EFFECTIVE STIFFNESS AND CARRY - OVER FACTORS FOR FLAT PLATES - MICRO CONCRETE MODEL STUDY

A Thesis
Presented to
The Faculty of Graduate Studies
The University of Manitoba

In Partial Fulfillment
of the Requirement for the Degree
Master of Science

by
A. Parnichkul
April, 1969.

PREFACE

This thesis is based on a study of the inter-action of flat plates with transversely loaded columns and shear walls. The study consisted of two experimental programs, which were carried out independently by Messrs A. Parnichkul and R. Nantasarn.

The first of these, conducted by Mr. Parnichkul, involved the fabrication and load testing of two 1/16 scale micro concrete flat plate models. The second, performed by Mr. Nantasarn, involved the construction and testing, by the Moiré method, of four 1/24 scale plastic plate models.

To avoid duplication and to facilitate comparisons between the two programs, both are reported on in this thesis.

ACKNOWLEDGEMENTS

The author wishes to express his sincere appreciation to G. A. Morris, Associate Professor, Department of Civil Engineering, for his continual guidance throughout this thesis as well as a careful checking of the final draft. Special thanks are due to A. M. Lansdown, Head of Department of Civil Engineering, J. D. Wiebe, Assistant Professor, Department of Civil Engineering and Mr. R. Petri whose advise during the work was valuable.

The author is also indebted to the Civil Engineering laboratory staff for their constructive help in the structural laboratory, and the Canadian International Development Agency for their financial support under the Colombo Plan.

TABLE OF CONTENTS

LIST OF FIGURES

LIST OF TABLES

CHAPTER I

INTRODUCTION

1.1 Object and Scope. In recent years the use of multistory buildings has grown rapidly for both residential and commercial purposes. As buildings increase in height, it becomes increasingly important to ensure adequate lateral stiffness against wind, seismic or blast loads. A commonly used type of structure which provides this lateral stiffness consists of a central core, which acts as a shear wall and accommodates elevators, stairs and services, surrounded by peripheral and possibly interior columns. The floor systems generally consist of flat plates, flat slabs, waffle slabs or concrete joints.

In the lateral load analysis of such shear wall-frame structures, the structure is often idealized as a series of parallel planar frames for which the "beams" are portions of the floor systems. One of the most complex problems in the analysis is the estimation of the effectiveness of the floor systems in resisting the relations of the shear walls and columns. In the past, it has sometimes been assumed for analysis purposes that the frame carries only vertical loads while shear walls resist all lateral loads. If, however, the shear wall-frame interaction is considered, the frame and shear walls tend to prevent each other from taking their natural free deflected shapes and a redistribution of forces among them will result. The calculated stiffness of the structure will also be increased. The force distribution in the structure depends on the stiffness of the members connecting the frame and the shear walls.

For flat plate shear wall structures, the stiffnesses of the connecting members depend on the widths of the plates that are effective in resisting lateral loads.

The object of this study was to measure experimentally the stiffness and carry-over factors for flat plates loaded by couples produced by loads applied transversely to columns and shear walls of various dimensions and shapes. The stiffness factors are used to compute effective slab widths for the various type of structure. The effective slab width is the width of a rectangular beam that would have the same flexural stiffness at a laterally loaded column or shear wall as the actual flat plate.

Four 1/24 scale plexiglas and two 1/16 scale micro concrete flat plate models were used in the tests. Each model consisted of several continuous flat plate panels supported by peripheral columns and loaded by couples applied transversely either to central column or shear wall stubs or to peripheral column stubs.

1.2 Relationship to Previous Tests. Interaction of wideplates with laterally loaded columns and shear walls has been treated analytically and experimentally by several investigators. Tsuboi and Kawaguchi [1] carried out tests on nine mortar plate models loaded through column stubs, and compared their test results with those from an elastic finite difference analysis. They reported effective plate widths based on stiffness factors for interior columns.

Khan and Sbarounis,[2] investigating the "Interaction of Shear Wall and Frames" reported an approximate solution obtained from simple mathema-

tical and physical models. The analytical study was supported by a syplified elastic model test showing good agreement. Also the results of their study of column plate interaction were in close agreement with those of Tsuboi and Kawaguchi.

Brochie and Russel[3] who studied an entire flat plate structure presented an analytical study (assuming elastic behavior) of flat plates subjected couples produced by lateral loads acting on the columns. They assumed the plate to be supported on an elastic medium with a variable modulus of elasticity and the loads were assumed applied directly to the plate. They expressed their findings in terms of effective plate widths.

Carpenter[4] studied the subject of effective plate stiffness and reported effective slab widths which were in good agreement with those obtained by Brochie and Russel, although they were based on different definitions of stiffness. While Carpenter used the moment rotation characteristic of one column with other columns remaining fixed, Brochie rotated simulteneously every column on the axis of rotation and obtained a somewhat lower stiffness due to the transverse carry-over factor.

Bernard and Schweighofer [5] studied plexiglas models subjected to lateral loads. Each model consisted of two shear walls connected by a series of plates of varying sizes. Test results showed a good agreement with an analytical study employing Rosman's formula. When the width of the plates was increased, different stress values resulted. It was reported that the difference could be caused by stress concentrations due to unconnected shear walls. The tests verified that within the elastic rang the entire width of the prototype plate could be considered as effective stiffness for frame action for two coupled shear walls. Carry-over factors

were not considered in this study.

The ACI Building Code[6] 318 - 63 does not recommended specific values for effective stiffness, but does imply in Sec. 2102(g), the participation of the entire panel width for transfering unbalanced moment. The pertinent section states: "When concerning with lateral loads, the moment shall be distributed between the column and middle strips in the same proportions as prescribed for negative moments due to gravity loads." A further statement in the same section reads in part, "A slab width between lines that are 1.5t each side of the column may be considered effective."

Distasio and Van Buren,[7] developing an analytical procedure for transfering moment between columns and a flat plate floor, suggested that the lateral force moments be split into two parts; one part was carried in direct bending from the slab into the column. The critical section was assumed at a distance equal to the slab thickness outside the column periphery. The other part, in the same critical section, was carried by torsional moment. Concrete and steel bars passing through this section were considered to produce resisting shearing stresses.

The studies cited above investigated the interaction of flat plates and laterally loaded columns or rectangular shear walls. In this study, an attempt is made to corelate with results of previous studies and to extend them to include shear walls of various sizes and shapes.

CHAPTER II

THEORETICAL CONSIDERATIONS

2.1 Introduction. The general elastic plate theory has been used by Carpenter[4] to analyse a flat plate to which couples have been applied by laterally loaded columns. While finite element or finite difference methods could be used to extend this analysis to plates loaded through shear walls, only an experimental study is undertaken here. Plate deflections and slopes under known loadings are measured and the plate stiffness and carry-over factors calculated from the appropriate applied loads and measured deflections.

2.2 Stiffness Factors. The definitions of the stiffness and carry-over factors used for the plate are those normally used in the slope - deflection equations. The factors are derived by considering a member AB subjected to transverse loads and end forces as shown in Fig. 2.2.1

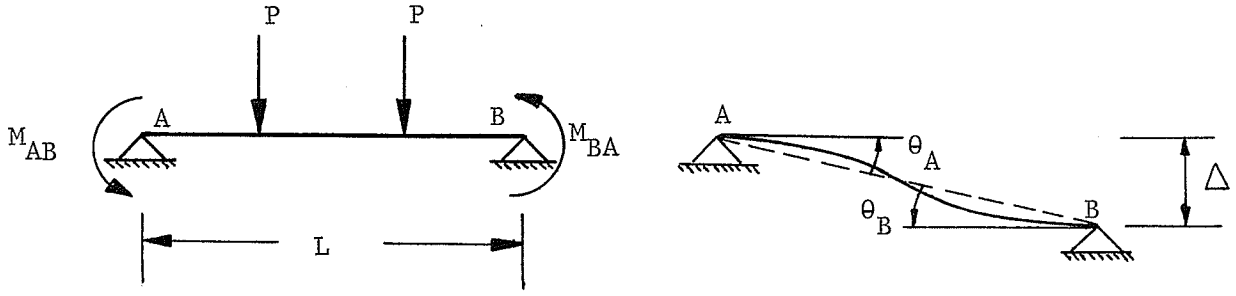

Fig 2.2.1 Loads and Displacements for Member AB

Assuming clockwise moments and rotations to be positive, and assuming displacement to be positive for clockwise rotation of the member about end A (all signs shown here are negative) the following relationships are obtained:

$$M_{AB} = \frac{2EI}{L}\left(2\theta_A + \theta_B - \frac{3\Delta}{L}\right) \pm M_{FAB} \quad \ldots\ldots \quad 2.2.1$$

$$M_{BA} = \frac{2EI}{L}\left(2\theta_B + \theta_A - \frac{3\Delta}{L}\right) \pm M_{FBA} \quad \ldots\ldots \quad 2.2.2$$

where, M_{AB}, M_{BA} = moments on ends A and B respectively,

M_{FAB}, M_{FBA} = fixed end moments on ends A and B respectively,

θ_A, θ_B = rotations of ends A and B relative to line AB,

Δ = transverse displacement of end B relative to end A,

L = span length of member,

P = any arbitrary load,

E = Young's Modulus of Elasticity,

and I = moment of inertia of the member.

The above two equations are known as the slope - diflection equations. For a continuous flat plate as shown in Fig. 2.2.2, if a moment, M_{AB}, is applied at the support AA, the slope - deflection equation may be simplified as follow:

Let the span length L, the width b and the depth d of the member be the same as the span length L_x, the equivalent width L_y and the thick-

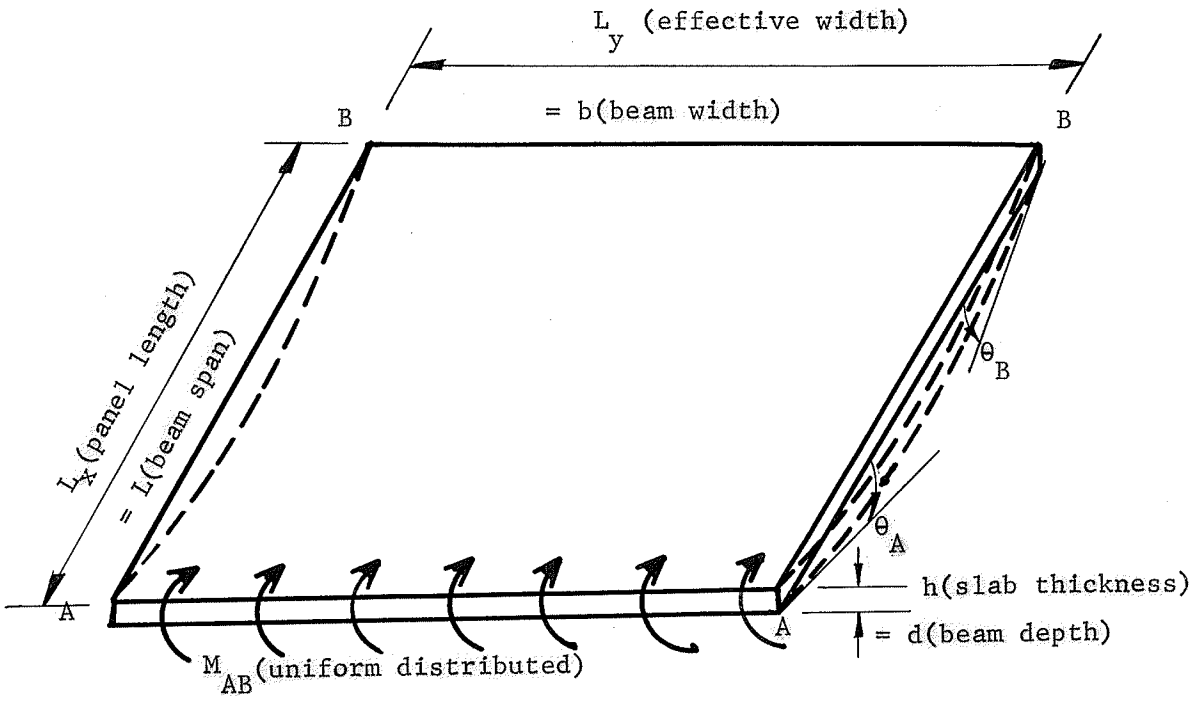

Fig. 2.2.2 Imaginary Beam of a Flat Plate.

ness h of the flat plate, thus creating a hypothetical wide shallow member.

From equation 2.2.1, since $M_{FAB} = 0$,

$$M_{AB} = \frac{2 E I}{L} \left(2\theta_A - \theta_B - \frac{3 \Delta}{L} \right) \quad \ldots\ldots \quad 2.2.3$$

where θ_A , θ_B = clockwise rotation and counter clockwise rotation of ends A and B of the plate respectively,

I = the moment of inertia of the plate,

and the other terms are defined as for the beam.

If end B of the member is fixed and end A is restrained from translation (pinned), θ_B and Δ become zero and then

$$M_{AB} = \frac{4 E I \theta_A}{L_x} \quad \ldots\ldots\ldots\ldots\ldots \quad 2.2.4$$

or $$\frac{M_{AB}}{\theta_A} = \frac{4 E I}{L_x} \quad \ldots\ldots\ldots\ldots\ldots \quad 2.2.5$$

Equation 2.2.5 gives the moment - rotation relationship for the plate, and is used to define the stiffness factor which is designated as

$$K = \frac{M_{AB}}{\theta_A} = \frac{4 E I}{L_x} \quad \ldots\ldots\ldots\ldots\ldots \quad 2.2.6$$

where $$I = \frac{L_y h^3}{12} \quad \ldots\ldots\ldots\ldots\ldots \quad 2.2.7$$

Combining equations 2.2.6 and 2.2.7

$$K = \frac{4\,E}{L_x}\left(\frac{L_y\,h^3}{12}\right) = \frac{E\,L_y\,h^3}{3\,L_x} \qquad \ldots\ldots \quad 2.2.8.$$

The stiffness factor can be determined experimentally by applying known moments M_{AB} and measuring the resulting plate rotations θ_A. When the stiffness factor has been determined, the effective width of the plate, L_y, can be calculated from equation 2.2.8, and is:

$$L_y = \frac{3\,K\,L_x}{E\,h^3} \qquad \ldots\ldots \quad 2.2.9$$

2.3 Carry - Over Factors. The carry-over factor for a member AB is the ratio of the moment M_{BA} produced at fixed support B, to the moment M_{AB} applied at a simply supported end A. Since it is difficult to measure the fixing moment at a plate support, the principle of superposition was used in obtaining the carry-over factors.

To illustrate the procedure beam ABC in Fig. 2.3.1 is considered. End C is fixed while points A and B are simply supported. In Fig. 2.3.1(a), a clockwise moment, M_{BA}, is applied at B and caused rotations θ_{A1} and θ_{B1} at A and B respectively. Moment, M_{BA}, is now removed and a clockwise moment, M_{AB}, is applied at end A as shown in Fig.2.3.1(b). The resulting rotations at A and B are θ_{A2} and θ_{B2} respectively.

Since M_{BA} causes a rotation θ_{A1} at A, and

M_{AB} causes a rotation θ_{A2} at the same point A,

the moment at A required to produce rotation θ_{A1} at point A is $M_{AB}\ \theta_{A1}\ /\ \theta_{A2}$.

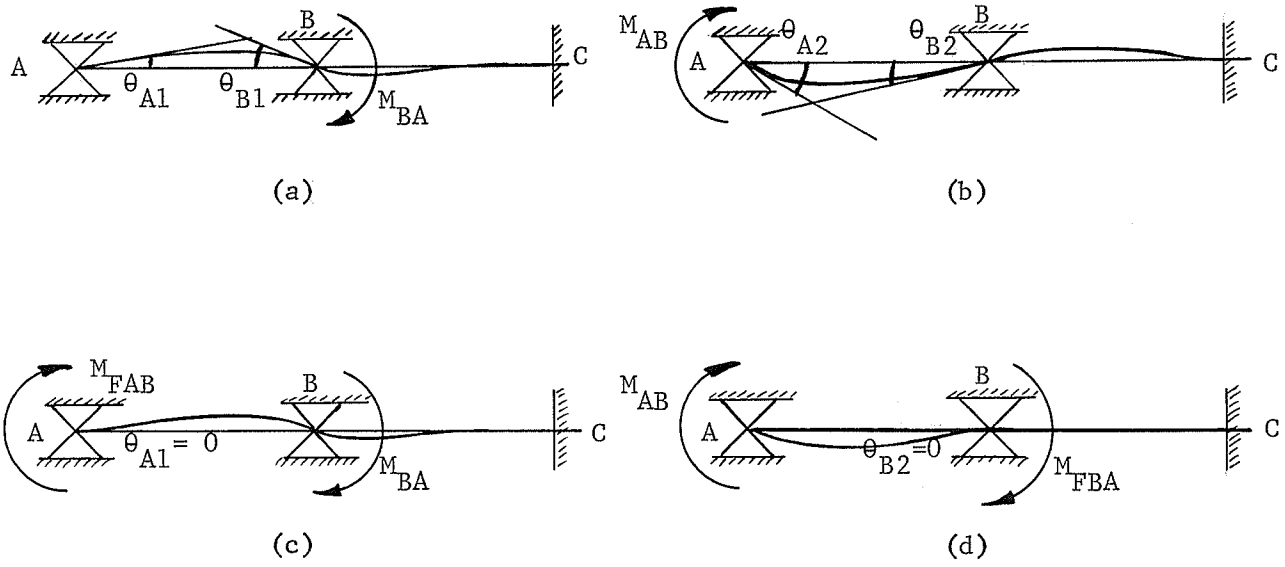

Fig. 2.3.1 Superposition

If the total rotation at A is to be made zero, an imaginary clockwise moment equal to $M_{AB}\ \theta_{A1}\ /\ \theta_{A2}$ should be applied at point A at the same time as M_{BA} is applied at point B. This imaginary moment is called the fixed end moment A to B or M_{FAB} as shown in Fig. 2.3.1(c).

Then the carry-over factor due to M_{BA} is equal to the fixed end moment M_{FAB} divided by the moment $M_{BA}/2$ or

$$C_{BA} = \frac{2\ M_{AB}\ \theta_{A1}}{\theta_{A2}\ M_{BA}} \qquad \ldots\ldots\ 2.3.1$$

In the same way if θ_{B2} is to be kept at zero when M_{AB} is applied, the fixed end moment B to A or M_{FBA} is equal to $M_{BA}\ \theta_{B2}/\ \theta_{B1}$ as shown in Fig. 2.3.1(d). Therefore,

$$C_{AB} = \frac{M_{BA}\ \theta_{B2}}{\theta_{B1}\ M_{AB}} \qquad \text{..... 2.3.2}$$

Equation 2.3.1 is used to determine the carry-over factors for panels loaded at interior columns of shear walls, while equation 2.3.2 is used to determine the carry-over factors for panels loaded at exterior columns.

2.4 Measurement of Stiffness Factor for Model C1. For micro - concrete model C1 (shown in Fig. 2.4.1), the section modulus of the loaded column was very small compared to that for the plate and it was impossible to obtain sufficiently large plate deflections by applying lateral loads to the column. Consequently, the following procedure had to be used to determine the stiffness factor for the plate.

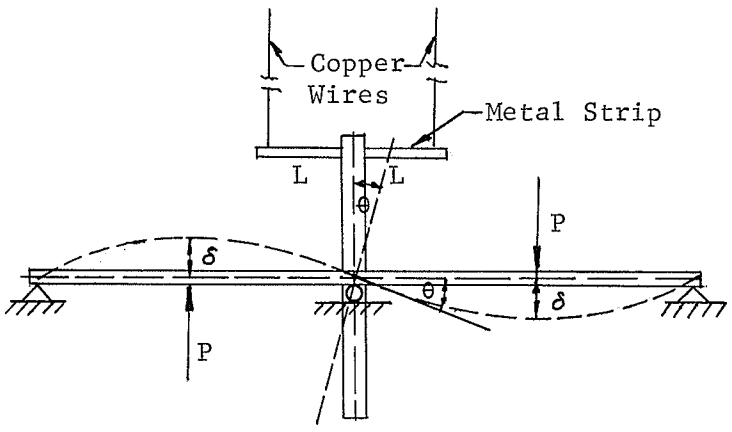

Fig. 2.4.1 Model C1

A pair of loads P were applied to the slab at equal distances from the exterior column as shown in Fig. 2.4.1. A metal strip fixed to the column, was connected to deflection gauges by means of copper wires and used to accurately measure the column rotations.

From the reciprocal theorem

$$2 P \delta = M \theta \qquad \ldots\ldots\ldots\ldots \quad 2.4.1$$

where θ = the column rotation produced by loads P,

δ = the slab deflection at each load P that would result from a moment M applied to the column.

If M is assumed to be unity, then equation 2.4.1 becomes

$$\delta = \frac{\theta}{2 P} \qquad \ldots\ldots\ldots\ldots \quad 2.4.2$$

By varying the points of load application, a series of θ values was obtained and the corresponding deflections calculated and plotted. The slope α of the plate was then measured from the deflection curve, and the stiffness factor calculated from;

$$K = \frac{M}{\alpha} = \frac{1}{\alpha} \qquad \ldots\ldots\ldots\ldots \quad 2.4.3$$

stiffness calculations for loads P of 50, 100 and 150 lbs. are included in Appendix C.

CHAPTER III

EXPERIMENTAL PROCEDURE

PART A PLASTIC MODELS

3.1 Description of Models. Four 1/24 scale flat plate models designated P1, P2, P3 and P4 were tested. Their dimentions are given in Figs. 3.1.1, 3.1.2, 3.1.3 and 3.1.4 respectively. Panel widths for models P2, P3 and P4 were varied to accomodate shear walls of various shapes.

The models were designed in such a way that loading could be applied through either the center column or shear wall, or one or two of the exterior columns along the same loading line. All exterior columns remained fixed when the center column or a shear wall was being loaded.

The models were cut from a sheet of 1/4 in. thick black plexiglas (acrylic sheet). Fixed columns were simulated by column stubs cut from 1/2 in. square steel bar with 1/4 in. diameter holes drilled through their centres to clamp them to the plate and loading frame. They were 1/2 in. in height except for those in the line of loading, which were 3/4 in. in height. The loaded columns had the same cross-sectional dimensions as the fixed columns and were 3½ in. in height. A V-notch was made on each loaded column stub at 2 7/8 in. from the plate in order to provide a 6 in. moment arm. The rectangular shear walls were cut from black plexiglas sheets and cemented to the top and bottom of the plate to simulated a shear wall passing through a flat

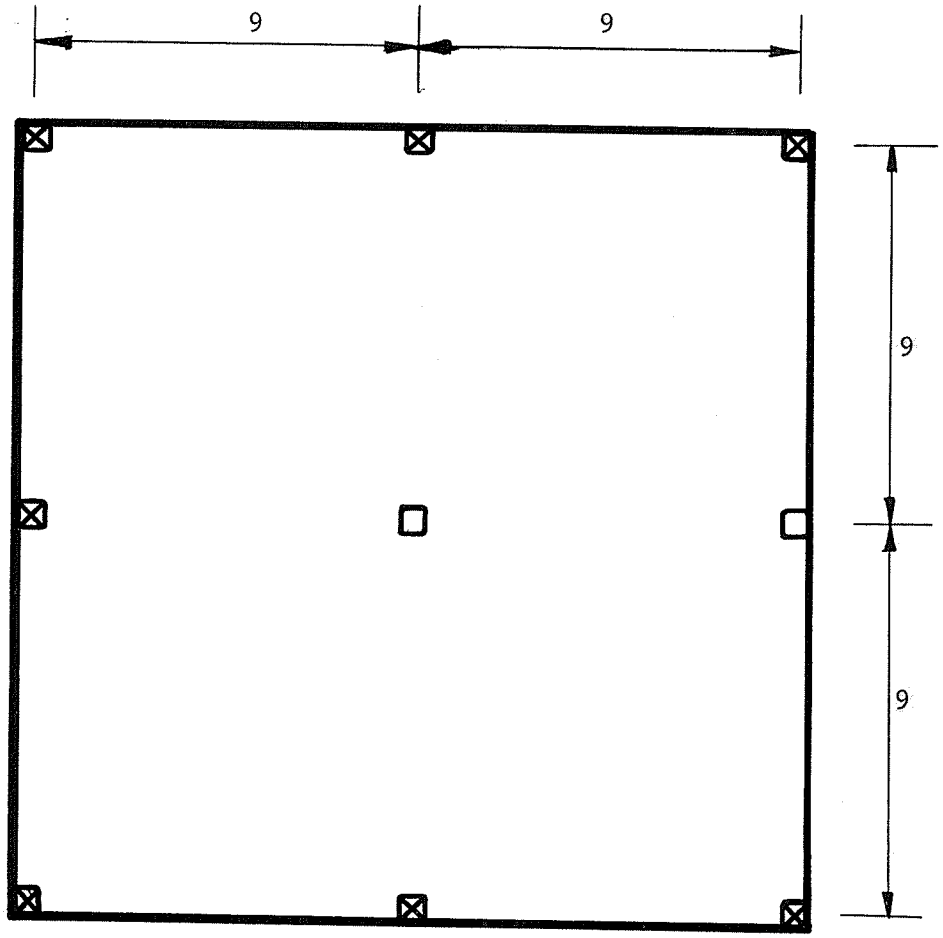

PLAN

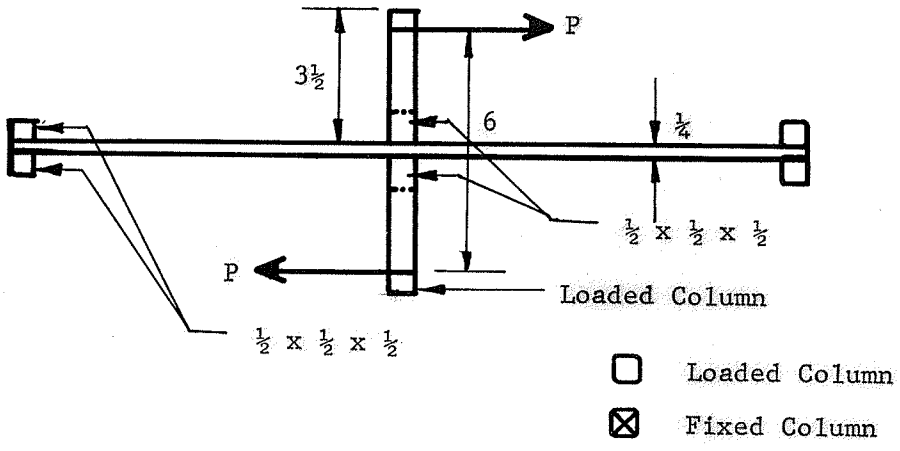

SECTION

Fig. 3.1.1 Model P1

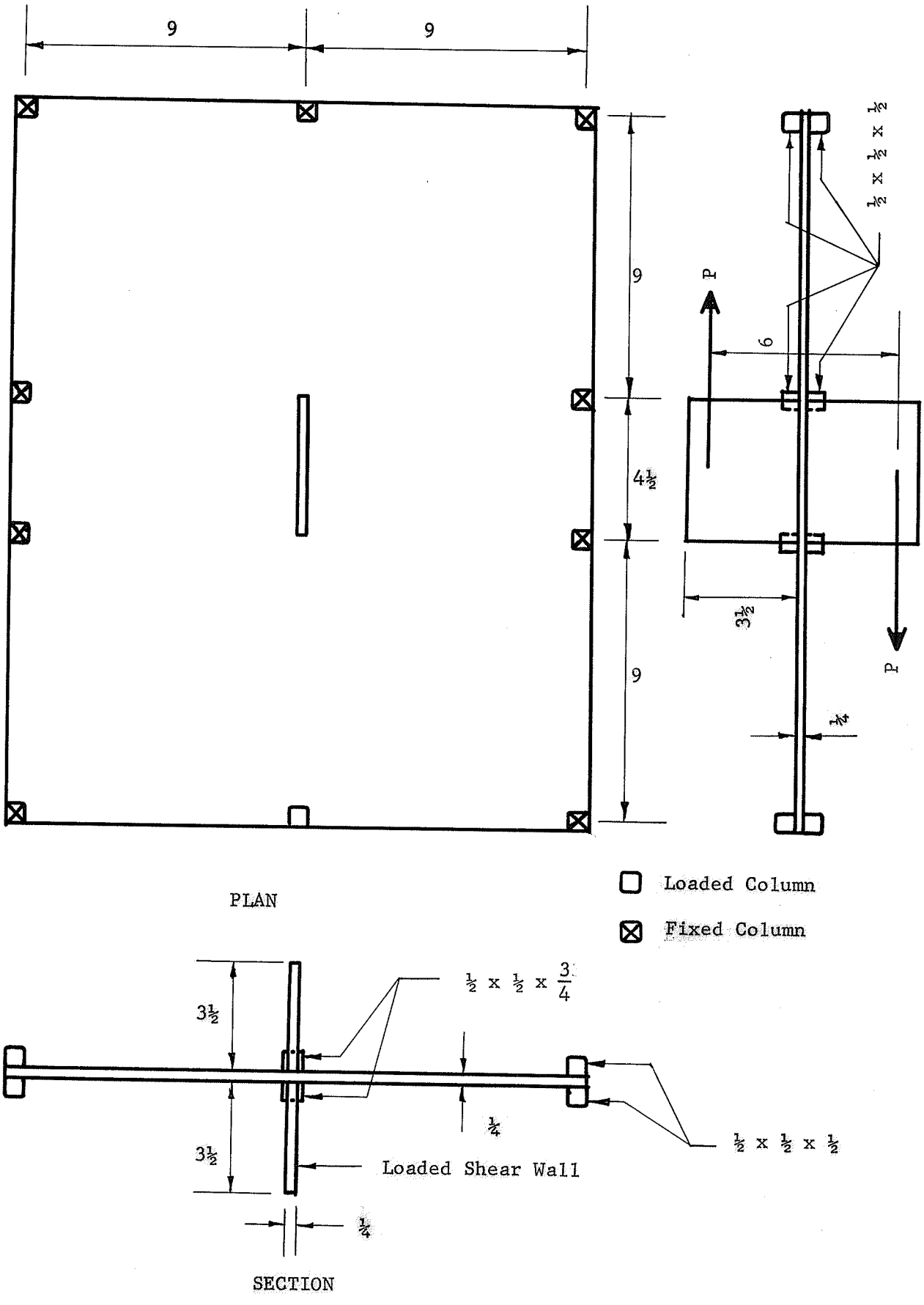

Fig. 3.1.2 Model P2

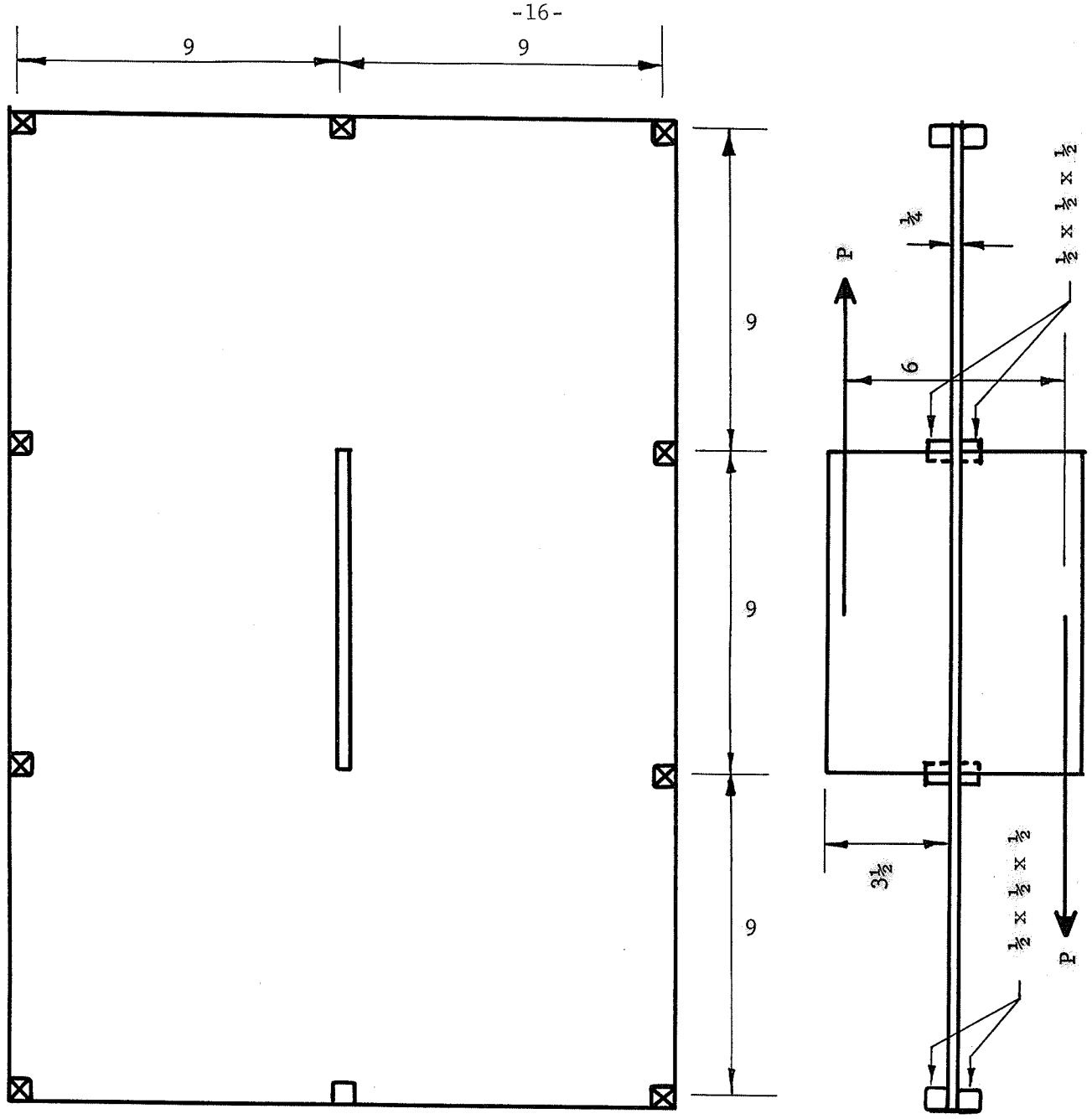

Fig. 3.1.3 Model P3.

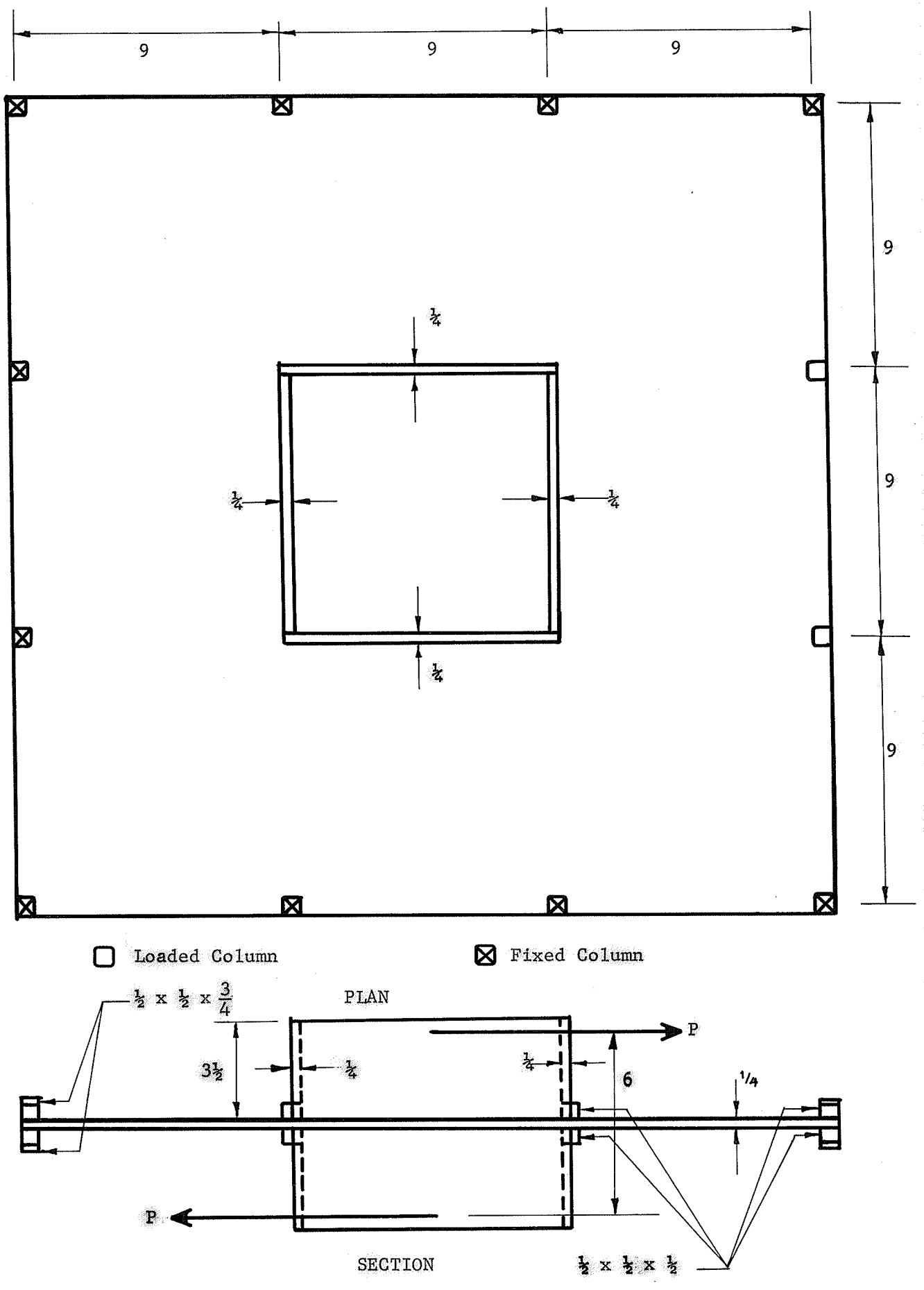

Fig. 3.1.4 Model P4

plate floor. The box shear wall was fabricated by cementing sheets together and then cementing the assembly to the plate. Jaybond GC-2 acrylic adhesive cement was used for cementing all joints. In order to provide a 6 in. couple arm, a 3/16 in. diameter hole was drilled through each shear wall at a point 2 7/8 in. from the plate, to accomodate a loading yoke.

3.2 Experimental Procedure. The Moire' apparatus shown in Fix. A -2 was used to measure the plate slopes for all plastic models. The principles of the Moire' technique are summarized in Appendix A. All models were positioned vertically and bloted to the frame shown in Fig. 3.2.1. Since the slope and deflections parallel to the direction of loading (the vertical direction) only were required, the screen was always positioned such that the ruled lines were horizontal.

Each model was subjected to four different types of loading, designated A, B, C and D illustrated in Figs. 3.2.2, 3.2.3, 3.2.4. and 3.2.5. Loading type A was used to determine the plate stiffness factor loaded at an interior column or shear wall by a couple of forces 6 in. apart acting in upward and downward directions. The forces were provided by weights attached to steel cables which were connected to a pair of galvanized steel strips that were placed on either side of the column or shear wall. The upward force was applied by means of a pulley system. The pulleys were calibrated to correct for friction force.

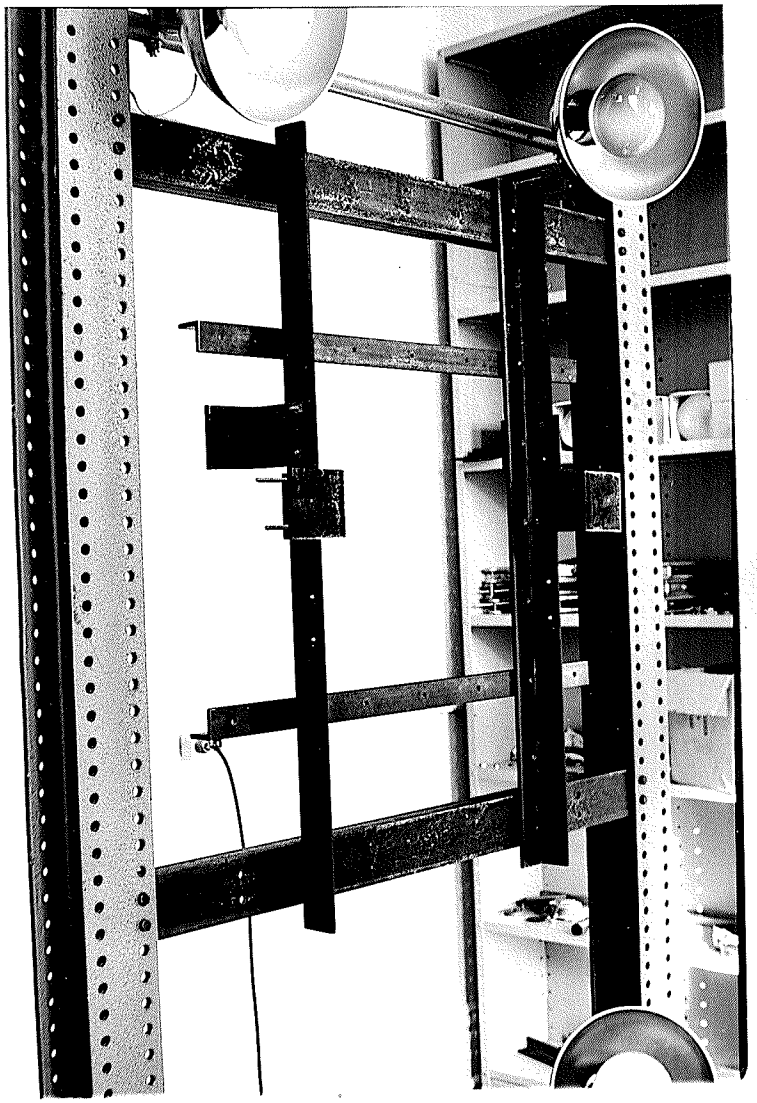

Fig. 3.2.1 Loading Frame

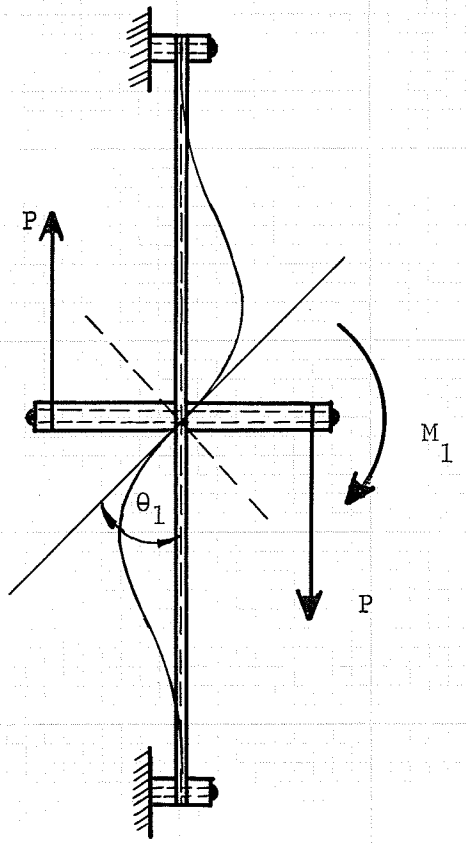

Fig. 3.2.2. Load Type A.

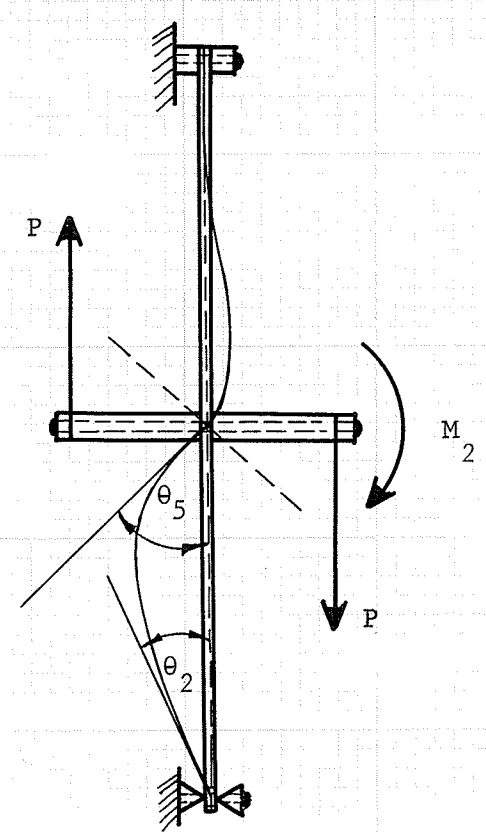

Fig. 3.2.3. Load Type B.

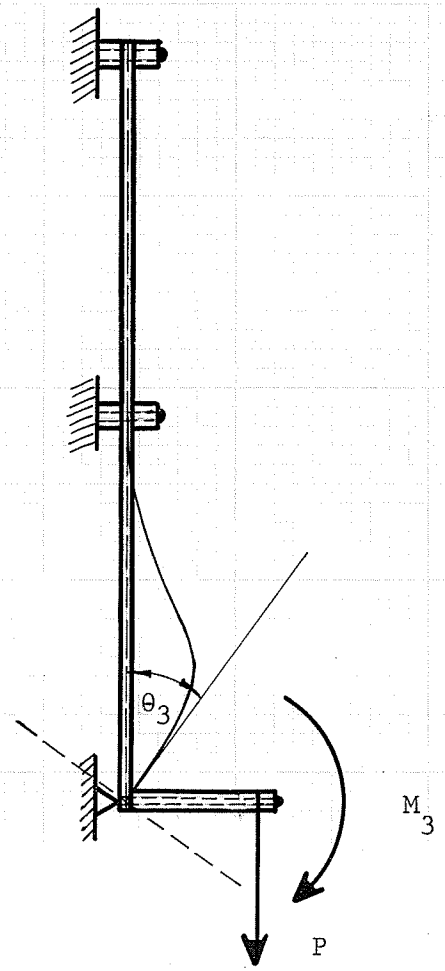

Fig. 3.2.4 Load Type C.

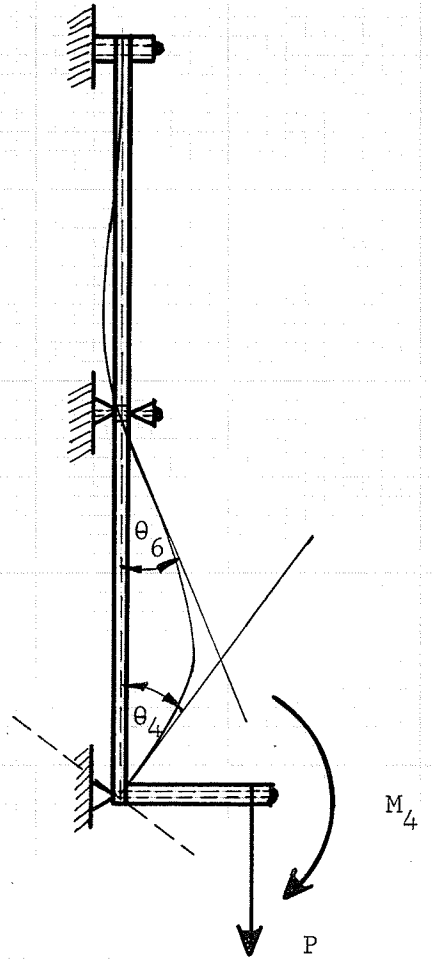

Fig. 3.2.5 Load Type D.

Loading type C was used to measure the stiffness of the plate loaded at an exterior column or in the case of model P4, at two adjacent exterior columns. Since the lateral couples applied to the exterior columns tended to cause lateral deflection of the plate at these columns, it was necessary to provide simple supports for the plate at the loaded columns to restrain the slab laterally as indicated in Figs. 3.2.4 and 3.2.5. All supports except the loaded column were fixed to the loading frame. For model P2, P3, and P4 the shear walls were restrained by angles which were bloted to the frame.

Since the fixing moment at a fixed column could not be measured directly, loading types B and D were applied, and the reciprocal theorem used to compute moments, as discussed in chapter 2. Loading type B was similar to type A except that one exterior column on the loading line was replaced by a simple support as shown in Fig. 3.2.3. Loading type D was similar to type C except that the slab was simply supported at the interior column or shear wall.

3.3 Properties of Plate Material. Eight specimens cut from the same plexiglas sheet as were the model plates, were used to test the flexural properties of the material. The tests conformed to ASTM Specification D790-66 Procedure A, Test for Flexural Properties of Plastic.[8] The specimens were 5 x 1 x 1/4 ins. and were loaded with the 1 in. dimension horizontal on a 4 in. span, using a universal testing machine. The supports had 3/8 in. radii and the radius of the loading head was 1 in. The rate of crosshead motion was set at 0.167 in./min. The load -

deflection curves are presented in Appendix B where the flexural properties are also calculated.

Table B - 1 shows the material properties as computed from the test results, and the average values. The other physical properties of the plexiglas used may be obtained from the manufacturer's cataloque.(9)

3.4 Photographic Technique. The curvatures and rotations of the model plates were obtained from photographs of interference fringes obtained using the Moire' apparatus.

Kodak D - 19 Developer and Kodak Metallographic plate were used in the photography. The camera was first focused on the unloaded model and a sharp image of lines of the Moire' screen obtained on the ground glass window of the camera. This was accomplished by completely opening the diaphragm and viewing the image on the ground glass with a magnifying glass. During focusing the photoflood lamps were switch on. After focusing, the diaphragm was set to its smallest opening (f:32) to obtain good contrast. The double exposures of the unloaded and loaded model were then made, and the photographic plate developed. The picture was fixed with the Kodak Fixer, washed under running water and allowed to dry at room temperature. Kodak Bromide Paper F - 3 Single Weight and Kodak Dektol Developer were used for obtaining enlargements, which were made to one half scale.

The camera of the Moire' apparatus is located behind the ruled screen and the photographs were taken through a hole at the center of the screen. A difficulty was encountered due to a reflection from the

cylindrical inner surface of the hole which produced a black circular ring on the photographs. This could not be prevented either by painting the surface black or by moving the screen. However, it was minimized by raising the photographic plate and lowering the screen to focus at the area of interest on the model. The dark spot, which appears on the most of Moire' photos is the image of the opening through which the photos were taken.

To obtain photos with clear, sharp interference patterns it is essential that the reflecting surface of the model be clean and dust free. Since it is extremely difficult to clean the surface without scratching it, great care should be exercised to avoid the forming of dust on the models.

Four types of loading which have been described previously were used for each model plate. Because of the sizes of the models and the Moire' apparatus, it was impossible to photograph the whole plate. Furtunately all loadings used gave symmetrical fringe patterns (an example of which is given in Fig. 3.4.1), and only the lower half of the model was photographed and used for fringe measurements.

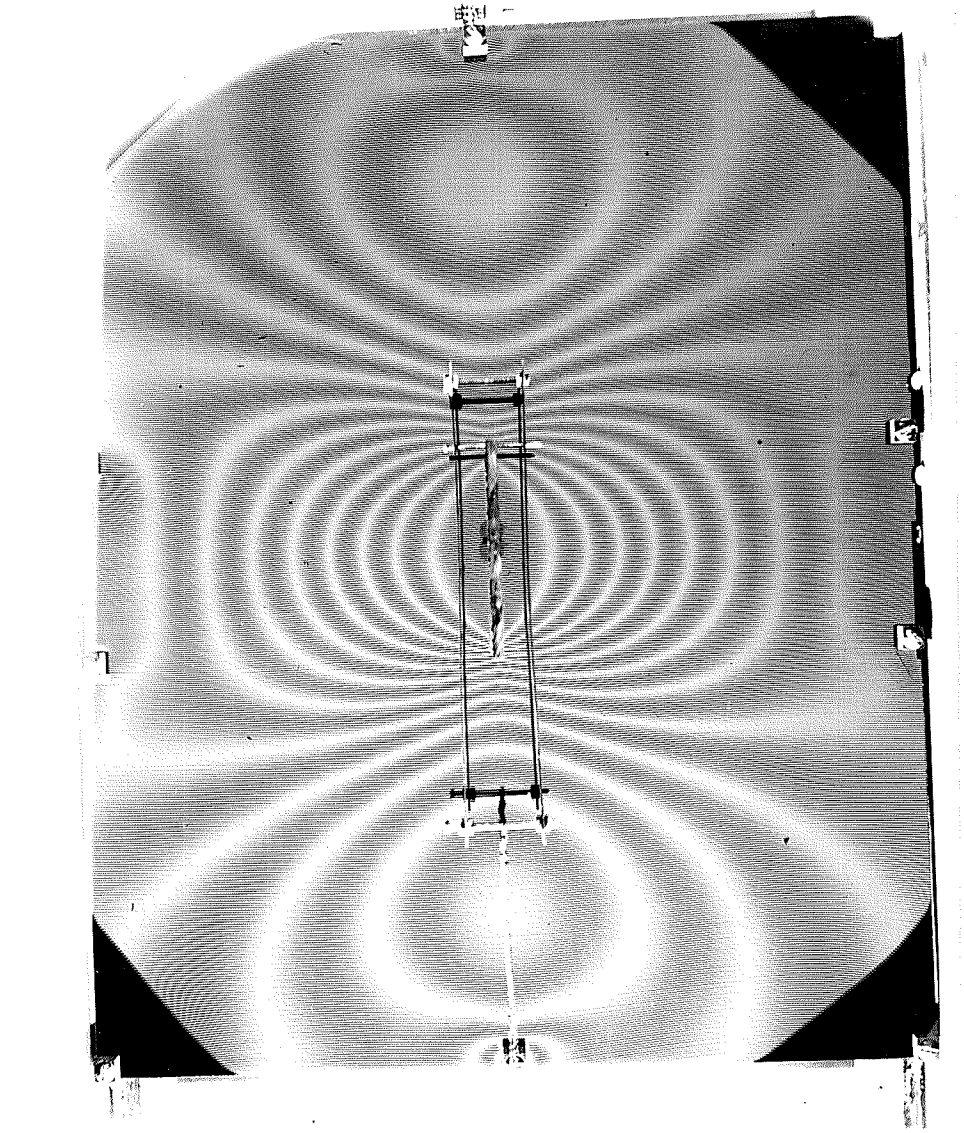

Fig. 3.4.1 Symetrical Fringes for Model P2 Load Type A.

(obtained by positioning model as far as possible from the camera)

PART B REINFORCED CONCRETE MODELS

3.5 Description of Test Structures. The two micro concrete models, designated C1 and C2 and shown in Figures 3.5.1 and 3.5.2 respectively were tested. Model C1 had four square flat plate panels with peripheral columns and one central column. Model C2 had three panels in one direction two in the other, and a central rectangular shear wall whose width covered a full panel.

(a) Prototype The concrete models were designed to represent flat plate floors with 16 foot square panels, a 6 in. slab and 12 in. square columns. No drop panels or column capitals were used. The height of each story for the prototype was assumed to be 10 ft. The rectangular shear wall for model C2 corresponded to a 17 ft. wide, 8 in. thick wall for the prototype. The prototype was designed according to the 318-63 ACI Building Code,[6] using the empirical method of Section 2104. The live load assumed was 60 psf and the dead load of the slab was 75 psf, giving a total load of 135 psf. Three thousand pound concrete with an allowable compressive stress of 1350 psi and an allowable shear stress of $2\sqrt{f'_c}$ or 110 psi was assumed. An allowable stress of 50% of the minimum yield strength or 20 ksi was assumed for the reinforcement.

(b) Models A scale factor of 1/16 was used for the two models. This yielded a model panel length of 12 in. and a slab thickness of 3/8 in. Three quarter in. square by one half in. thick steel blocks were used to simulate fixed columns for both models. Three sixteenth in. diameter bolts, passed through the steel blocks and the plate, were used to fasten the models to a loading frame. Other columns and

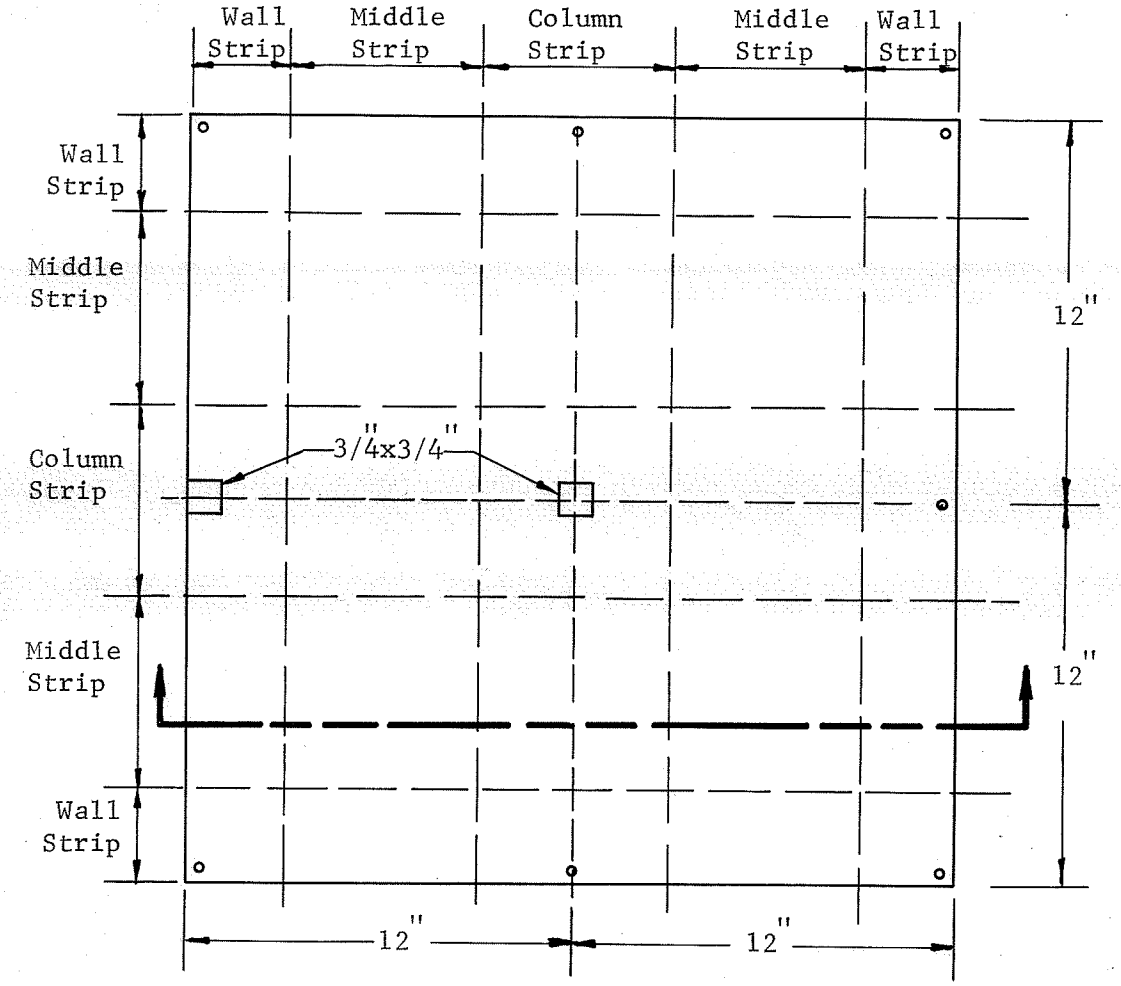

Plan

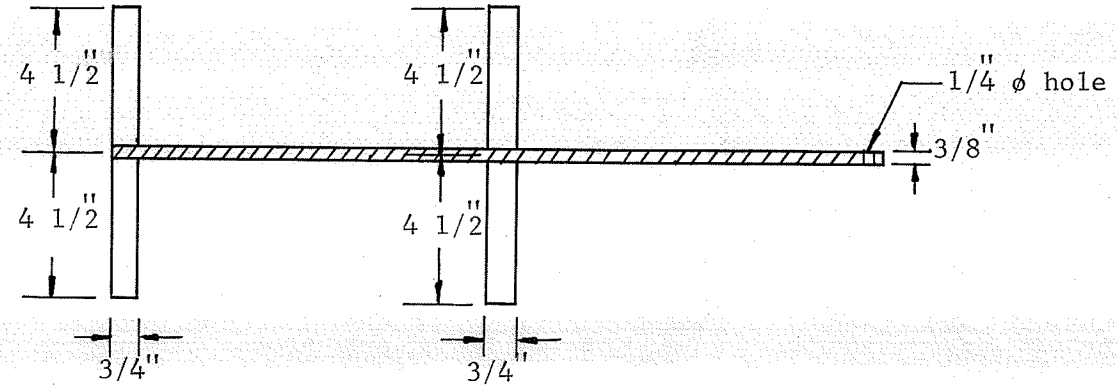

Section

Fig.3.5.1 Model C1

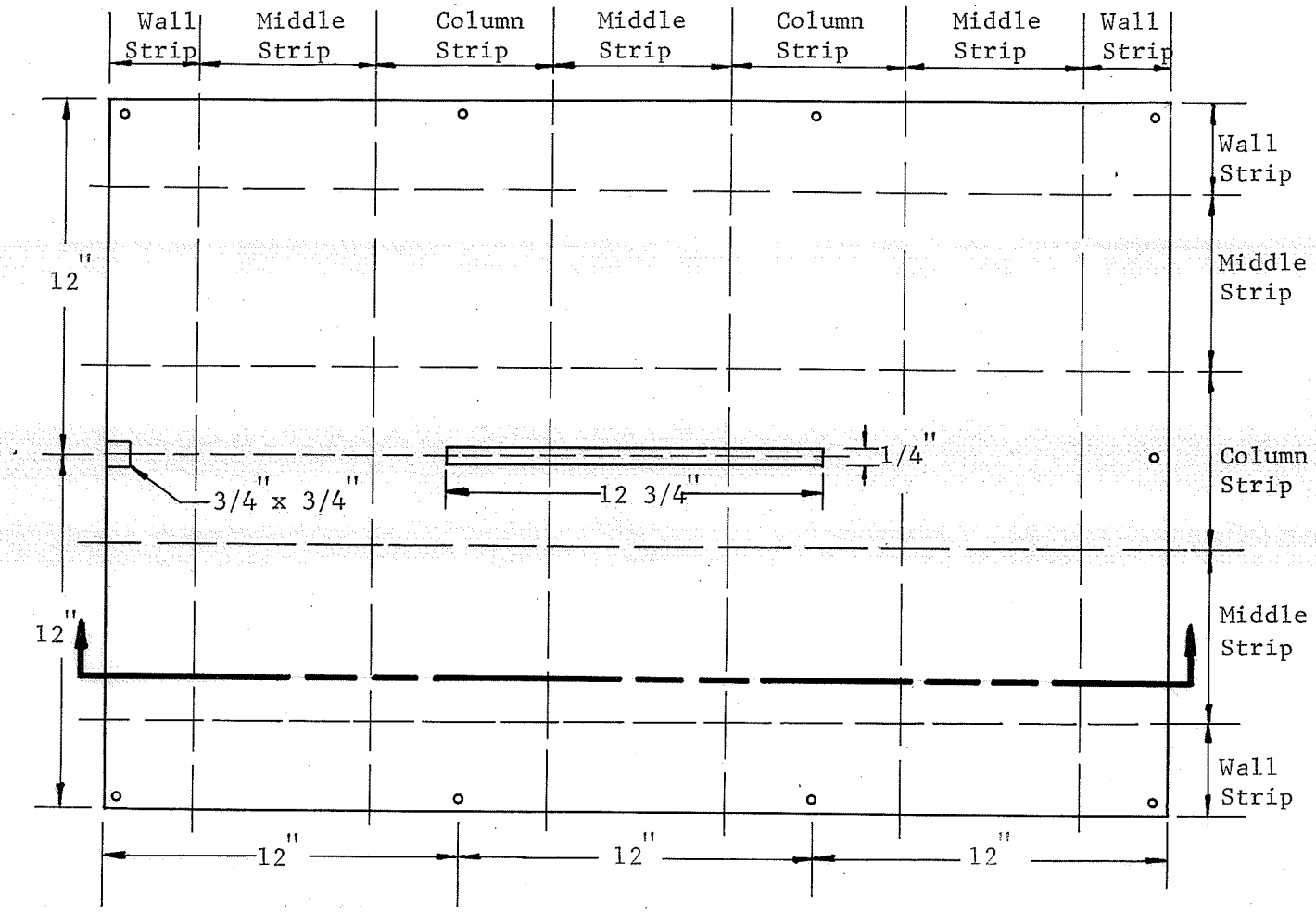

Plan

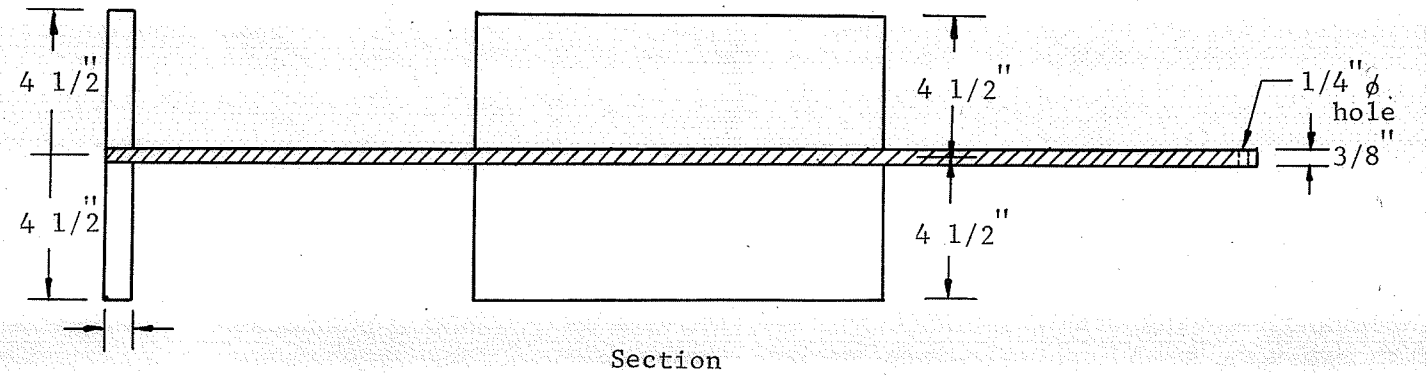

Section

Fig.3.5.2 Model C2

the shear wall were cast from mortar. The dimensions of the shear wall for model C2 were 12 3/4 in. by 1/2 in. The heights of shear wall and column stubs were 4 1/4 in.

A 0.038 in. diameter music wire (piano wire) was used as slab reinforcement and 0.067 in. diameter wire was used for column and shear wall reinforcement. Column ties were fabricated from 0.015 in. diameter copper wire. Of the wire used, only the 0.038 in. diameter music wire was annealed. The slab reinforcement patterns for models C1 and C2 are shown in Figures 3.5.3 and 3.5.4 respectively.

The design method, design loads and allowable stresses of models C1 and C2 were the same as those for the prototypes.

(c) Design of the Models Because the design loads and allowable stresses were the same for both models and prototypes, the following force conversions had to be used:

$$P_p = S_f \left(S_L \right)^2 P_m$$

and

$$M_p = S_f \left(S_L \right)^3 M_m$$

where P_p, M_p = Forces, moments on prototypes

P_m, M_m = Forces, moments on models

S_f = Stress scale factor = f_{sp}/f_{sm} = 1

S_L = Length scale factor = 16

The unit stresses and moduli used for models were:

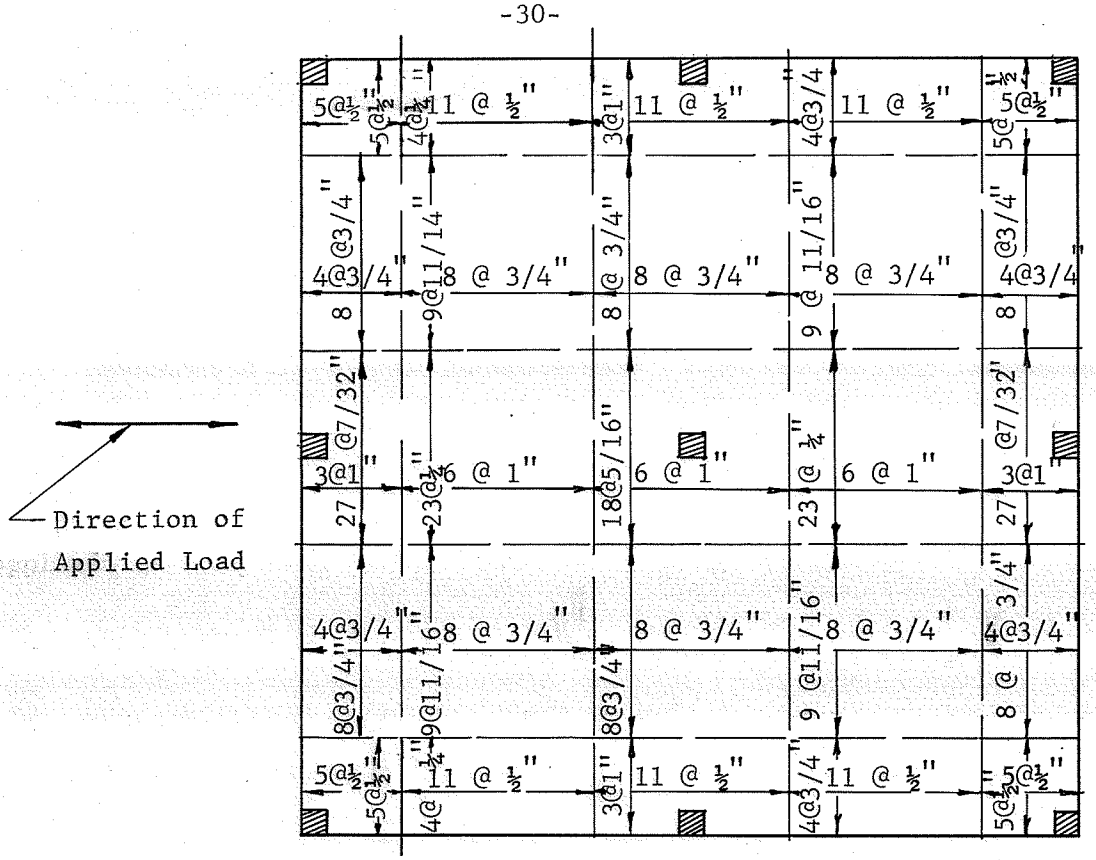

Positive Reinforcement

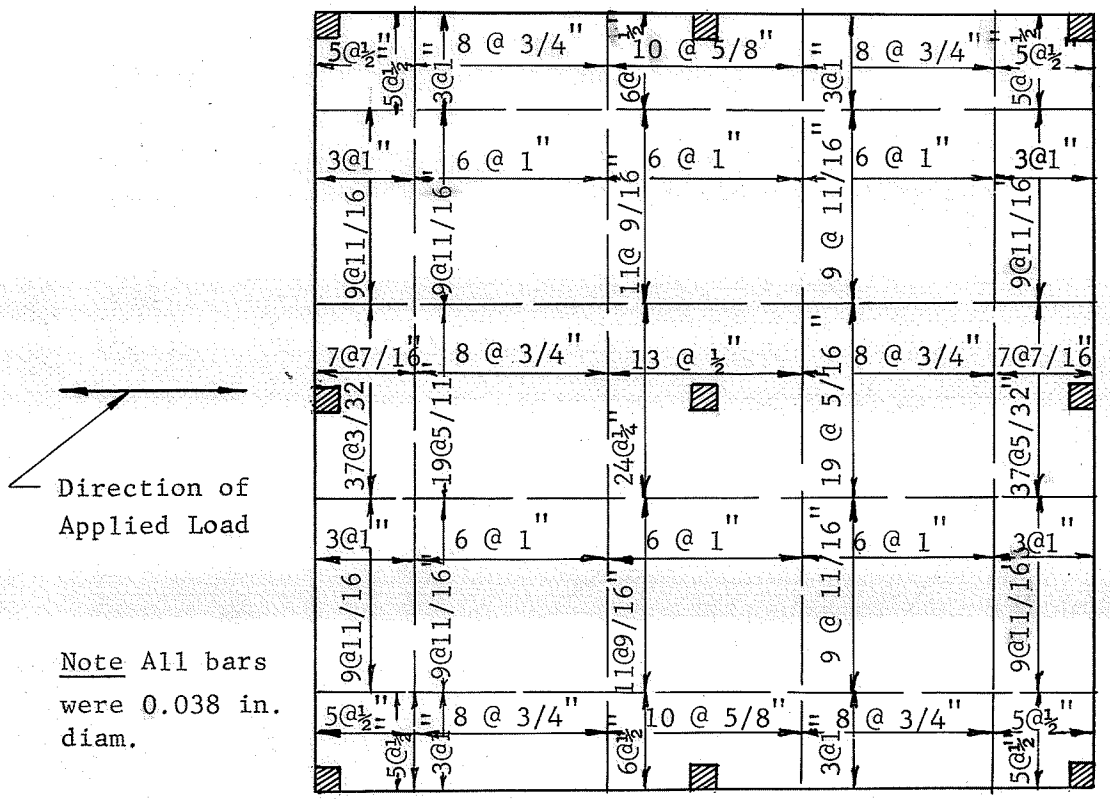

Note All bars were 0.038 in. diam.

Negative Reinforcement

Fig. 3.5.3 Wire Reinforcement Model C1

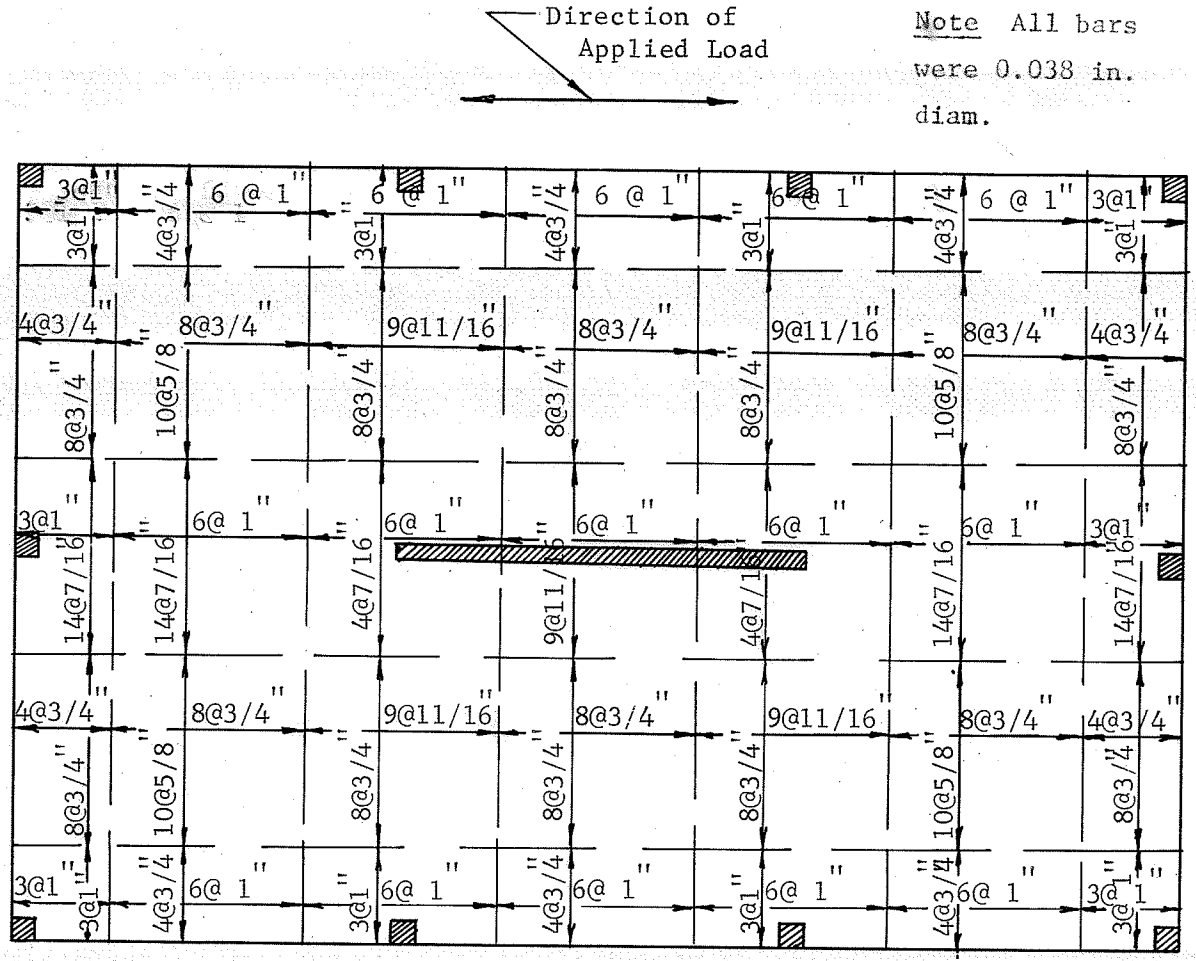

Fig.3.5.4 Wire Reinforcement, Model C2

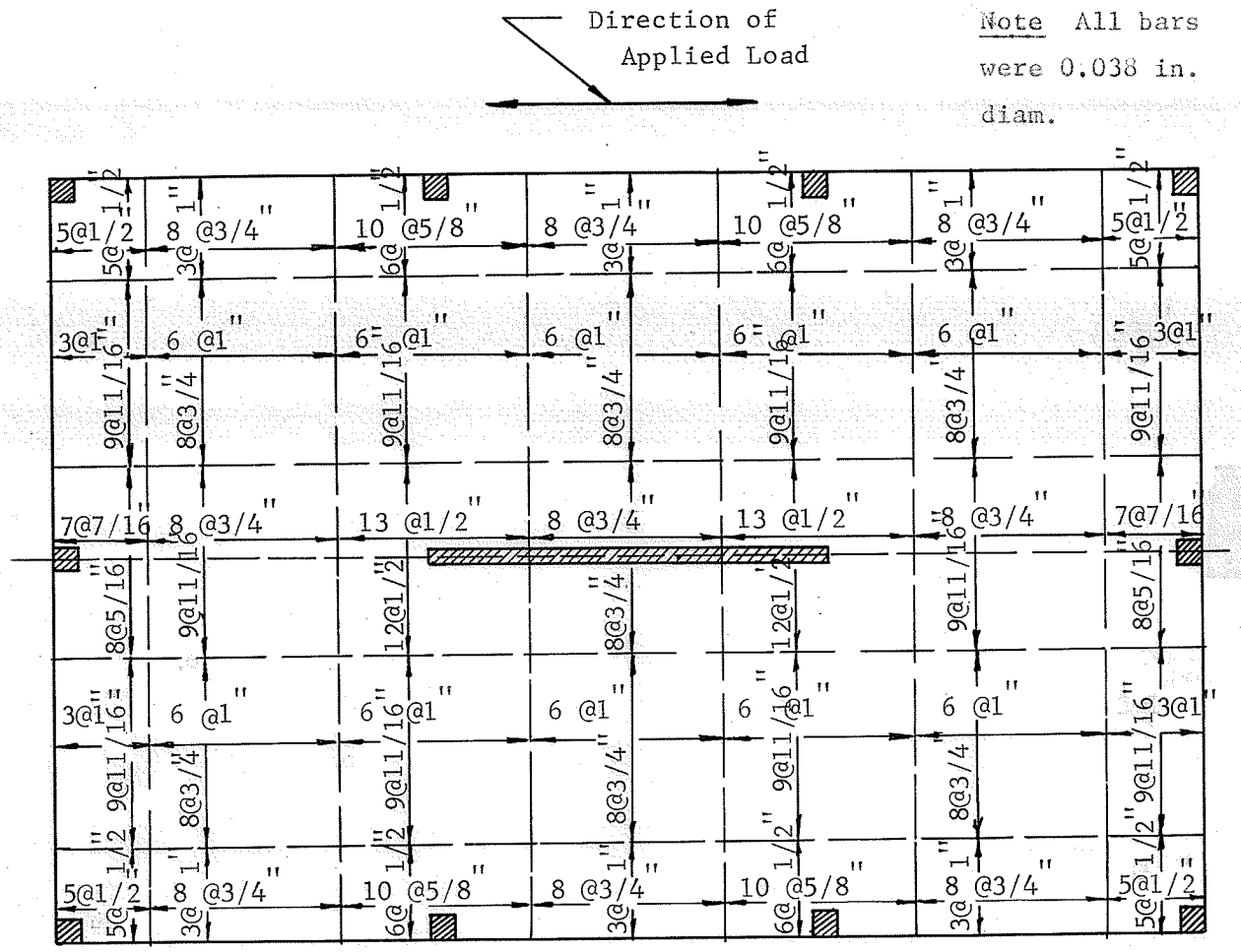

Negative Reinforcement

Fig.3.5.4 Wire Reinforcement, Model C2

f'_c	=	3000	psi
f_y	=	40000	psi
E_s	=	30×10^6	psi
E_c	=	3×10^6	psi
n	=	10	

The properties of the concrete used for the model structures were similar to those of a typical concrete that would be used for the prototype. Because the models were to simulate the prototype, the steel reinforcement for the models required the same pertinent properties as that for the prototype. Music wire suitably treated, served the purpose satisfactory.

3.6 Material Property Control

(a) Introduction Remarks Micro concrete models are composed of only two important materials; namely mortar and reinforcing wires. In order to simulate the properties of the concrete and reinforcement in the full-scale structure, both the mortar and reinforcing wire have to be carefully prepared. As noted by Petri,[10] the location of the material is one problem, while continuous supply with consistant properties is an other. The latter is generally more prominent because of the fact that the quality control of commercially available materials is not sufficiently good for model construction.

(b) Mortar In the model structure, the strength of the mortar has to be equal to that of concrete in the prototype. The workability of the mortar must be moderate. A stiff mix results in poor workability and

makes the removal of voids and air pockets difficult. On the other hand, if the mortar is too wet, excessive shrinkage occurs. Also the proportions of components of the mortar must be consistent. Because of the small size and quantities involves, materials of consistent properties must be exactly proportioned.

The fine aggregate used was 100% Selkirk Silica Sand with a specific gravity of 2.67. The sand was obtained from the Selkirk Silica Co. Ltd. in three sizes: $16^{\#}$ - $30^{\#}$, $30^{\#}$ - $60^{\#}$, and $60^{\#}$ - $100^{\#}$. Three gradations designated type A, B and C, were tested to obtain the gradation that would yield the highest strength. Type A was obtained from Portland Cement Association Bulletin D113.[11] Type B was obtained from the Magazine of Concrete Research Vol. 14 No.40, March 1962.[12] Type C was adapted from the Structural Research Series Bulletin No.256 University of Illinois.[13] Sieve analysis for the three gradations used are shown in Table I and the particle size distribution curves are shown in Fig. 3.6.1.

Trial batches using the three gradations were mixed, using a w/c ratio of 0.6 and agg/c ratio 0.3. DAREX AEA air entrainment agent was used in each mix. Nine 1 in. by 2 in. cylinders, cast in the plastic moulds shown in Fig. 3.6.2, were cast from each mix cured in air. The average compressive strengths of type A, B and C were 3986, 4085, and 4922 psi respectively. The reason that type C gave the highest strength can be explained by the fact that it had a smaller volume of voids than either type A or B. For this reason, it needed less cement paste. The arrangement of sand particles was another possible reason for the highest strength

TABLE I

Particle Size Distribution of Sands

U.S. Sieve No.	Type A % retained	Type B % retained	Type C % retained
8	0	0	0
16	20	0	1.40
30	20	30	25.60
50	10	35	23.55
60	--	--	6.50
100	16	35	25.75
200	--	--	12.90
F.M.	1.76	1.95	3.14

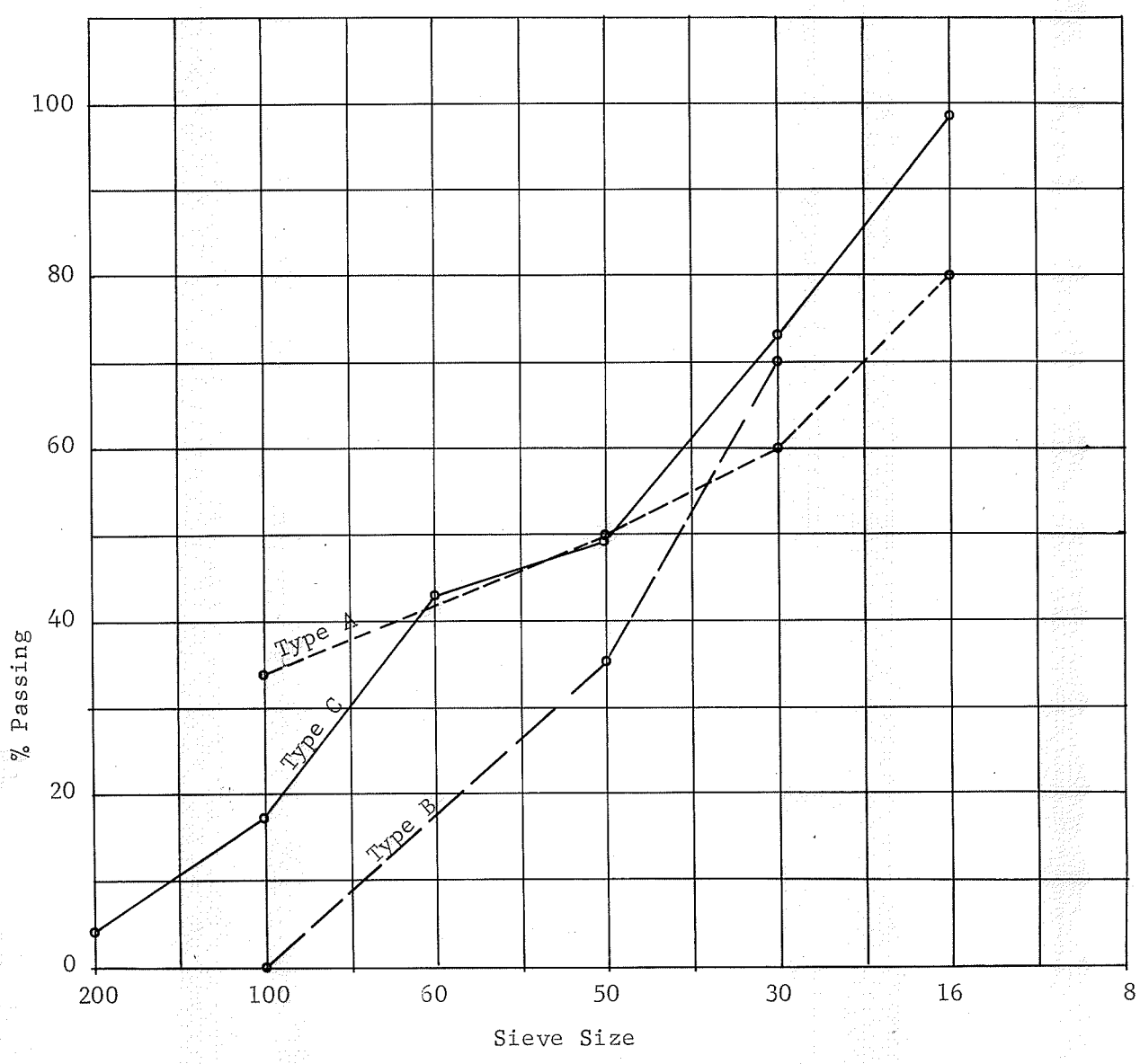

Fig.3.6.1 Particle Size Distribution Curves

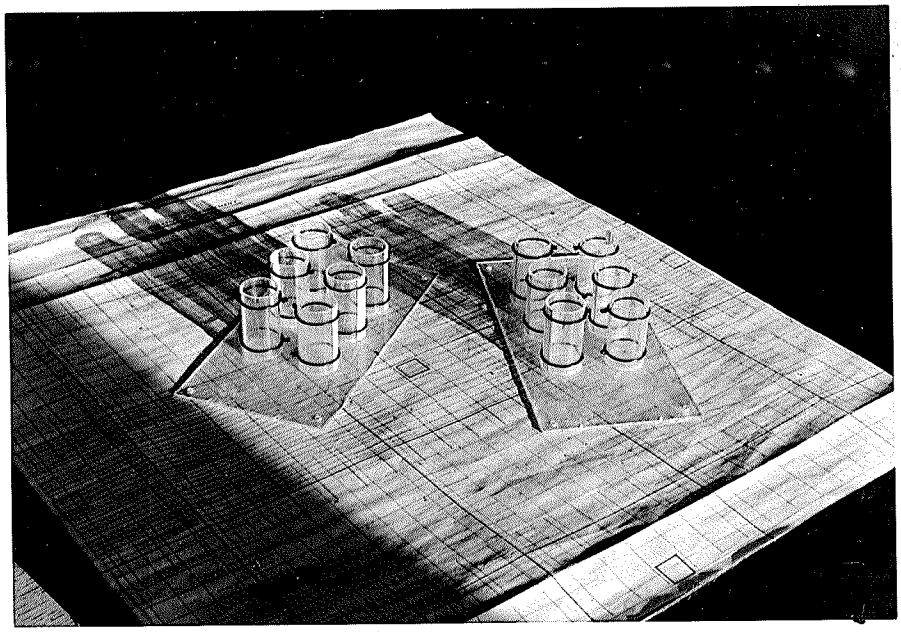

Fig. 3.6.2 Cylinder Moulds

of type C.

The material used for the concrete models were:high early strength Portland Cement, Sieved Sand, air entrainment agent and water.

The air entrainment agent had an important effect on the results as it increased the strength and workability of the concrete for a given cement or water content. DAREX AEA was used at the rate of 3/4 fluid ounces per sack of cement.

The 3/4 cu.ft. capacity electric mixer, shown in Fig. 3.6.3 was used for mixing all concrete for the models. The duration of mixing was 3 minutes. The proportions finally selected were: sand 21.0 lbs., cement 6.0 lbs., water 4.08 lbs., w/c ratio 0.68 and air entrainment agent 1.95 c.c. All materials were measured by weight to the nearest ounce on a balance scale.

Table II shows strengths for trial mixes employing gradation C. Both the w/c ratio and the agg/c ratio were varied. Seven cylinders were cast from each mix. Workability, type of vibration and method of curing were recorded for each. Crushing strength vs w/c ratio curves were plotted in Fig. 3.6.4. Each point on the "air-dried" curves represents an average strength of 4 cylinders, and each point on the "humid-room" curves represents the average of 3 cylinders.

(c) Reinforcing Steel The small wires used in model construction should have similar properties to those of the prototype reinforcement. Consequently it was desired to achieve a yield stress of 40 ksi to correspond to the yield stress for intermediate grade steel and to scale down the diameters of the prototype reinforcing bars by a factor of 16.

Fig. 3.6.3 Electric Mixer

TABLE II

Preliminary Mortar Design

Mix No.	w/c	agg/c	Pozz.	Curing time (days)	f'_c (psi) Humid room	f'_c (psi) Air dried	Workability	Vibration
1	0.41	2.4	No	7	7225	6425	Impossible	Rodding and Vibrating
	"	"	"	"	6275	6100		
	"	"	"	"	6475	6550		
	"	"	"	"		8225		
					ave.	ave.		
					6658	6825		
2	0.45	"	"	"	6050	6175	Possible	"
	"	"	"	"	5925	6100		
	"	"	"	"	6275	6025		
	"	"	"	"		5750		
					ave.	ave.		
					6080	6010		

(Continued)

Mix No.	w/c	agg/c	Pozz.	Curing time (days)	f'_c (psi) Humid room	f'_c (psi) Air dried	Workability	Vibration
3	0.52	2.4	No	7	5400	5200	Good	Rodding and Vibrating
	"	"	"	"	5250	6400		
	"	"	"	"	5800	5525		
	"	"	"	"		6000		
					ave.	ave.		
					5480	5780		
4	0.65	"	No	7	4275	4400	High Slump	Rodding and Vibrating
	"	"	"	"	4950	4950		
	"	"	"	"	4875	4700		
	"	"	"	"		4225		
					ave.	ave.		
					4700	4570		

(Continued)

Mix No.	w/c	agg/c	Pozz.	Curing time (days)	f'_c (psi)		Workability	Vibration
					Humid room	Air dried		
5	0.53	3.0	No	7	5150	5275	Good	Rodding and Vibrating
	"	"	"	"	5425	6600		
	"	"	"	"	5475	5425		
						6325		
					ave.	ave.		
					5350	5906		
6	0.60	"	"	"	4475	4925	Good	"
	"	"	"	"	5400	4350		
	"	"	"	"	5775	4300		
	"	"	"	"		5125		
					ave.	ave.		
					5083	4663		

(Continued)

Mix No.	w/c	agg/c	Pozz.	Curing time (days)	f'_c (psi) Humid room	f'_c (psi) Air dried	Workability	Vibration
7	0.71	3.0	No.	7	4525	3750	High Slump	Rodding and Vibrating
	"	"	"	"	3850	4025		
	"	"	"	"	3700	4175		
	"	"	"	"		4375		
					ave.	ave.		
					4025	4080		
8	0.82	"	"	"	1925	1950	Very High Slump	"
	"	"	"	"	2500	2925		
	"	"	"	"	2025	2625		
	"	"	"	"		1950		
					ave.	ave.		
					2150	2362		

(Continued)

Mix No.	w/c	agg/c	Pozz.	Curing time (days)	f'_c (psi)		Workability	Vibration
					Humid room	Air dried		
9	0.61	3.5	Yes	7	4525	5100	Good	Rodding and Vibrating
	"	"	"	"	4275	5150		
	"	"	"	"	4225	4575		
	"	"	"	"		4400		
					ave.	ave.		
					4342	4806		
10	0.68	"	"	"	3725	4000	Good	"
	"	"	"	"	3775	3850		
	"	"	"	"	3250	3500		
	"	"	"	"		3550		
					ave.	ave.		
					3583	3725		

(Continued)

Mix No.	w/c	agg/c	Pozz.	Curing time (days)	f'_c (psi)		Workability	Vibration
					Humid room	Air dried		
11	0.74	3.5	Yes	7	3050	2800	High Slump	Rodding and Vibrating
	"	"	"	"	3150	2850		
	"	"	"	"	2825	3025		
	"	"	"	"		3150		
					ave.	ave.		
					3008	2956		
12	0.85	"	"	"	2125	2000	Very High Slump	"
	"	"	"	"	2000	2175		
	"	"	"	"	1975	2150		
	"	"	"	"		----		
					ave.	ave.		
					2033	2108		

(Continued)

Mix No.	w/c	agg/c	Pozz.	Curing time (days)	f'_c (psi)		Workability	Vibration
					Humid room	Air dried		
13	0.65	4.2	Yes	7	3150	3600	Impossible	Rodding and Vibrating
	"	"	"	"	3075	3850		
	"	"	"	"	3300	3925		
	"	"	"	"		3850		
					ave.	ave.		
					3175	3780		
14	0.72	"	"	"	3050	2550	Good	Rodding and Vibrating
	"	"	"	"	3075	2200		
	"	"	"	"	2675	2250		
	"	"	"	"		2800		
					ave.	ave.		
					2933	2450		

(Continued)

Mix No.	w/c	agg/c	Pozz.	Curing time (days)	f'_c (psi) Humid room	f'_c (psi) Air dried	Workability	Vibration
15	0.80	4.2	Yes	7	2425	2450	Good	Rodding and Vibrating
	"	"	"	"	2325	2450		
	"	"	"	"	2500	2175		
	"	"	"	"		2150		
					ave.	ave.		
					2420	2306		
16	0.87	"	"	"	1825	1675	High Slump	"
	"	"	"	"	1600	1950		
	"	"	"	"	1775	1875		
	"	"	"	"		----		
					ave.	ave.		
					1733	1833		

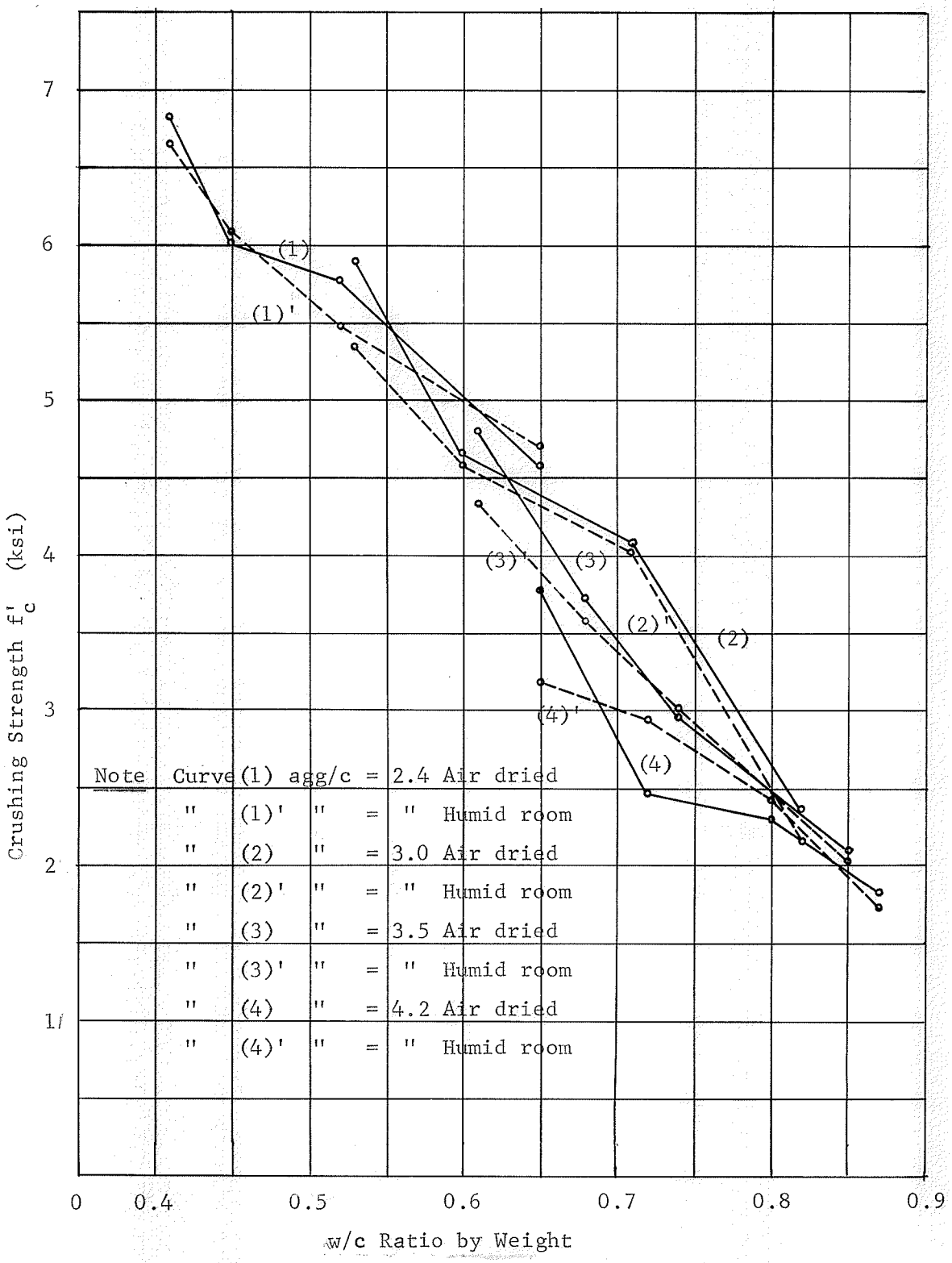

Fig.3.6.4 Crushing Strength vs w/c Ratio

It was not possible to find a wire to meet these requirements exactly. However, it was possible to obtain high strength music wire of the correct diameter and by heat treating it for different lengths of time obtain the proper yield point.

In this annealing process, various lengths of wire were placed in a rack which was then placed in a small oven and held at a constant temperature for a certain time. The rack was then removed and the wires were allowed to cool in air. For 0.038 in. diameter wire, a temperature of 1700°F and a 2 hours duration was found to be satisfactory. A larger diameter wire would require a longer annealing time.

After cooling in air, the wires were placed in a 1 litre capacity glass cylinder containing dilute acid (1 part hydrochloric, 3 parts water) for about ten minutes, then rinsed and dried.

Figure 3.6.5 shows the stress-strain curves for a typical wire before and after annealing. The value of the modulus of elasticity was reduced from 28000 ksi to 26000 ksi during the annealing process. Table III gives the values of the yield strengths for eight samples of the annealed wire. The value assumed as the yield point for the slab reinforcement was 46.25 ksi. The coefficient of variation of the slab steel yield point was 10.8%.

3.7 Construction of Test Structures

(a) Construction Considerations Great care was necessary in the construction of the concrete models because small errors in measuring or placing the wire reinforcement in the models could correspond to

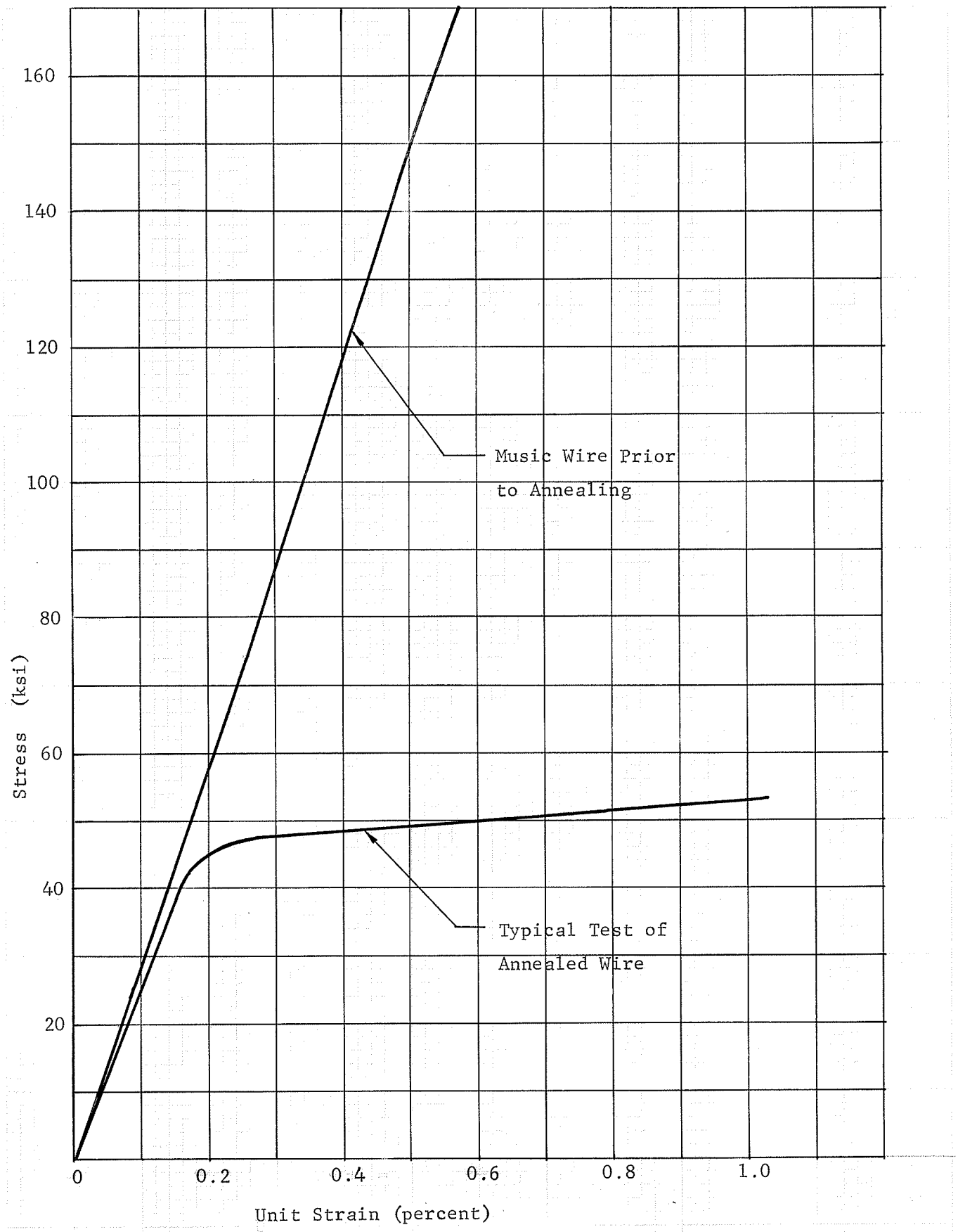

Fig.3.6.5 Stress-Strain Curve for Music Wire

TABLE III

Yield Point of Annealed Wires

Sample No.	f_y (ksi)	$f_{y\ ave.}$ (ksi)
1	47.7	
2	39.8	
3	42.4	
4	40.5	
5	50.3	46.25
6	52.0	
7	45.2	
8	52.3	

relatively large errors in the prototype. An approximation of $\pm 5\%$ of construction error was allowed, while a tolerance of ± 0.02 in. was allowed for the thickness of the slab, span length and the placement of reinforcement.

(b) Formwork The formwork for each model consisted of a single 1/2 in. thick plywood sheet lined with a 1/8 in. thick plastic sheet. The plastic sheet was used to prevent water absorption from the mortar by the plywood. Plastic strips 3/8 in. deep and 1/2 in. wide were screwed on the form to provide edge forms for the slab and serve as a guide for the screed. The slab forms are shown in Fig. 3.7.1 and 3.7.2. The column forms and the shear wall form for model C2 were made from 1/2 in. thick plastic sheet. The joints were screwed together and sealed by a double coating of plastic glue. It was found that glued joints between the columns and slab form for model C1 separated during vibration, and screwed joints were used for model C2.

To provide holes through the slab at fixed columns, 3/8 in long 1/4 in. outer diameter plastic tubes were screwed to the form. The plastic tubes were removed by drilling after casting and provided holes for bolting the slabs to the loading frame.

Holes of the appropriate sizes were provided at the centre and edge of the form to accommodate the column and shear wall stubs through which the loading was to be applied.

Each form was stiffened by a 2 in. by 4 in. timber frame which was designed to minimize deformation of the form during casting and vibrating.

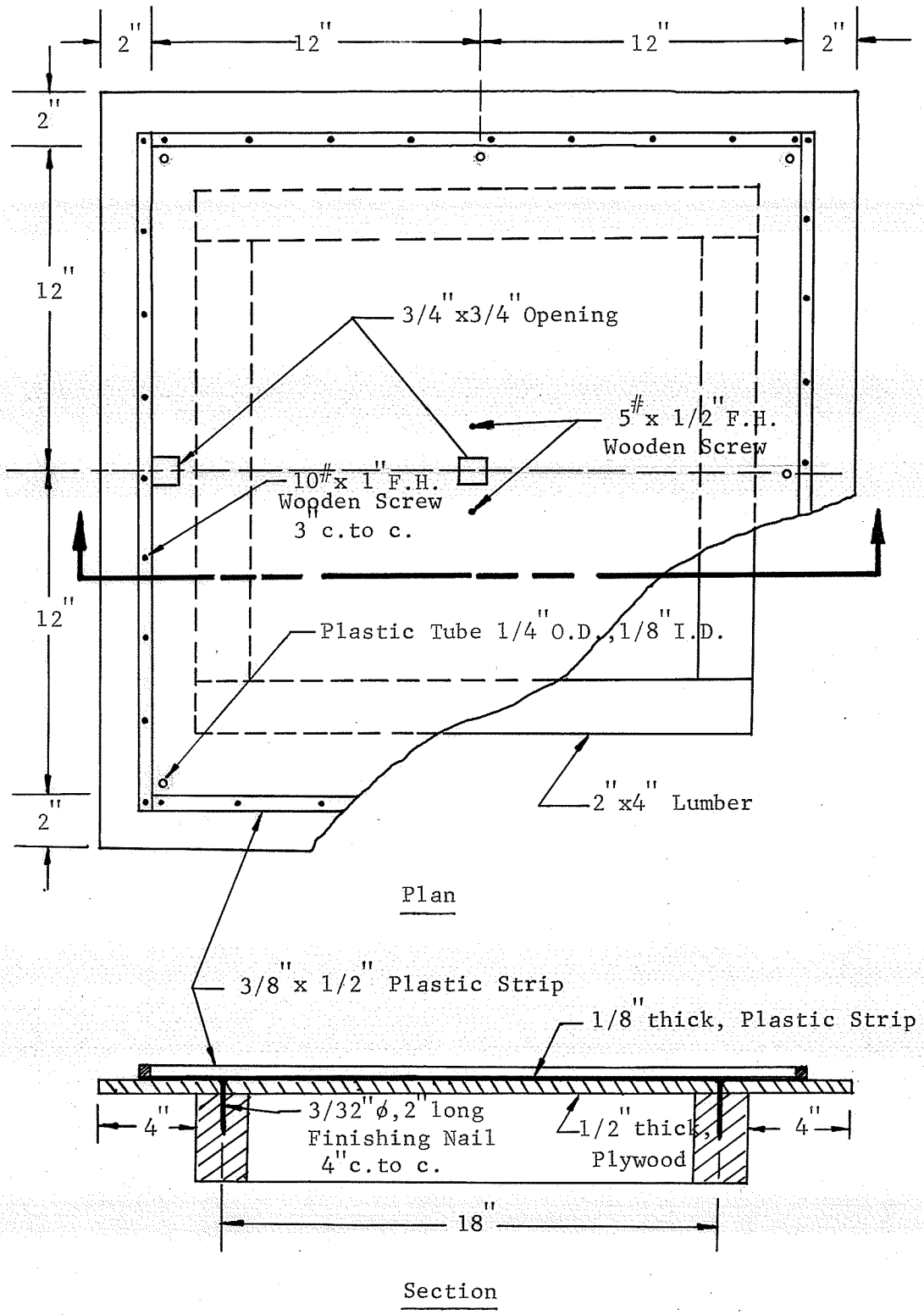

Fig.3.7.1 General View of Form Work, Model C1

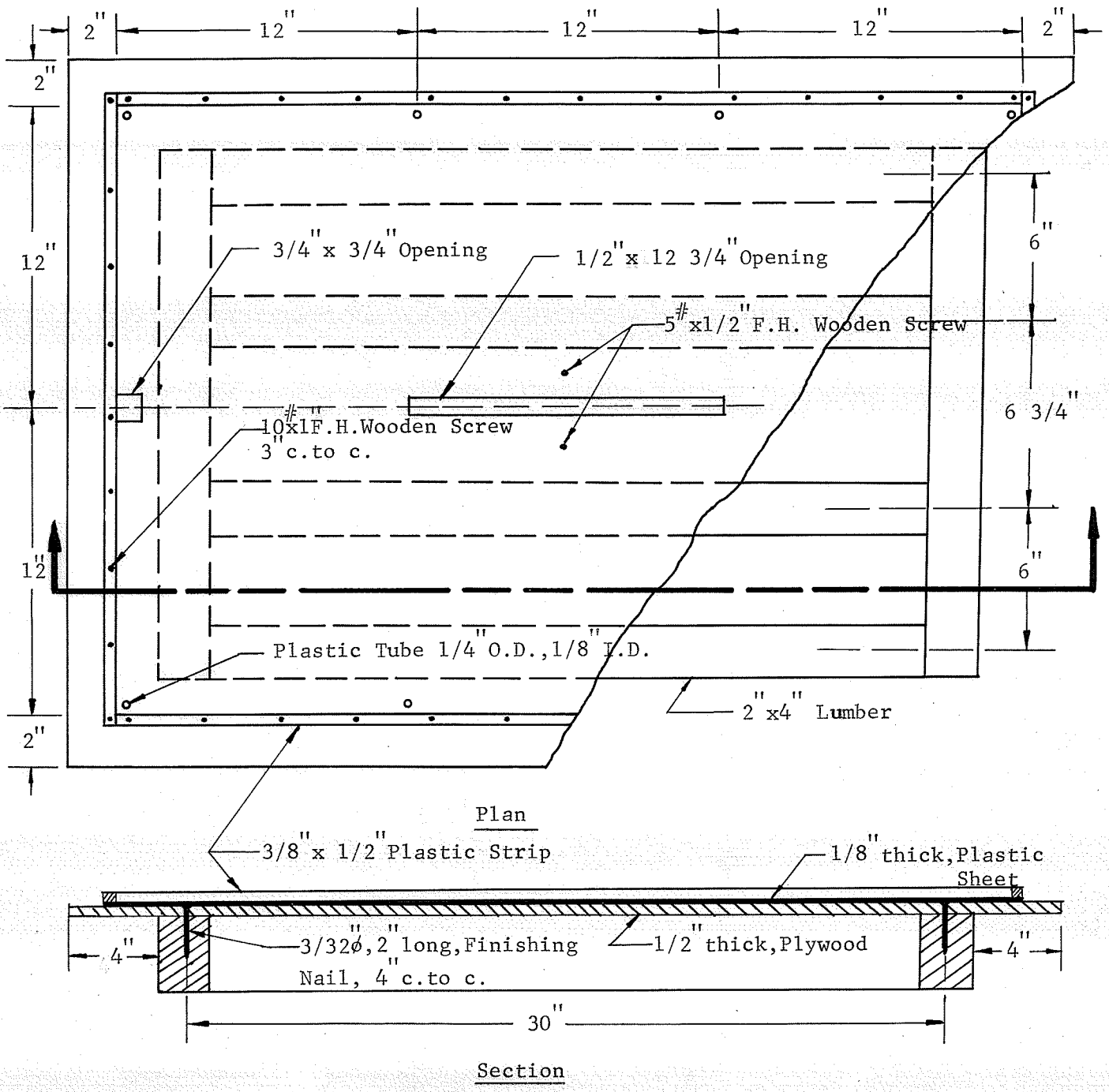

Fig.3.7.2 General View of Form Work, Model C2

(c) Reinforcement Fabrication

1. Slab Reinforcement Fabrication For convenience, the wires were taped to a plywood sheet which had the same dimensions as the slab see Fig. 3.7.3. The orthogonal sets of reinforcing wires were soldered at the joints to maintain the correct spacing between individual wires. An oxygen acetylene torch was used for the soldering. It was discovered that for a time consumption of a few seconds with a flame length 1/8 in., the yield strength was not effected.

2. Column, Shear Wall Reinforcement Fabrication

Music wire of 0.067 in. diameter was used for column and shear wall reinforcement. This wire was not annealed because the study did not require accurate simulation of the column and shear wall behaviour.

Column reinforcement cages were fabricated using 4 in. square, 1/4 in. thick plywood templates. Longitudinal wires of the correct length were passed through accurately located holes in the templates and 0.015 in. ties were bent to a square shape around the main reinforcement and soldered. The spacing of the ties was about 3/4 in. It was impossible to pass a completed column reinforcing cage through the slab reinforcing mat because of the close spacing of the wires in the mat. Thus the half-completed steel cage was positioned and then the other half was fabricated.

The shear wall reinforcement was fabricated in the same manner. Fig. 3.7.4 shows the column and shear wall reinforcement.

(d) Placement of Reinforcement Before the column steel cages were positioned, both positive and negative slab reinforcement was placed.

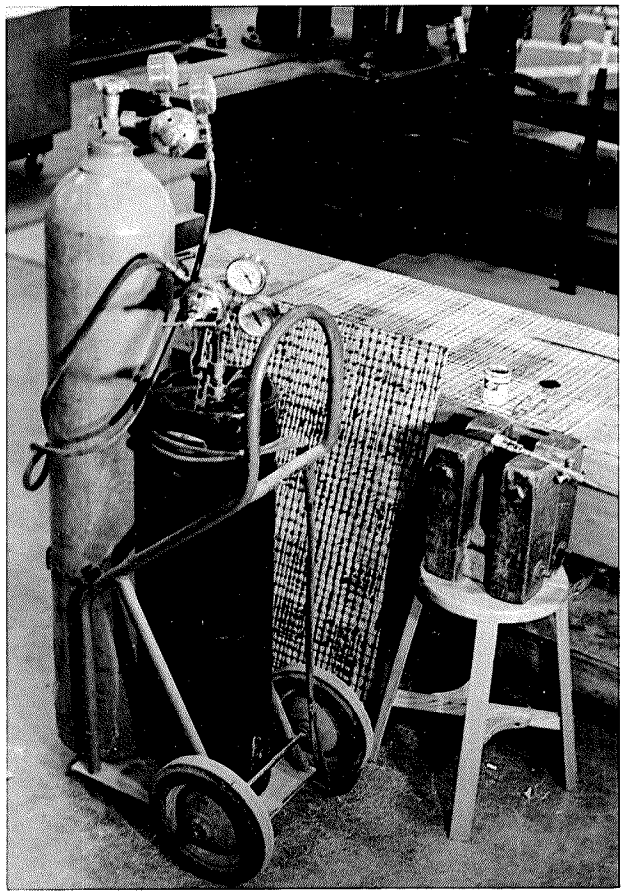

Fig. 3.7.3 Plywood Sheet and Soldering Device for Fabricating Slab Reinforcement.

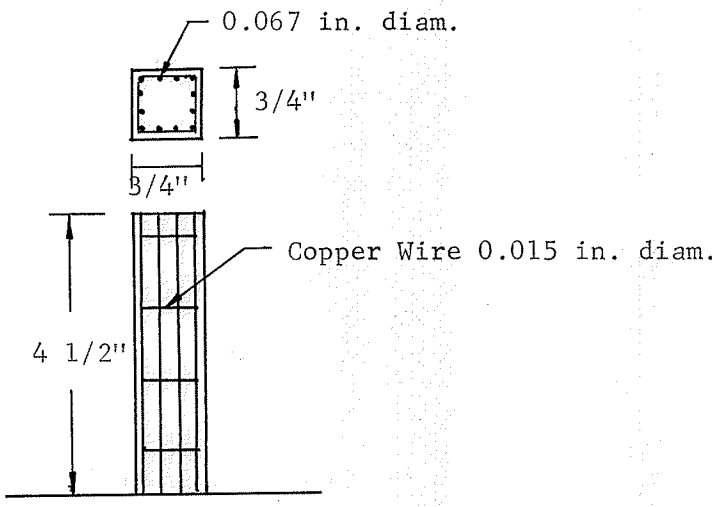

Column Reinforcement

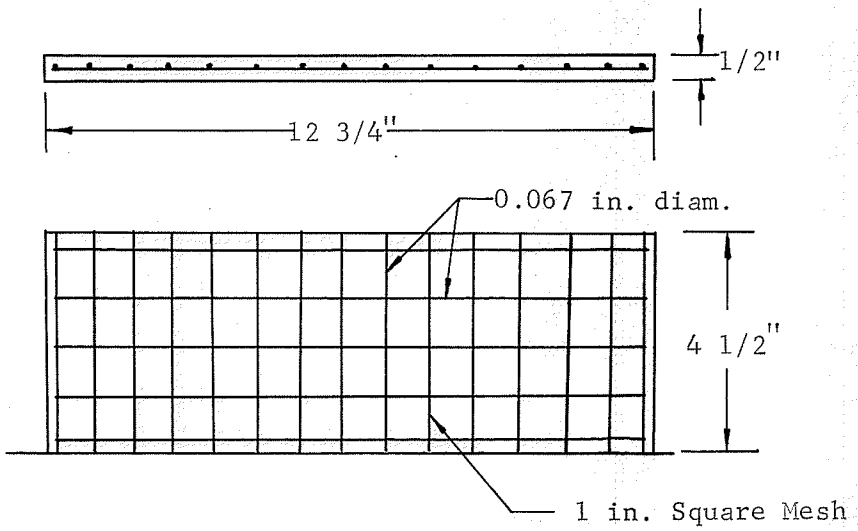

Shear Wall Reinforcement

Fig.3.7.4 Steel Reinforcement of Column and Shear Wall

The positive slab reinforcement was supported on a 1/8 in. long piece of 0.038 in. diameter bar spaced at approximately 1 in. intervals through out the slab. For the negative reinforcement, steel spacers of the proper diameter were used as chairs to place the reinforcing mats at the correct height. The chairs were positioned at about 1 in. intervals throughout the slab. Figure 3.7.5 shows the placement of chairs and steel bars.

The mat was tied down using 0.01 in. diameter copper wires passing through one sixteenth in. diameter holes in the slab form. Careful checks were made to insure sufficient tie-downs and to assure the correct positioning of all wires. Then the holes on the slab form were glued and final checks were made to assure that all joints were watertight. Fig. 3.7.6 shows the view of reinforcement for model C1 in place ready for casting.

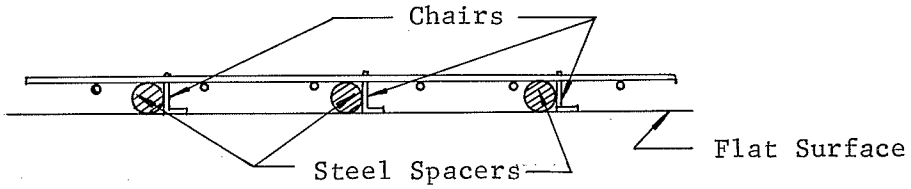

Negative Reinforcement

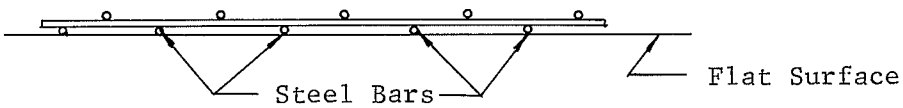

Positive Reinforcement

Fig. 3.7.5 Slab Reinforcement Spacers

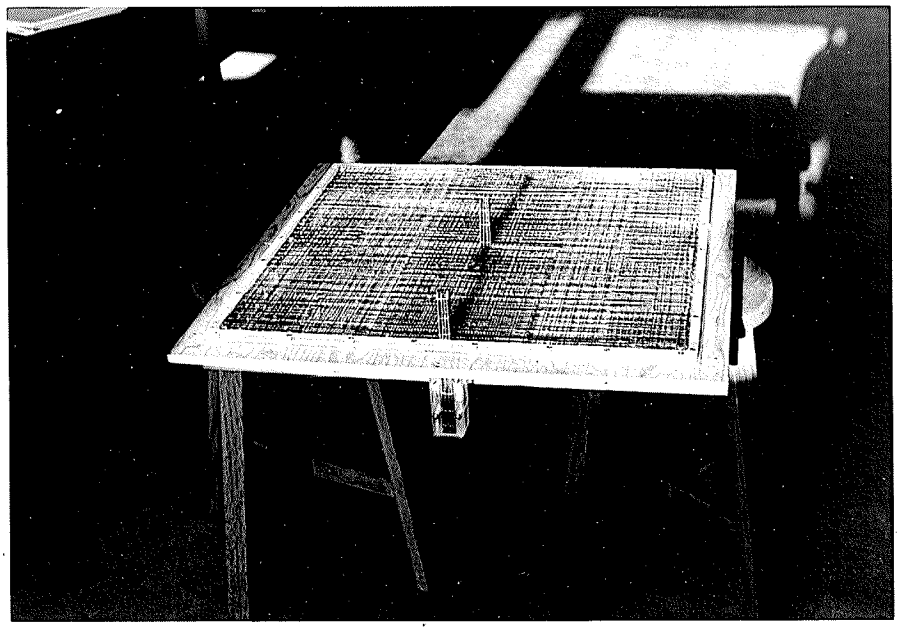

Fig. 3.7.6 Over-all view of the Reinforcement - Model C1

(e) Casting

1. Casting and Curing The lower portions of the columns and shear wall and the slabs were cast as a unit. Fig. 3.7.7 shows the casting operation. A small massage vibrator was used on the under side of the slab form at points close to the columns and the shear wall, a concrete vibrator was used at the edge of the form.

A wooden 2 in. by 4 in. screed was used to screed the slab surface. Two 3 in. by 6 in. and twelve 1 in. by 2 in. control cylinders were cast from each mix. Seven hours after casting, the surface of the slab and all cylinders were coated with white shellac to minimize moisture loss. After the surface had dried, the slab and cylinders were covered with wet burlap and a plastic membrane as shown in Fig. 3.7.8. One day later, the upper portions of the columns and the shear wall were cast. The control cylinders were removed from the moulds, coated with shellac and stored with the slab.

2. Material Properties The control cylinders were tested three days after loading of the models (at an age of 40 days). The average compressive strength of the 1 in. by 2 in. cylinders was 3080 psi.

Stress-strain curves obtained from the tests of the 3 in. by 6 in. cylinders are shown in Fig. 3.7.9. The average value of the initial tangent modulus from the curves was 3.14×10^3 ksi. and secant modulus was 2.85×10^3 ksi.

(f) Condition of Structures at Beginning of Testing The structures were cured under moist condition for seven days and the

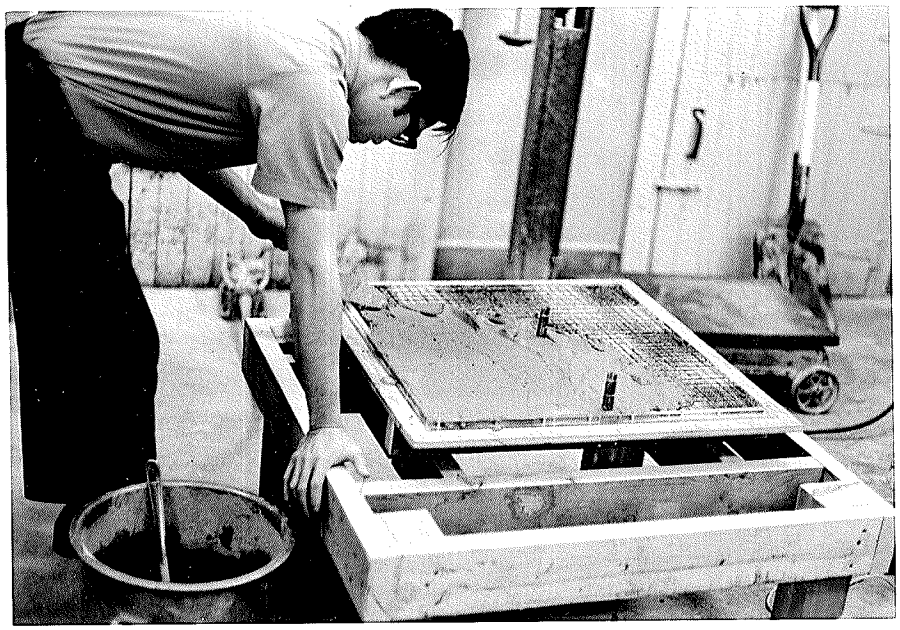

Model C1

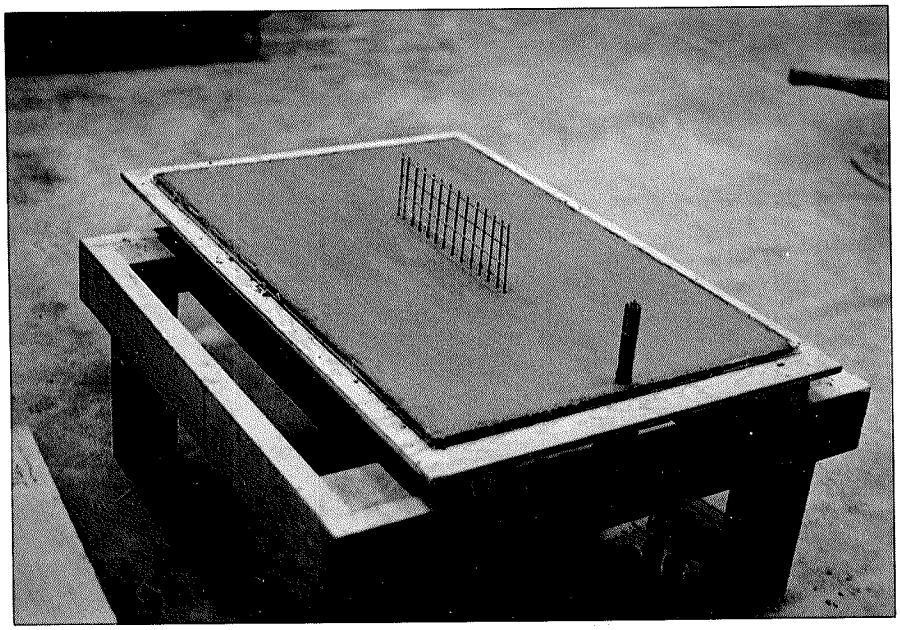

Model C2

Fig. 3.7.7 Models during pouring

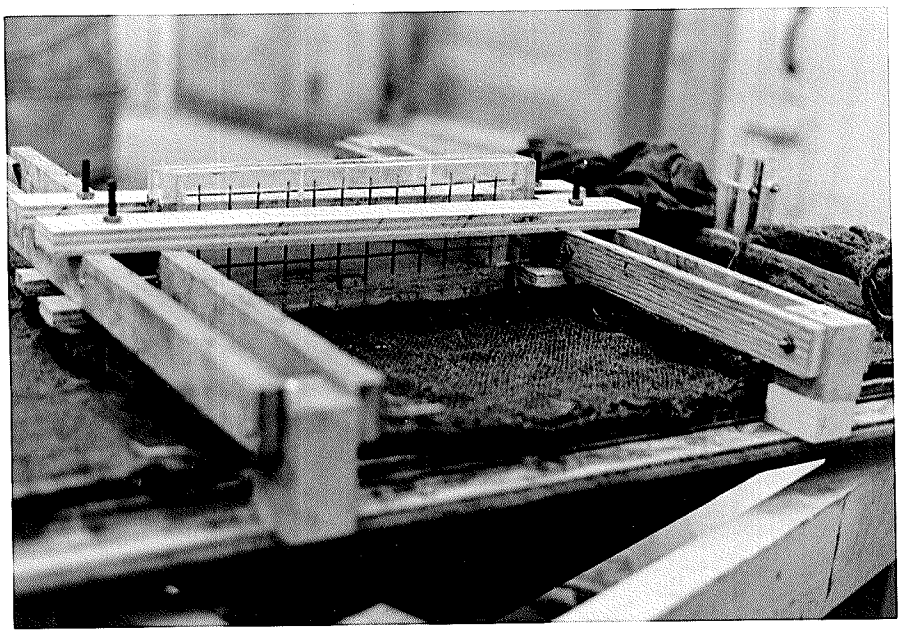

Fig. 3.7.8 Curing of Slab C2

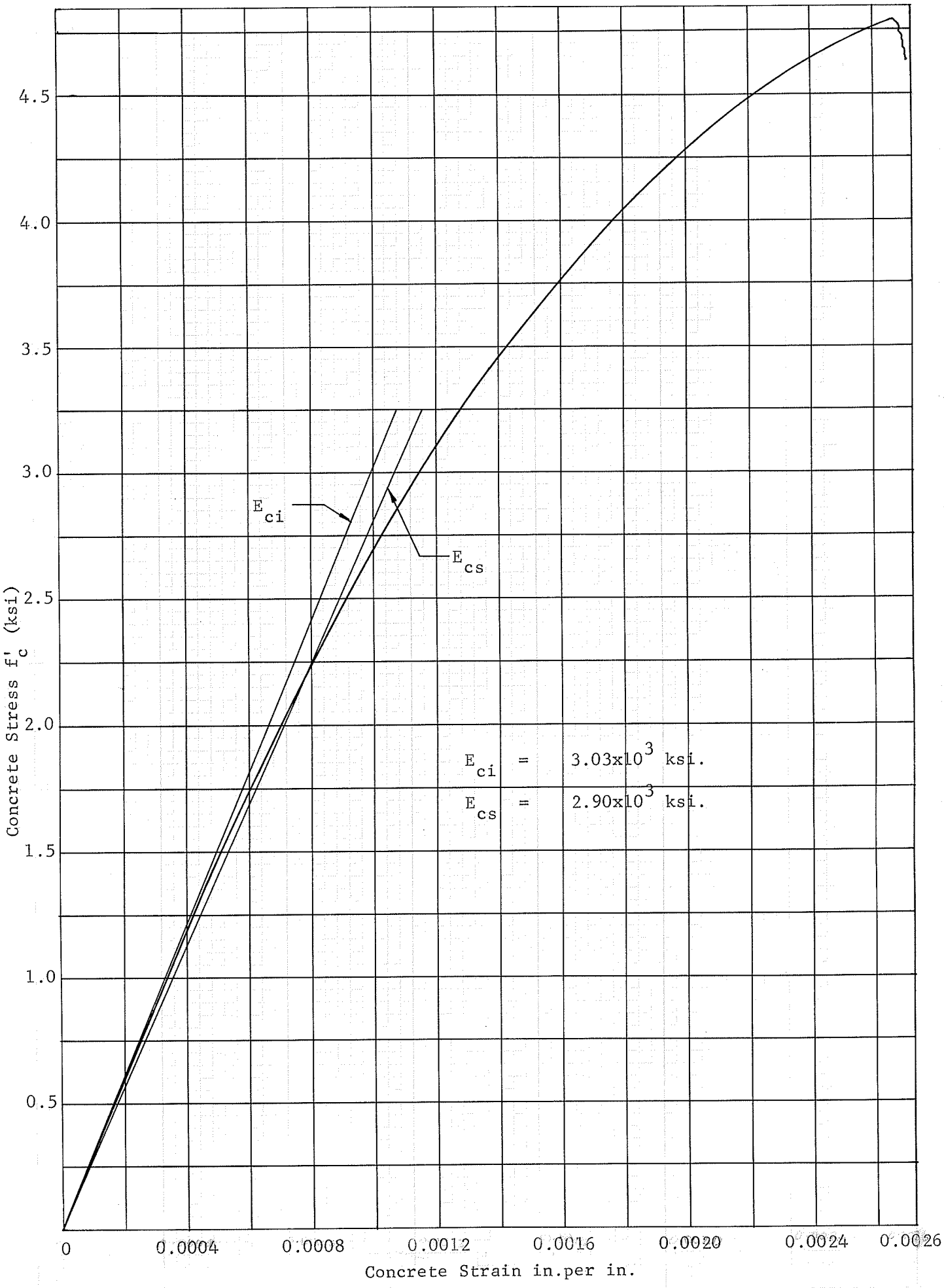

Fig.3.7.9 Stress-Strain Curve

forms removed on the eighth day. The slabs were carefully examined with a magnifying glass for any damage or cracking that may have occurred. There were no cracks but several voids were observed; primarily in the columns of the model C1 and on the slab closed to the shear wall of model C2.

Patching was carried out with the slabs in an inverted position. A cement-sand mixture was used to fill the voids. After patching, the entire structures were moist cured an additional three days.

3.8 Loading System and Deflection Apparatus

(a) Loading Frame The loading frame consisted of four 2 in. by 2 in. by 1/4 in. angles embedded in a square 4 1/2 ft. by 4 1/2 ft. and 8 in. thick concrete base slab. These angles served as columns supporting a system of 3 in. by 1 1/2 in. by 1/4 in. channels. The columns were stiffened by four 2 in. by 2 in. by 1/4 in. angle horizontal braces bolted near the tops of the columns. Two of them acted as beams to carry channel supports to which the 1/2 in. long steel bars which simulated the fixed columns for the test structures were bolted. To stabilize the frame laterally, two 1 1/4 in. by 1 1/4 in. by 1/4 in. angle braces were used on each side of the frame. All joints on the frame used 3/8 in. diameter bolts. Fig. 3.8.1 shows the loading frame and concrete base slab.

(b) Loading System The loading systems for test structures C1 and C2 were different. In the case of structure C1, vertical loads were applied to the slab as described in Chapter II. Six 1/8 in. dia-

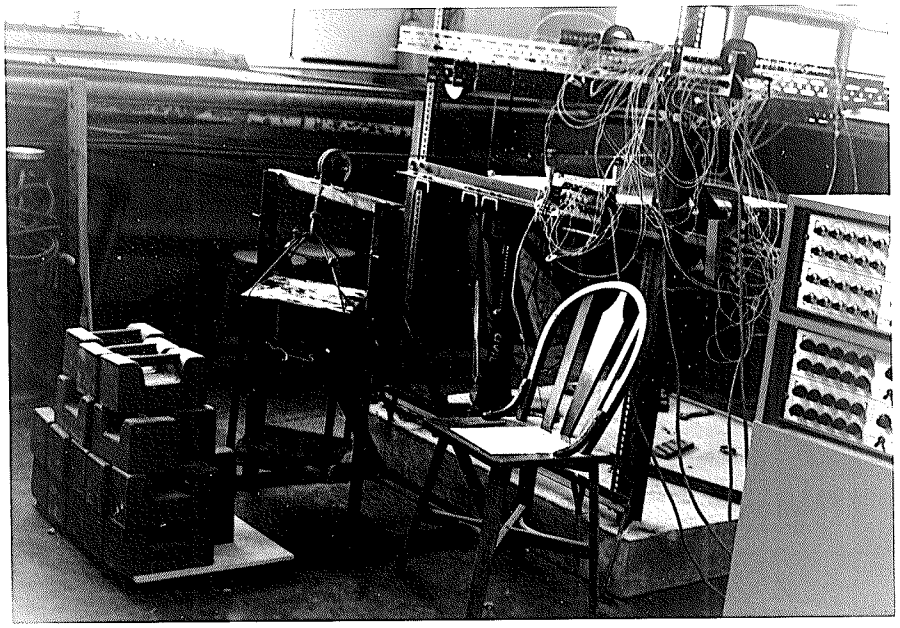

Fig. 3.8.1 Loading Frame

meter holes were drilled on either side of the column along the slab centre line. A 3/32 in. diameter threaded steel rod was used to support the loads in each direction. The downward force was provided by suspended weights while a tail nut fixed to Dillon Gauge was tightened to give the upward force simultaneously. The pointer on the gauge showed the magnitude of load, loads were applied at each pair of 1/8 in. diameter holes in turn. Fig. 3.8.2 shows how the Dillon Gauge was fixed to the frame.

Structure C2 was loaded by horizontal forces applied to the column or shear wall 3 3/4 in. above and below the mid plane of the slab. The forces were provided by suspending weights from flexible steel wires running over fixed pulleys. The pulleys were calibrated to account for friction loss. Fig. 3.8.3 shows the method of load application.

Pairs of steel plates 1/8 in. thick, 1 in. wide and 28 in. long were used as loading yokes for the shear wall, as indicated in Fig. 3.8.4

(c) Deflection Apparatus. Because the slab deflections were relatively small, special deflection measuring gauges were fabricated. They consisted of 0.01 in. thick 3/4 in. wide 2 3/4 in. long, cantilevered brass strips with a strain gauge mounted on the top face close to the clamped end. Each strip was clamped between two 1/2 in. thick 3/4 in. wide 2 in. long steel plated which could be bolted to a dexiom angle. The deflection of the free end of the brass strip was measured in terms of the strain gauge reading. Fig. 3.8.5 shows the deflection measuring device.

Many such devices were made and all were calibrated individually.

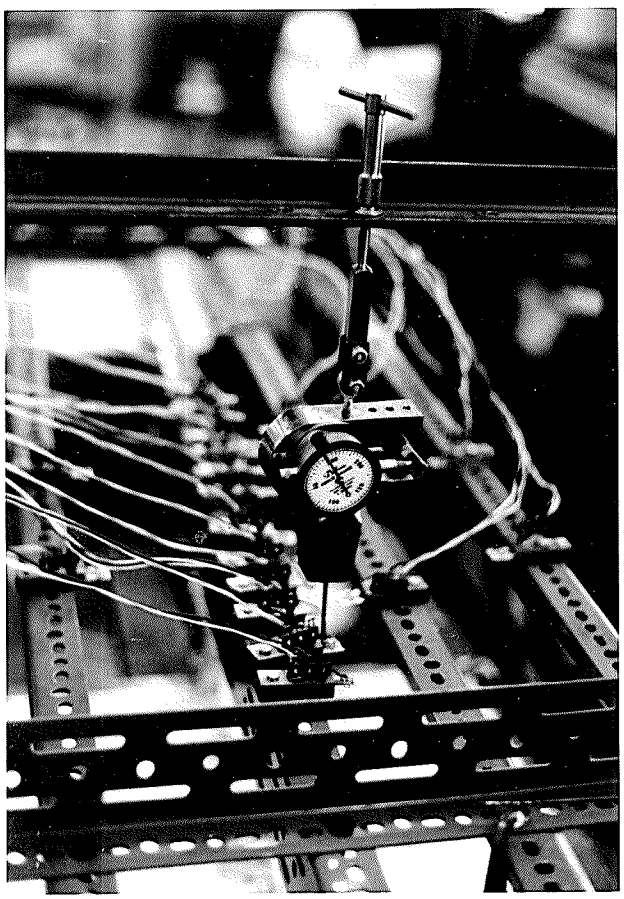

Fig. 3.8.2 Dillon Gauge

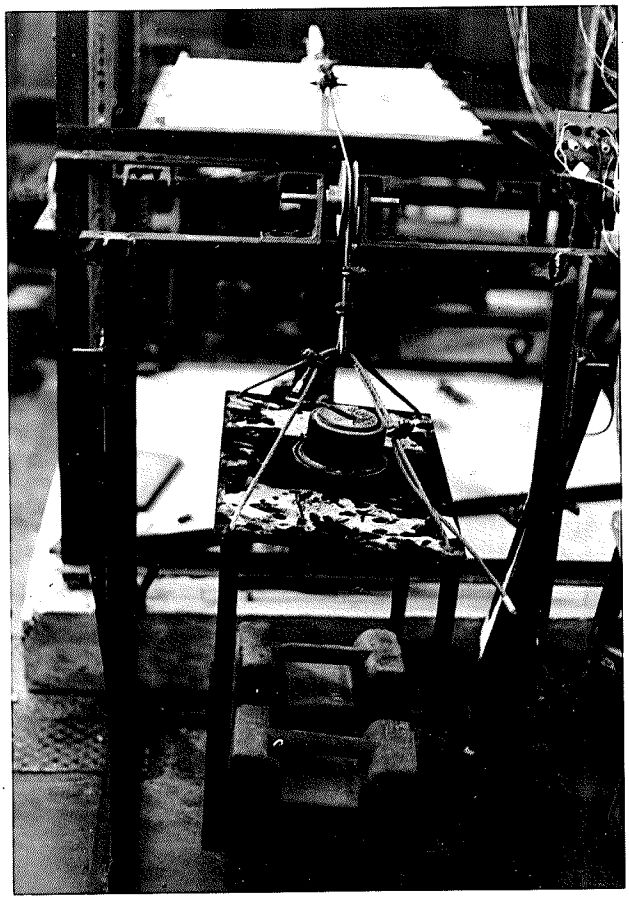

Fig. 3.8.3 Load Application of Model C2

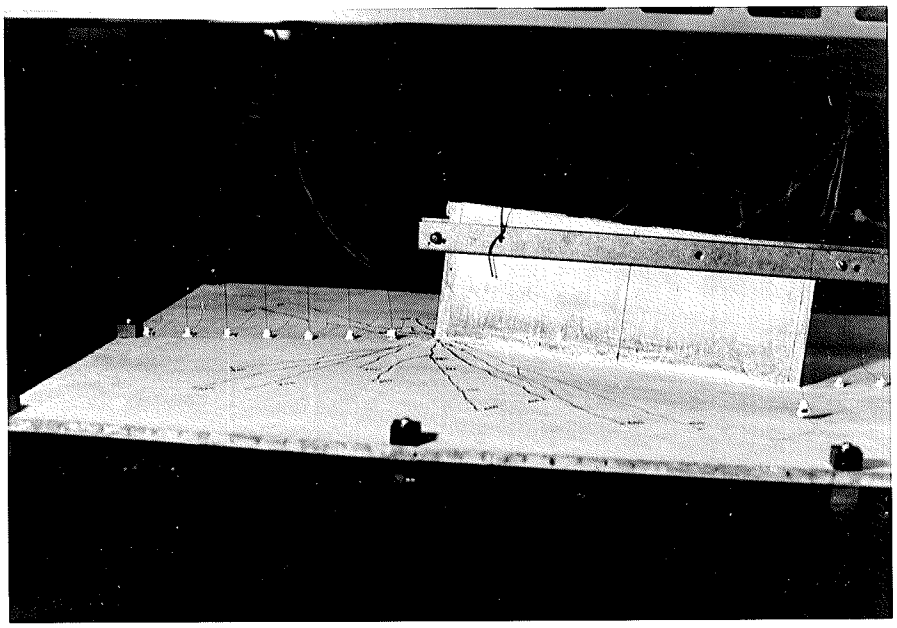

Model C2

Fig. 3.8.4 Steel Yokes used for Load Application

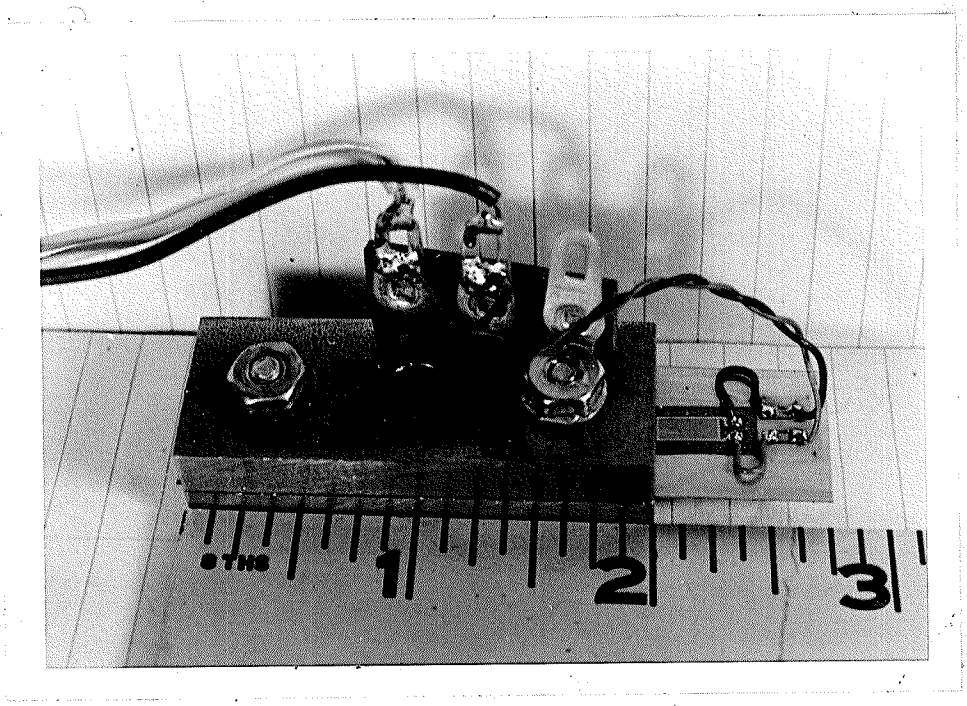

Fig. 3.8.5 Deflection Measuring Device

The calibration apparatus is shown in Fig. 3.8.6. During calibration an initial strain gauge reading was recorded with the brass strip free. Then the pointer of a 0.0001 in. increment dial gauge was brought into contact with the bottom surface of the strip while a fine thread screw from the top maintained the initial reading on the strain indicator. The dial gauge reading was noted. By turning the top screw in increments, the deflection was recorded on the dial gauge and on the strain indicator. This gave the relationship between the vertical deflection of the strip and the strain indicator reading. The calibration was performed twice for each gauge; for increasing deflections, and for decreasing deflections. Fig. 3.8.7 shows a typical calibration curve.

During the testing, deflection measurements were made using a 0.009 in. diameter copper wire connecting the slab and the free end of the cantilevered brass strip. Thus it was necessary to correct for the elastic elongation of the wire. In order to do this a wire was glued to the free end of the strip and a load of approximately 60 grams applied. The load was increased or decreased until the deflection of the strip was within the calibrated range. The true deflection at the free end of the wire was then obtained by substracting the elongation of the wire from the deflection determined from the strain indicator reading.

Small 3/8 in. by 1/4 in. by 1/16 in. "L" shaped steel strips were glued to the slab at points where the deflection was to be measured. The free end of the wire was pulled down till the strain indicator reading was close to that obtained during the calibration, and then glued to the leg of the steel strip. A plumb line was used to properly position

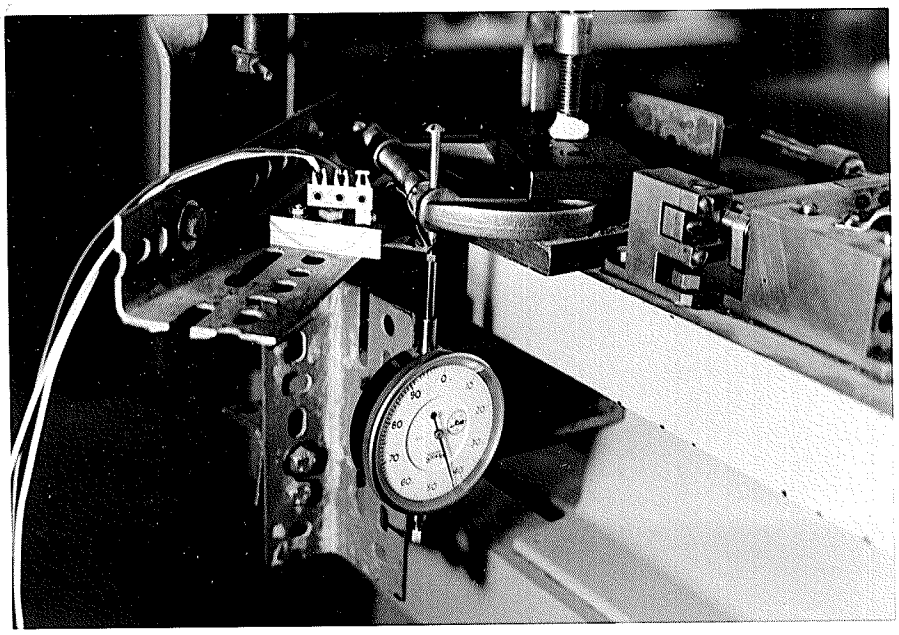

Fig. 3.8.6 Set up Measuring Device

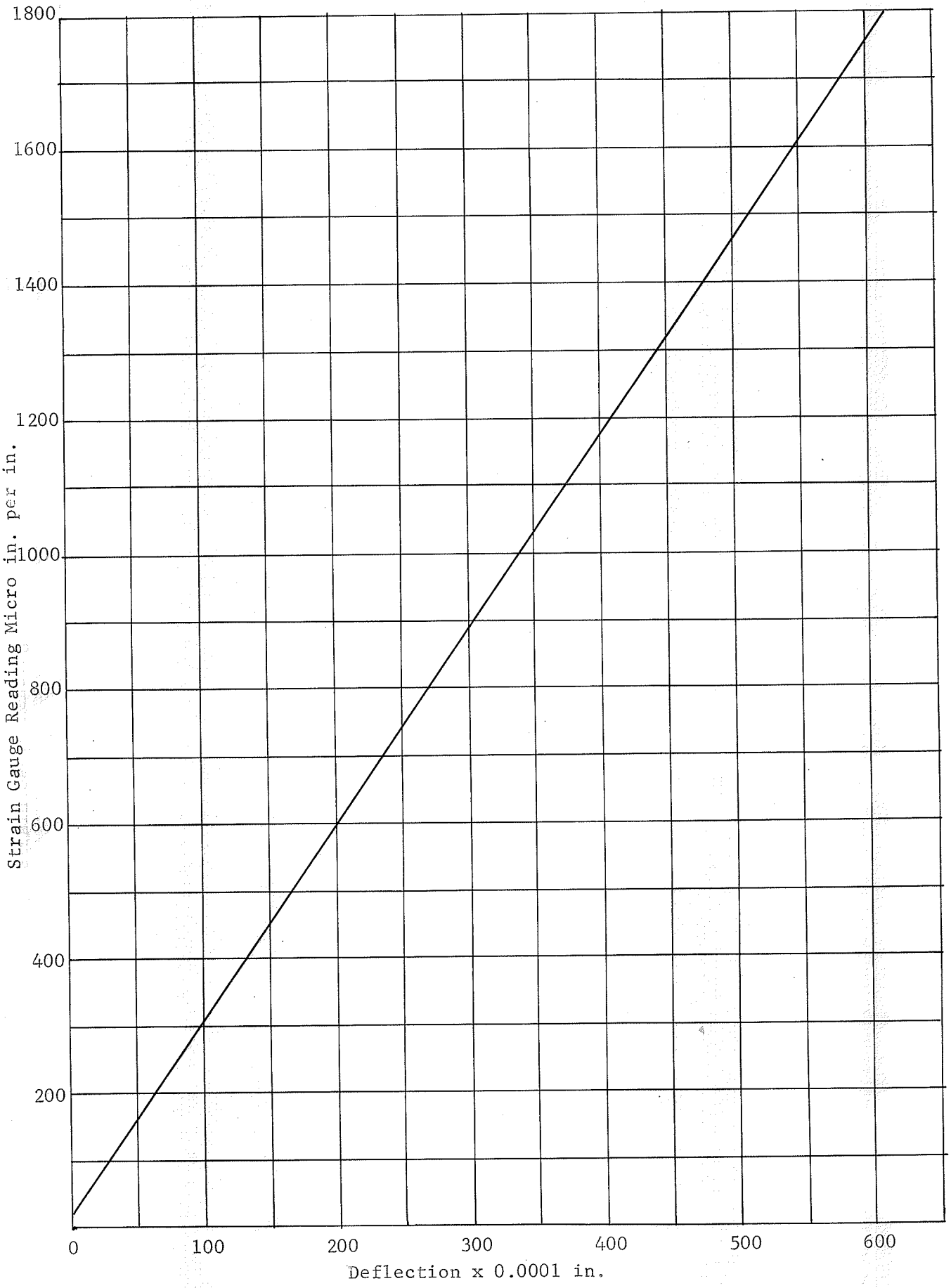

Fig.3.8.7 Typical Calibration Curve for Deflection Measuring Gauges.

the deflection measuring devices on the dexiom frame.

For model C2, sixteen deflection measuring devices were spaced along the centre line of the slab. Typical deflection curves are shown in Figs. C - 7, C - 8, C - 9, C - 10, C - 11, Appendix C. A describe strain indicator was used to record all deflection gauge readings.

CHAPTER IV

DISCUSSION OF TEST RESULTS

4.1 Test Results for Plastic Models. Deflections and slopes of models P1, P2 and P3 were calculated along the loading line which passed through the centre column or shear wall. For model P4 which involved a box type of shear wall, deflections and slopes were calculated along the two loading lines which joined the edges of the shear wall and the exterior columns. The calculated deflections and slopes are shown in Appendix A.

The relative deflection between any two points is the integration of the slope between them, or the area under the slope curve. Since all columns, and shear walls were assumed to prevent lateral deflection of the plate, the area under the slope curve from the exterior column to the point of maximum deflection should always equal that between the centre column or shear wall and the point of maximum deflection.

The calculated deflections in Appendix A show small relative deflections between the exterior column and the interior column or shear wall. For load types A and B of all model plates, these differences did not exceed 3 percent. This may be regarded as an error in interpretation of the photographs. In the case of load types C and D, the differences range from 1 percent to 9 percent. The error may due partly to movement of the plate supports normal to the plate surface. This discrepancy may also be due to discontinuity of the plate rigidity. The loaded column was rested on a knife-edge support and its positioning may

have affected the movement of the column.

Table 4.1.1 summarizes the applied loadings and resulting plate rotations. The moments and rotations are classified according to the type of loading and model. The stiffness, and carry-over factors and the effective widths obtained are presented in Table 4.1.2 Values are listed for panel loaded by an interior column or shear wall and for a panel loaded by an exterior column. The stiffness factors K were calculated from equation 2.2.6, while the effective widths were obtained from equation 2.2.9. The carry-over factors were obtained from equation 2.3.1 for the interior column loading and from equation 2.3.2 for the exterior column loading.

The reliability of the test results is mostly dependent on;

1. the reliability of the instrumentation,
2. the precision in scale reduction of the photographs

and 3. the interpretation of the photograph to obtain curvatures and rotation.

Plate slopes obtained using the Moire' method are a function of the size of the plate, the distance between the plate and the ruled screen, and the spacing of the lines ruled on the screen. When the last two variables are kept constant, the slope values obtained are dependent on the size of the plate only. The error due to the size of the plate has been studies by Ligthenber.[15] For sizes of the plate from 0.5 to 0.8 of the distance between the plate and the screen, the errors are of the order of 1 to 4 percent. The Moire' method

TABLE 4.1.1

Applied Moments and Rotations for Plastic Models

Model \ Load Type	A	B	C	D
P1	P = 5 lbs. M_1 = 30 in.-lb. θ_1 = 0.0129 rad.	P = 5 lbs. M_2 = 30 in.-lb. θ_2 = 0.00255 rad. θ_5 = 0.01375 rad.	P = 5 lbs. M_3 = 15 in.-lb. θ_3 = 0.0113 rad.	P = 5 lbs. M_4 = 15 in.-lb. θ_4 = 0.0192 rad. θ_6 = 0.002 rad.
P2	P = 10 lbs. M_1 = 60 in.-lb. θ_1 = 0.00922 rad.	P = 10 lbs. M_2 = 60 in.-lb. θ_2 = 0.004 rad. θ_5 = 0.0089 rad.	P = 5 lbs. M_3 = 15 in.-lb. θ_3 = 0.01285 rad.	P = 5 lbs. M_4 = 15 in.-lb. θ_4 = 0.0143 rad. θ_6 = 0.000775 rad.
P3	P = 20 lbs. M_1 = 120 in.-lb. θ_1 = 0.0075 rad.	P = 20 lbs. M_2 = 120 in.-lb. θ_2 = 0.00636 rad. θ_5 = 0.00808 rad.	P = 5 lbs. M_3 = 15 in.-lb. θ_3 = 0.012 rad.	P = 5 lbs. M_4 = 15 in.-lb. θ_4 = 0.0175 rad. θ_6 = 0.00075 rad.
P4	P = 20 lbs. M_1 = 120 in.-lb. θ_1 = 0.0045 rad.	P = 20 lbs. M_2 = 120 in.-lb. θ_2 = 0.00636 rad. θ_5 = 0.0059 rad.	P = 5 lbs. M_3 = 15 in.-lb. θ_3 = 0.0133 rad.	P = 5 lbs. M_4 = 15 in.-lb. θ_4 = 0.015 rad. θ_6 = 0.0012 rad.

TABLE 4.1.2

Stiffnesses, Effective Widths and Carry-Over Factors for Plastic Models

Model	Interior Column (Shear Wall) Loading			Exterior Column Loading		
	Stiffness K in.-lb./rad.	Effective Width L_y in.	Carry-Over Factor	Stiffness K in.-lb./rad.	Effective Width L_y in.	Carry-Over Factor
P1	2,300	10.00	0.1330	1,325	5.70	0.290
P2	6,500	28.10	0.1400	1,165	5.02	0.348
P3	16,000	69.00	0.0910	1,250	5.40	0.743
P4	26,650	115.00	0.1560*	1,250	5.40	0.815*

* Calculations are based on one exterior column only.

is used primarily in the study of moments in flat plates.[15],[16],[17] Kupta and Vaughen[17] used this method in conjunction with a computer program to investigate the curvatures and relative deflectionsof flat plates. Deflections at three points, obtained by reaching the point by different routes were compared. The differences were found to be as large as 3 percent.

Precision in scale of the prints is very important since the deflections under investigation are extremely small compared to the dimensions of the plate. Since the deflections and the angles of rotation are so small, human errors which may occur in the interpretation of fringes and in the measurement of the areas under the slope curves may be significant.

4.2 Test Results for Concrete Models. The test results for the concrete models are presented in Appendix C. The computed values of the stiffness factors and effective widths are summarized in Table 4.2.1

TABLE 4.2.1

Stiffness and Carry-Over Factors and Effective Widths for Concrete Models.

Model	Interior Column (Shear Wall) Loading			Exterior Column Loading		
	Stiffness in.-lb./rad.	Effective Width in.	Carry-Over Factor	Stiffness in.-lb./rad.	Effective Width in.	Carry-Over Factor
C1	32,328	7.24	-	-	-	-
C2	448,800	101.00	0.1492	47,100	10.60	0.666

Because the central column for model C1 was not sufficient stiff to transmit the required moments to the plate, the indirect loading procedure discussed in Section 2.4 was necessary, and stiffness factors and effective slab widths were determined only for the interior column loading.

Three different load levels were tabulated in Appendix C. The coefficient of variation of computed stiffness factors and effective widths agreed within 4.07 percent, the average values can be seen from Table 4.2.1.

For model C2, stiffness and carry-over factors and effective slab widths were determined for both interior and exterior column (shear wall) loadings, and are tabulated in Table 4.2.1. Each of the tabulated values was obtained by averaging values obtained for either four or five different load levels. The individual values and the corresponding load levels are also tabulated in Appendix C.

The coefficient of variations are as follows.

Load Applied by Interior Shear Wall.

Stiffness factor (and effective width)	11.85	%
Carry-over factor	7.75	%

Load Applied by Exterior Column

Stiffness factor (and effective width)	11.10	%
Carry-over factor	6.57	%

After the elastic stiffness and carry-over factors had been determined for model C2, the model was loaded to failure by loads applied

transversely to the shear wall. Fifty pound loading increments were used and cracking was first observed at a load of 250 lb. at which time the maximum plate deflection was 0.0493 in. The first crack initiated on the top of the slab at the point where slab and shear wall met, and propagated across the width of the panel in a direction perpendicular to the shear wall. At a load of 350 lb., another crack appeared on the top of the slab but at other side of the shear wall and had a similar direction. At a load of 400 lb., long diagonal cracks formed between the edges of the shear wall and the peripheral columns. Many cracks extended from the edges of the shear wall towards the corners of the slab. Fig. 4.2.1 shows cracking lines of the slab. At failure load maximum deflection was 0.142 in.

An ultimate strength analysis of model C2 is presented in Appendix D. Yield line theory was used to find the ultimate load.

4.3 Discussion and Comparison of Test Results. As mentioned in chapter I, five plexiglas and two micro concrete models were tested. Plexiglas models P1 and P3 were similar to concrete models C1 and C2 respectively, and Table 4.3.1 shows the comparison of the results obtained from the similar models.

The computed effective width for the interior column loading of model C1 was smaller than that for model P1. This different may be due partly to the different values of Poison's ratio for the material used. However, the discrepancy is probably largely due to the unreliability of the result for model C1, since it was obtained by a rather indirect pro-

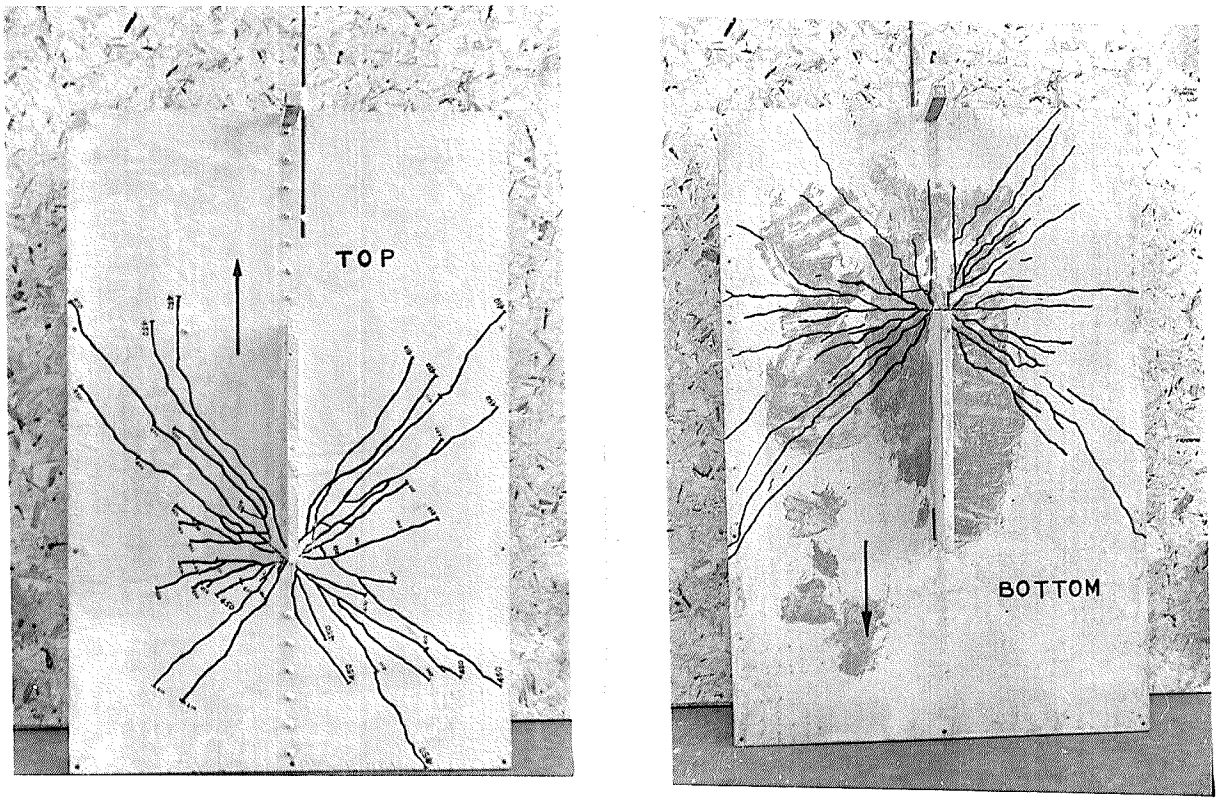

Fig. 4.2.1 Cracking Lines on the Slab C2

cedure. Unfortunately the stiffness factor for the exterior column loading and carry-over factors could not be obtained for model C1.

TABLE 4.3.1

Model	Interior Column (Shear Wall) Loading			Exterior Column Loading		
	Stiffness in.-lb./rad.	Effective Width in.	Carry-Over Factor	Stiffness in.-lb./rad.	Effective Width in.	Carry-Over Factor
P1	2,320	10.00	0.133	1,325	5.70	0.290
C1	32,400	7.36	-	-	-	-
P3	16,000	69.00	0.091	1,250	5.40	0.743
C2	448,800	101,00	0.1492	47,100	10.60	0.666

For model P3, the effective widths for both the interior and exterior loading were smaller than those for model C2. This could be explained by the fact that the models were made from materials which have different values of Poison's ratio and in addition, while model P3 was homogenous and isotropic, model C2 was not. The carry-over factors for exterior column loading for models P3 and C2 agree within ±10 percent. While the carry-over factors for the panel laoded by the interior shear wall do not agree axactly, the factors have the same order of magnitude. Because of their relatively small magnitude, an axact agreement would probably extremely difficult to obtain. The discrepancy may be largely due to the difficulty of simulating complete fixity, or a smooth pin at the plate supports.

The results of this investigation are compared with those from previous studies in Figs. 4.3.1, 4.3.2 and 4.3.3. Fig. 4.3.1 shows plots of effective width/actual panel width vs column panel width ratios for panels loaded through an interior column. From the figure, it can be seen that the effective widths and stiffness factors for interior column loading are extremely sensitive to the size and shape of the interior column. For model C1 with a column-to-panel width ratio of 1/16, the average value of the effective width obtained from three set of loadings (50, 100 and 150 lbs.) was 0.61 of the actual panel width. This was slightly smaller than the values obtained by Brotchie and Russel[3] who reported a range of 0.67 and 1.67 for column to - panel width ratio of 1/20 to 1/7. The value obtained from model C1 is also smaller than that obtained by Carpenter[4] who reported that the full slab width may be used for the column-to-panel width ratio of 1/14. For model P1 the effective width obtained can be seen to be approximately 16 percent higher than the value obtained by Carpenter for the same column panel width ratio.

Fig. 4.3.2 shows effective width/actual panel width vs column panel width ratios for panels loaded through exterior columns. For this loading of all model plates the effective panel widths vary little. When the plate is subjected to a moment at exterior column, it appears that the moment does not distribute into the interior panel. This resulted in the same stiffness regardless of the size and shape of the interior supports. The stiffness factor obtained for model P1 is about 24 per-

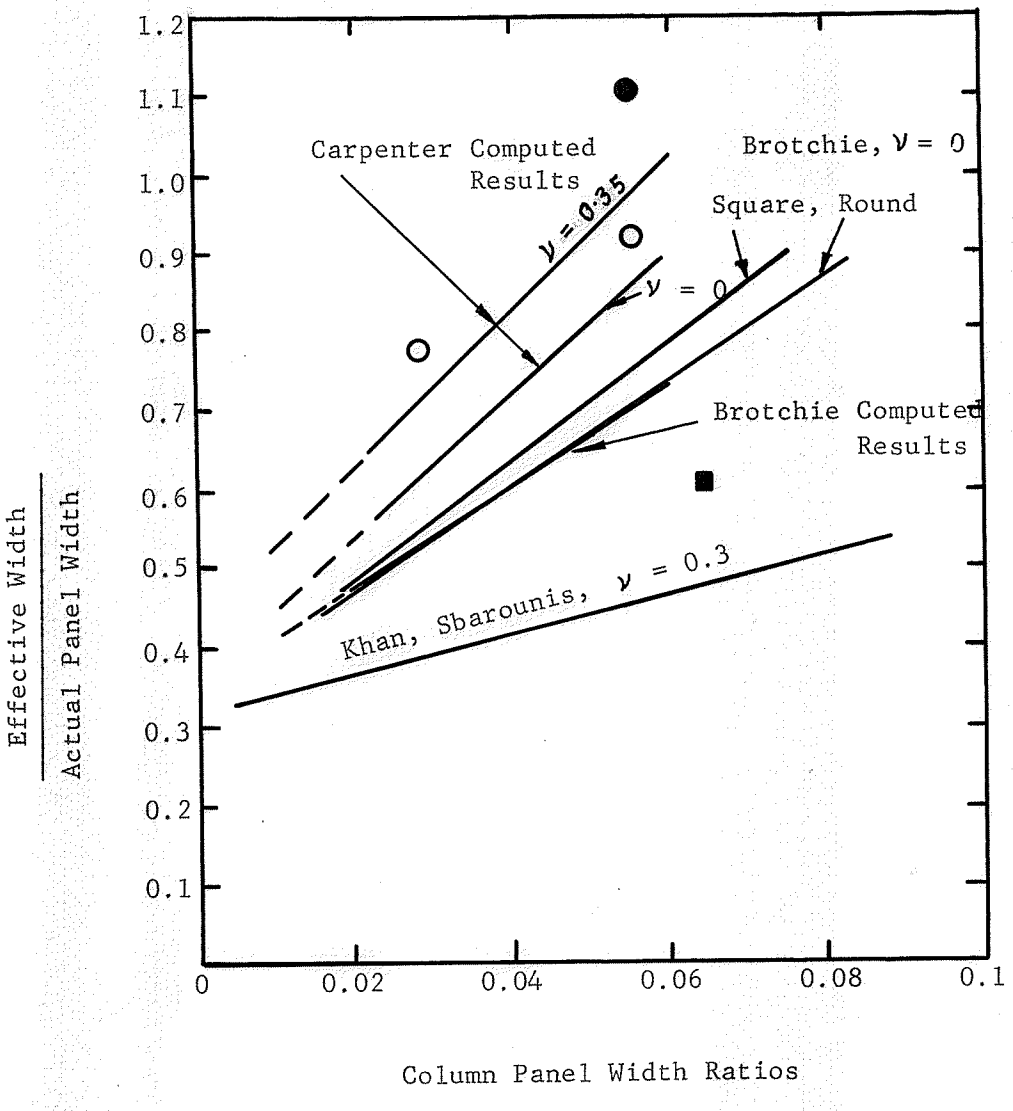

Key

○ Test Results Obtained by Carpenter

● Test Result Model P1

■ Test Result Model C1

Fig. 4.3.1 Stiffness of Slab Element Interior Column Loading

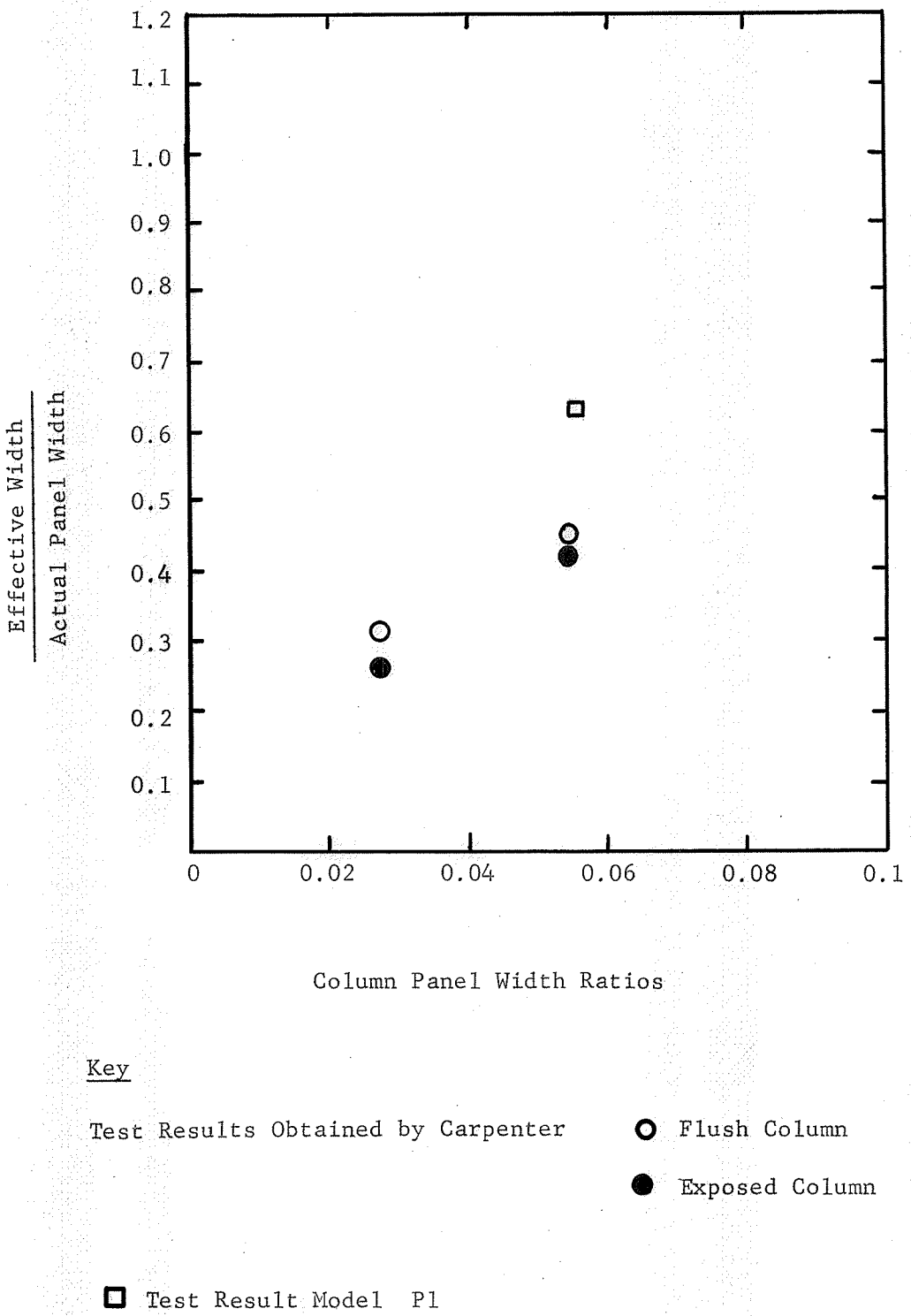

Fig. 4.3.2 Stiffness of Slab Element Exterior Column Loading

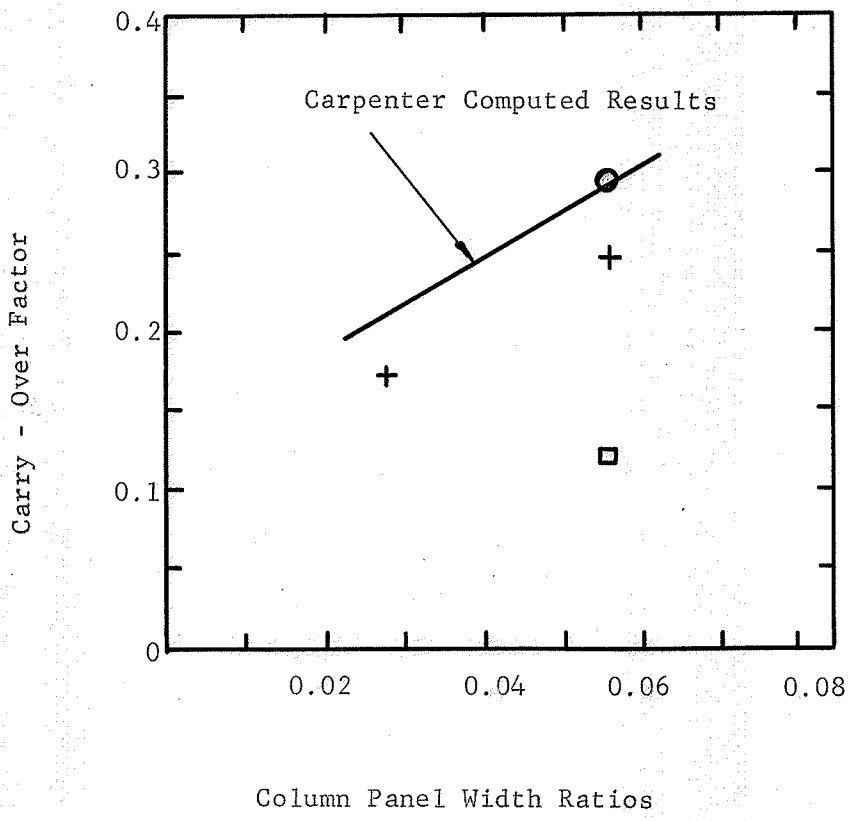

Key

+ Carpenter Experimental Interior Column

□ Panel Loaded by Interior Column Model P1

○ Panel Loaded by Exterior Column Model P1

Fig. 4.3.3 Carry - Over Factor for Slab Element

cent higher than that obtained by Carpenter for a model with similar geometry and the same column panel width ratio.

The carry-over factor for panel loaded by interior columns is extremely small compared with those obtained analytically using an equivalent beam. Fig. 4.3.3 shows a comparison of the carry-over factor from the interior column of model P1 with value obtained by Carpenter for the same column panel width ratio. The value is approximately 45 percent lower than that obtained by Carpenter. The carry-over factors for panel loaded by interior column or shear wall are approximately the same for all models except P3 indicating that the carry-over factor from an interior column or shear wall is almost independent of the size and shape of the column or shear wall.

For exterior column loading the carry-over factors ranged from 0.29 to 0.815, the higher values corresponding to the stiffer interior shear walls.

Little published information is available on the effective stiffness of plates loaded by transverse loads applied to shear walls. Barnard and Schwaighofer[5] conducted a study of structures including shear walls coupled by a slab. They reported that the entire width of phototype plate can be considered as effective for frame action for the shear walls connected by a plate. This result is in agreement with the test results obtained in the study since for model P2, P3, P4 and C2 effective widths much greater than the actual panel width were obtained. It is obvious from the large values obtained, that effective panel width is not a suitable criterion for expressing the effective stiffness of the slab in a

flat plate - shear wall structure. Consider for example the typical floors illustrated in Fig. 4.3.4. Because of the positioning of the shaded exterior columns in Fig. 4.3.4(a) large torsional moments will be developed in the centre panels when the structure is subjected to shearing loads parallel to the shear wall. For the structure in Fig. 4.3.4(b) these torsional moments will not be present, and the apparent slab siffness will therefore be greater reduced.

It is thus obvious that the "effective slab width" is a function not only of the slab thickness and panel size, but also of the geometry of the whole structure and therefore not a suitable criterion for speficying plate stiffness.

Model C2 was tested up to failure. When failure occured the observed ultimate load was 450 lbs. compared with the computed strength from Appendix D which was 471 lbs. for first collapse mechanism and 499 lbs. for the second collapse mechanism.

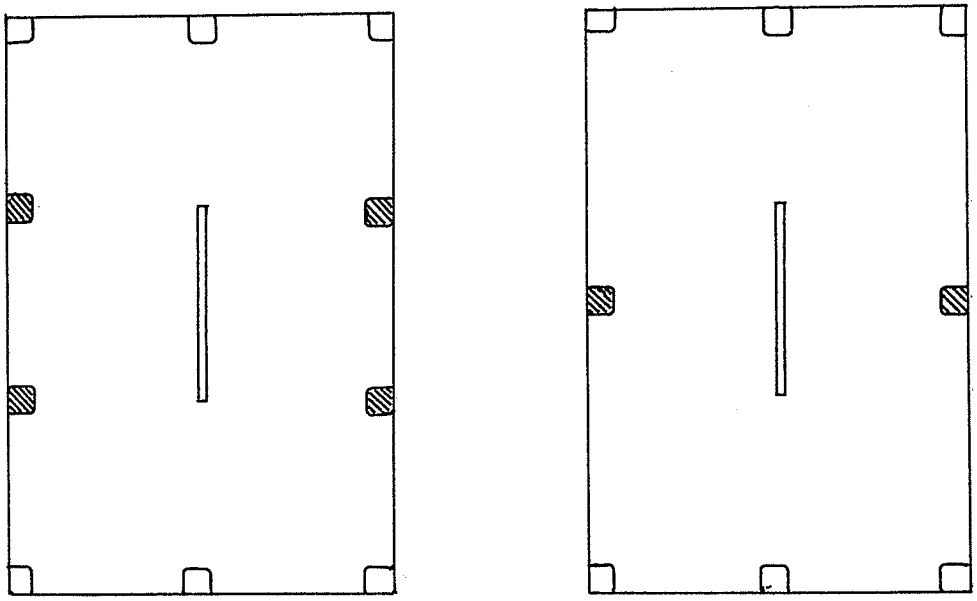

(a) (b)

Fig. 4.3.4 Comparison of Two Types of Shear Wall Structure.

CHAPTER V

CONCLUSIONS AND SUGGESTIONS FOR FURTHER STUDY

5.1 Conclusions. An experimental study of stiffness and carry-over factors for elastic plates loaded by transverse loads applied to columns and various shapes of shear wall has been made. For a shear wall structure subjected to lateral loads the following conclusions are made.

1. For flat plate loaded only through interior columns, the effective panel widths range approximately from 0.6 to 1.1 of the true panel width. It may be concluded that, for a column panel width ratio of 1/10 or greater, the full slab width may be assumed effective.

2. For a flat plate loaded through exterior columns, the effective panel width is independent of the shape and size of interior supports. The effective widths obtained were approximately 0.6 of the true width for model P series and 0.88 for model C2.

3. Values of the carry-over factor for a flat plate panel loaded through an exterior column ranged from 0.29 to 0.815, depending on the size and shape of the fixed interior column or shear wall.

4. Carry-over factors from a loaded interior column or shear wall are relatively small, and practically independent of the size and shape of the interior column or wall. Values ranging from 0.091 to 0.156 were obtained.

5 Effective widths of panel loaded through interior shear walls ranged from 3 to 12 times the true panel width. The large values obtained indicate that effective slab width is an unsuitable criterion for

indicating the efffective stiffness of flat plate - shear wall structures.

Micro concrete model C2 was loaded to failure, which resulted from flexural failure in the slab combined with punching shear at the edge of the shear wall. The experimental ultimate load was in good agreement with the results of a yield line analysis, the effective slab width reduces as ultimate moment approaches. This can be explained by the fact that as the ultimate load approaches, large deformations occur with very little increase in the slab moment capacity. Thus the stiffness factor at the ultimate load decrease.

5.2 Suggestion for Further Study. Further study is recommended to establish suitable effective plate widths or stiffness and carry-over factors for plate loaded through shear walls with various geometries. The effect of slab openings near shear walls or columns should be further investigated. Similar investigations to this one should be performed for flat slabs and concrete joist floors. The experimental results obtained should be corelated with analytical studies that could be performed using finite element or finite difference techniques. Because of the unsuitability of the effective width criterion, further studies to obtain different criteria for representing slab stiffness for shear wall buildings should be made. Finally the behavior of flat plate and flat slab - shear wall structures in the inelastic region requires considerably more study.

REFERENCES

1. Tsuboi and Kawaguchi, " On Earthquake Resistant Design of Flat Slabs and Concrete Shell Structures," The Second World Conference on Earthquake Engineering, Tokyo 1960.

2. Khan Fazlur R. and Sbarounis, John A., " Interaction of Shear Walls and Frames," Journal of the Structural Division, ASCE Proceedings Vol.90, ST 3, June 1964.

3. Brotchie, John F., and Russell, J.J., " Flat Plate Structures," Part I. Journal of the American Concrete Institute, Proc. 61, No. 8, August 1964.
Part II. available from American Concrete Institute, Detroit, Michigan.

4. Carpenter, J. E., " Flexural Characteristics of Flat Plate Floors in Buildings Subjected to Lateral Loads " Ph. D Thesis, Purdue University, June 1965.

5. Bernard, P. R. and Schweighofer, J. " Interaction of Shear Walls Connected Solely to Slabs," The International Syposium on Tall Buildings, University of Southampton, London, April 1966.

6. American Concrete Institute, " Building Code Requirements for Reinforced Concrete," ACI Standard 318 - 63, June 1963.

7. Di Stasio, Joseph and Van Buren, M.P., " Transfer of Bending Moment Between Flat Plate Floor and Column," Journal of The American Concrete Institute, Proc. 57, No. 3, September 1960.

8 Standard Method of Test for Flexural Properties of Plastic,, ASTM Designation : D 790 - 66, Book of ASTM Standards, Vol. 27, 1967.

9. Canadian Plastic for Industry, Catalogue, Johnson Industrial Plastics Ltd., 1968.

10. Robert Petri, " Model Analysis of a Ten Storey Building," M. Sc. Thesis, University of Manitoba, 1965.

11. Donald D. Magura, " Structural Model Testing Reinforced and Prestressed Mortar Beams," Portland Cement Association, Research and Development Laboratories, January 1967.

12. Johnson, R. Paul, " Strength tests on Scaled - Down Concretes Suitable for Models, With a Note on Mixed Design," Magazine of Concrete Research, Vol. 14, No.40, March 1962.

13. Shewmaker, R. E., Xanthakis, M. and Sozen, M. A., " Very Small Scale Reinforced Concrete Multi-Panel Flat Slabs," A Report on a Research Project, University of Illinois, Urbana, Illinois, June 1963.

14. Weibe, J. D., " Preparation of Influence Surfaces for a

Simply Supported Square Plate by the Moire' Method," M. Sc. Thesis, University of Manitoba, 1967.

15. Ligtenberg, F. K., " The Moire' Method, a New Experimental Method for the Determination of Moments in Small Slab Models," Proc. Soc. Exp. Stress Analysis, XII (2), 1954.

16. Vreedenberg, C.G.J., and Van Wijngaarden, H., " New Progress in Our Knowledge About the moment Distribution in Flat Slabs by Means of the Moire' Method," Proc. Soc. Exp. Stress Analysis, XII (2), 1954.

17. Gupta, K.K., and Vaughan, R.C., " Determination of Elastic Moments in Flat - Plate and Lift - Slab Structures by the Moire' Method," Experimental Mechanics, Vol. 8, No. 4, April 1968.

APPENDIX A

A - 1 Basic Principle of the Moire' Method. The Moire' Method is an experimental procedure for measuring the slopes of a deflected plexiglas plate model. If the slopes are established along a set of parallel lines, a slope diagram can be drawn. The slope curve along any given line can then be integrated to obtain a deflection diagram along that line.

A model plate with a reflecting surface is clamped to a loading frame in front of a ruled screen, as shown in Fig. A - 1. The unloaded model is photographed through a small opening in the screen, and a reflected image of the ruled dark and light lines on the screen obtained. For example, the image of a dark line at point Q would be reflected from point P on the plate and would appear at point S on the film. The model is then loaded and rephotographed. If point P on the model rotates through an angle $\emptyset$, the image of a new point R appears at S. If point R on the screen coincides with a dark line, point S on the photo will be dark. Otherwise it will be somewhat lighter in color. This gives interference patterns on the photographic plate and produces Moire' fringes as shown in Figs.A - 3, A - 5, A - 7, etc. These fringes represent contours of constant slope, and since the slope along each fringe is constant, it follows that the change of slope between the contours corresponding to two consecutive fringes must also be constant. This constant "C" is dependent on the interval of ruling screen, "d" and on the distance between the screen and the model plate, "a" shown in Fig. A - 1.

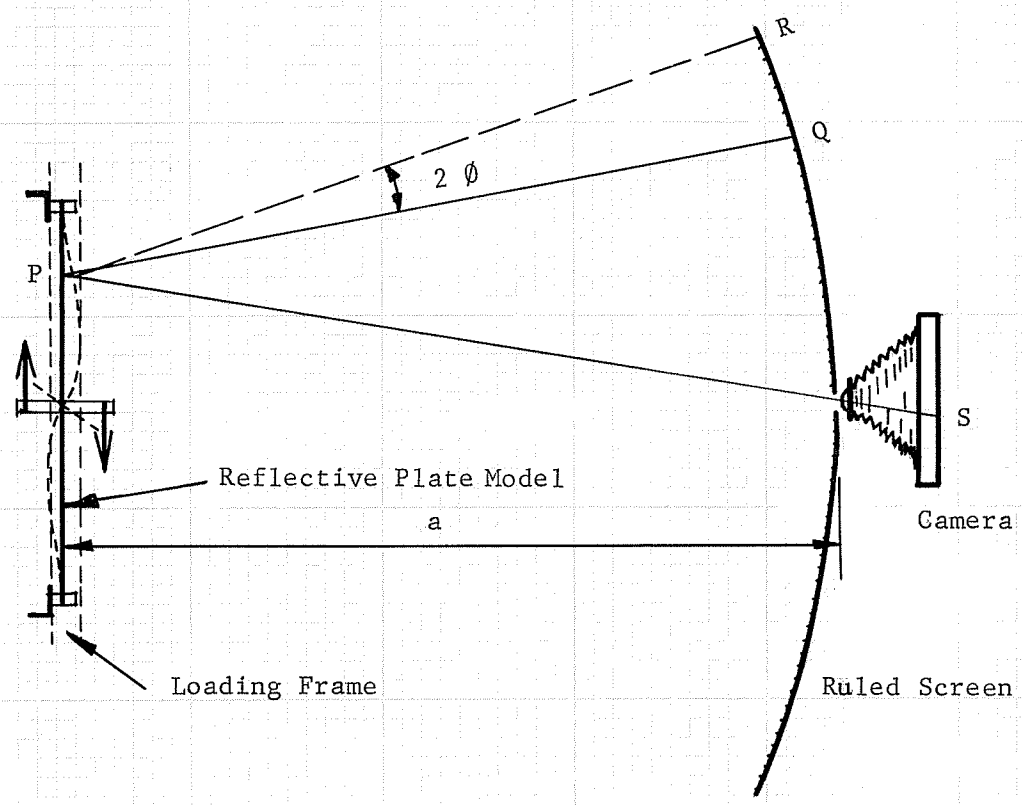

Fig. A - 1 Basic Principle of Morie' Method

The evaluation of the constant "C" is described by J. Weibe[14] and for the M 1/03 apparatus used in this study C = 0.0015. Fig. A - 2 shows two views of the Moire' apparatus.

A - 2 Determination of Slope Curve from Moire' Photographs. If a Moire' photograph of a model plate is taken with the rulings of the screen in the x- direction (horizontal), a curve of $\partial w/\partial y$ along a line parallel to the y- direction (vertical) may be obtained as follows:

A line is drawn parallel to the y-axis as shown in Figs. A - 3, A - 5, A - 7, etc., this line intersects a number of fringes. The centres of the fringes along the line are then projected downward and plotted as shown in Figs. A - 4, A - 6, A - 8, etc. Values of slope are then plotted to obtain a curve of slope $\emptyset_y$ vs distance along the line.

The fringes are numbered staring from the zero fringe, which represents zero slope (i.e. a zero value for QR in Fig. A - 1) In Figs. A - 3, A - 5, A - 7, etc., for examples, the zero fringe is the one that extends from the exterior fixed columns. The slope (in a direction perpendicular to the ruled lines on the screen) at any point is thus the fringe order at the point times C.

A - 3 Calculation of Stiffnessess and Carry - Over Factors. The Moire' fringe patterns and the plots of the computed plate slopes and deflections are presented in Figs. A - 3 to A - 34. The calculations for the stiffness, effective width and carry-over factor are also included. The last two calculations are based on the following physical properties and dimensions:

Fig. A-2 Moire' Apparatus Type M 1/03

1.	Young's Modulus of Elasticity of Plexiglas,	E =	441,000	psi.
2.	Average thickness of the plate,	t =	0.243	in.
3.	Panel length of the plate,	L_x =	9.00	in.

Fig. A - 3 Photograph of Model P1 Load Type A.

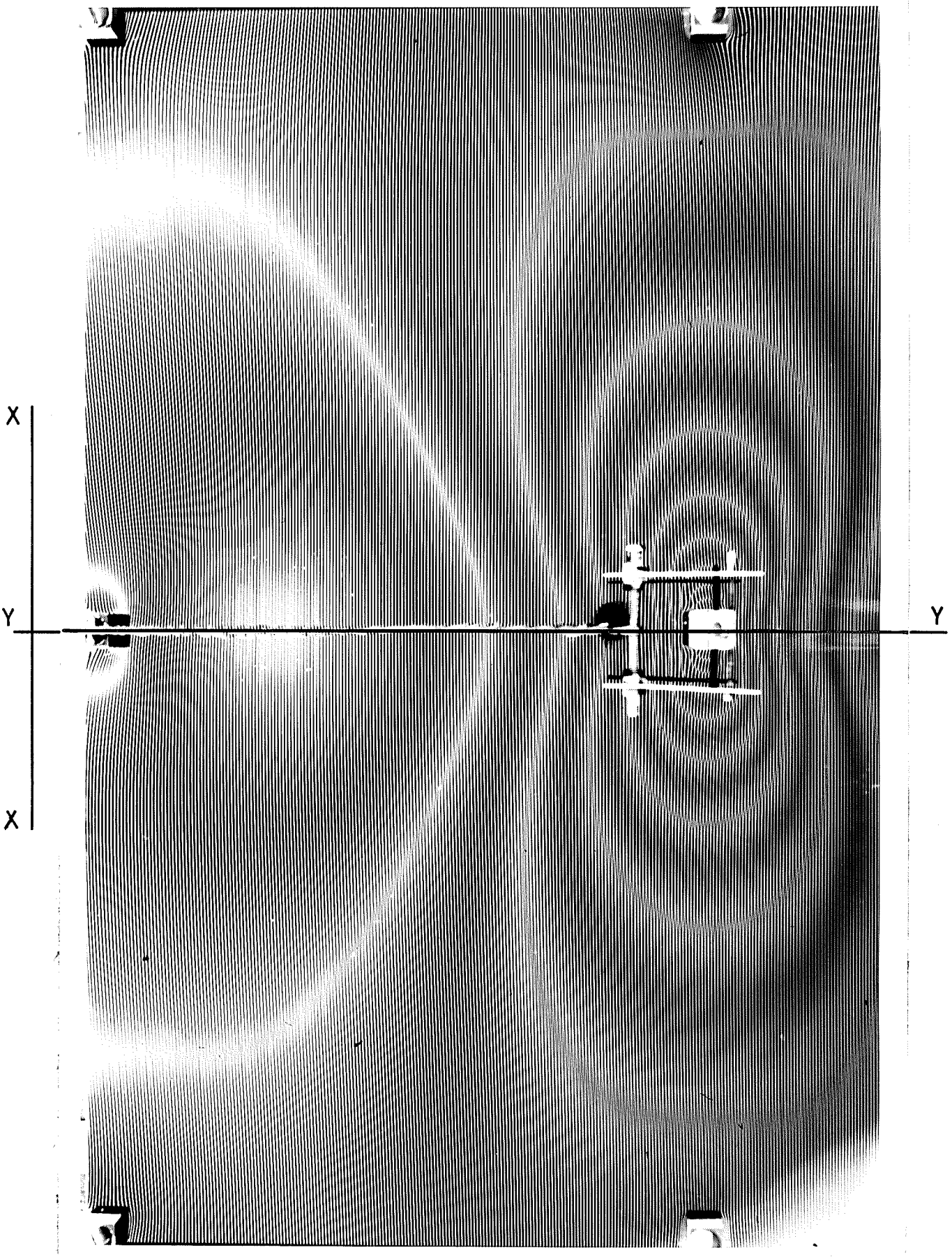

Fig. A - 4 Slope and Deflection Curves Model P1 Load Type A.

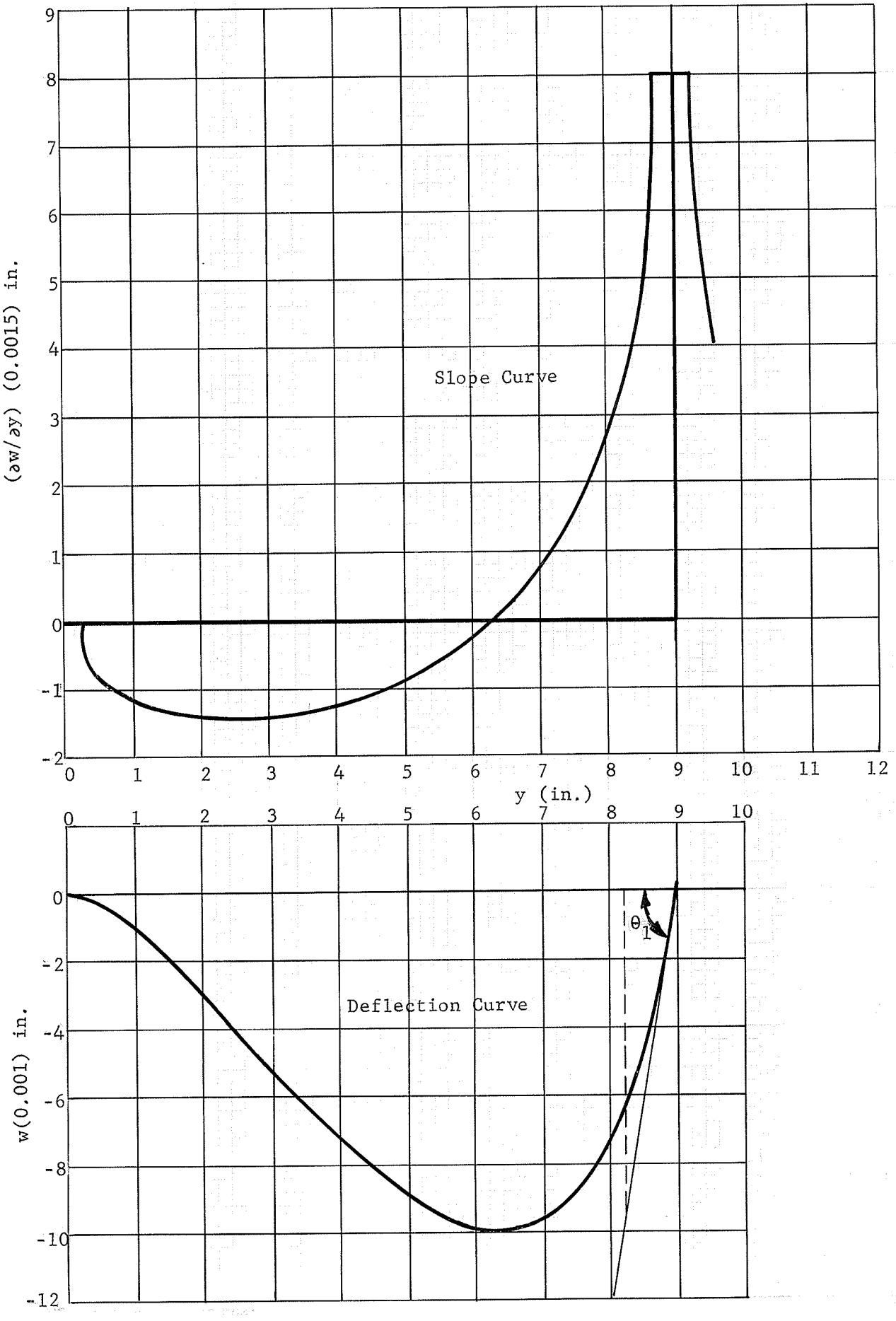

$y_1 - y_2$ in.	$\int_{y_2}^{y_1} (\partial w/\partial y)\, dy$ in.	$\Sigma \int_{y_2}^{y_1} (\partial w/\partial y)\, dy$ in.
0 - 1	-0.00105	-0.00105
1 - 2	-0.00196	-0.00301
2 - 3	-0.00220	-0.00521
3 - 4	-0.00210	-0.00731
4 - 5	-0.00168	-0.00899
5 - 6.35	-0.00100	-0.00999
6.35 - 7	0.00033	-0.00966
7 - 8	0.00231	-0.00735
8 - 9	0.00760	0.00025
M_1 = 30 lb.-in.,		θ_1 = 0.0129 rad.

Slope and Deflection Calculations Model P1 Load Type A.

TABLE A - 1

Stiffness and Effective Width Calculations.

$$K = \frac{M_1}{\theta_1} = 2320 \text{ lb.-in./rad.}$$

$$L_y = \frac{3 K L_x}{E h^3}$$

$$= \frac{3 \times 2320 \times 9}{441{,}000 \times (0.243)^3}$$

$$= 10.00 \text{ in.}$$

Fig. A - 5 Photograph of Model P1 Load Type B.

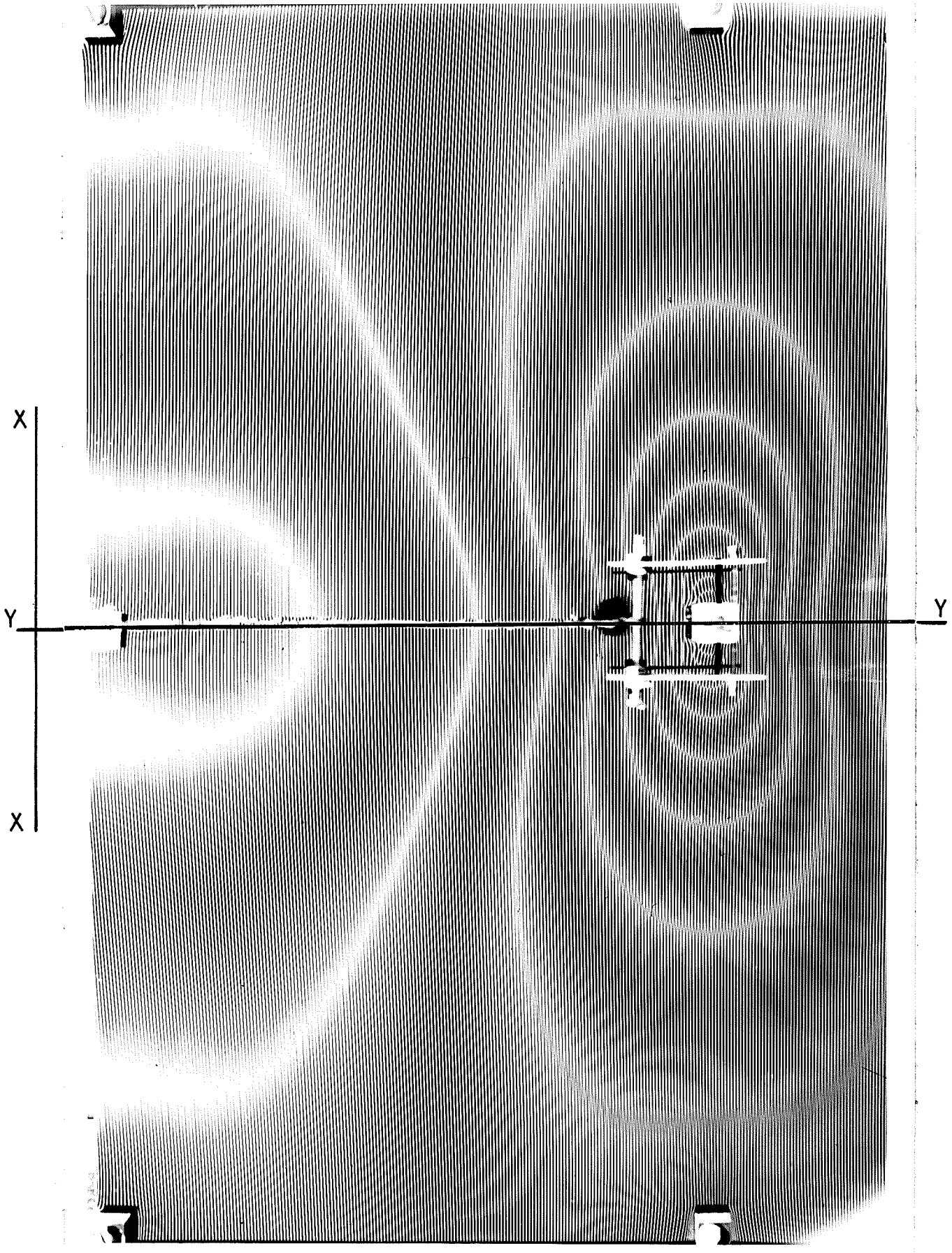

Fig. A - 6 Slope and Deflection Curves Model P1 Load Type B.

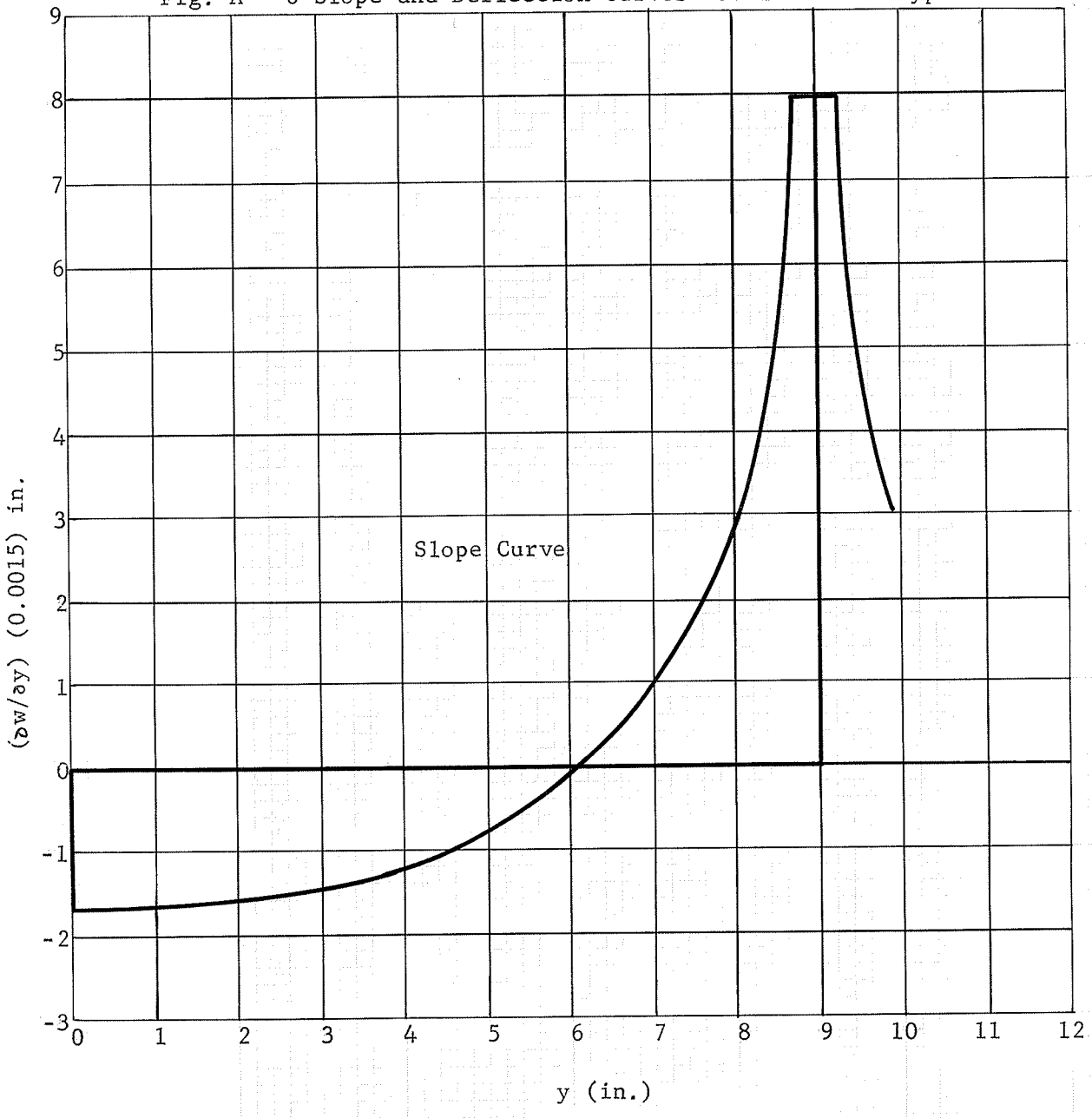

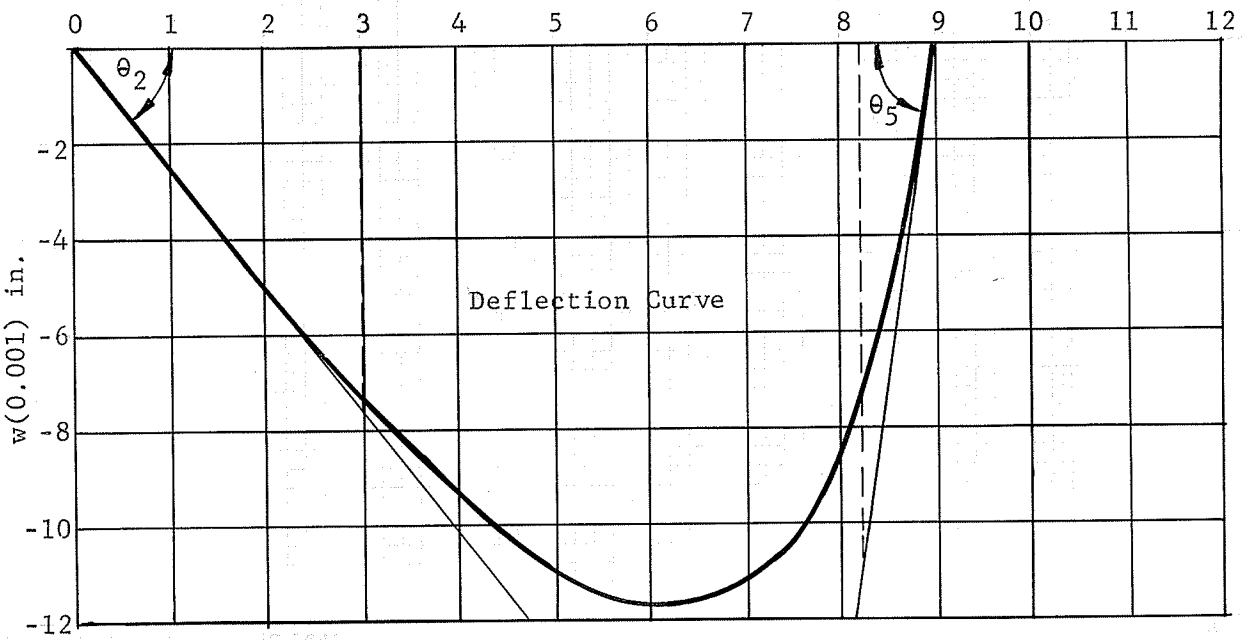

$y_1 - y_2$ in.	$\int_{y_2}^{y_1} (\partial w/\partial y)\, dy$ in.	$\sum \int_{y_2}^{y_1} (\partial w/\partial y)\, dy$ in.
0 - 1	-0.00255	-0.00255
1 - 2	-0.00250	-0.00505
2 - 3	-0.00234	-0.00739
3 - 4	-0.00207	-0.00946
4 - 5	-0.00157	-0.01103
5 - 6.15	-0.000735	-0.011765
6.15 - 7	0.000554	-0.011211
7 - 8	0.00270	-0.008511
8 - 9	0.00840	-0.000111

M_2 = 30 lb.-in., θ_2 = 0.00255 rad., θ_5 = 0.01375 rad.

Slope and Deflection Calculations Model P1 Load Type B.

TABLE A - 2

Fig. A - 7 Photograph of Model P1 Load Type C.

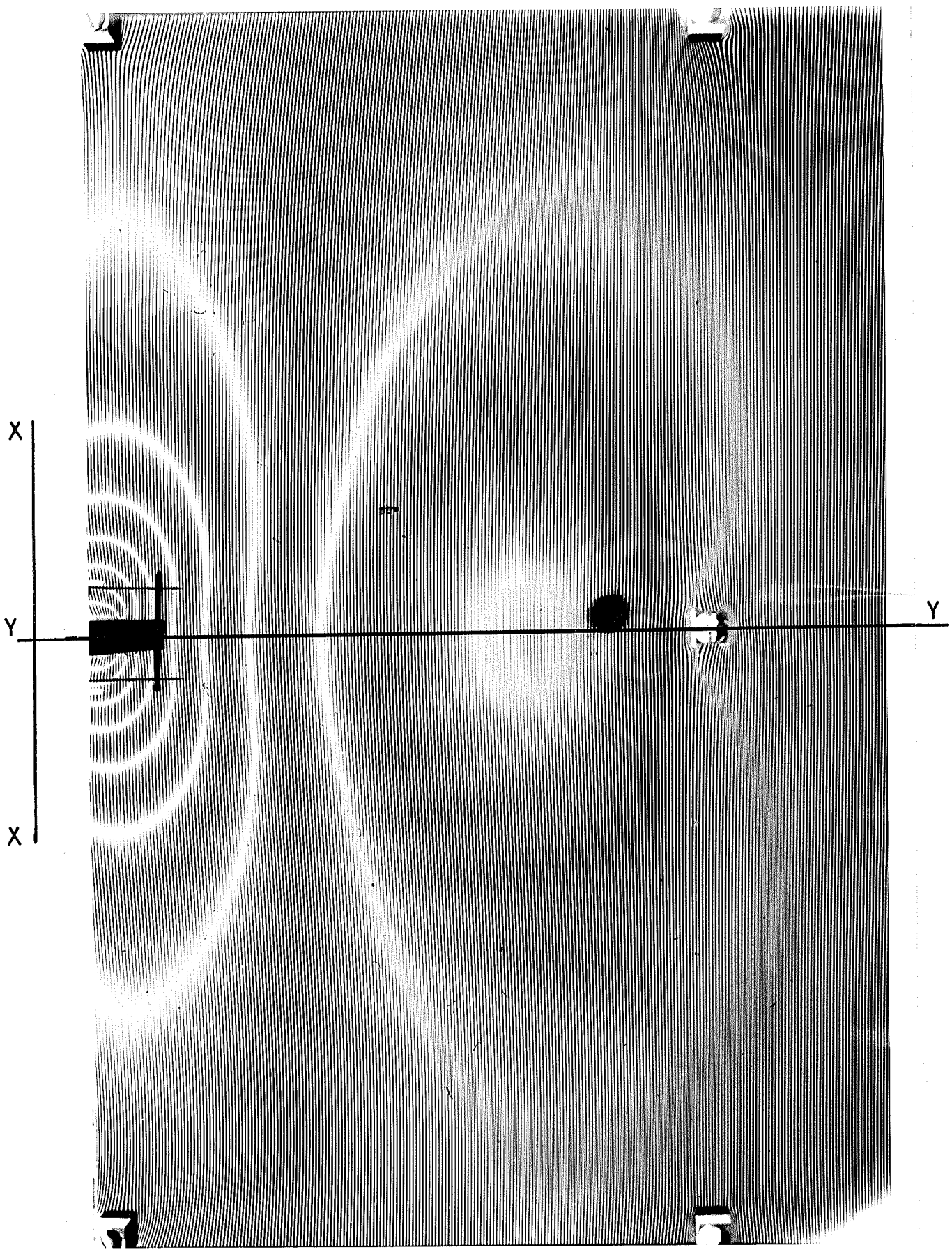

Fig. A - 8 Slope and Deflection Curve Model P1 Load Type C.

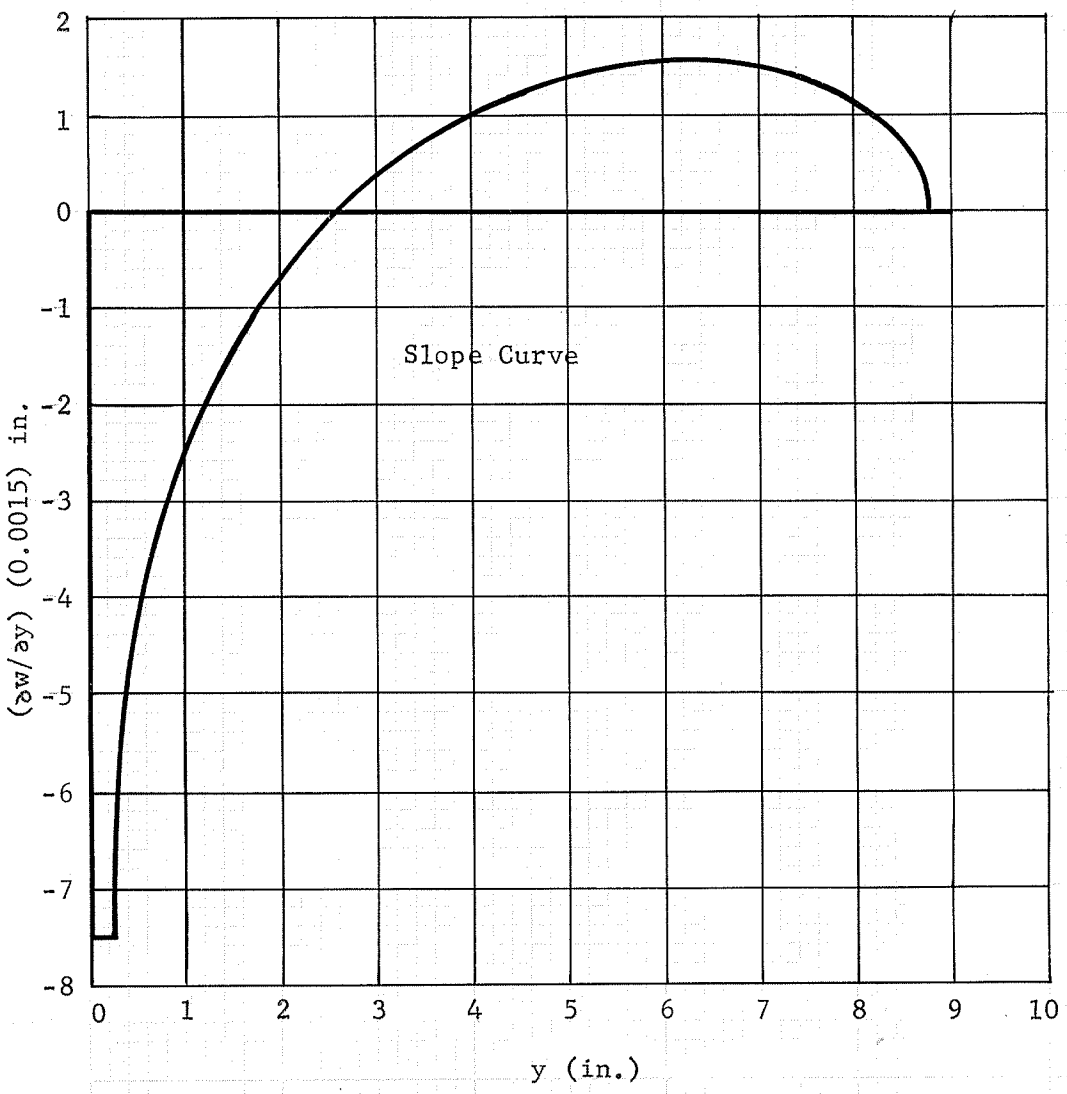

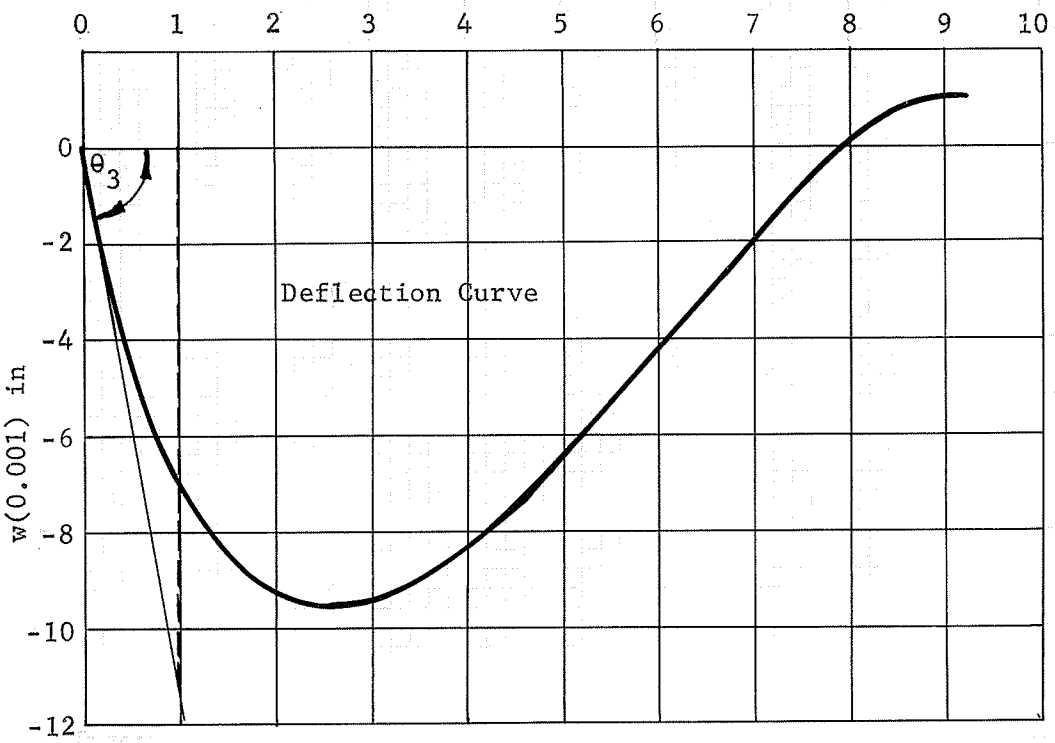

$y_1 - y_2$ in.	$\int_{y_2}^{y_1} (\partial w/\partial y)\, dy$ in.	$\sum \int_{y_2}^{y_1} (\partial w/\partial y)\, dy$ in.
0 - 1	-0.00714	-0.00714
1 - 2	-0.00220	-0.00934
2 - 2.55	-0.000285	-0.009625
2.55 - 4	0.00120	-0.008425
4 - 5	0.00184	-0.00685
5 - 6	0.00225	-0.004335
6 - 7	0.00228	-0.002055
7 - 8	0.00204	-0.000015
8 - 9	0.00096	0.000975
M_3 = 15 lb.-in.,		θ_3 = 0.0113 rad.

Slope and Deflection Calculations Model P1 Load Type C.

TABLE A - 3

Stiffness and Effective Width Calculations.

$$K = \frac{M_3}{\theta_3} = 1325 \text{ lb.-in./rad.}$$

$$L_y = \frac{3 K L_x}{E h^3}$$

$$= \frac{3 \times 1325 \times 9}{441{,}000 \times (0.243)^3}$$

$$= 5.70 \text{ in.}$$

Fig. A - 9 Photograph of Model P1 Load Type D.

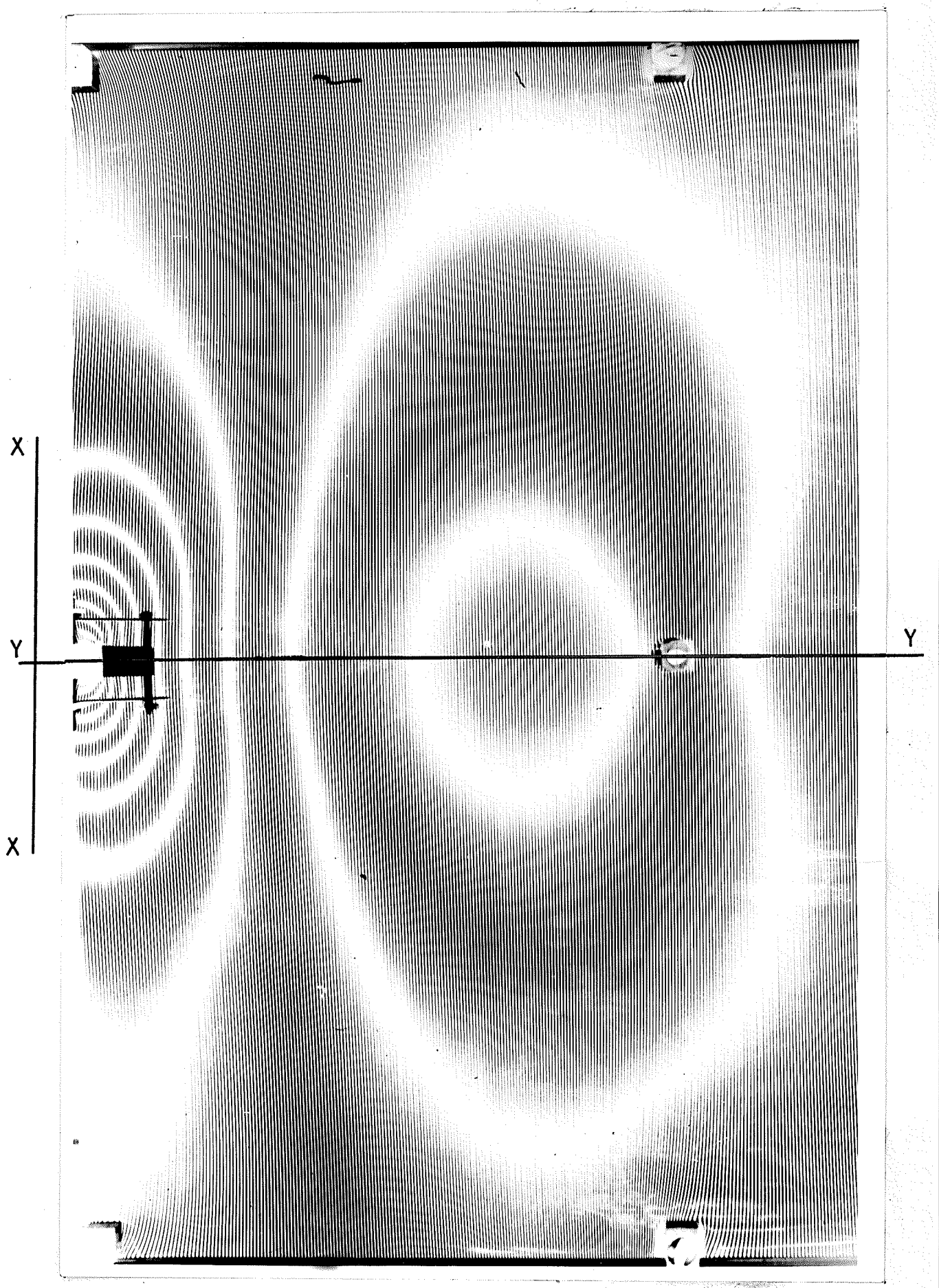

Fig. A - 10 Slope and Deflection Curves Model P1 Load Type D.

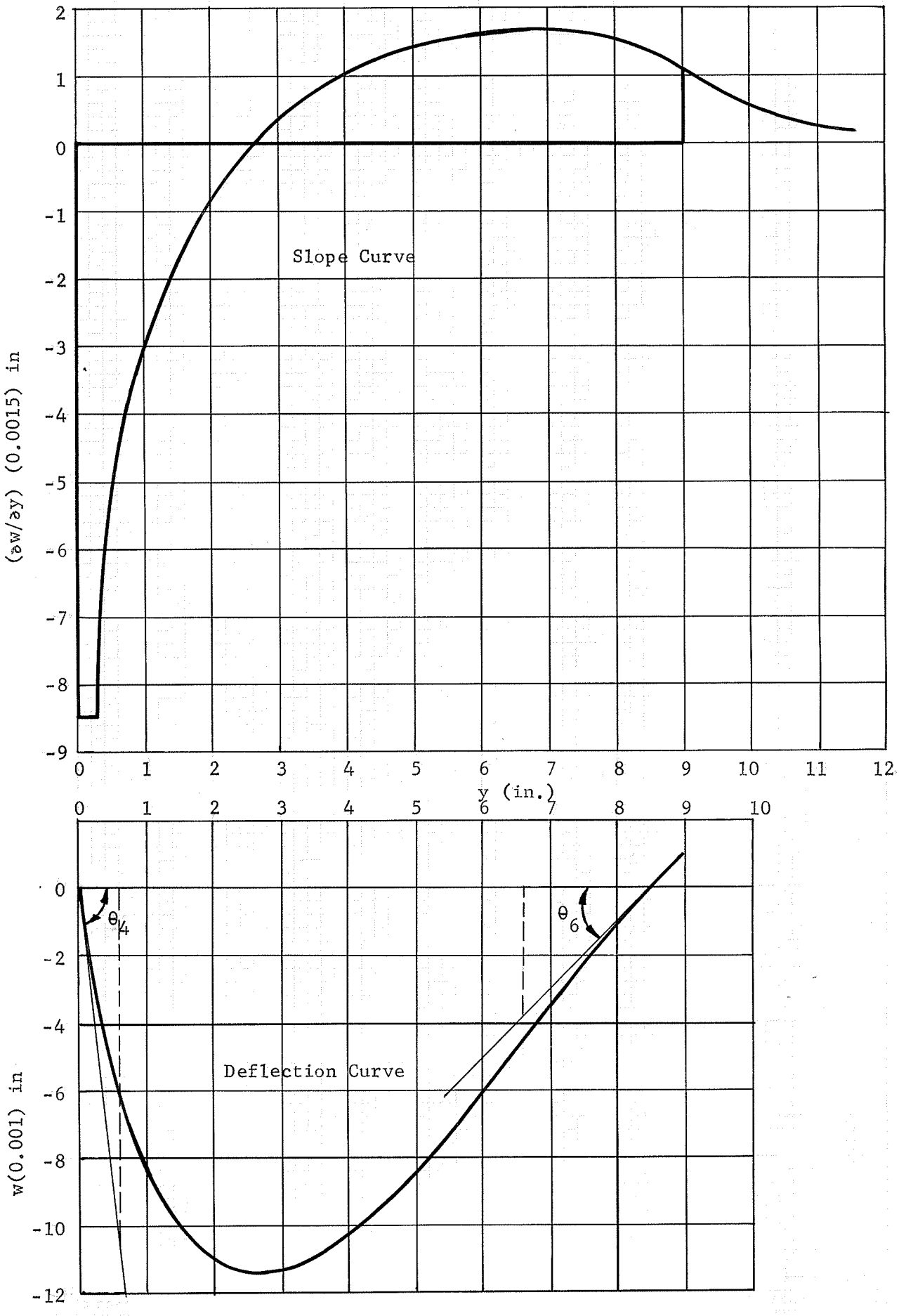

$y_1 - y_2$ in.	$\int_{y_2}^{y_1} (\partial w/\partial y)\, dy$ in.	$\sum \int_{y_2}^{y_1} (\partial w/\partial y)\, dy$ in.
0 - 1	-0.00845	-0.00845
1 - 2	-0.00272	-0.01117
2 - 2.65	-0.00039	-0.01156
2.65 - 4	0.00121	-0.01035
4 - 5	0.00192	-0.00843
5 - 6	0.00234	-0.00609
6 - 7	0.00253	-0.00356
7 - 8	0.00250	-0.00106
8 - 9	0.00206	0.001

M_4 = 15 lb.-in., θ_4 = 0.0192 rad., θ_6 = 0.002 rad.,

M_2 = 30 lb.-in., θ_2 = 0.00255 rad., θ_5 = 0.01375 rad.

Slope and Deflection Calculations Model P1 Load Type D.

TABLE A - 4

Carry - Over Factors Calculations.

$$C_{interior} = \frac{2\, M_4\, \theta_2}{M_2\, \theta_4} = \frac{2 \times 15 \times 0.00255}{30 \times 0.0192}$$

$$= 0.133$$

$$C_{exterior} = \frac{M_2\, \theta_6}{M_4\, \theta_5} = \frac{30 \times 0.002}{15 \times 0.0137}$$

$$= 0.29$$

Fig. A - 11 Photograph of Model P2 Load Type A.

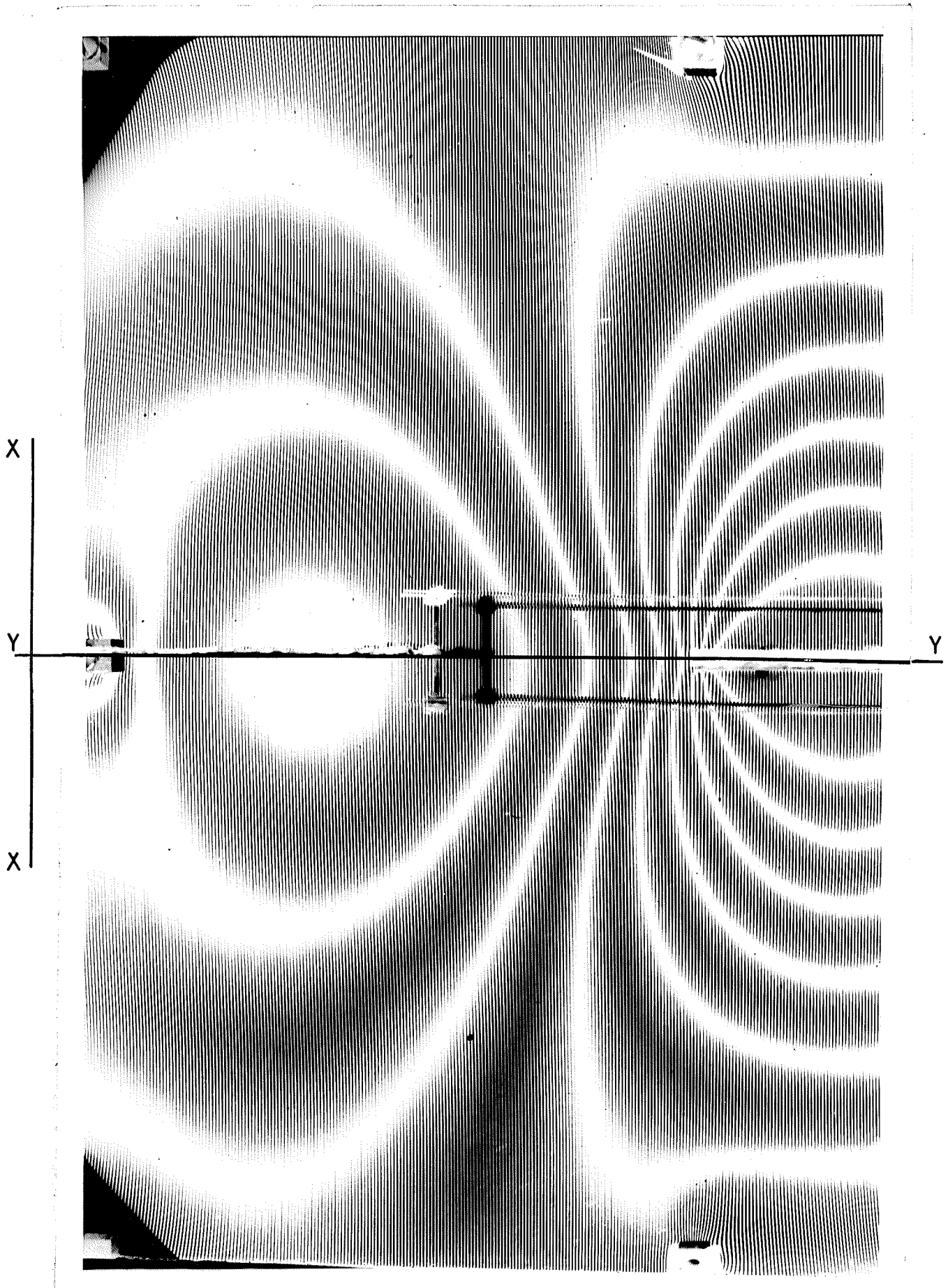

Fig. A - 12 Slope and Deflection Curves Model P2 Load Type A.

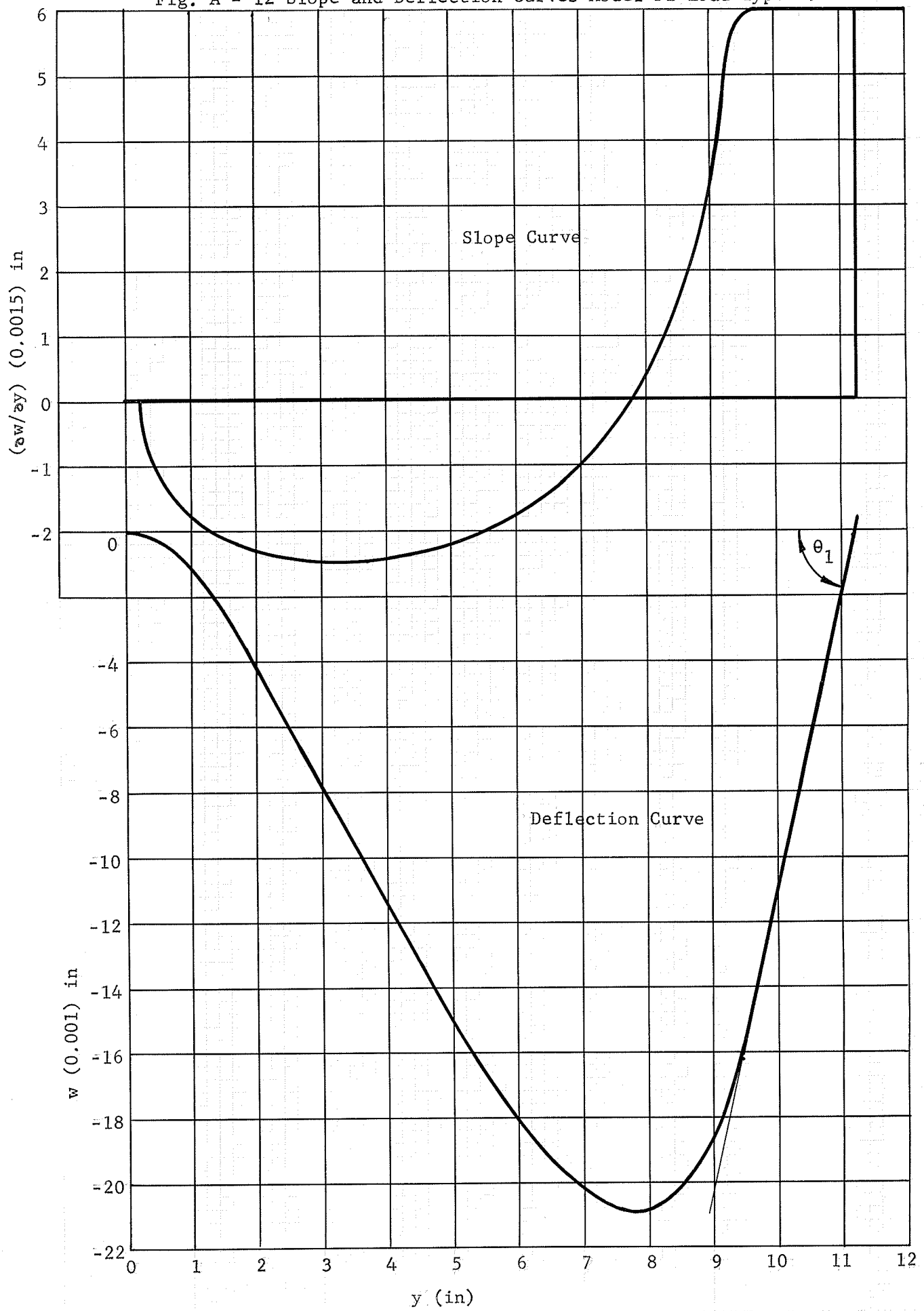

$y_1 - y_2$ in.	$\int_{y_2}^{y_1} (\partial w/\partial y)\, dy$ in.	$\sum \int_{y_2}^{y_1} (\partial w/\partial y)\, dy$ in.
0 - 1	-0.001035	-0.001035
1 - 2	-0.00318	-0.004215
2 - 3	-0.00362	-0.007835
3 - 4	-0.00375	-0.011585
4 - 5	-0.00352	-0.015105
5 - 6	-0.00307	-0.018175
6 - 7	-0.00216	-0.020335
7 - 7.8	-0.00069	-0.021025
7.8 - 9	0.00223	-0.018795
9 - 10	0.00795	-0.010845
10 - 11	0.00900	-0.001845
11 - 11.25	0.00225	0.000405

M_1 = 60 lb.-in., θ_1 = 0.00922 rad.

Slope and Deflection Calculations Model P2 Load Type A.

TABLE A - 5

Stiffness and Effective Width Calculations.

$$K = \frac{M_1}{\theta_1} = 6500 \text{ lb.-in./rad}$$

$$Ly = \frac{3 K L_x}{E h^3} = \frac{3 \times 6500 \times 9}{441{,}000 \times (0.243)^3}$$

$$= 28.10 \text{ in.}$$

Fig. A - 13 Photograph of Model P2 Load Type B.

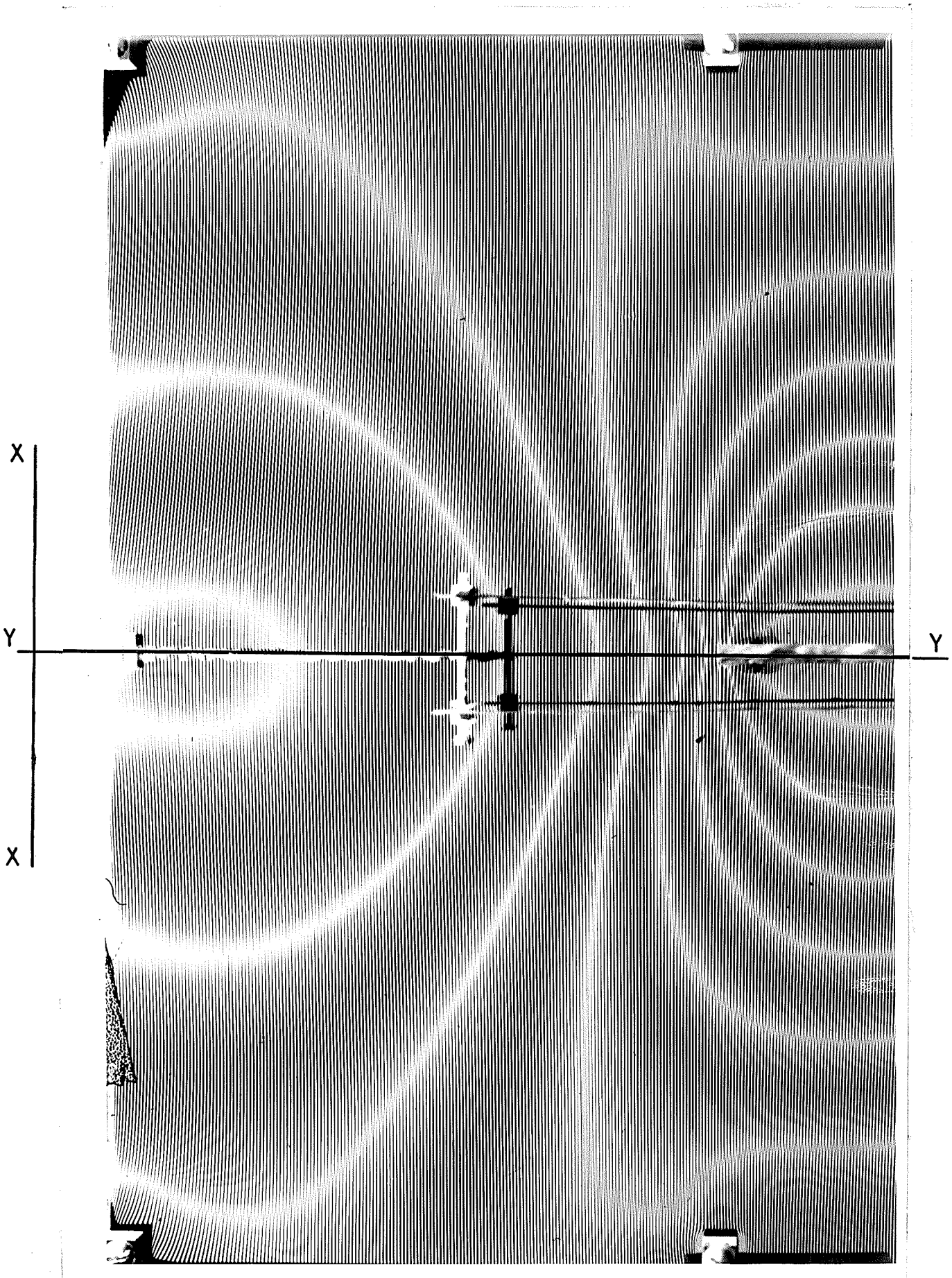

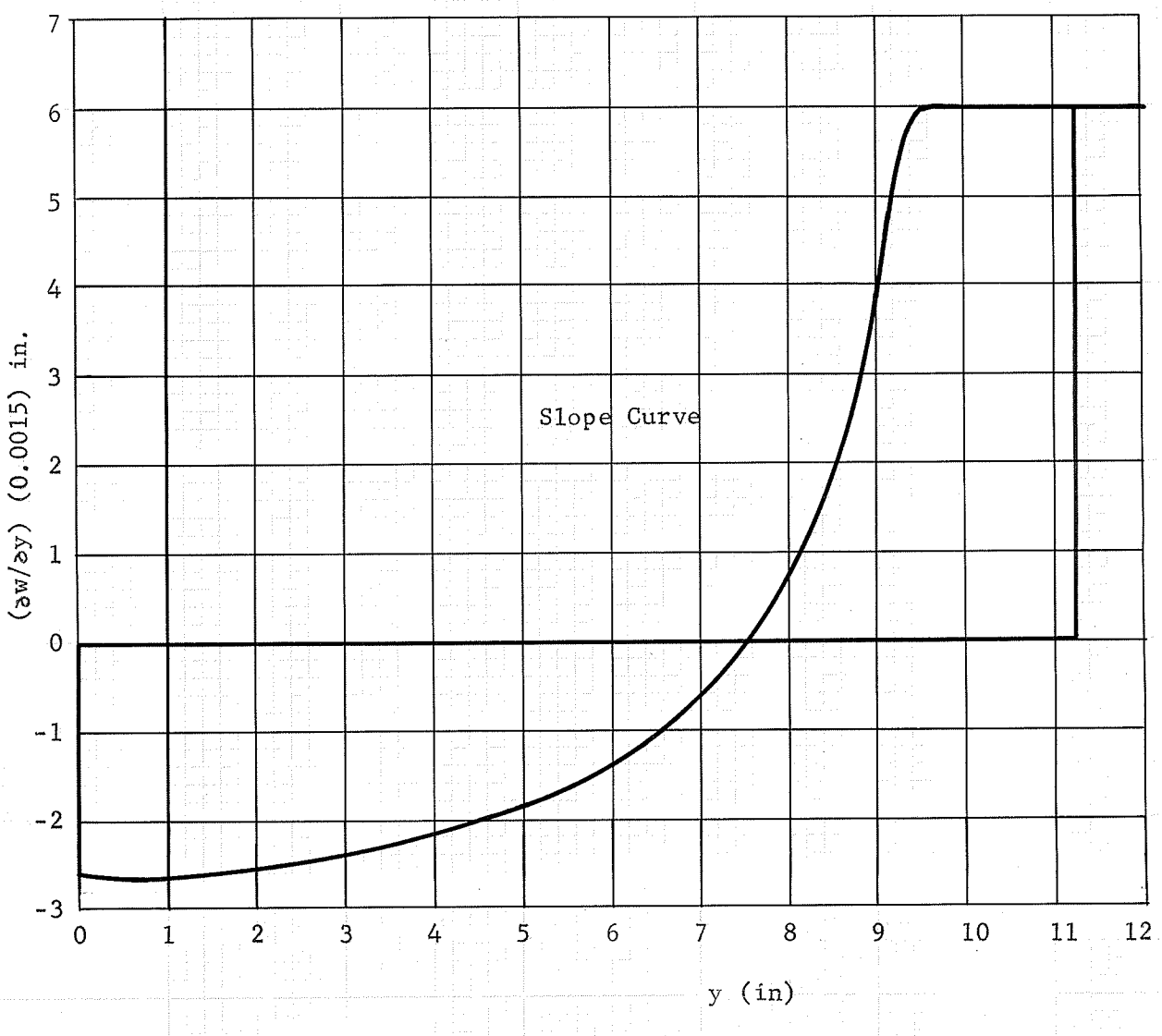

Fig. A - 14 Slope and Deflection Curves

Model P2 Load Type B

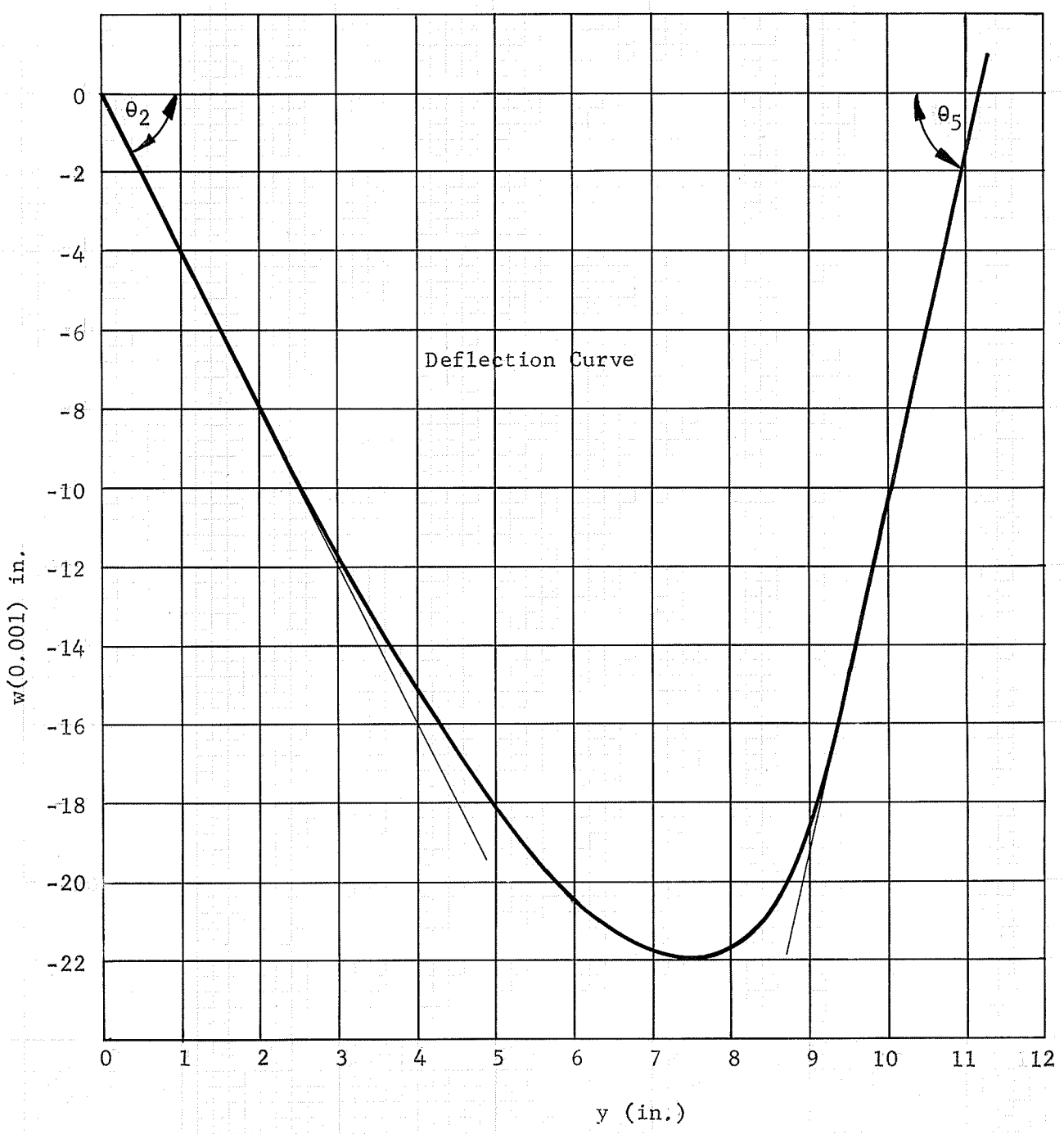
0
-2
-4
-6
-8
-10
-12
-14
-16
-18
-20
-22
w(0.001) in.
θ2
θ5
Deflection Curve
0
1
2
3
4
5
6
7
8
9
10
11
12
y (in.)

Fig. A - 14

$y_1 - y_2$ in.	$\int_{y_2}^{y_1} (\partial w/\partial y)\, dy$ in.	$\sum \int_{y_2}^{y_1} (\partial w/\partial y)\, dy$ in.
0 - 1	-0.00398	-0.00398
1 - 2	-0.00393	-0.00791
2 - 3	-0.00375	-0.01166
3 - 4	-0.00345	-0.01511
4 - 5	-0.00304	-0.01815
5 - 6	-0.00248	-0.02063
6 - 7	-0.00140	-0.02177
7 - 7.6	-0.00030	-0.02207
7.6 - 8	-0.000225	-0.021845
8 - 9	0.00287	-0.018975
9 - 10	0.00834	-0.010635
10 - 11	0.00900	-0.001635
11 - 11.25	0.00225	0.000615

M_2 = 60 lb.-in., θ_2 = 0.004 rad., θ_5 = 0.0089 rad.

Slope and Deflection Calculations Model P2 Load Type B.

TABLE A - 6

Fig. A - 15 Photograph of Model P2 Load Type C.

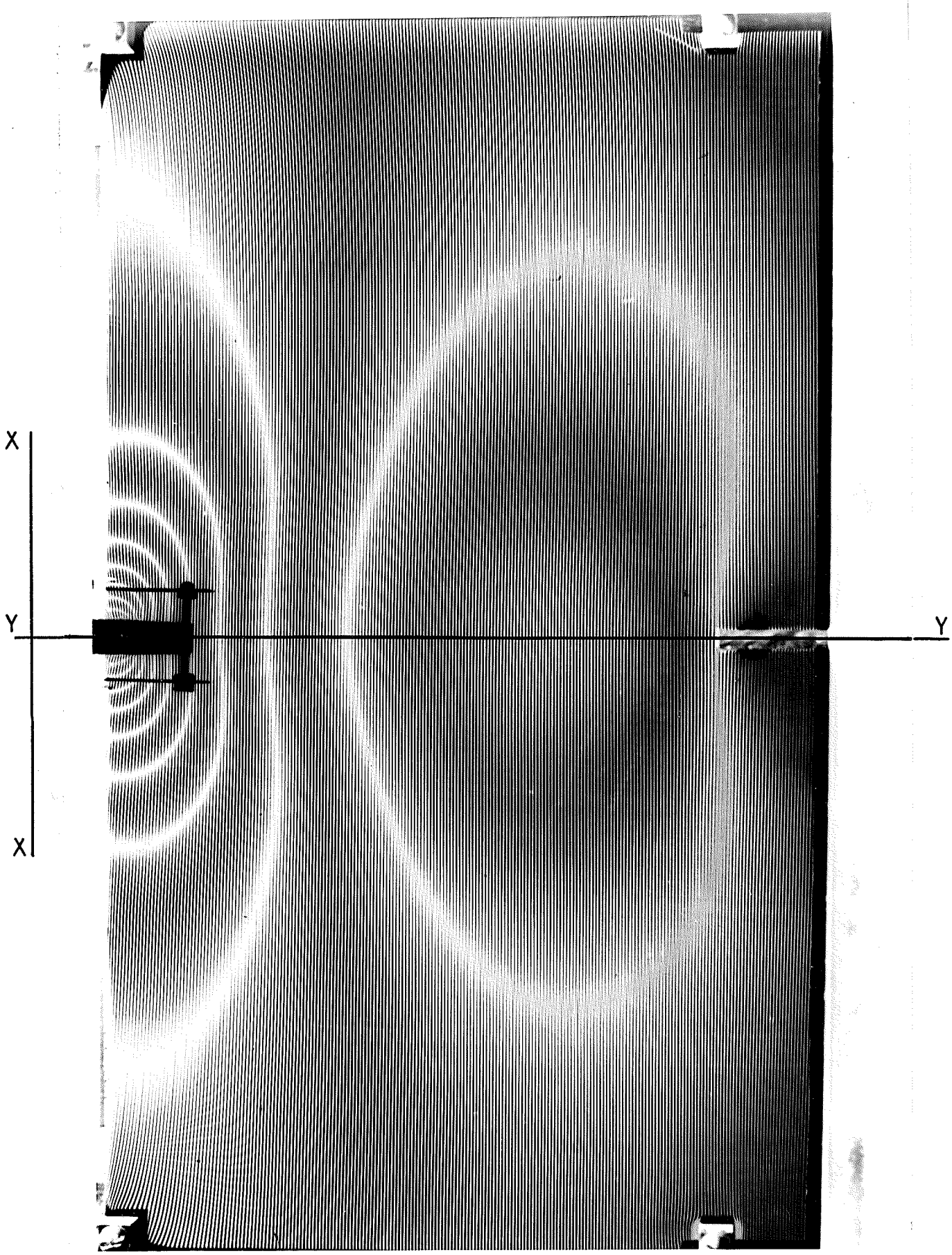

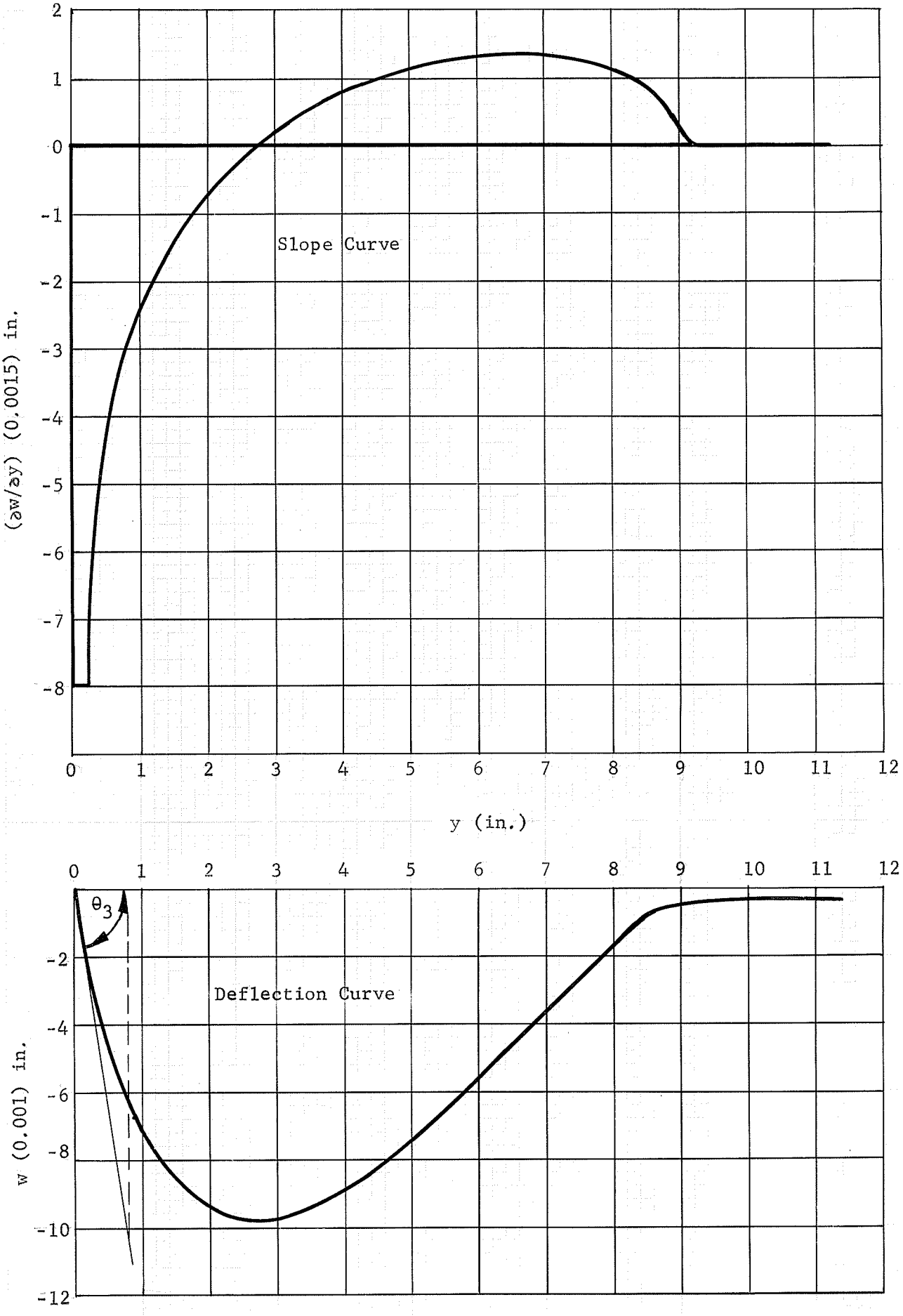

Fig. A - 16 Slope and Deflection Curves Model P2 Load Type C

$y_1 - y_2$ in.	$\int_{y_2}^{y_1} (\partial w/\partial y)\, dy$ in.	$\sum \int_{y_2}^{y_1} (\partial w/\partial y)\, dy$ in.
0 - 1	-0.00736	-0.00736
1 - 2	-0.00219	-0.00955
2 - 2.7	-0.00033	-0.00988
2.7 - 4	0.00087	-0.00901
4 - 5	0.001485	-0.007525
5 - 6	0.00186	-0.005665
6 - 7	0.002025	-0.003640
7 - 8	0.00192	-0.001720
8 - 9	0.00138	-0.000340
9 - 11.5	0.00000	-0.000340
M_3 = 15 lb.-in.,		θ_3 = 0.01285 rad.

Slope and Deflection Calculations Model P2 Load Type C.

TABLE A - 7

Stiffness and Effective Width Calculations.

$$K = \frac{M_3}{\theta_3} = 1165 \text{ lb.-in./rad.}$$

$$L_y = \frac{3 K L_x}{E h^3}$$

$$= \frac{3 \times 1165 \times 9}{441{,}000 \times (0.243)^3}$$

$$= 5.02 \text{ in.}$$

Fig. A - 17 Photograph of Model P2 Load Type D.

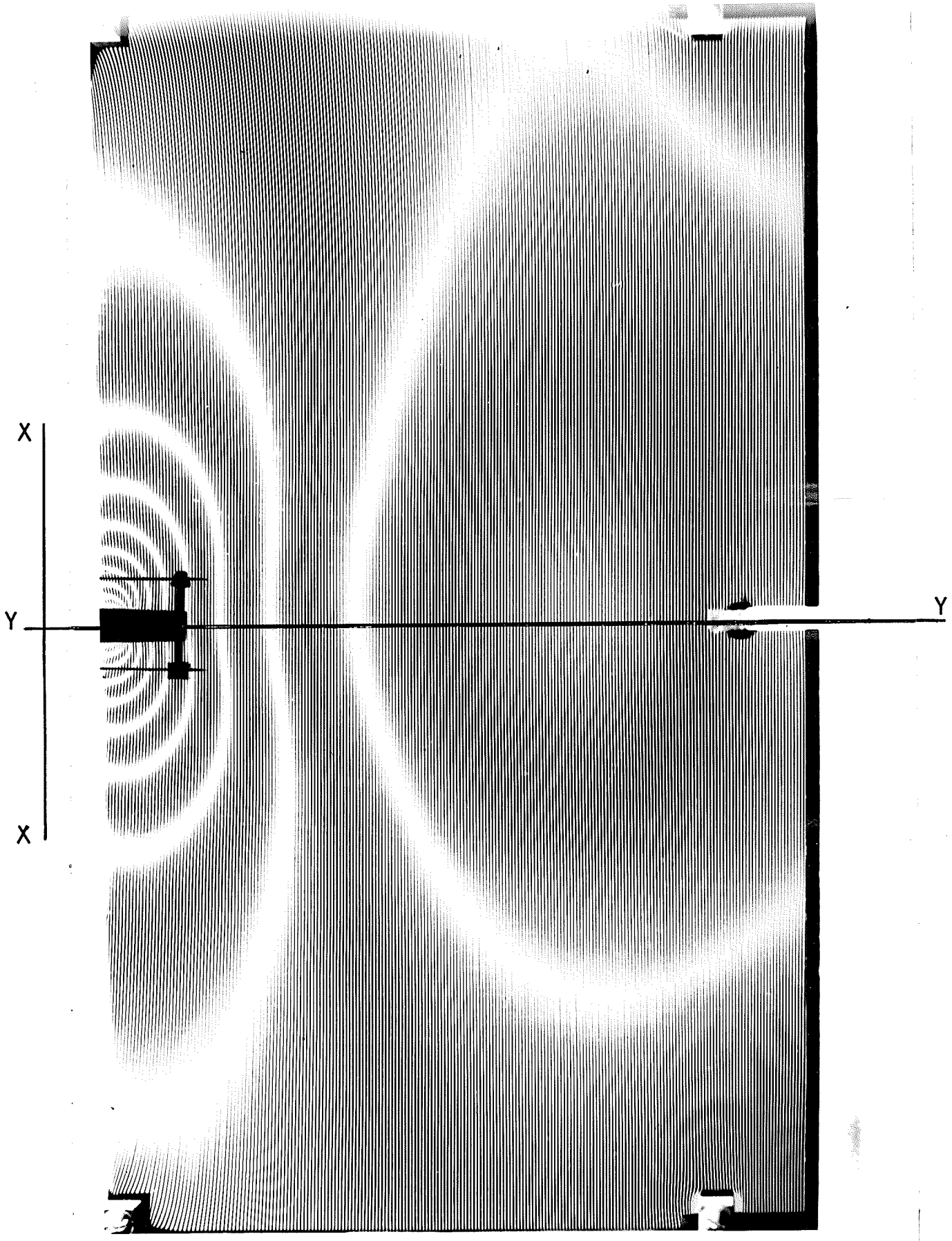

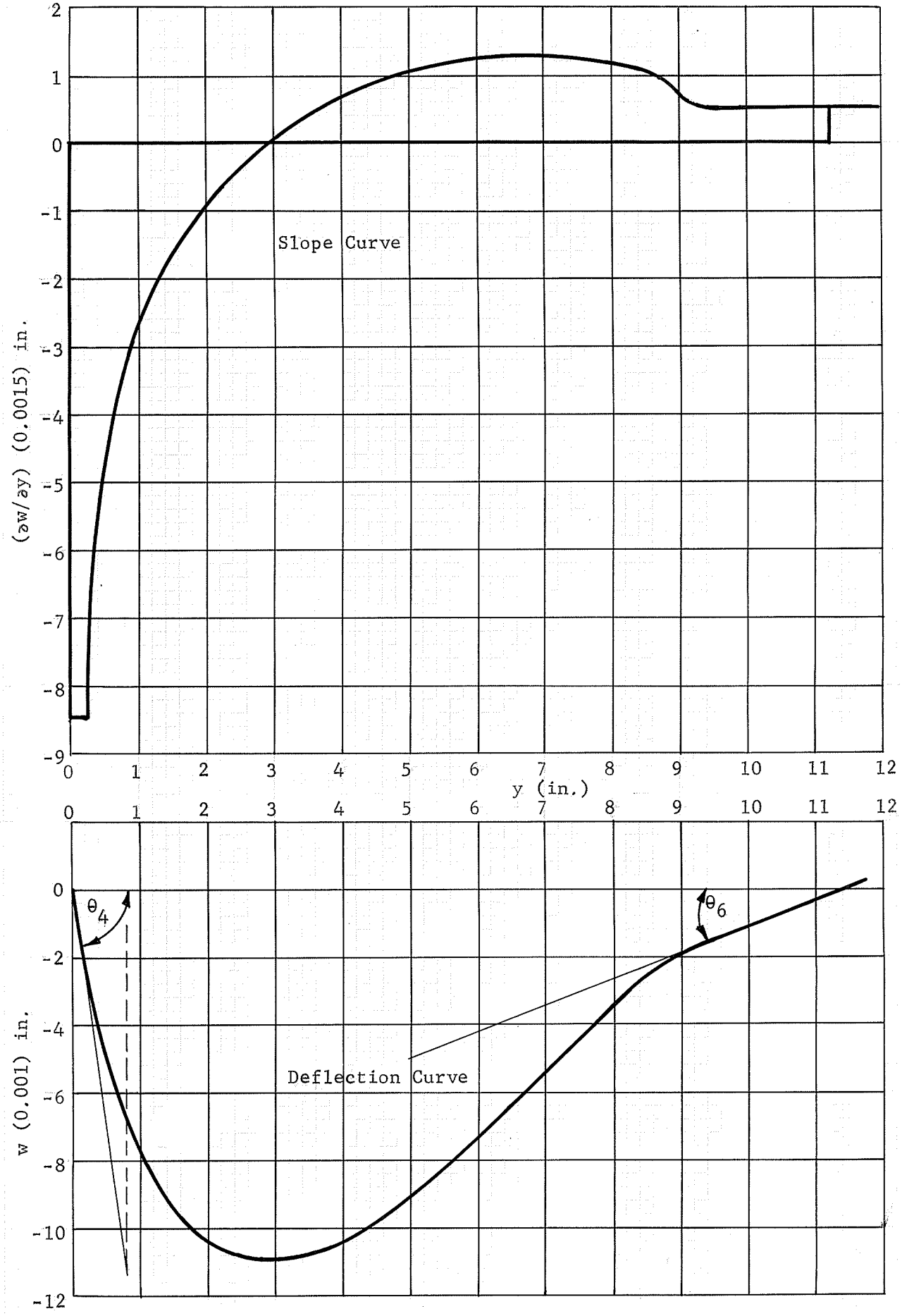

Fig. A - 18 Slope and Deflection Curves Model P2 Load Type D.

$y_1 - y_2$ in.	$\int_{y_2}^{y_1} (\partial w/\partial y)\, dy$ in.	$\sum \int_{y_2}^{y_1} (\partial w/\partial y)\, dy$ in.
0 - 1	-0.00792	-0.00792
1 - 2	-0.00252	-0.01044
2 - 2.9	-0.00060	-0.01104
2.9 - 4	0.000585	-0.010455
4 - 5	0.001335	-0.009120
5 - 6	0.00177	-0.00735
6 - 7	0.00195	-0.00542
7 - 8	0.001905	-0.003495
8 - 9	0.00156	-0.001935
9 - 10	0.00081	-0.001125
10 - 11	0.00075	-0.000375
11 - 11.25	0.00018	-0.000195

M_4 = 15 lb.-in., θ_4 = 0.0143 rad., θ_6 = 0.000775 rad.

M_2 = 60 lb.-in., θ_2 = 0.004 rad., θ_5 = 0.0089 rad.

Slope and Deflection Calculations Model P2 Load Type D

TABLE A - 8

Carry - Over Factors Calculations.

$$C_{interior} = \frac{2 M_4 \ \theta_2}{M_2 \ \theta_4} = \frac{2 \times 15 \times 0.004}{60 \times 0.0143} = 0.14$$

$$C_{exterior} = \frac{M_2 \ \theta_6}{M_4 \ \theta_5} = \frac{60 \times 0.000775}{15 \times 0.0089}$$

$$= 0.348$$

Fig. A - 19 Photograph of Model P3 Load Type A.

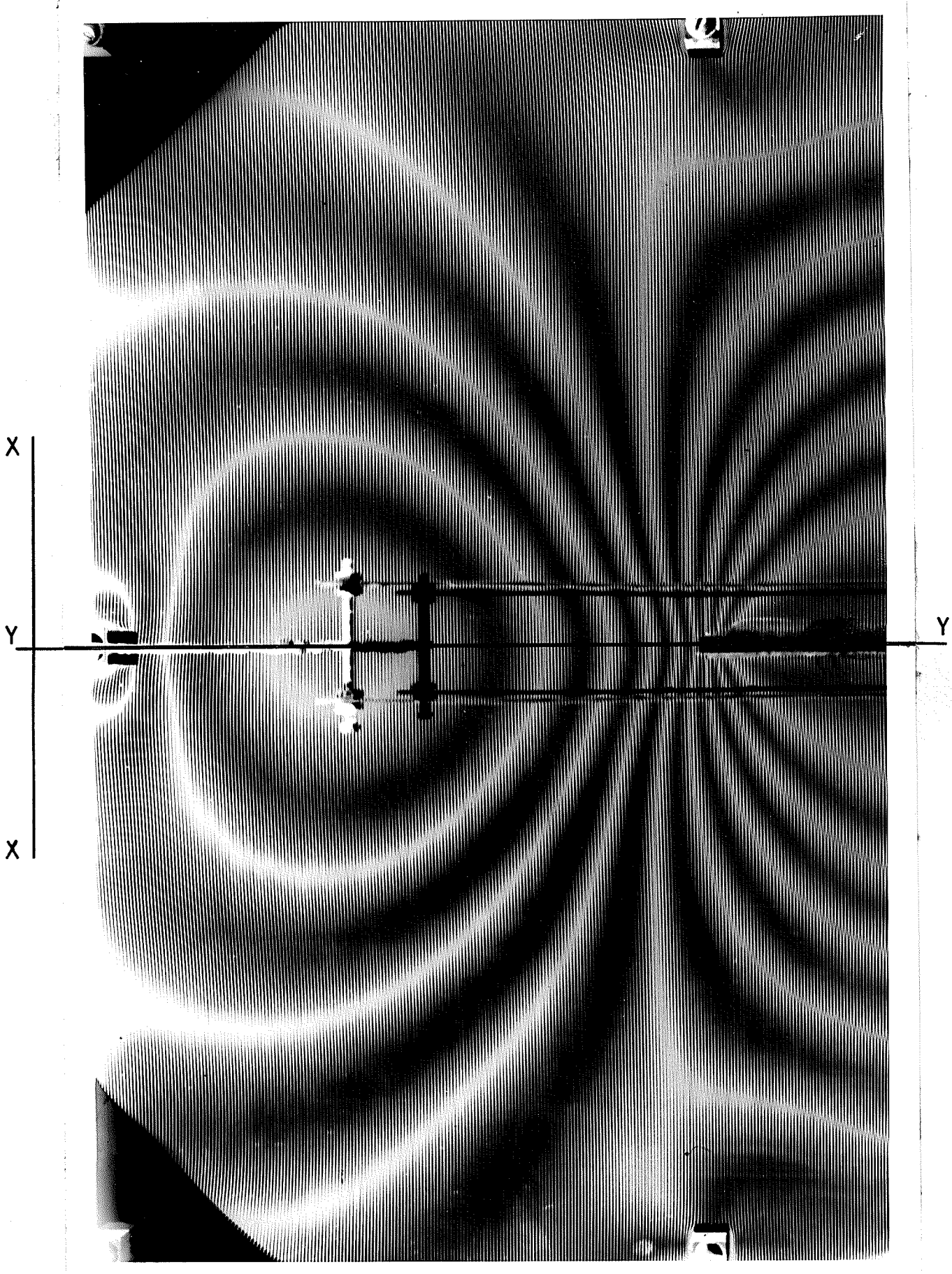

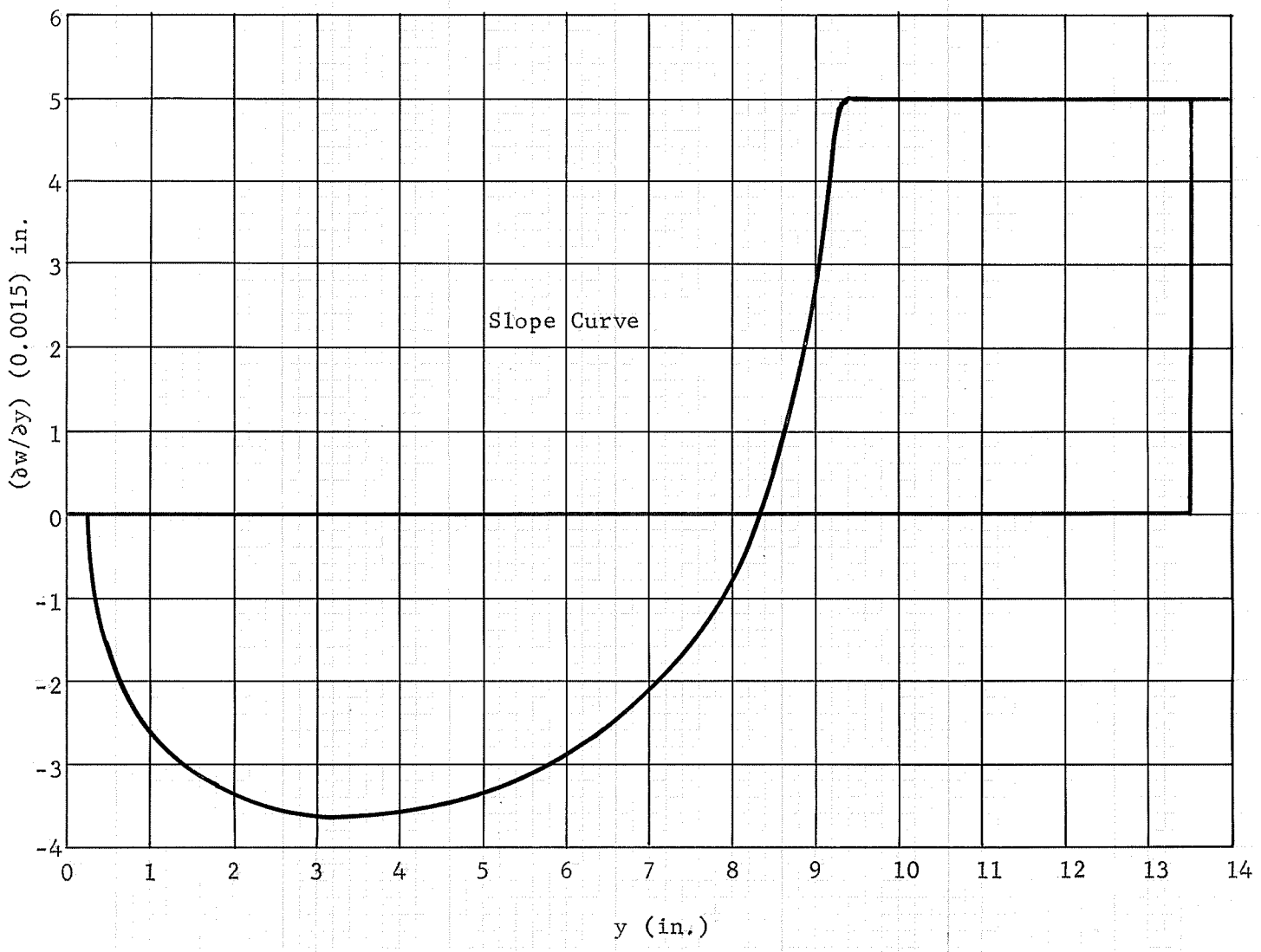

Fig. A - 20 Slope and Deflection Curves

Model P3 Load Type A.

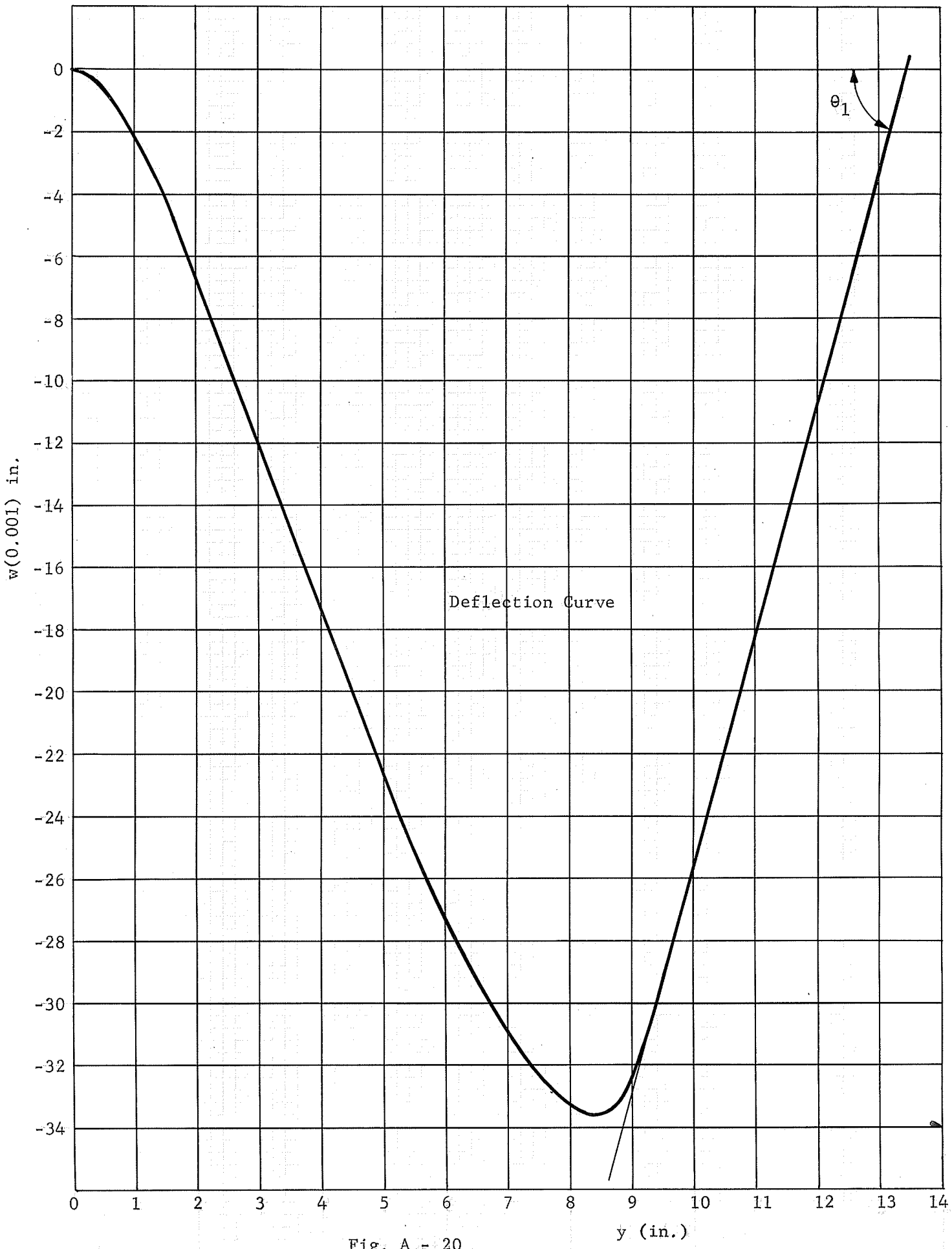
0
-2
-4
-6
-8
-10
-12
-14
-16
-18
-20
-22
-24
-26
-28
-30
-32
-34
w(0.001) in.
Deflection Curve
θ_1
0
1
2
3
4
5
6
7
8
9
10
11
12
13
14
y (in.)

Fig. A - 20

$y_1 - y_2$ in.	$\int_{y_2}^{y_1} (\partial w/\partial y)\, dy$ in.	$\sum \int_{y_2}^{y_1} (\partial w/\partial y)\, dy$ in.
0 - 1	-0.00208	-0.00208
1 - 2	-0.00457	-0.00665
2 - 3	-0.00528	-0.01193
3 - 4	-0.00540	-0.01733
4 - 5	-0.00523	-0.02256
5 - 6	-0.00473	-0.02729
6 - 7	-0.00380	-0.03109
7 - 8	-0.00231	-0.03340
8 - 8.35	-0.000255	-0.033655
8.35 - 9	0.00100	-0.032655
9 - 10	0.00680	-0.025855
10 - 11	0.00750	-0.018355
11 - 12	0.00750	-0.010855
12 - 13	0.00750	-0.003355
13 - 13.5	0.00375	0.000395

M_1 = 120 lb.-in., θ_1 = 0.0075 rad.

Slope and Deflection Calculations Model P3 Load Type A.

TABLE A - 9

Stiffness and Effective Width Calculations.

$$K = \frac{M_1}{\theta_1} = 16{,}000 \text{ lb.-in./rad.}$$

$$L_y = \frac{3 K L_x}{E h^3} = \frac{3 \times 16{,}000 \times 9}{441{,}000 \times (0.243)^3}$$

$$= 69.00 \text{ in.}$$

Fig. A - 21 Photograph of Model P3 Load Type B.

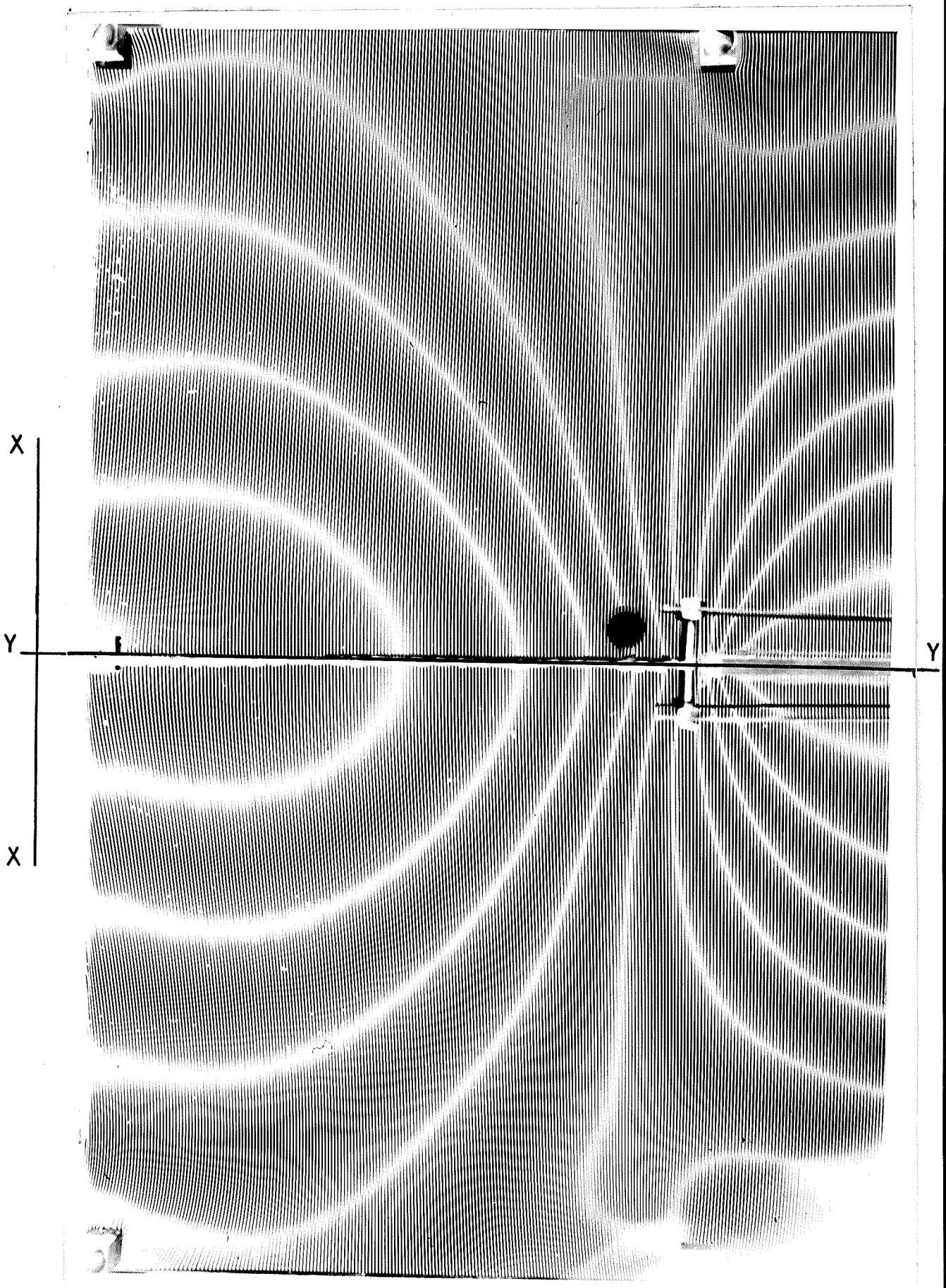

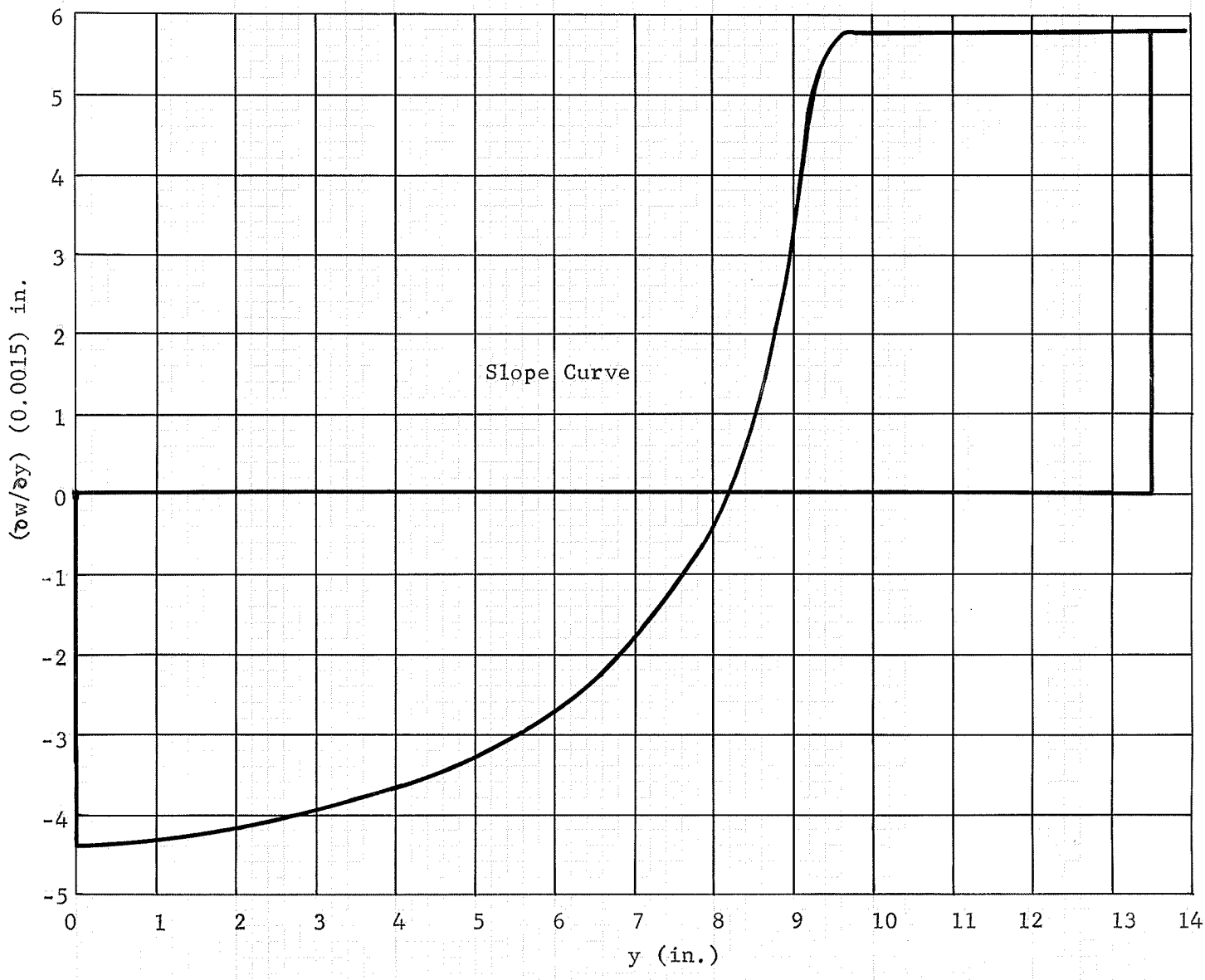

Fig. A - 22 Slope and Deflection Curves

Model P3 Load Type B

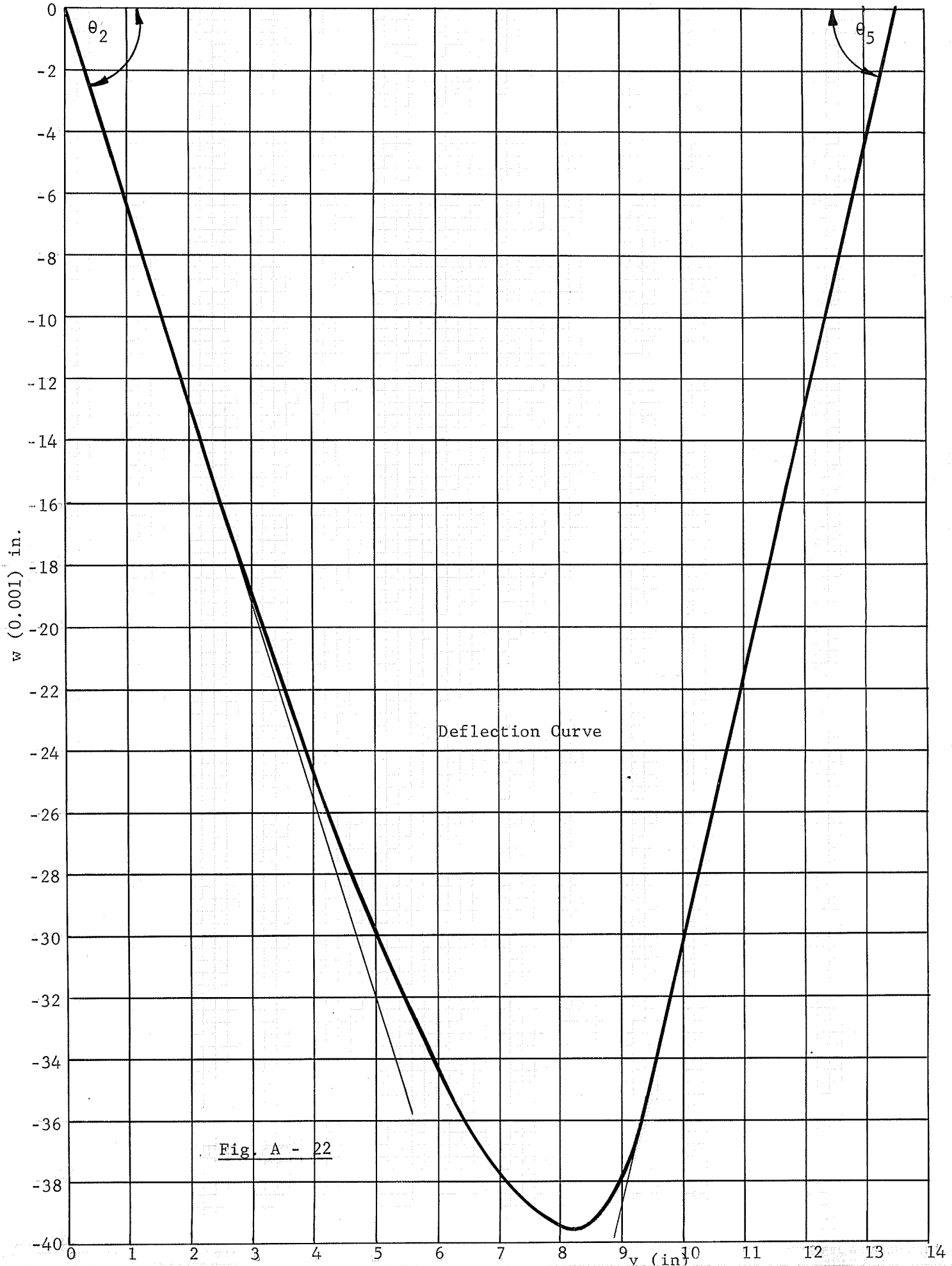
θ2
θ5
0
-2
-4
-6
-8
-10
-12
-14
-16
-18
-20
-22
-24
-26
-28
-30
-32
-34
-36
-38
-40
w (0.001) in.
0
1
2
3
4
5
6
7
8
9
10
11
12
13
14
v (in)
Deflection Curve

Fig. A - 22

$y_1 - y_2$ in.	$\int_{y_2}^{y_1} (\partial w/\partial y)\, dy$ in.	$\sum \int_{y_2}^{y_1} (\partial w/\partial y)\, dy$ in.
0 - 1	-0.00653	-0.00653
1 - 2	-0.00635	-0.01288
2 - 3	-0.00608	-0.01896
3 - 4	-0.00570	-0.02466
4 - 5	-0.00522	-0.02988
5 - 6	-0.00450	-0.03438
6 - 7	-0.00344	-0.03782
7 - 8.2	-0.00186	-0.03968
8.2 - 9	0.00156	-0.03812
9 - 10	0.00780	-0.03032
10 - 11	0.00870	-0.02162
11 - 12	0.00870	-0.01292
12 - 13	0.00870	-0.00422
13 - 13.5	0.00435	-0.00013

M_2 = 120 lb.-in., θ_2 = 0.00636 rad., θ_5 = 0.00808 rad.

Slope and Deflection Calcuations Model P3 Load Type B

TABLE A - 10

Fig. A - 23 Photograph of Model P3 Load Type C.

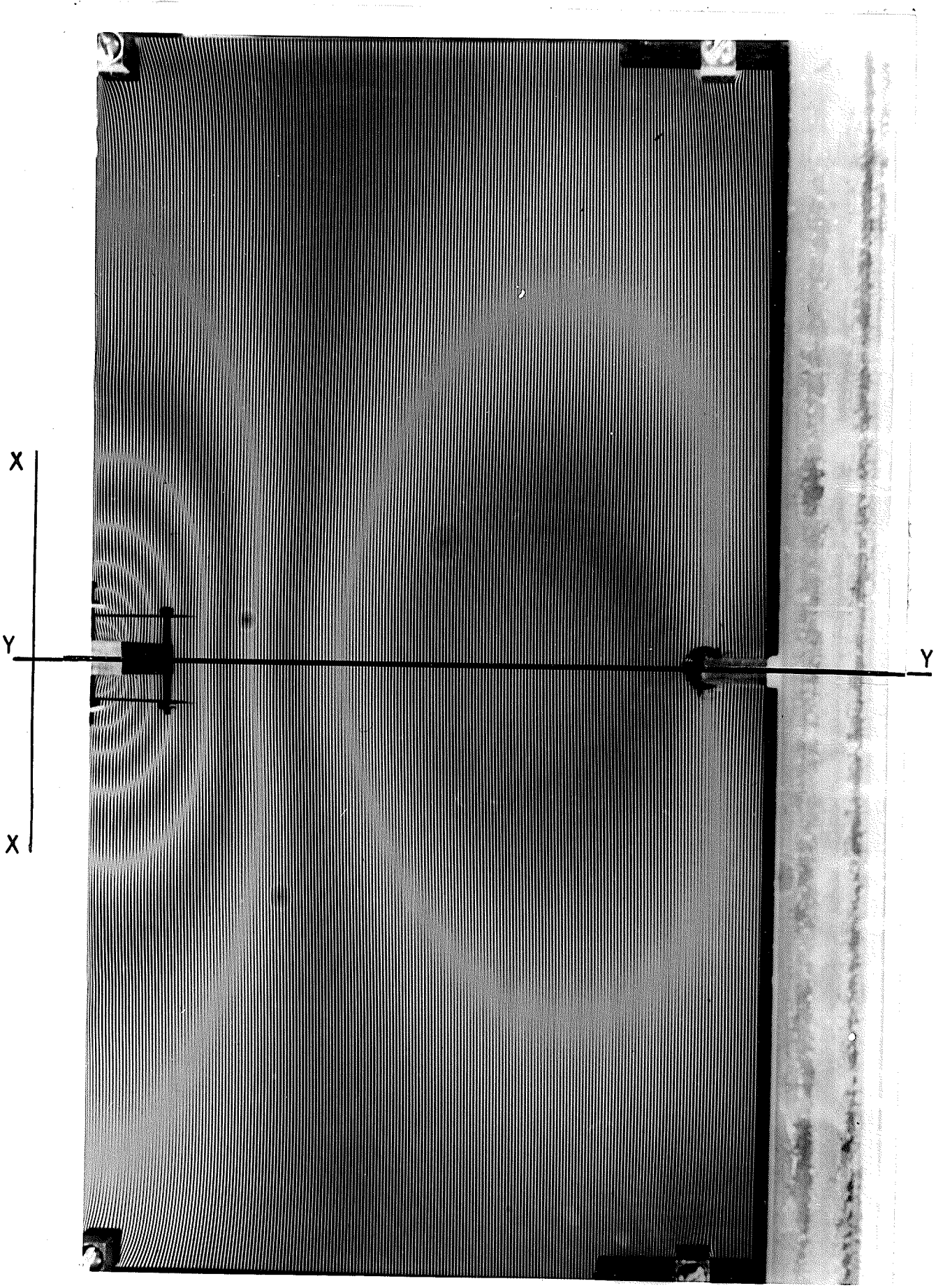

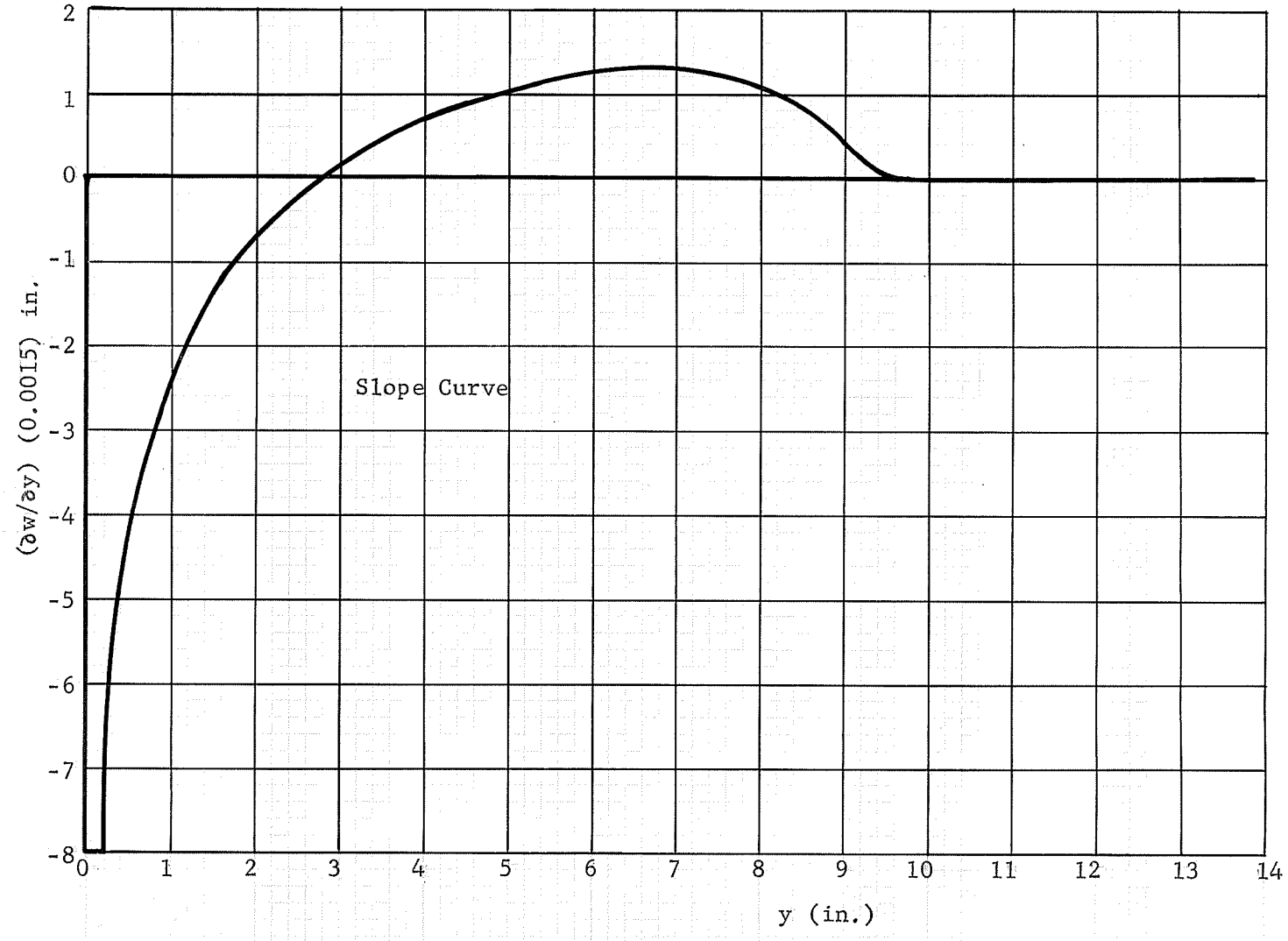

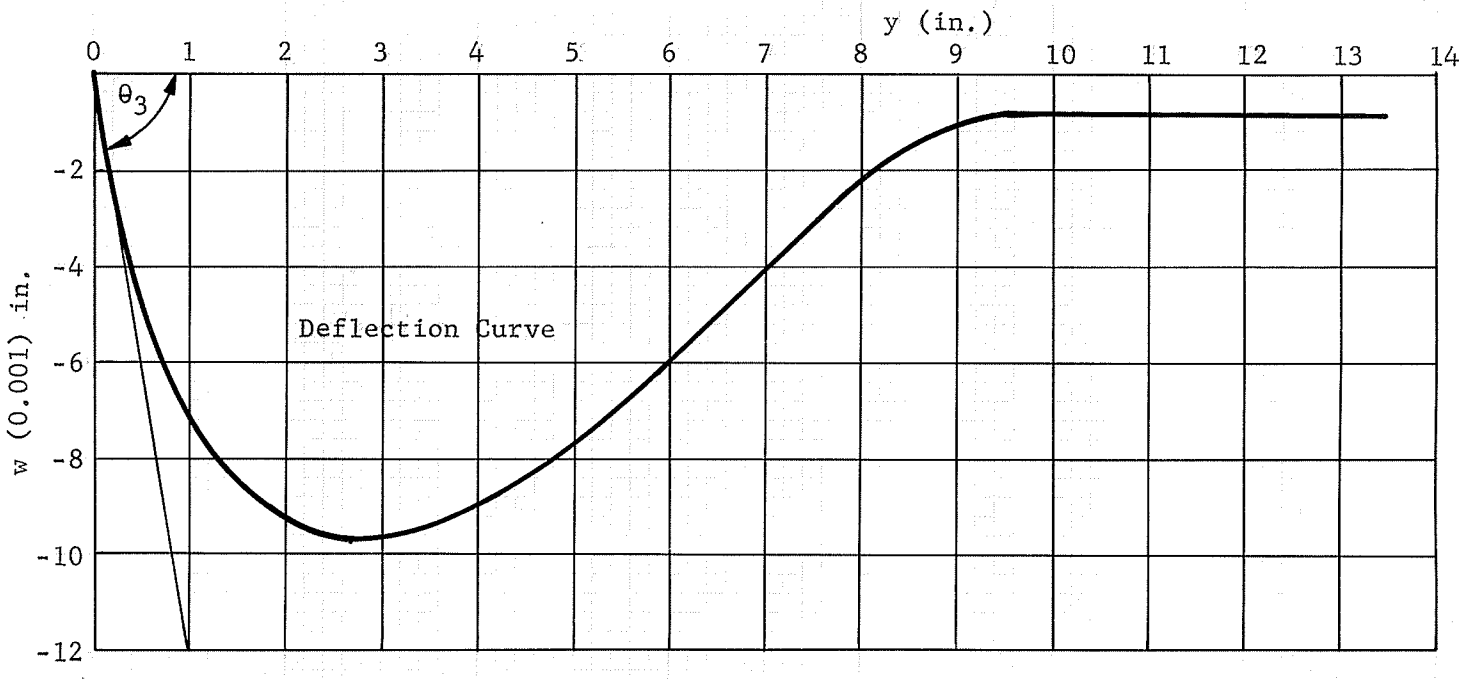

Fig. A - 24 Slope and Deflection Curves Model P3 Load Type C.

$y_1 - y_2$ in.	$\int_{y_2}^{y_1} (\partial w/\partial y)\, dy$ in.	$\sum \int_{y_2}^{y_1} (\partial w/\partial y)\, dy$ in.
0 - 1	-0.00722	-0.00722
1 - 2	-0.00214	-0.00936
2 - 2.75	-0.00075	-0.009735
2.75 - 4	0.000585	-0.009150
4 - 5	0.00132	-0.00783
5 - 6	0.00175	-0.00608
6 - 7	0.00195	-0.00413
7 - 8	0.00186	-0.00227
8 - 9.6	0.001422	-0.000848

M_3 = 15 lb.-in., θ_3 = 0.0012 rad.

Slope and Deflection Calculations Model P3 Load Type C.

TABLE A - 11

Stiffness and Effective Width Calculations.

$$K = \frac{M_3}{\theta_3} = 1250 \text{ lb.-in./rad.}$$

$$L_y = \frac{3 K L_x}{E h^3}$$

$$= \frac{3 \times 1250 \times 9}{441{,}000 \times (0.243)^3}$$

$$= 5.40 \text{ in.}$$

Fig. A - 25 Photograph of Model P3 Load Type D.

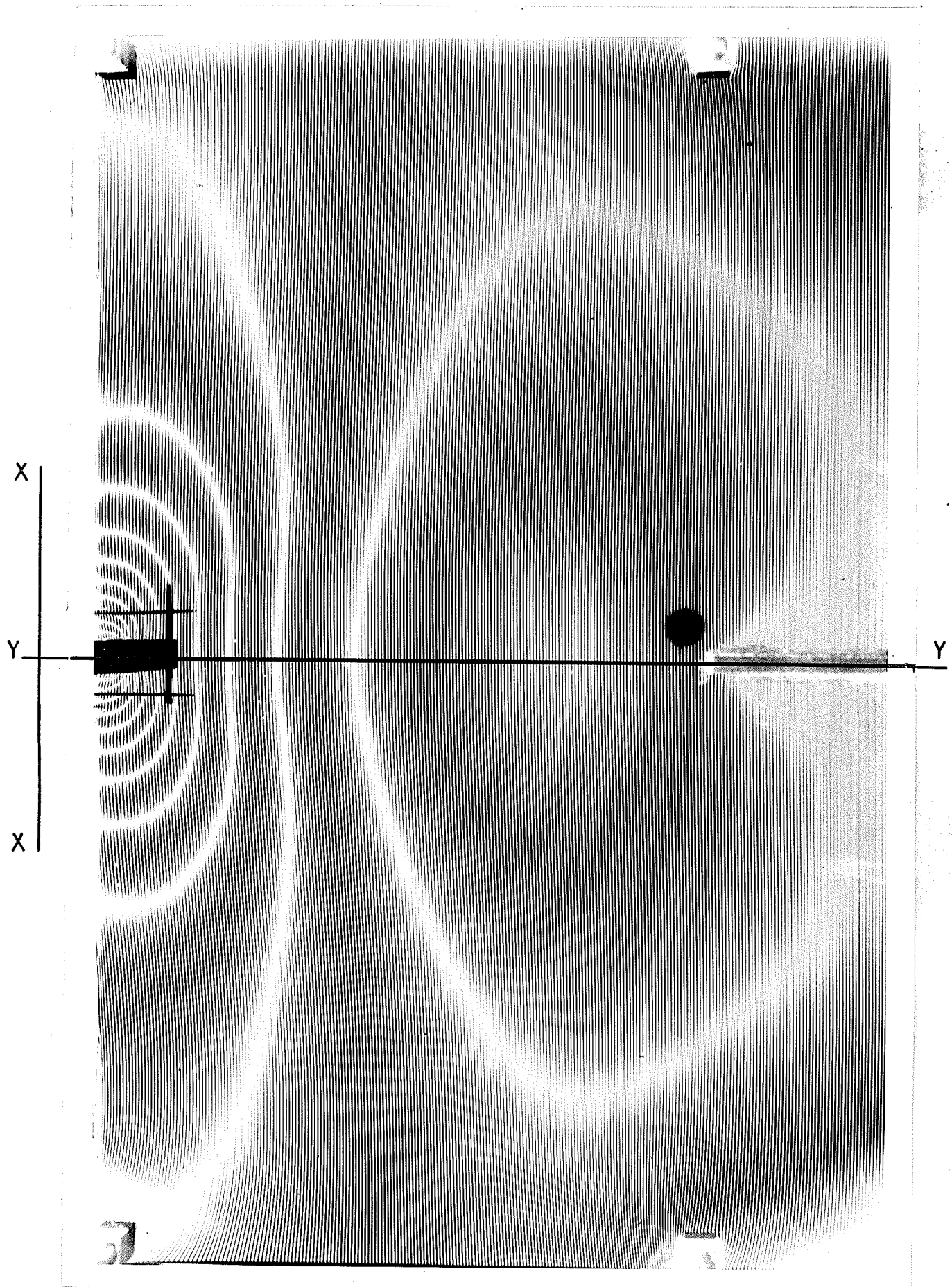

Fig. A - 26 Slope and Deflection Curves Model P3 Load Type D.

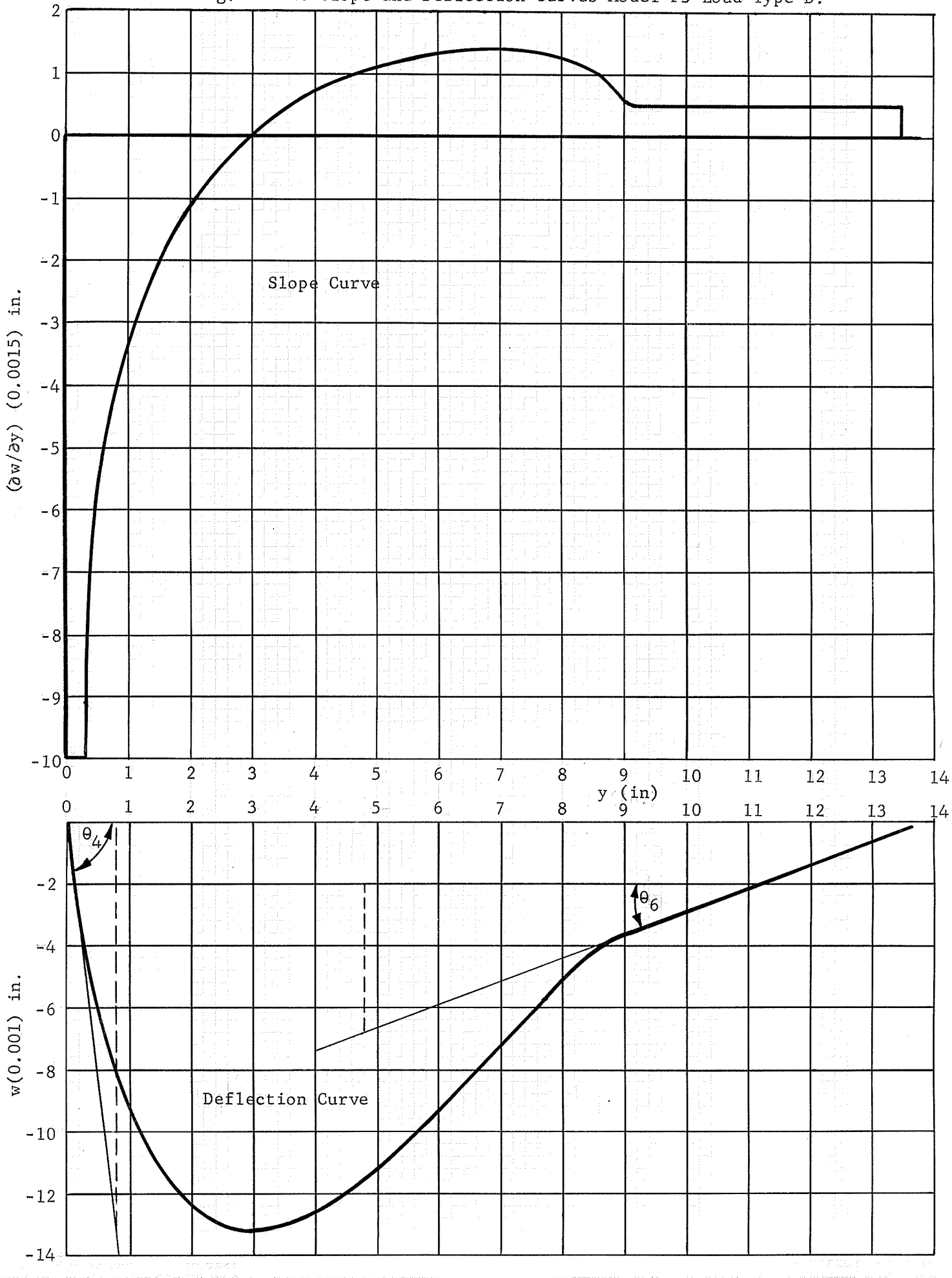

$y_1 - y_2$ in.	$\int_{y_2}^{y_1} (\partial w/\partial y)\, dy$ in.	$\sum \int_{y_2}^{y_1} (\partial w/\partial y)\, dy$ in.
0 - 1	-0.00940	-0.00940
1 - 2	-0.00312	-0.01252
2 - 2.95	-0.000705	-0.013225
2.95 - 4	0.00060	-0.012625
4 - 5	0.00141	-0.011215
5 - 6	0.001875	-0.009340
6 - 7	0.00210	-0.00724
7 - 8	0.00207	-0.00517
8 - 9	0.00156	-0.00361
9 - 10	0.00075	-0.00286
10 - 11	0.00075	-0.00211
11 - 12	0.00075	-0.00136
12 - 13	0.00075	-0.00061
13 - 13.5	0.000375	-0.000235

M_4 = 15 lb.-in., θ_4 = 0.0175 rad., θ_6 = 0.00075 rad.

M_2 = 120 lb.-in., θ_2 = 0.00636 rad., θ_5 = 0.00808 rad.

Slope and Deflection Calcuations Model P3 Load Type D.

TABLE A - 12

Carry - Over Factors Calculations.

$$C_{interior} = \frac{2 M_4\, \theta_2}{M_2\, \theta_4} = \frac{15 \times 0.00636 \times 2}{120 \times 0.0175} = 0.091$$

$$C_{exterior} = \frac{M_2\, \theta_6}{M_4\, \theta_5} = \frac{120 \times 0.00075}{15 \times 0.00808} = 0.743$$

Fig. A - 27 Photograph of Model P4 Load Type A.

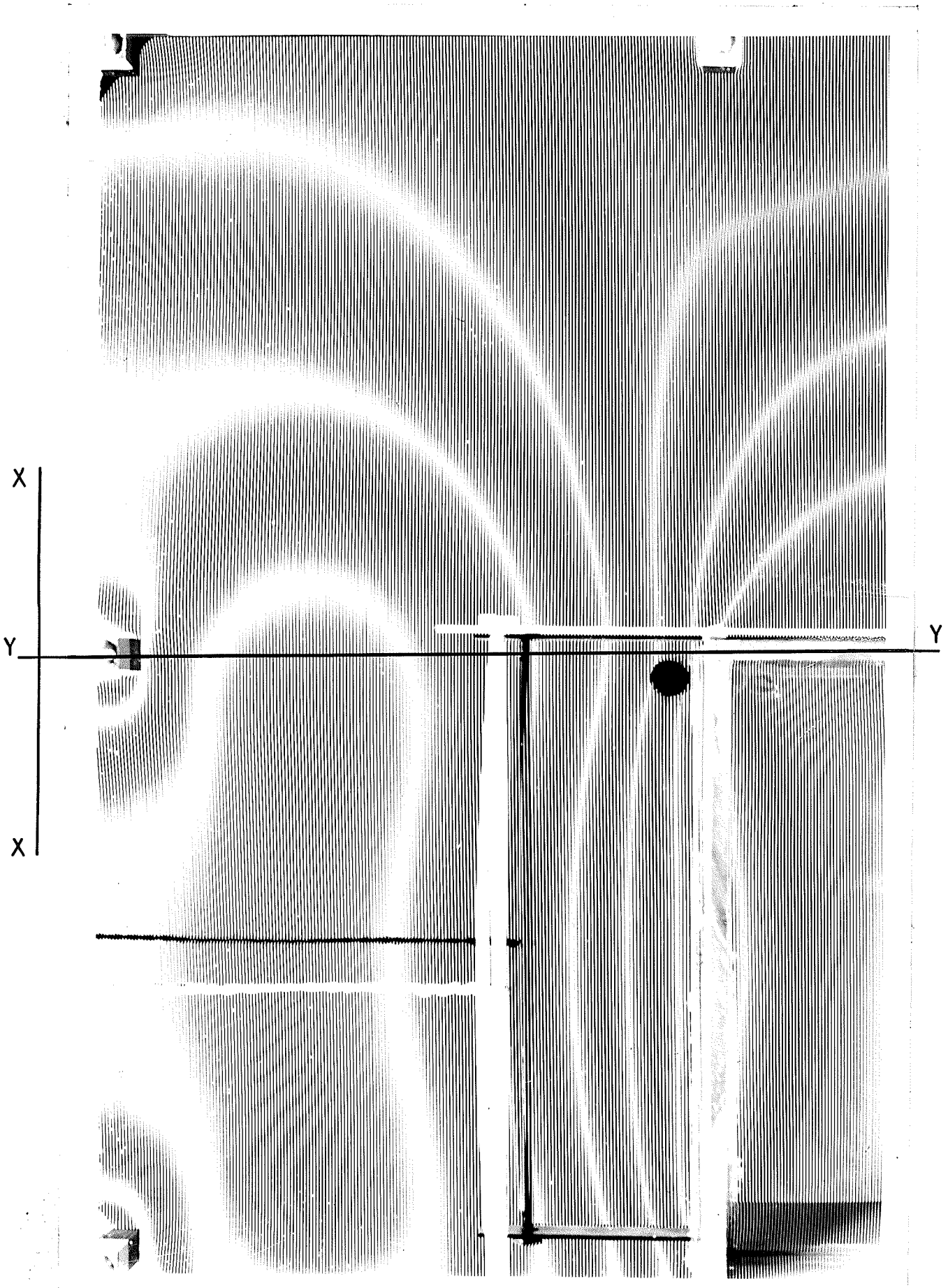

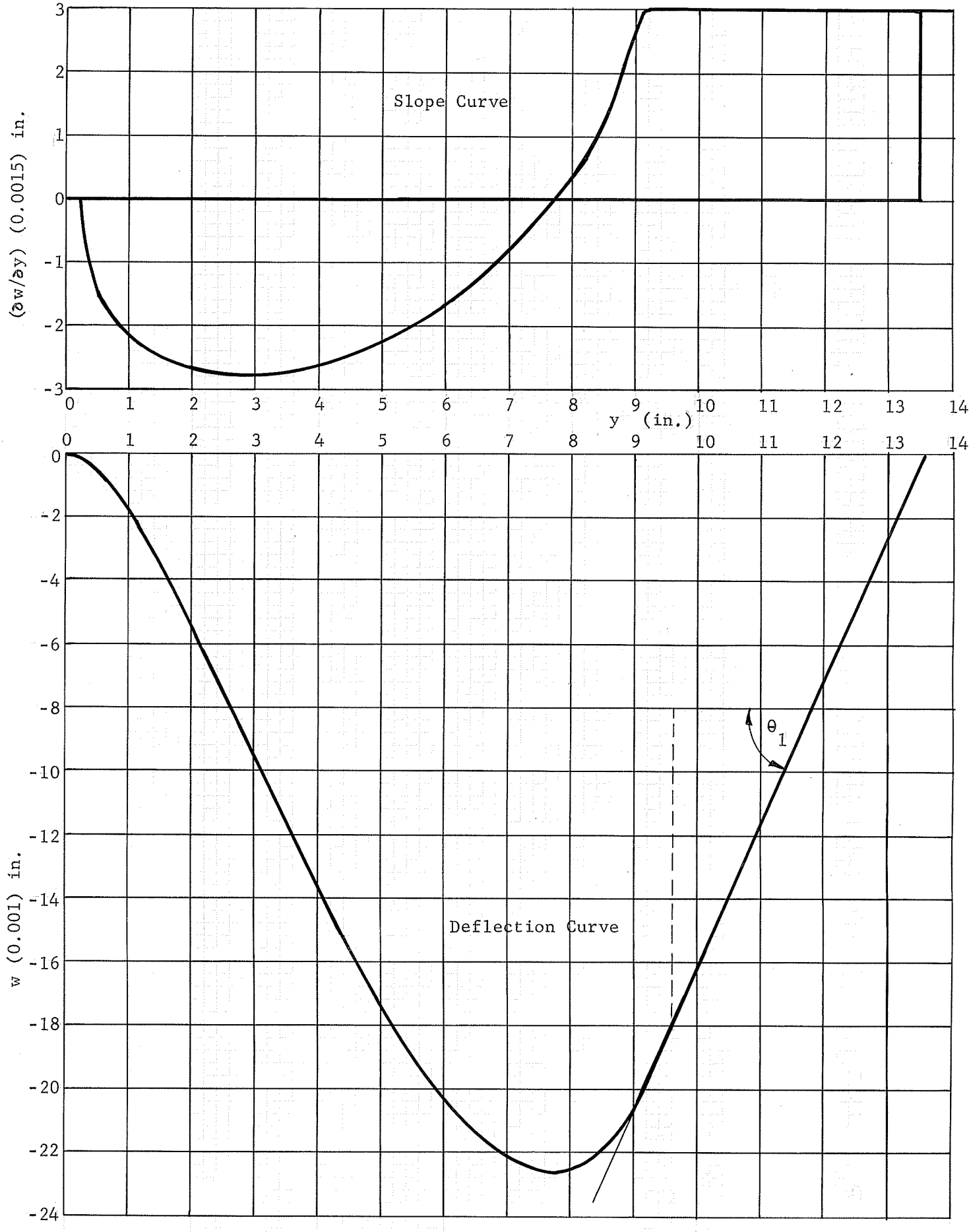

Fig. A - 28 Slope and Deflection Curves Model P4 Load Type A.

$y_1 - y_2$ in.	$\int_{y_2}^{y_1} (\partial w/\partial y)\, dy$ in.	$\sum \int_{y_2}^{y_1} (\partial w/\partial y)\, dy$ in.
0 - 1	-0.001815	-0.001815
1 - 2	-0.003720	-0.005535
2 - 3	-0.004140	-0.009675
3 - 4	-0.004110	-0.013785
4 - 5	-0.003675	-0.017460
5 - 6	-0.002855	-0.020315
6 - 7	-0.001905	-0.022220
7 - 7.75	-0.000480	-0.022700
7.75 - 9	0.001980	-0.020720
9 - 10	0.004470	-0.016250
10 - 11	0.004500	-0.011750
11 - 12	0.004500	-0.007250
12 - 13	0.004500	-0.002750
13 - 13.5	0.002250	-0.000500
M_1 = 120 lb.-in.		θ_1 = 0.0045 rad.

Slope and Deflection Calculations Model P4 Load Type A.

TABLE A - 13

Stiffness and Effective Width Calculations.

$$K = \frac{M_1}{\theta_1} = 26{,}650 \text{ lb.-in/rad.}$$

$$L_y = \frac{3 K L_x}{E h^3} = \frac{3 \times 26{,}650 \times 9}{441{,}000 \times (0.243)^3}$$

$$= 115.00 \text{ in.}$$

Fig. A - 29 Photograph of Model P4 Load Type B.

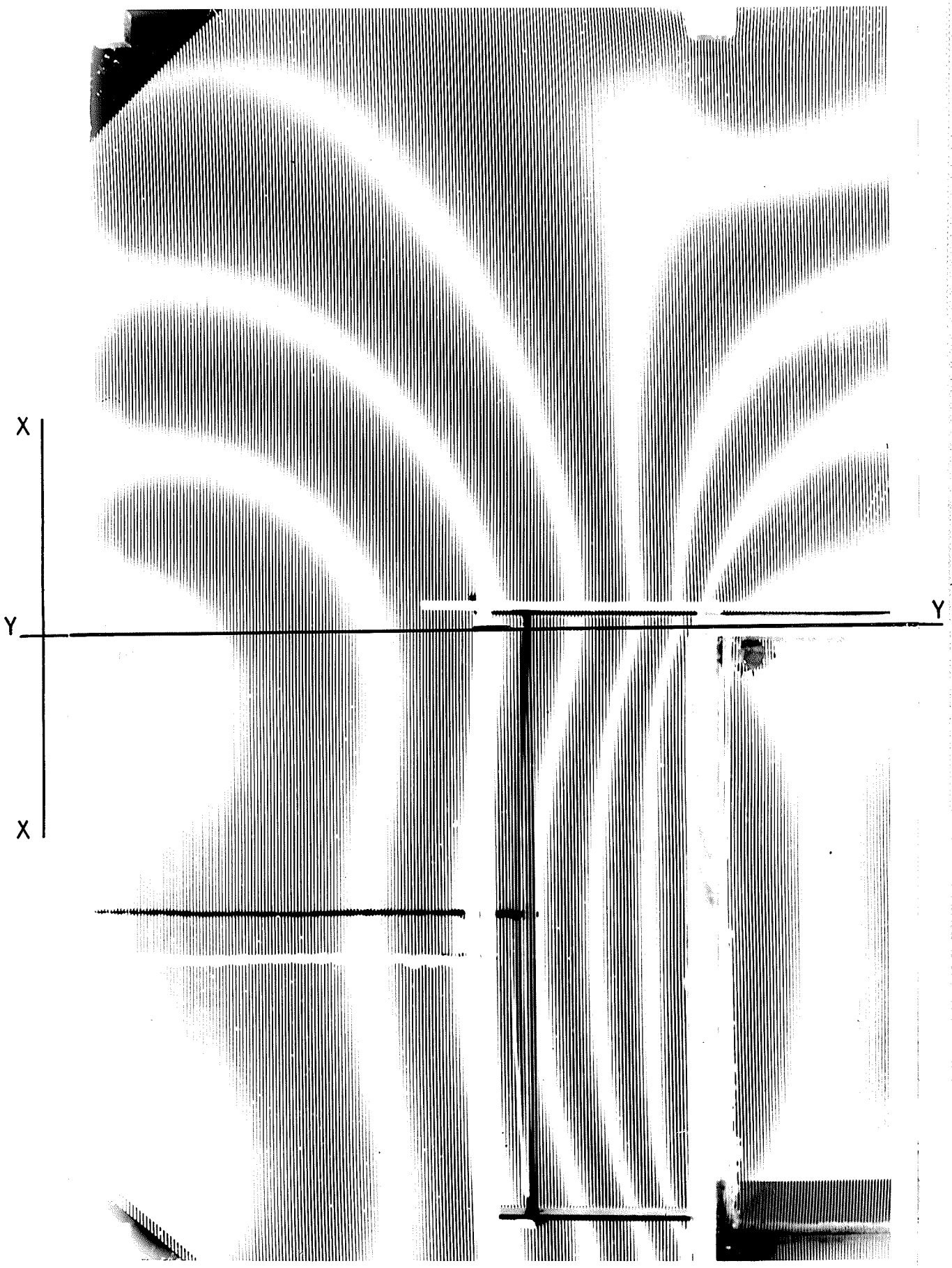

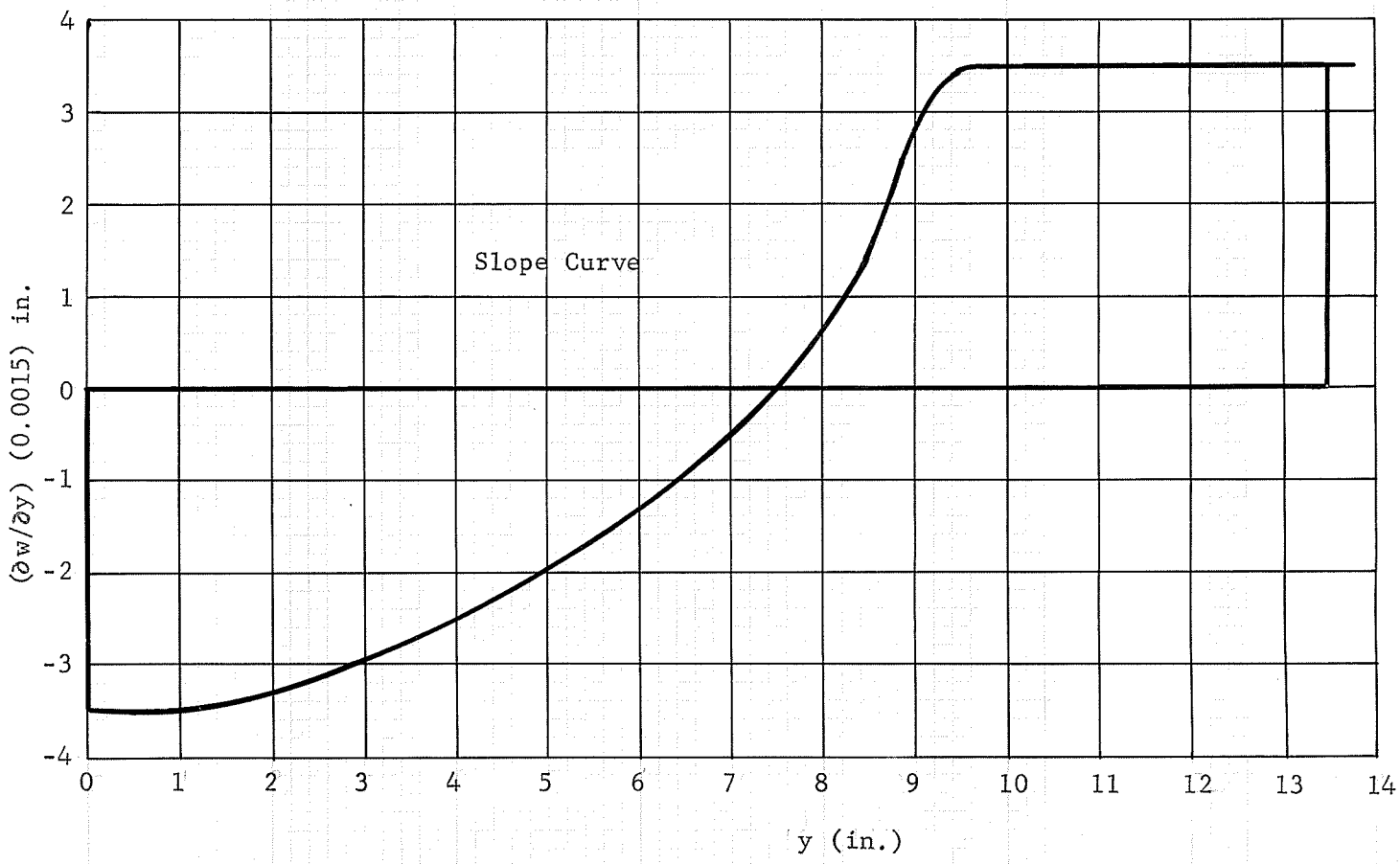

Fig. A - 30 Slope and Deflection Curves

Model P4 Load Type B.

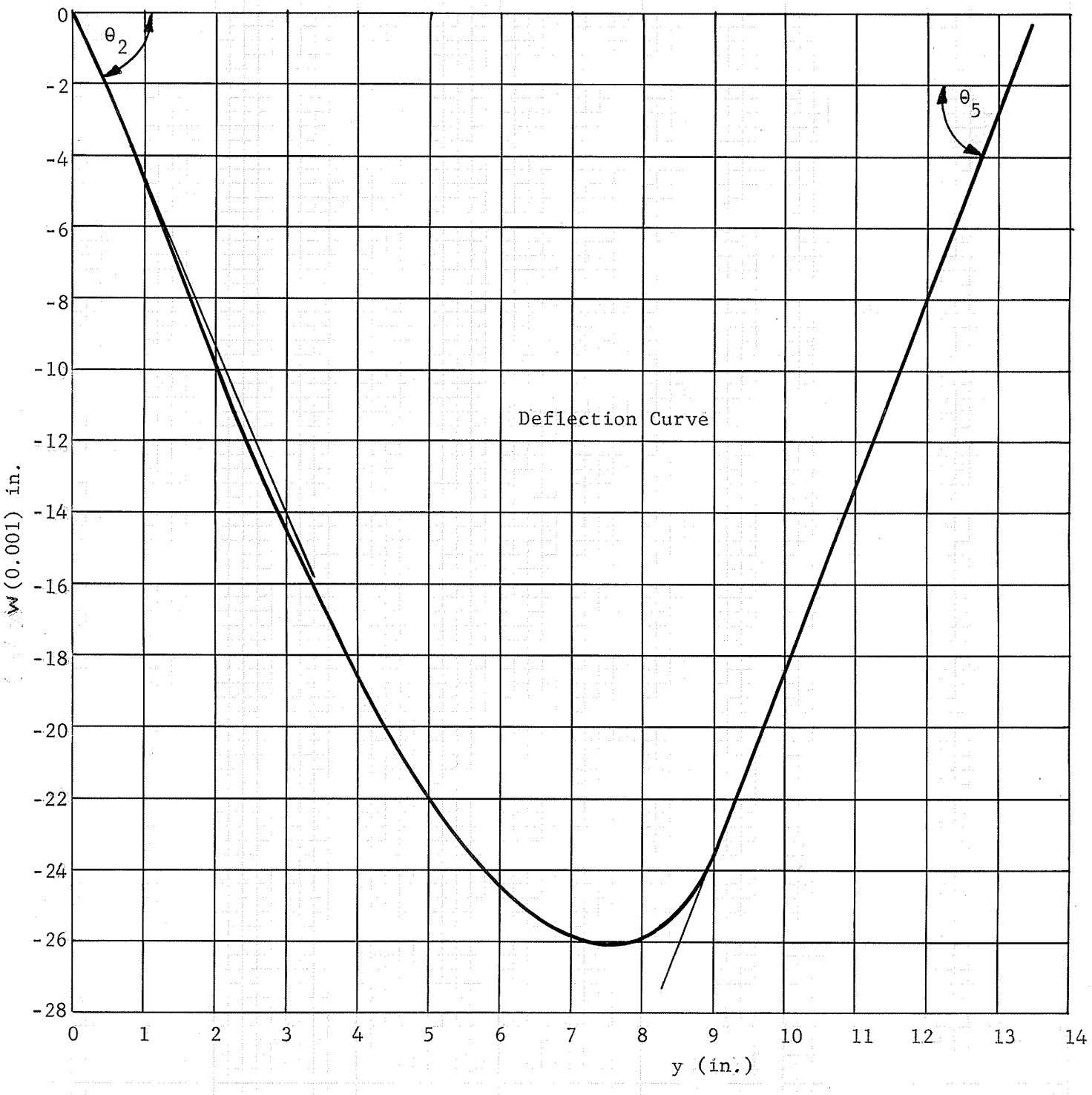
θ2
θ5
Deflection Curve
w(0.001) in.
y (in.)
0
-2
-4
-6
-8
-10
-12
-14
-16
-18
-20
-22
-24
-26
-28
0
1
2
3
4
5
6
7
8
9
10
11
12
13
14

Fig. A - 30

$y_1 - y_2$ in.	$\int_{y_2}^{y_1} (\partial w/\partial y)\, dy$ in.	$\sum \int_{y_2}^{y_1} (\partial w/\partial y)\, dy$ in.
0 - 1	-0.00472	-0.00472
1 - 2	-0.00515	-0.00987
2 - 3	-0.00470	-0.01457
3 - 4	-0.00410	-0.01867
4 - 5	-0.00338	-0.02050
5 - 6	-0.00250	-0.02455
6 - 7	-0.00141	-0.02596
7 - 7.5	-0.000195	-0.026155
7.5 - 8	0.000195	-0.02596
8 - 9	0.00299	-0.02367
9 - 10	0.00502	-0.01865
10 - 11	0.00525	-0.01340
11 - 12	0.00535	-0.00185
12 - 13	0.00525	-0.00295
13 - 13.5	0.00262	-0.00033

M_2 = 120 lb.-in., θ_2 = 0.00467 rad., θ_5 = 0.0059 rad.

Slope and Deflection Calculations Model P4 Load Type B

TABLE A - 14

Fig. A - 31 Photograph of Model P4 Load Type C.

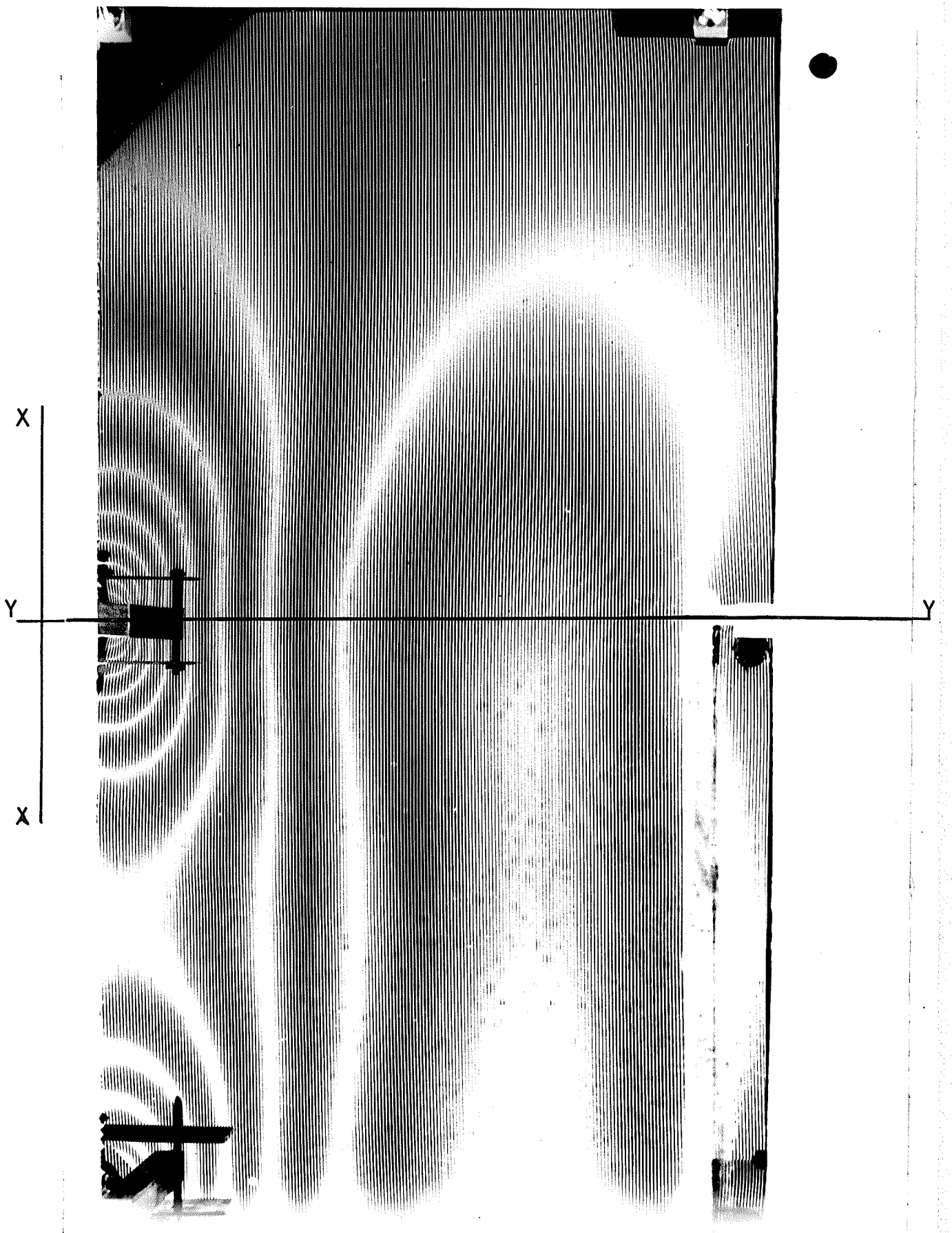

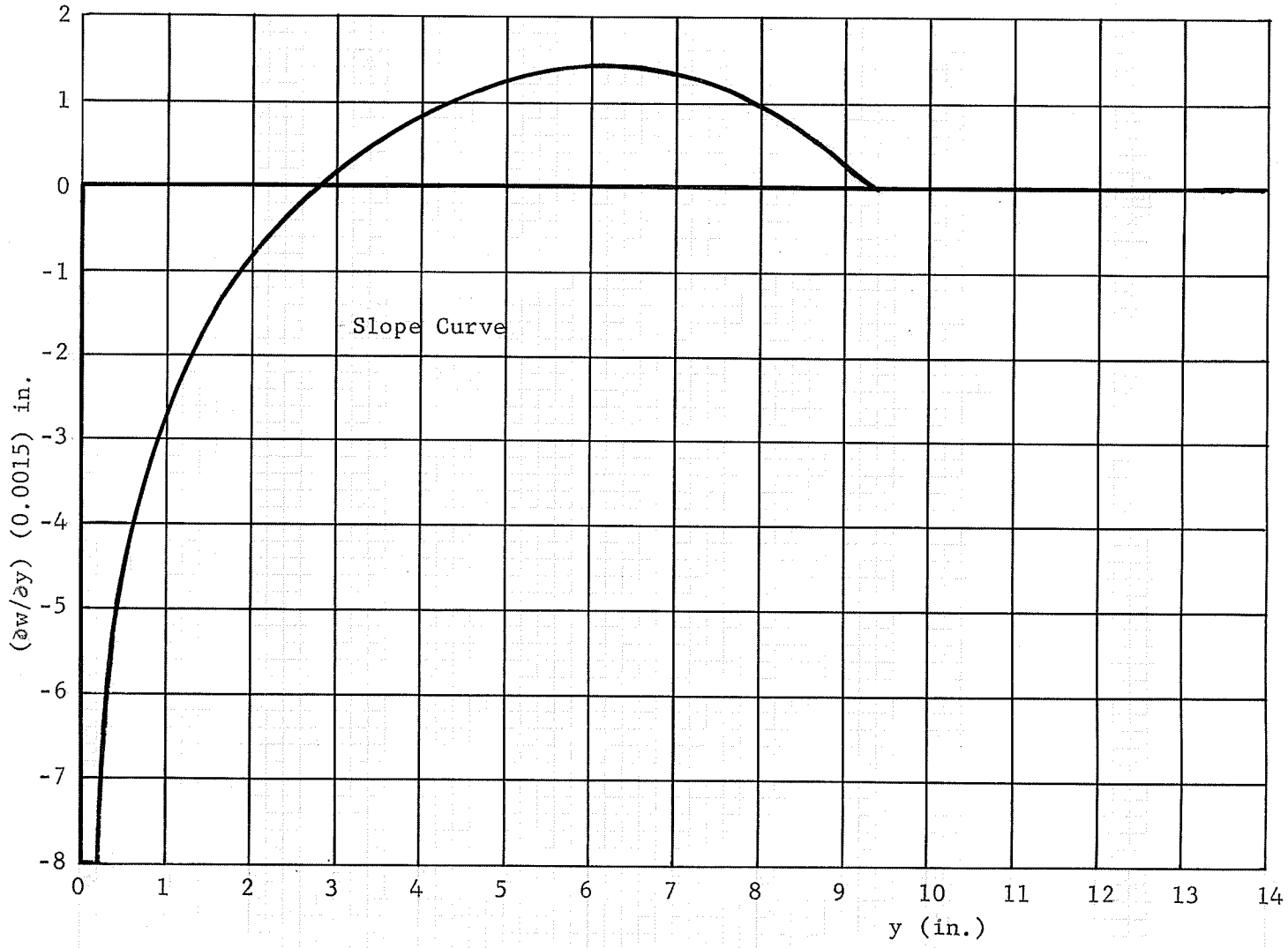

Fig. A - 32 Slope and Deflection Curves Model P4 Load Type C.

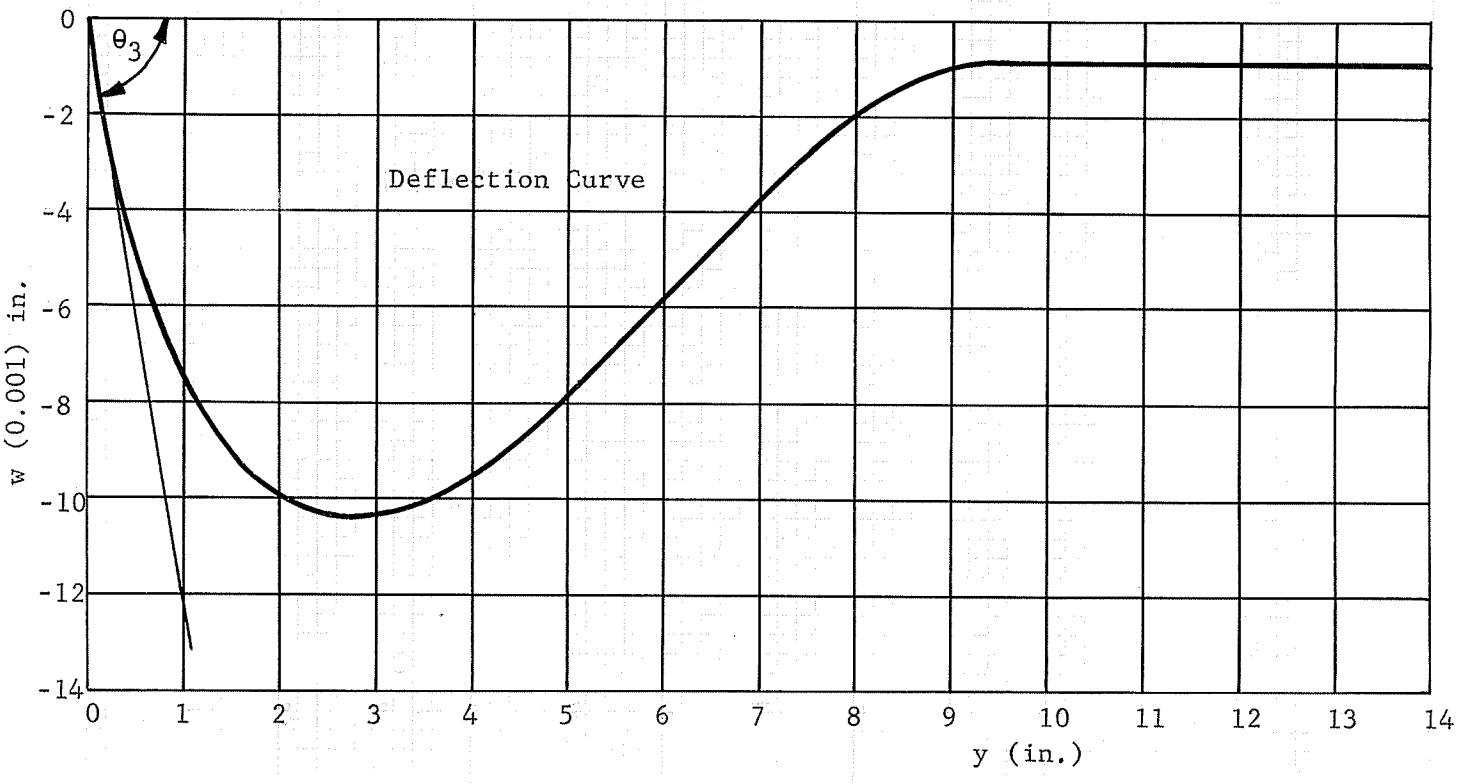

$y_1 - y_2$ in.	$\int_{y_2}^{y_1} (\partial w/\partial y)\, dy$ in.	$\sum \int_{y_2}^{y_1} (\partial \bar{w}/\partial y)\, dy$ in.
0 - 1	-0.00758	-0.00758
1 - 2	-0.00247	-0.01005
2 - 2.75	-0.000435	-0.010485
2.75 - 4	-0.000855	-0.00963
4 - 5	0.00165	-0.00798
5 - 6	0.00207	-0.00591
6 - 7	0.00217	-0.00374
7 - 8	0.00181	-0.00193
8 - 9.3	0.00111	-0.00082
M_3 = 15 lb.-in.,		θ_3 = 0.012 rad.

Slope and Deflection Calculations Model P4 Load Type C.

TABLE A - 15

Stiffness and Effective Width Calculations.

$$K = \frac{M_3}{\theta_3} = 1250 \text{ lb.-in./rad.}$$

$$L_y = \frac{3 K L_y}{E h^3}$$

$$= \frac{3 \times 1250 \times 9}{441{,}000 \times (0.243)^3}$$

$$= 5.40 \text{ in.}$$

Fig. A - 33 Photograph of Model P4 Load Type D.

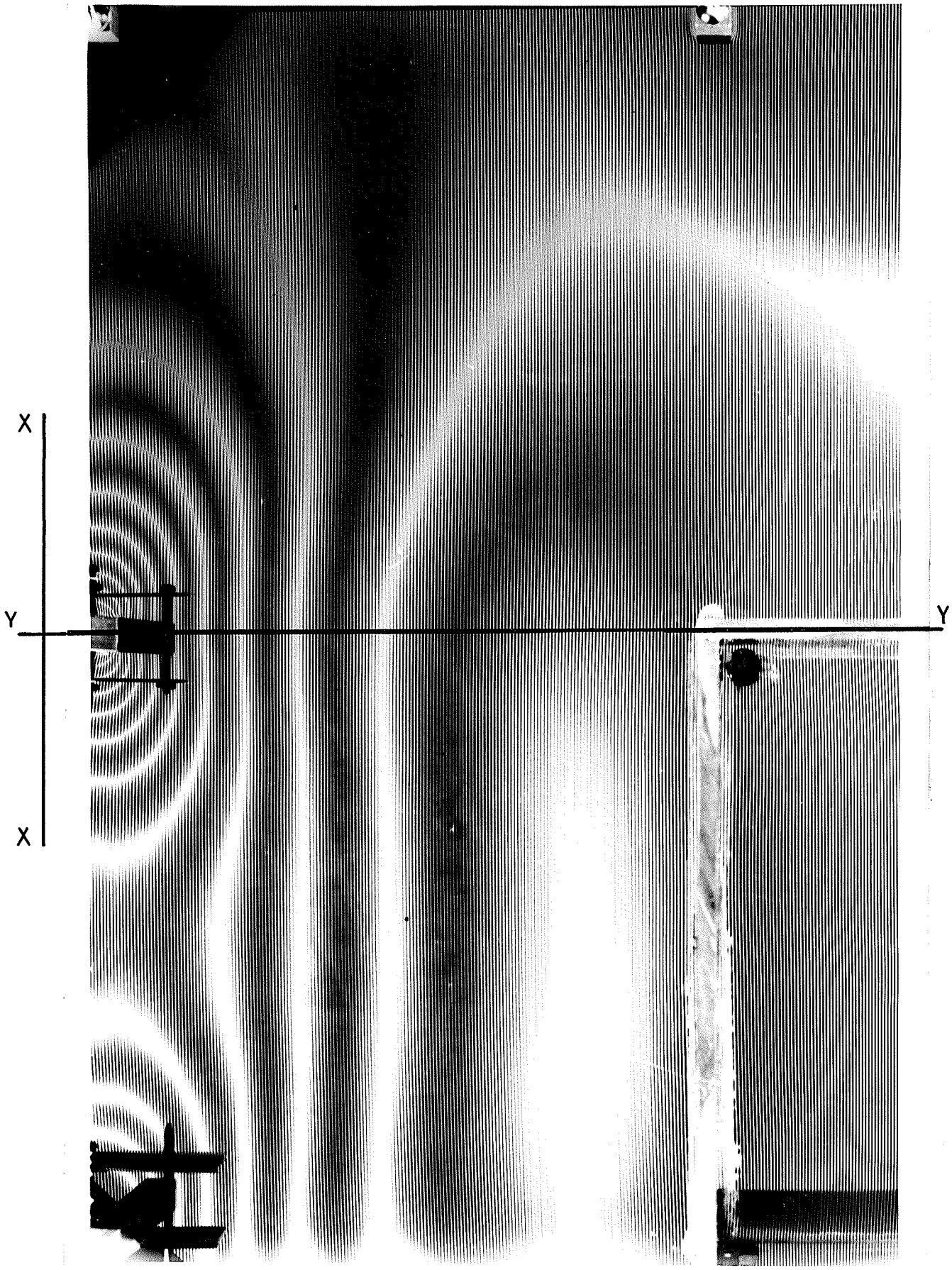

Fig. A - 34 Slope and Deflection Curves Model P4 Load Type D.

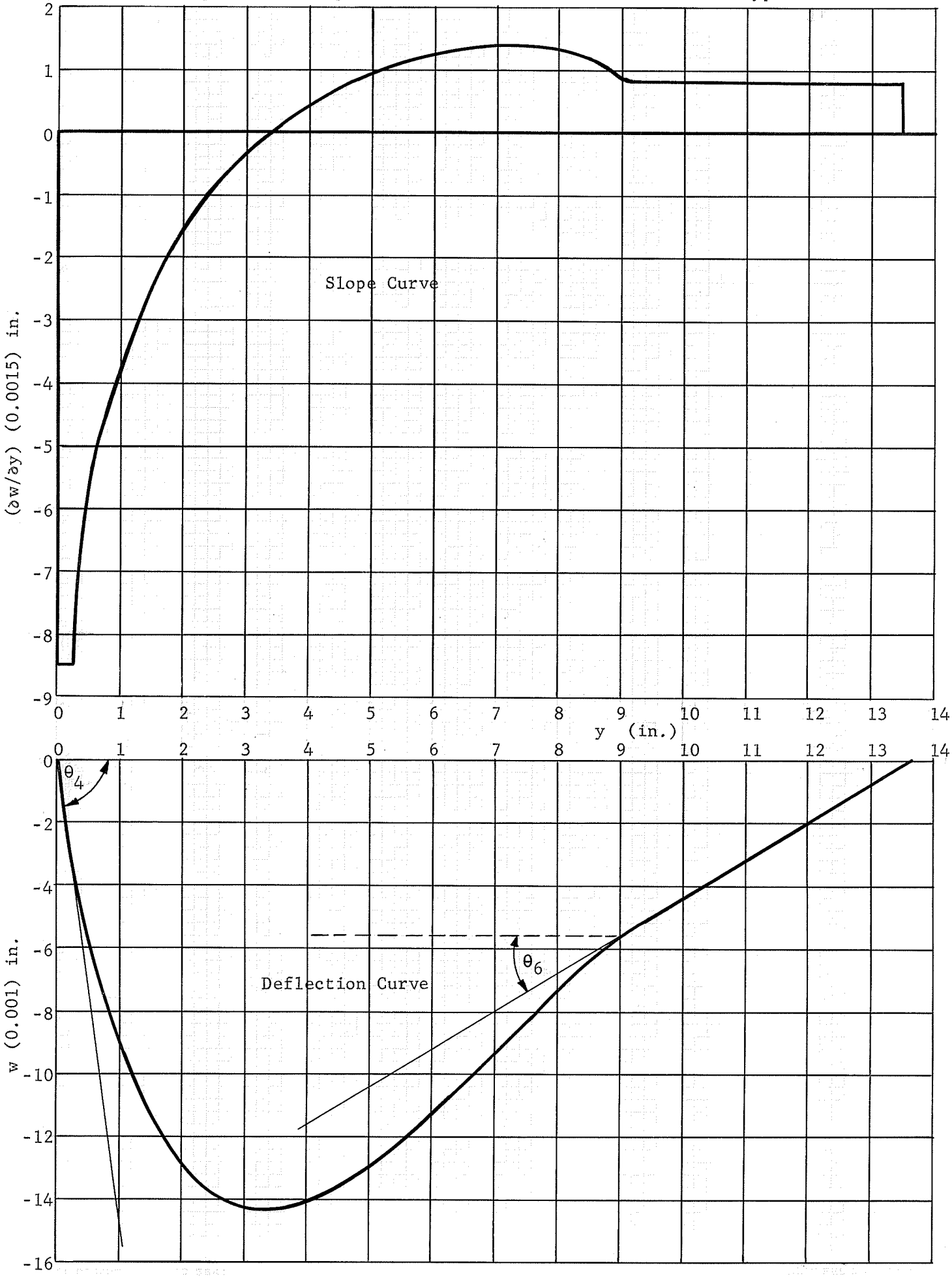

$y_1 - y_2$ in.	$\int_{y_2}^{y_1} (\partial w/\partial y)\, dy$ in.	$\sum \int_{y_2}^{y_1} (\partial w/\partial y)\, dy$ in.
0 - 1	-0.00910	-0.00910
1 - 2	-0.00389	-0.01292
2 - 3.4	-0.00144	-0.01436
3.4 - 4	0.00021	-0.01415
4 - 5	0.00108	-0.01307
5 - 6	0.001695	-0.011375
6 - 7	0.001995	-0.009380
7 - 8	0.00201	-0.007370
8 - 9	0.001755	-0.005615
9 - 10	0.001215	-0.004400
10 - 11	0.00120	-0.003200
11 - 12	0.00120	-0.002000
12 - 13	0.00120	-0.000800
13 - 13.5	0.00060	-0.000200

M_4 = 15 lb.-in., θ_4 = 0.015 rad., θ_6 = 0.0012 rad.

M_2 = 120 lb.-in., θ_2 = 0.00467 rad., θ_5 = 0.0059 rad.

Slope and Deflection Calculations Model P4 Load Type D.

TABLE A - 16

Carry - Over Factors Calculations.

$$C_{interior} = \frac{2M_4\ \theta_2}{M_2\ \theta_4} = \frac{2 \times 30 \times 0.00467}{120 \times 0.015} = 0.156$$

$$C_{exterior} = \frac{M_2\ \theta_6}{M_4\ \theta_5} = \frac{120 \times 0.0012}{30 \times 0.0059} = 0.815$$

APPENDIX B

B - 1 Determination of the Flexural Properties of the Plexiglas.

1. Flexural strength (Modulus of Repture);

$$S = \frac{3\,P\,L}{2\,b\,d^2} \qquad \text{.....B - 1}$$

2. Maximum strain in outer fiber;

$$r = \frac{6\,D\,d}{L^2} \qquad \text{..... B - 2}$$

3. Tangent modulus of elasticity or modulus of elasticity;

$$E_B = \frac{L^3\,m}{4\,b\,d^3} \qquad \text{..... B - 3}$$

where, P = load at break in load-deflection curve (lbs.),

L = span length (in.),

b = width of beam (in.),

d = depth of beam (in.),

D = maximum deflection (in.),

and m = slope of the tangent to the initial straight - line portion of the load - deflection curve (lb./in.).

Specimen No.	S psi.	r in./in.	E_B psi.	Average thickness in.
1	12,250	0.0293	460,000	0.236
2	12,400	0.0300	440,000	0.23914
3	10,800	0.0328	430,000	0.2404
4	11,500	0.0232	434,000	0.2481
5	13,000	0.0314	440,000	0.24266
6	11,400	0.0260	420,000	0.2474
7	11,350	0.0246	440,000	0.2495
8	10,800	0.0222	464,000	0.23796
Average	11,900		441,000	0.2430

Flexural Properties of Plexiglas

TABLE B - 1

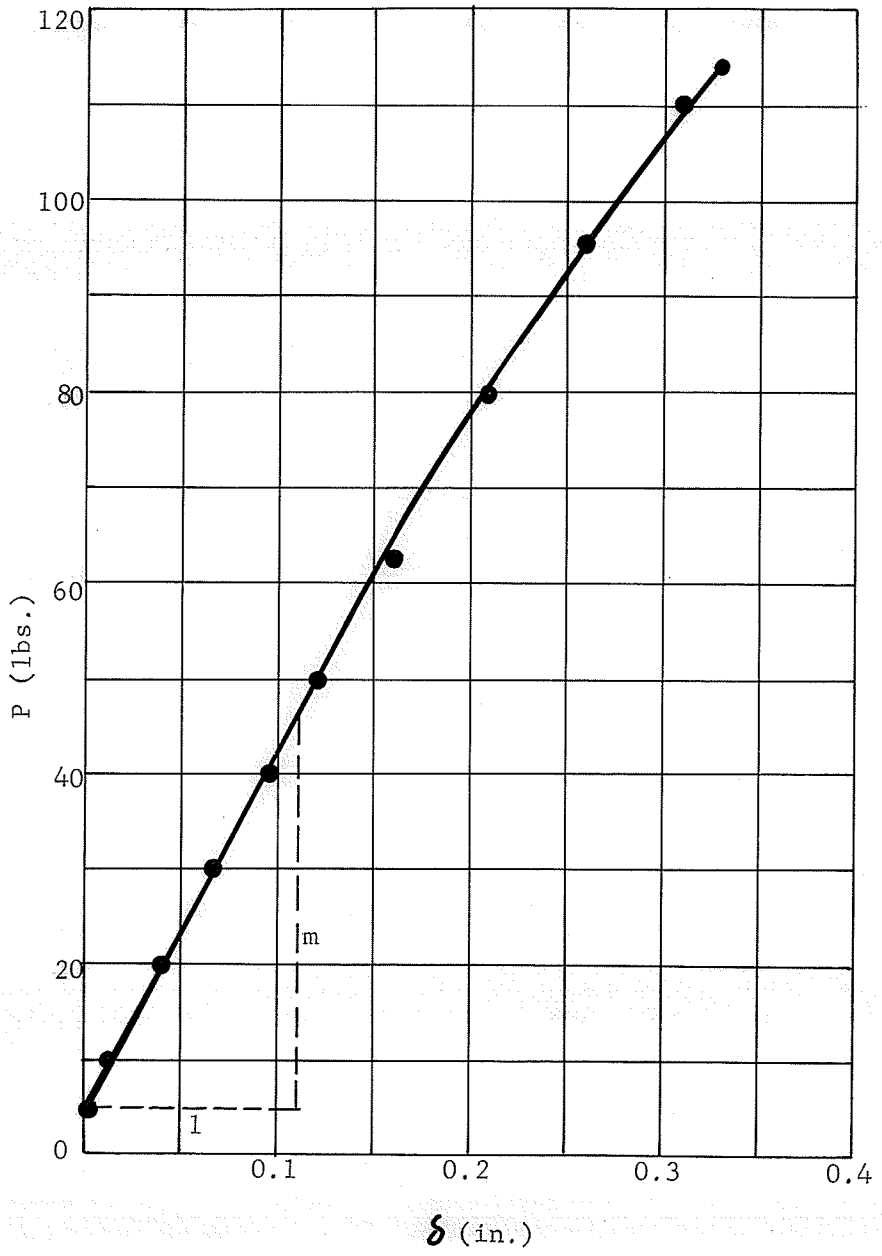

$P = 114$ lb.

$L = 4.0$ in.

$b_{av.} = 1.0097$ in.

$d_{av.} = 0.236$ in.

$D = 0.330$ in.

$m = 380$ lb./in.

$$S = \frac{3 \times 114 \times 4}{2 \times 1.0097 \times (0.236)^2}$$

$= 12,250$ psi.

$$r = \frac{6 \times 0.330 \times 0.236}{4 \times 4}$$

$= 0.0293$ in./in.

$$E_B = \frac{4 \times 4 \times 4 \times 380}{4 \times 1.0097 \times (0.236)^3}$$

$= 446,000$ psi.

Fig. B - 1 Determination of Flexural Properties of Plexiglas - Specimen No.1

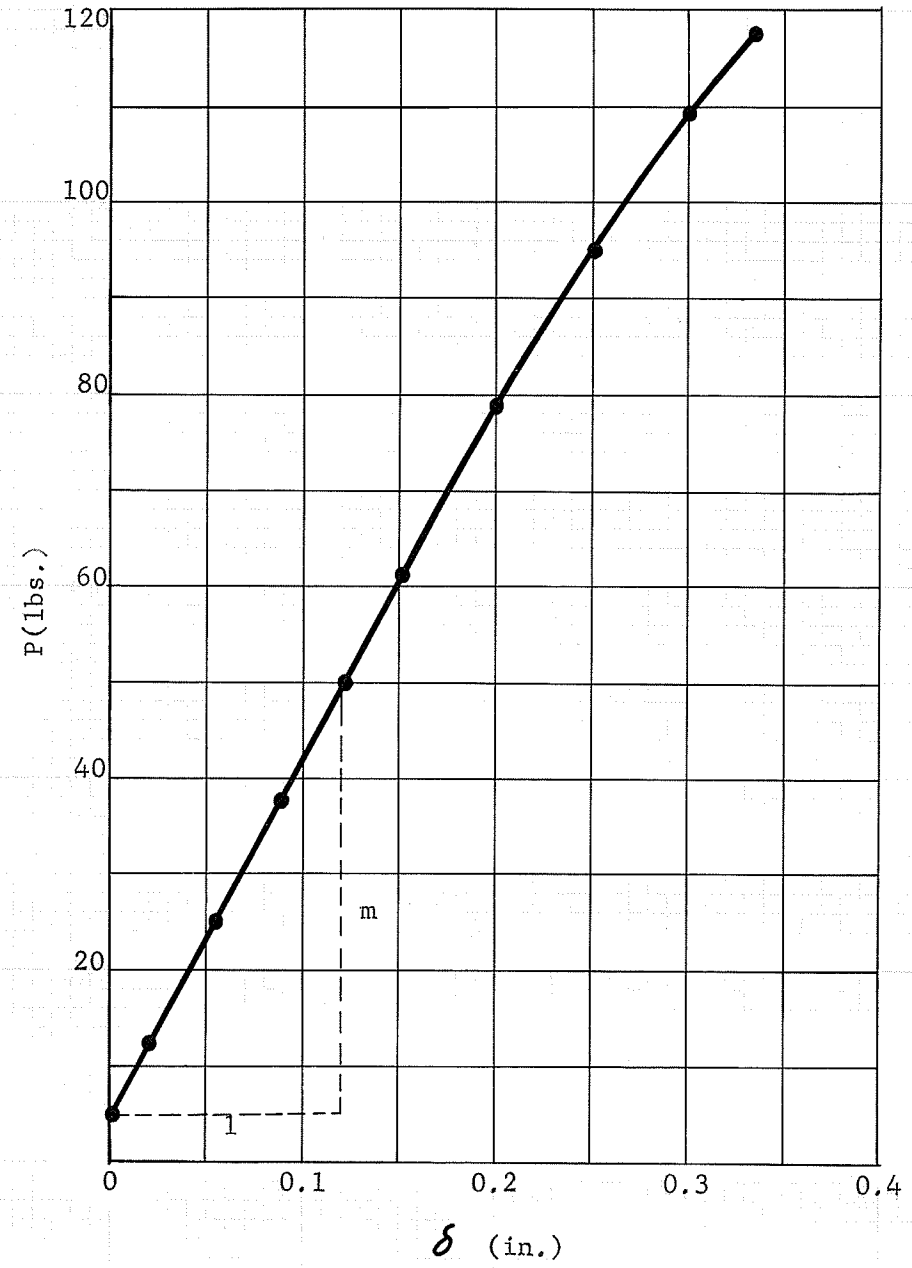

P	=	117.5	lb.
L	=	4.0	in.
$b_{av.}$	=	0.9968	in.
$d_{av.}$	=	0.23914	in.
D	=	0.335	in.
m	=	375	lb./in.
S	=	$\frac{3 \times 117.4 \times 4}{2 \times 0.9968 \times (0.23914)^2}$	
	=	12.400	psi.
r	=	$\frac{6 \times 0.335 \times 0.23914}{4 \times 4}$	
	=	0.03	in./in.
E	=	$\frac{4 \times 4 \times 4 \times 375}{4 \times 0.9968 \times (0.23914)^3}$	
	=	440,000	psi.

Fig. B - 2 Determination of Flexural Properties of Plexiglas -Specimen No.2.

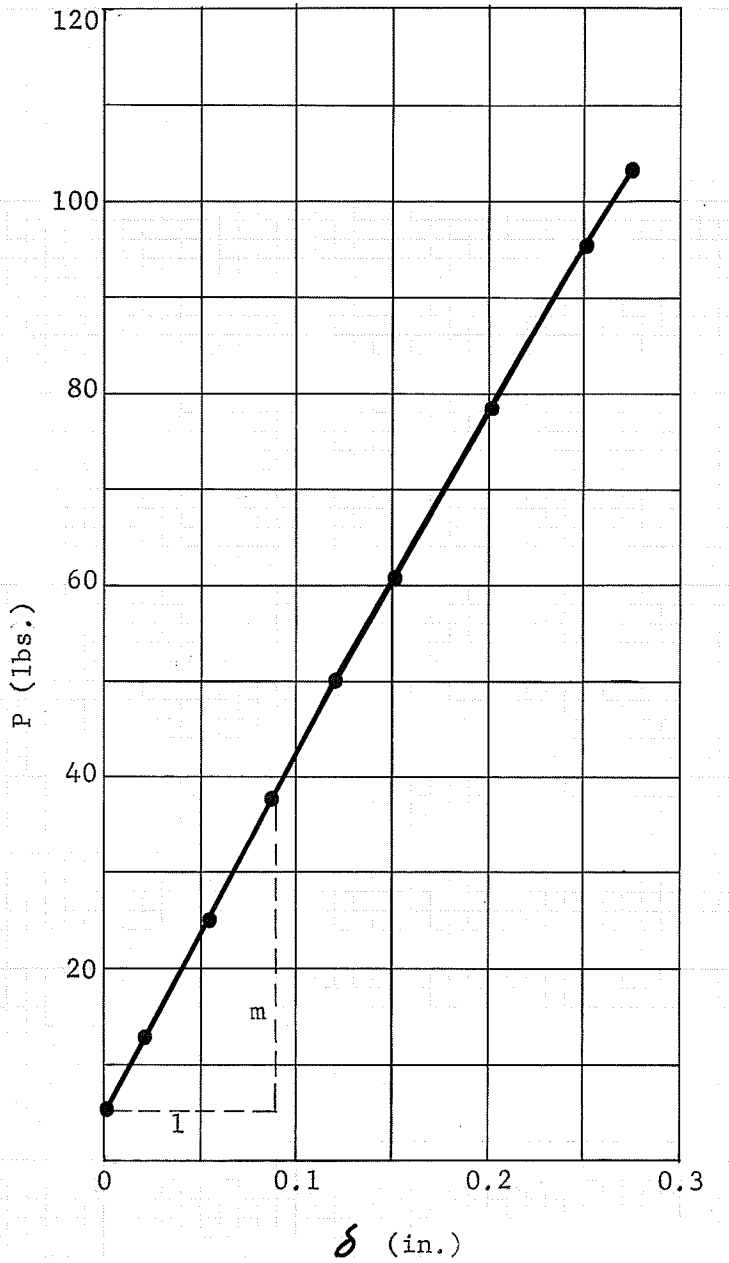

$P = 103.5$ lb.

$L = 4.0$ in.

$b_{av.} = 0.9958$ in.

$d_{av.} = 0.2404$ in.

$D = 0.275$ in.

$m = 370$ lb./in.

$$S = \frac{3 \times 103.5 \times 4}{2 \times 0.9958 \times (0.2404)^2}$$

$= 10{,}800$ psi.

$$r = \frac{6 \times 0.275 \times 4}{4 \times 4}$$

$= 0.0328$ in./in.

$$E_B = \frac{4 \times 4 \times 4 \times 370}{4 \times 0.9958 \times (0.2404)^3}$$

$= 430{,}000$ psi.

Fig. B - 3 Determination of Flexural Properties of Plexiglas - Specimen No.3

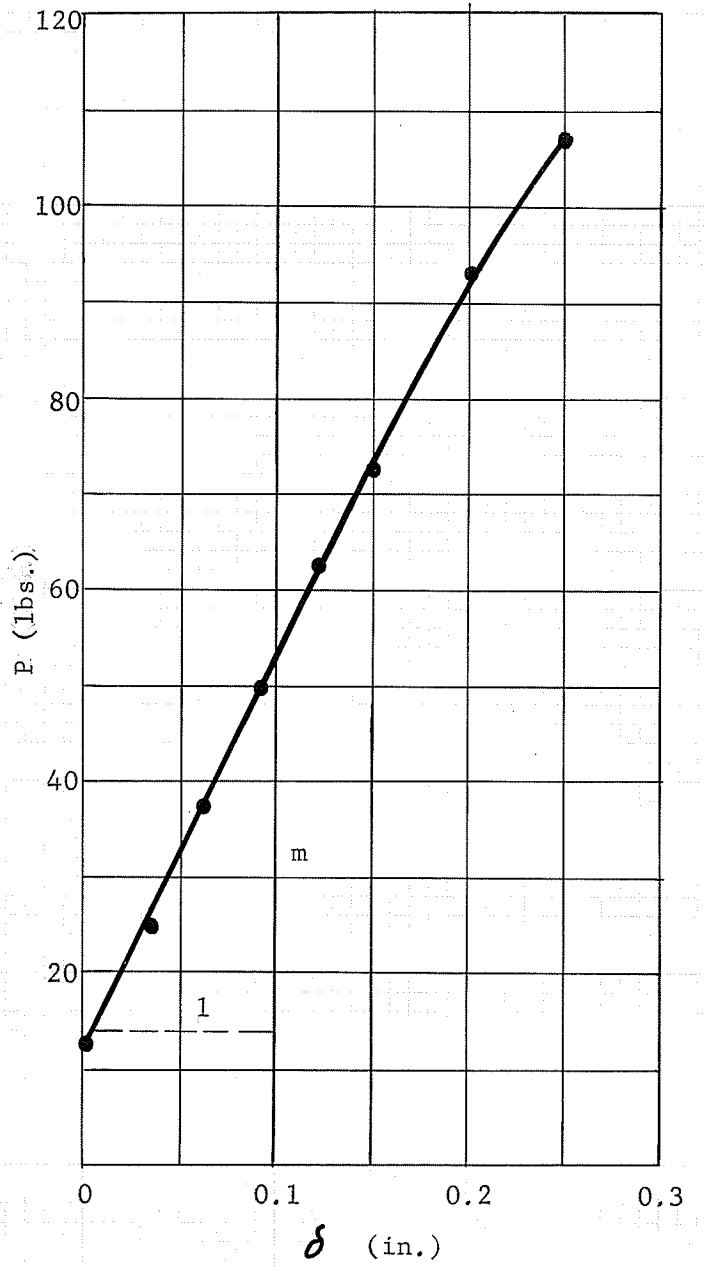

P	=	107	lb.
L	=	4.0	in.
$b_{av.}$	=	1.0114	in.
$d_{av.}$	=	0.2481	in.
D	=	0.25	in.
m	=	420	lb./in.

$$S = \frac{3 \times 107 \times 4}{2 \times 1.0114 \times (0.2481)^2} = 11{,}500 \text{ psi.}$$

$$r = \frac{6 \times 0.25 \times 0.2481}{4 \times 4} = 0.0232 \text{ in./in.}$$

$$E_B = \frac{4 \times 4 \times 4 \times 420}{4 \times 1.0114 \times (0.2481)^3} = 434{,}000 \text{ psi.}$$

Fig. B - 4 Determination of Flexural Properties of Plexiglas - Specimen No.4

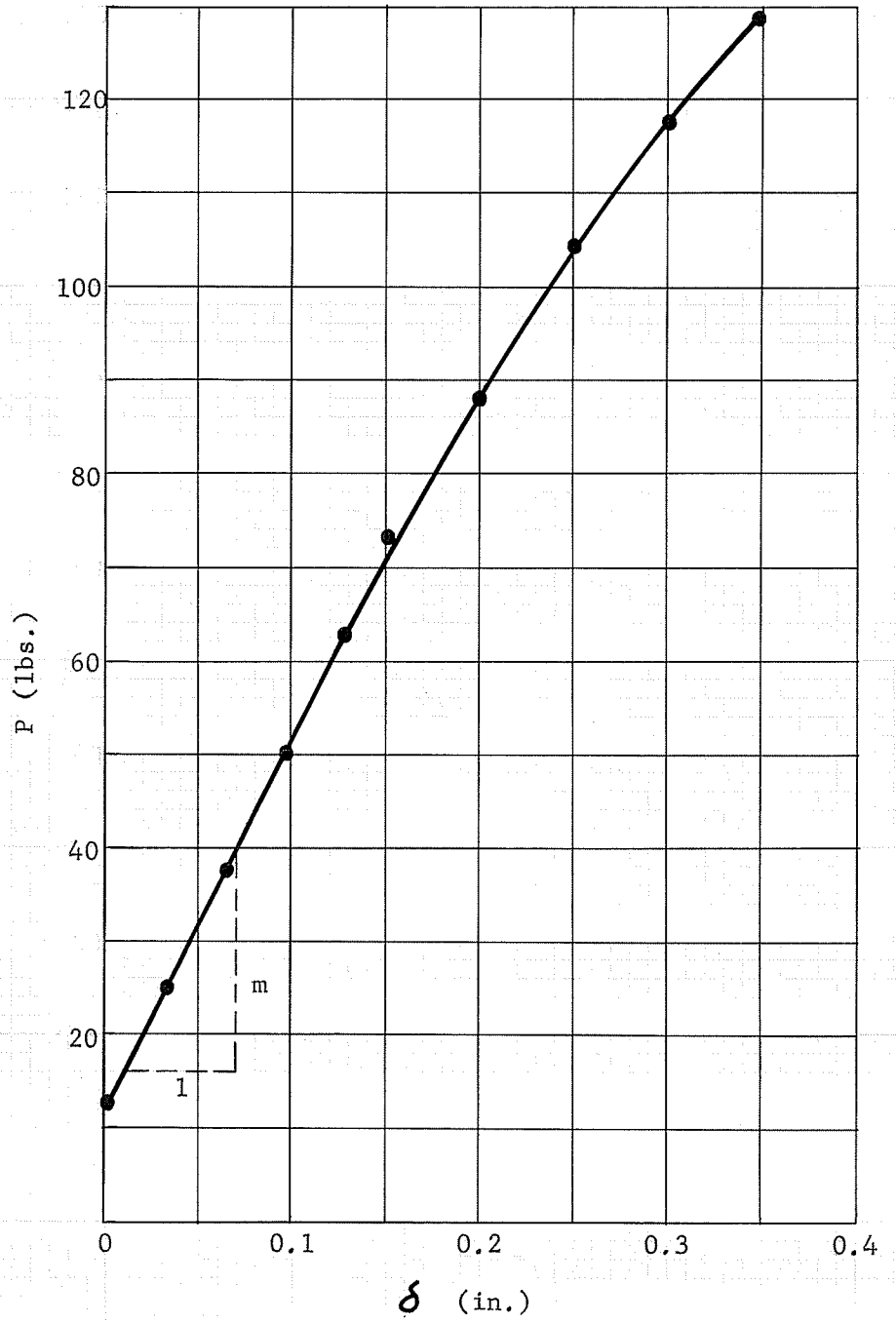

P	=	129	lb.
L	=	4.0	in.
$b_{av.}$	=	1.0173	in.
$d_{av.}$	=	0.24266	in.
D	=	0.346	in.
m	=	400	lb./in

$$S = \frac{3 \times 129 \times 4}{2 \times 1.0173 \times (0.24266)^2} = 13{,}000 \text{ psi.}$$

$$r = \frac{6 \times 0.346 \times 0.24266}{4 \times 4} = 0.0314 \text{ in./in.}$$

$$E_B = \frac{4 \times 4 \times 4 \times 400}{4 \times 1.0173 \times (0.24266)^3} = 440{,}000 \text{ psi.}$$

Fig. B - 5 Determination of Flexural Properties of Plexiglas - Specimen No. 5

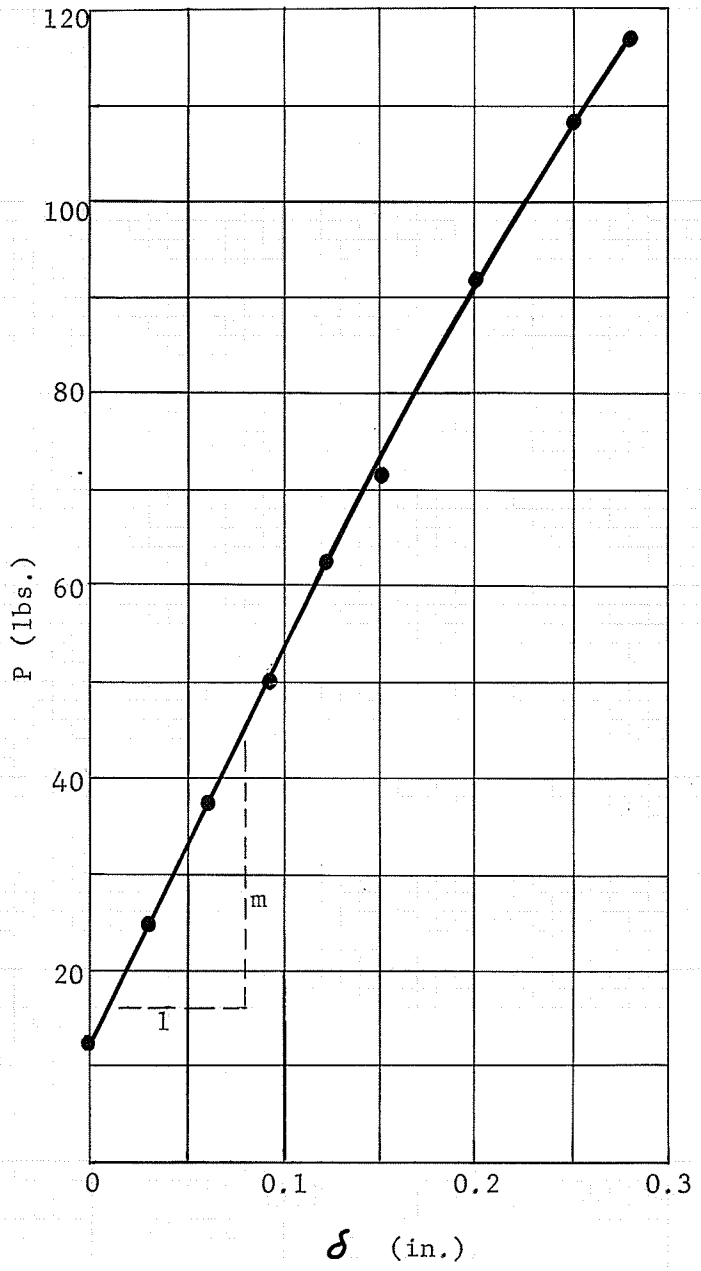

P	=	117	lb.
L	=	4.0	in.
$b_{av.}$	=	1.0092	in.
$d_{av.}$	=	0.2474	in.
D	=	0.28	in.
m	=	400	lb./in.
S	=	$\frac{3 \times 117 \times 4}{2 \times 1.0092 \times (0.2474)^2}$	
	=	11,400	psi.
r	=	$\frac{6 \times 0.28 \times 0.2474}{4 \times 4}$	
	=	0.026	in./in.
E_B	=	$\frac{4 \times 4 \times 4 \times 400}{4 \times 1.0092 \times (0.2474)^3}$	
	=	420,000	psi.

Fig. B - 6 Determination of Flexural Properties of Plexiglas - Specimen No. 6

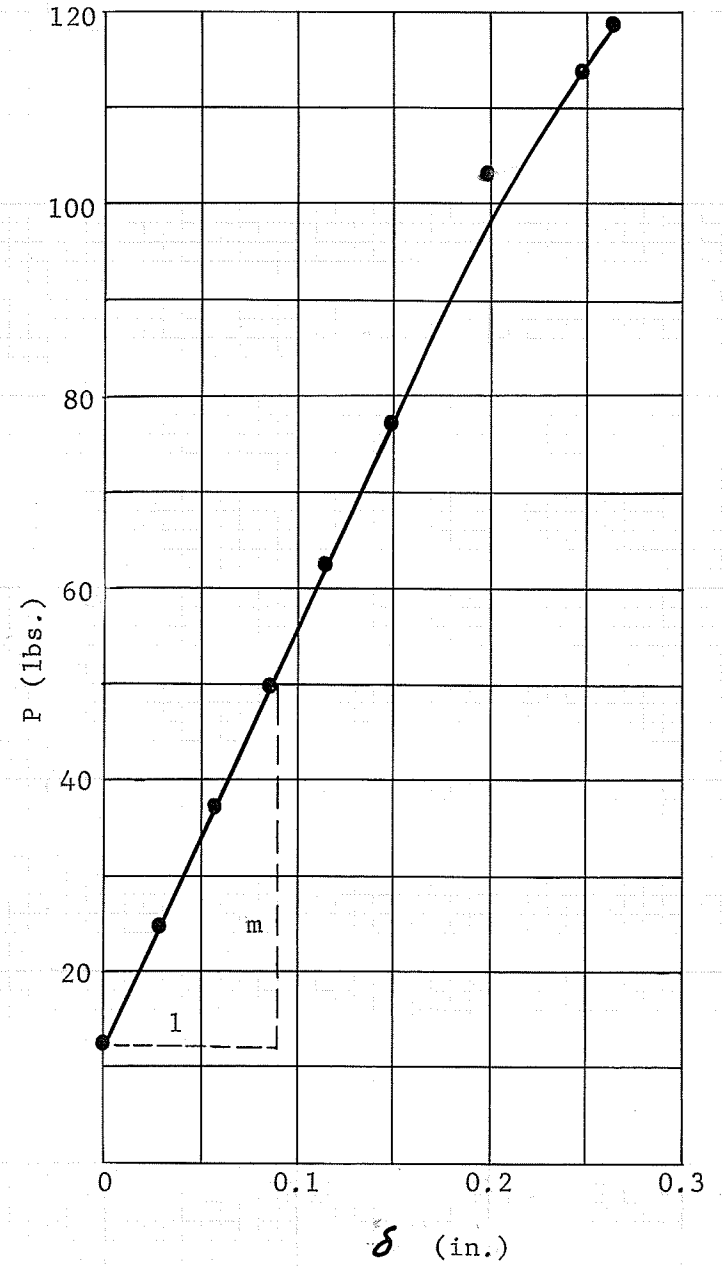

P	=	119	lb.
L	=	4.0	in.
$b_{av.}$	=	1.00926	in.
$d_{av.}$	=	0.2495	in.
D	=	0.264	in.
m	=	435	lb./in.
S	=	$\frac{3 \times 119 \times 4}{2 \times 1.00926 \times (0.2495)^2}$	
	=	11,350	psi.
r	=	$\frac{6 \times 0.264 \times 0.2495}{4 \times 4}$	
	=	0.0246	in./in/
E_B	=	$\frac{4 \times 4 \times 4 \times 435}{4 \times 1.00926 \times (0.2495)^3}$	
	=	440,000	psi.

Fig. B - 7 Determination of Flexural Properties of Plexiglas - Specimen No. 7

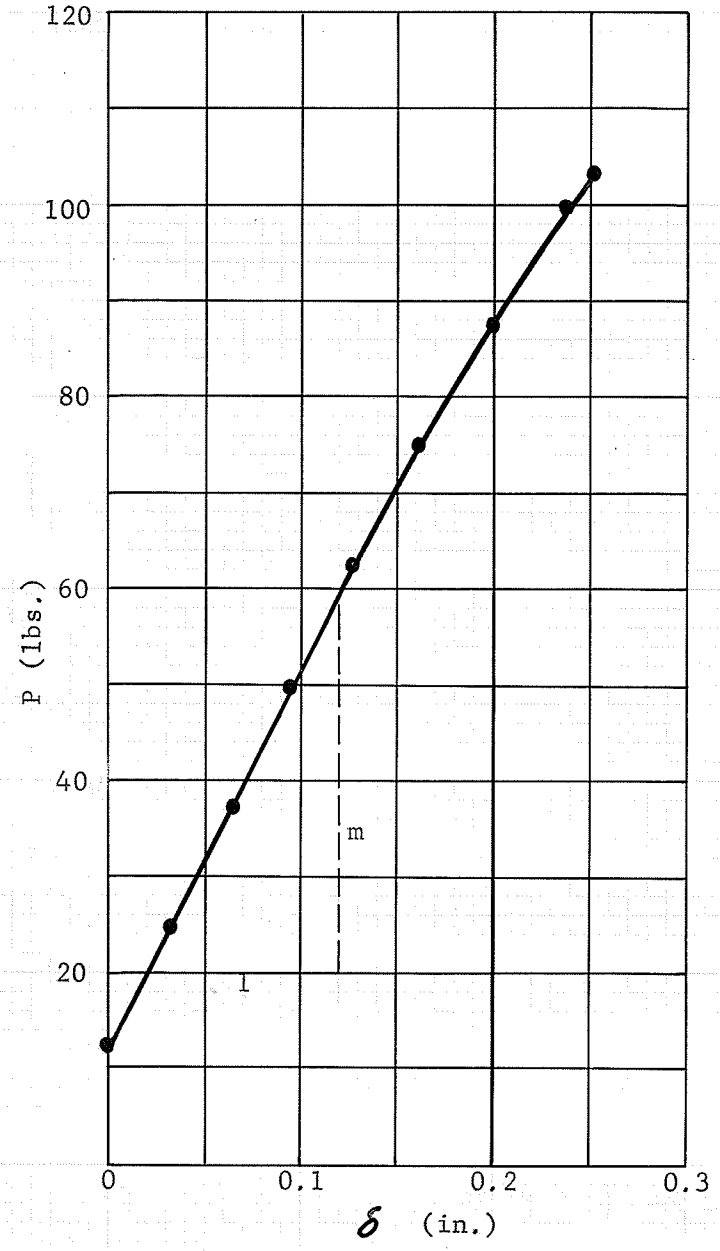

P	=	103	lb.
L	=	4.0	in.
$b_{av.}$	=	1.01196	in.
$d_{av.}$	=	0.23796	in.
D	=	0.25	in.
m	=	395	lb./in

$$S = \frac{3 \times 103 \times 4}{2 \times 1.01196 \times (0.23796)^2}$$

$$= 10,800 \text{ psi.}$$

$$r = \frac{6 \times 0.25 \times 0.23796}{4 \times 4}$$

$$= 0.0222 \text{ in./in.}$$

$$E_B = \frac{4 \times 4 \times 4 \times 395}{4 \times 1.01196 \times (0.23796)^3}$$

$$= 464,000 \text{ psi.}$$

Fig. B - 8 Determination of Flexural Properties of Plexiglas - Specimen No. 8

APPENDIX C

C - 1 Determination of Stiffness Factor for Model C1. Test structure C1 was loaded by a couple of loads P as shown in Fig. C - 1. The rotation θ of the plate at the centre column was obtained by measuring

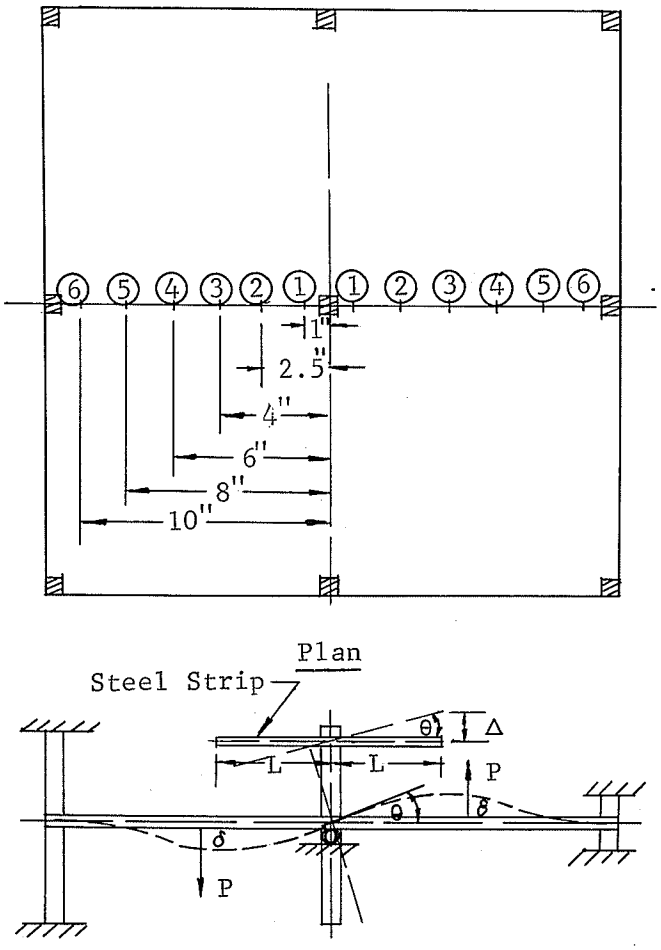

Fig. C-1 Test Structure C1

vertical deflections Δ at the ends of a steel strip glued to the column stub. Then, using the reciprocal theorem as discussed in Chapter II, the plate deflections δ at the points of load application were calculated from the equation:

$$\delta = \frac{M\,\theta}{2\,P}$$

where P = Load applied to slab

θ = Rotation of the column caused by loads P.

δ = Deflection of load point that would be caused by a moment M applied to the column.

Load points (1) to (6) in Fig. C - 1 were used, deflection curves drawn, and the stiffness factor calculated from

$$K = \frac{M}{\alpha}$$

where α = rotation at plate at centre column due to an applied moment M.

The plate deflections, calculated stiffness factors and effective slab widths for the three different load values P used are presented in Table C - 1. The corresponding deflection curves are shown in Figs. C - 2, C - 3 and C - 4.

Load 50 lbs.

Point	1	2	3	4	5	6
Deflection of steel strip(Δ) in in.	0.0052	0.0075	0.0083	0.0081	0.0056	0.0019
Rotation of steel strip(θ) in rad. L = 5.94 in.	0.00088	0.00125	0.00139	0.00137	0.00095	0.00033
Deflection of slab(δ) in in. = $M.\theta/2P$	0.0000088	0.0000126	0.0000139	0.0000137	0.0000095	0.0000033

From curve in Fig.C-2, α = 0.000030 rad.

Stiffness = 1/0.000030 = 33333 in.-lb./rad.

4EI/L = K = 33333 in.-lb./rad.

$$b = \frac{33333 \times 11.25}{4 \times 2.85 \times 10^{6}} \times \frac{12 \times 8 \times 8 \times 8}{3 \times 3 \times 3} = 7.50 \text{ in.}$$

Determination of Stiffness Factors for Model C1

Table C-1

Load 100 lbs.

Point	1	2	3	4	5	6
Deflection of steel strip(Δ) in in.	0.0112	0.0162	0.0174	0.0166	0.0125	0.0048
Rotation of steel strip(θ) in rad. L = 5.94 in.	0.00188	0.00272	0.00293	0.00295	0.00247	0.00080
Deflection of slab(δ) in in. = M.θ/2P	0.0000094	0.0000136	0.0000146	0.0000140	0.0000105	0.000004

From curve in Fig.C-3, α = 0.0000308 rad.

Stiffness = 1/0.0000308 = 32400 in.-lb./rad.

4EI/L = K = 32400 in.-lb./rad.

$$b = \frac{32400 \times 11.25}{4 \times 2.85 \times 10^6} \times \frac{12 \times 8 \times 8 \times 8}{3 \times 3 \times 3} = 7.30 \text{ in.}$$

Determination of Stiffness Factors for Model C1

Table C-1 (Continued)

Load 150 lbs.

Point	1	2	3	4	5	6
Deflection of steel strip(Δ) in in.	0.0168	0.0238	0.0279	0.0255	0.0182	0.0063
Rotation of steel strip(θ) in rad. L = 5.94 in.	0.00282	0.00399	0.00470	0.00429	0.00306	0.00105
Deflection of slab(δ) in in. = $M.\theta/2P$	0.0000094	0.0000133	0.0000160	0.0000143	0.0000102	0.0000035

From curve in Fig.C-4, α = 0.000032 rad.

Stiffness = 1/0.000032 = 31250 in.-lb./rad.

4EI/L = K = 31250 in.-lb./rad.

$$b = \frac{31250 \times 11.25}{4 \times 2.85 \times 10^6} \times \frac{12 \times 8 \times 8 \times 8}{3 \times 3 \times 3} = 6.92 \text{ in.}$$

$$\text{Average } b = \frac{7.50 + 7.30 + 6.92}{3} = 7.24 \text{ in.}$$

Determination of Stiffness Factors for Model C1

Table C-1 (Continued)

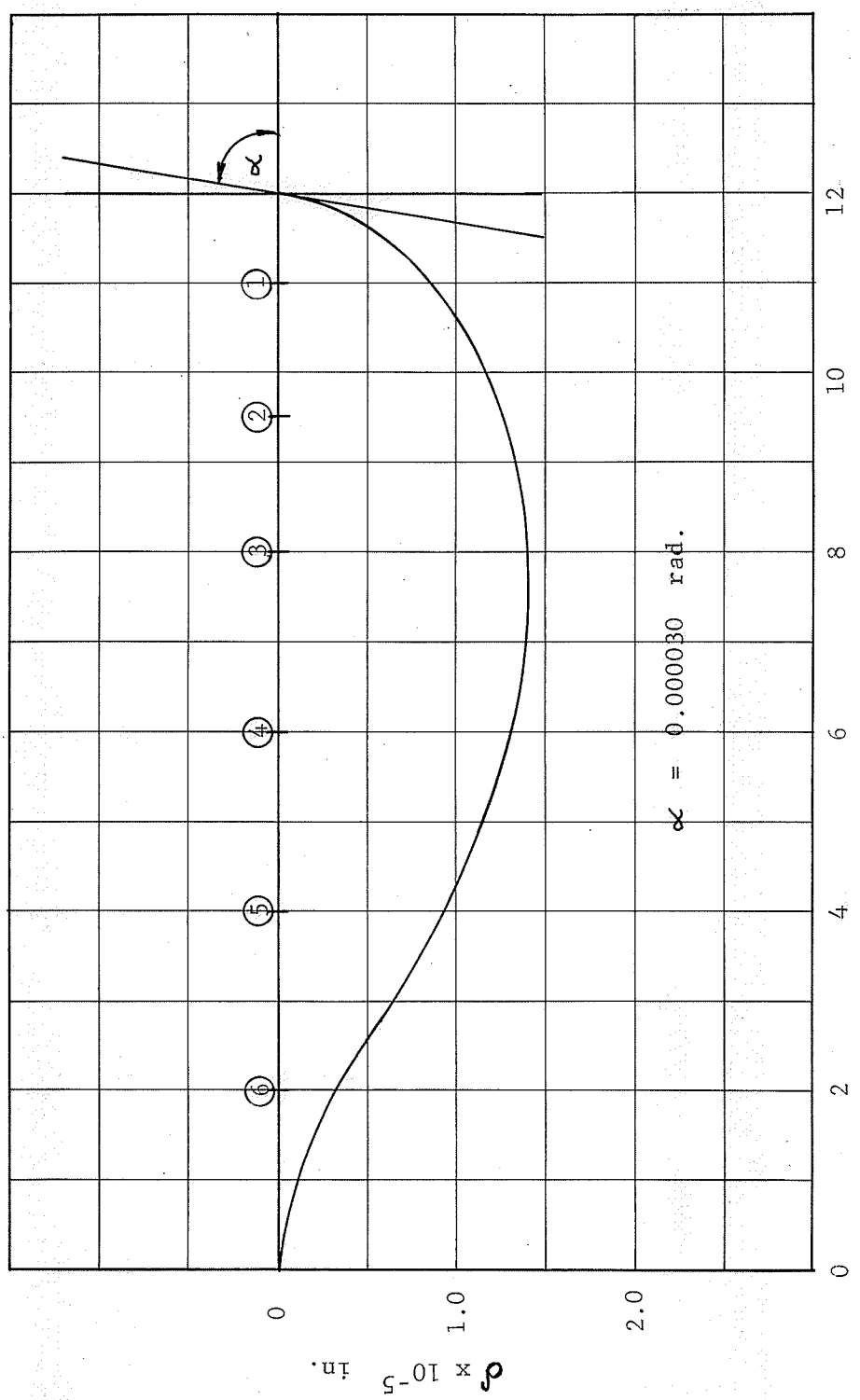

Fig. C-2 Deflection Curve of Loads 50 lbs.

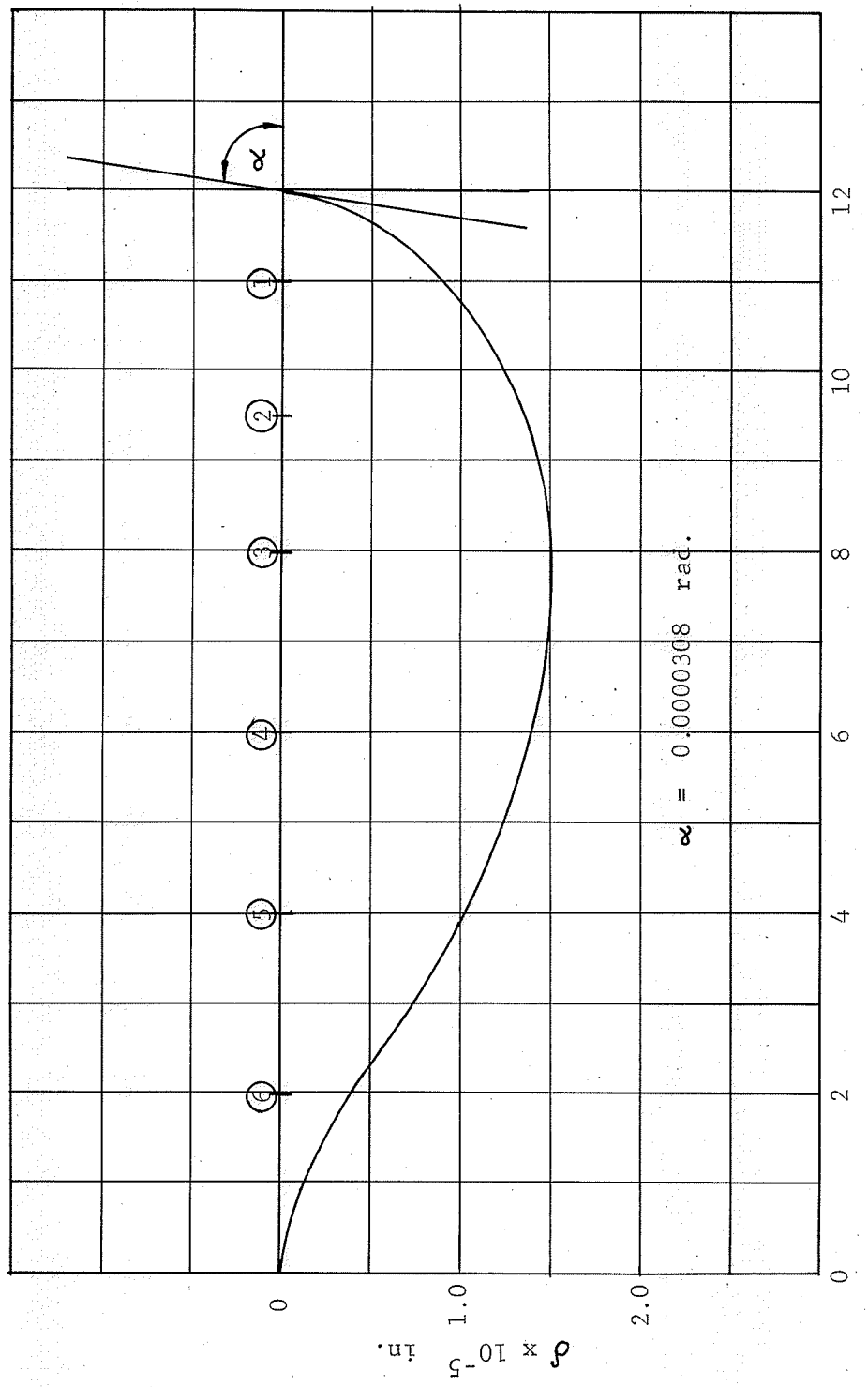

Fig. C-3 Deflection Curve of Loads 100 lbs.

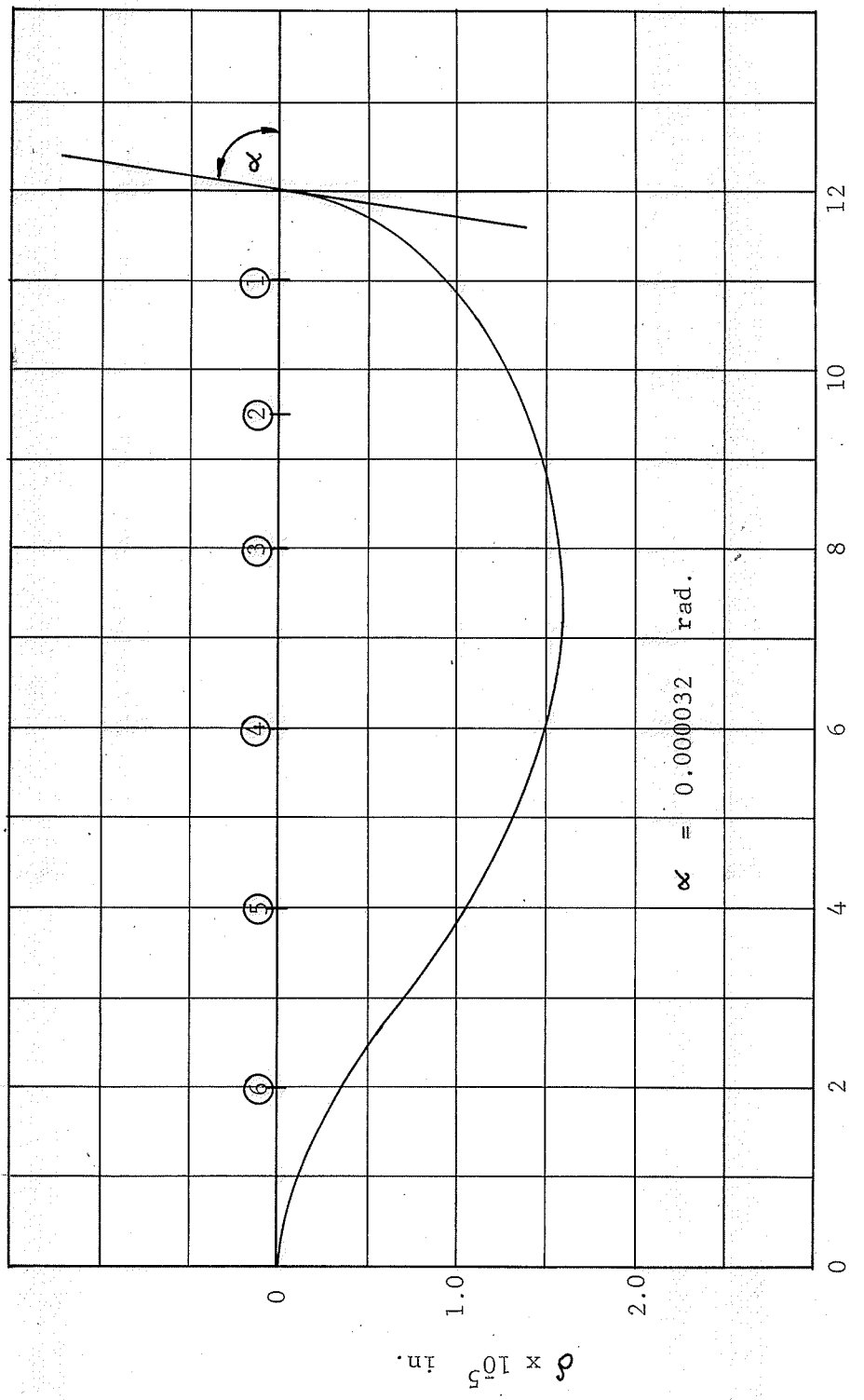

Fig. C-4 Deflection Curve of Loads 150 lbs.

C - 2 Determination of Stiffness Factors and Carry-Over Factors for Model C2.

The test structure C2, shown in Fig. C-5, was subjected to loading types A, B, C and D shown in Fig. C-6.

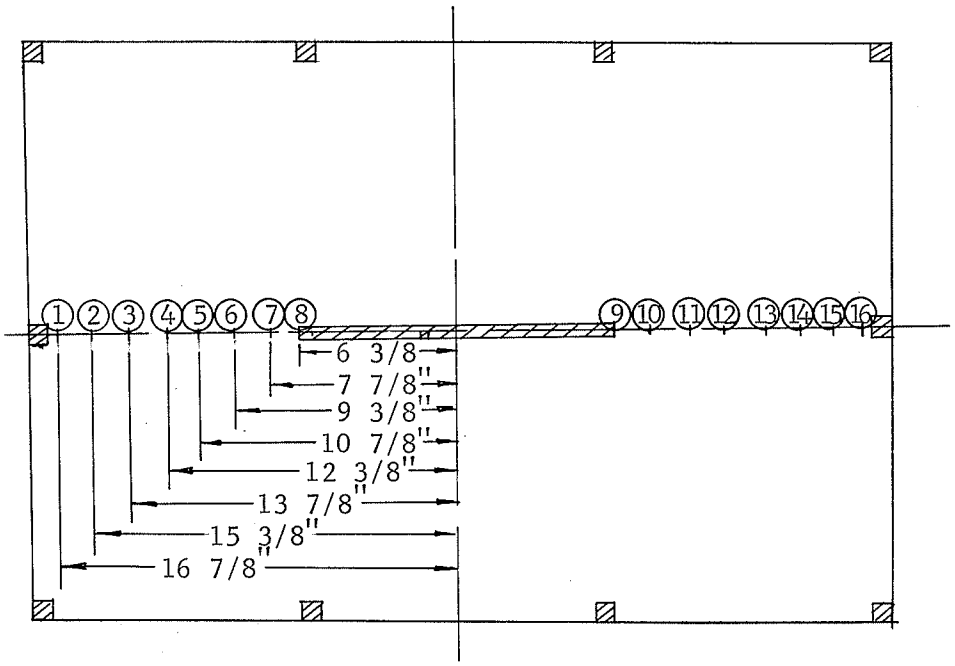

Plan

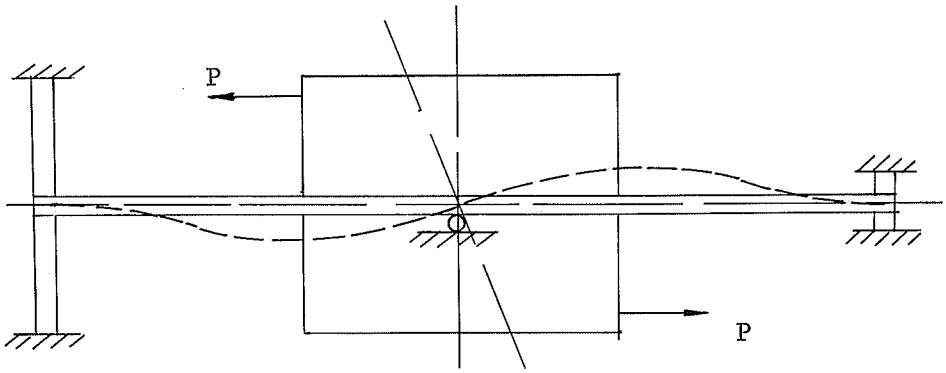

Elevation

Fig. C-5 Test Structure C2

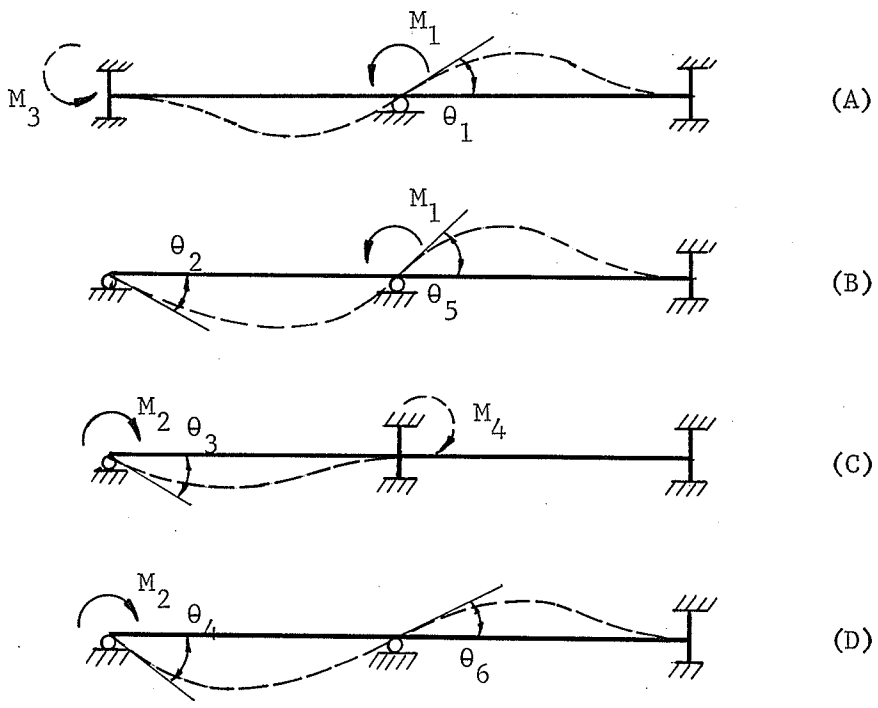

Fig. C-6 Load Types for Model C2

The measured plate deflections at point ① to ⑯ in Fig. C - 5 are presented in Table C - 2. The rotations θ_1, θ_2, θ_3, θ_4, θ_5, and θ_6 of the plate were obtained by measurement from the plotted plate deflection curves which are shown in Figs. C - 7, C - 8, C - 9, C - 10, C - 11. The plate stiffnesses and effective widths and carry-over factors were determined as outlined in Sections 2.2 and 2.3. Sample calculations for transverse loads of 150 lbs. applied to the shear wall and 40 lbs. loads at the edge column, are presented in Table C - 3. Tables C-4 and C-5 are the average values of stiffness factors, effective widths and carry-over factors respectively.

Point / Load lbs.	1	2	3	4	5	6	7	8	9	10	11	12	13	14	15	16
50	0.00025	0.0010	0.0017	0.0028	0.0034	0.0042	0.0047	0.0049	0.0050	0.0045	0.0040	0.0043	0.0025	0.0017	0.0009	0.0003
100	0.0005	0.0018	0.0036	0.0054	0.0069	0.0085	0.0095	0.010	0.0098	0.0088	0.0076	0.0064	0.0047	0.0030	0.0016	0.0005
150	0.0007	0.0025	0.0050	0.0078	0.0106	0.0128	0.0148	0.0152	0.0154	0.0140	0.0122	0.0098	0.0075	0.0042	0.0019	0.0005
200	0.0010	0.0040	0.0080	0.0119	0.0155	0.0187	0.0210	0.0220	0.0223	0.0202	0.0177	0.0143	0.010	0.006	0.0030	0.0001
250	0.0017	0.0052	0.0101	0.0163	0.0225	0.0275	0.0318	0.0332	0.0316	0.0293	0.0258	0.0213	0.0152	0.0087	0.0041	0.0010

Deflections of Plate in in., Load Type A

Table C-2

Point / Load lbs.	1	2	3	4	5	6	7	8	9	10	11	12	13	14	15	16
50	0.0005	0.0015	0.0024	0.0031	0.0038	0.0042	0.0047	0.0046	0.0049	0.0045	0.0038	0.0030	0.0020	0.0011	0.0005	0.0001
100	0.001	0.0029	0.0045	0.0060	0.0075	0.0087	0.0098	0.010	0.012	0.0095	0.0081	0.0065	0.0047	0.0029	0.0028	0.0003
150	0.0021	0.0047	0.0073	0.0093	0.0112	0.0131	0.0148	0.0152	0.0153	0.0146	0.0126	0.0106	0.0081	0.0056	0.0030	0.0005
200	0.0027	0.0072	0.0110	0.0145	0.0175	0.0210	0.0225	0.0230	0.0235	0.0220	0.0198	0.0167	0.0134	0.0095	0.0064	0.0080

Deflections of Plate in in., Load Type B

Table C-2 (Continued)

Point / Load lbs.	1	2	3	4	5	6	7	8	9	10	11	12	13	14	15	16
20	0.0009	0.0014	0.0013	0.0011	0.0008	0.0005	0.0001	0	0	0	0	0	0	0	0	0
30	0.0023	0.0035	0.0034	0.0029	0.0019	0.0008	0.0002	0	0	0	0	0	0	0	0	0
40	0.0033	0.0060	0.0057	0.0046	0.0031	0.0013	0.0004	0	0	0	0	0	0	0	0	0
50	0.0056	0.0086	0.0080	0.0066	0.0044	0.0021	0.0006	0	0	0	0	0	0	0	0	0

Deflections of Plate in in., Load Type C

Table C-2 (Continued)

Point / Load lbs.	1	2	3	4	5	6	7	8	9	10	11	12	13	14	15	16
10	0.0011	0.0016	0.0016	0.0018	0.0014	0.0012	0.0009	0.0006	0.0007	0.0007	0.0006	0.0005	0.0004	0.0002	0.00005	0.00002
20	0.0022	0.0032	0.0034	0.0032	0.0028	0.0023	0.0018	0.0014	0.0014	0.0013	0.0010	0.0009	0.0007	0.0003	0.00015	0.00002
30	0.0031	0.0051	0.0052	0.0048	0.0042	0.0034	0.0027	0.0020	0.0019	0.0018	0.0016	0.0013	0.0009	0.0005	0.0003	0.00005
40	0.0043	0.0068	0.0071	0.0066	0.0057	0.0048	0.0038	0.0029	0.0027	0.0025	0.0021	0.0017	0.0012	0.0007	0.0003	0.00005
50	0.0058	0.0093	0.0098	0.0090	0.0080	0.0066	0.0052	0.0038	0.0035	0.0031	0.0027	0.0021	0.0015	0.0009	0.0004	0.0001

Deflections of Plate in in., Load Type D

Table C-2 (Continued)

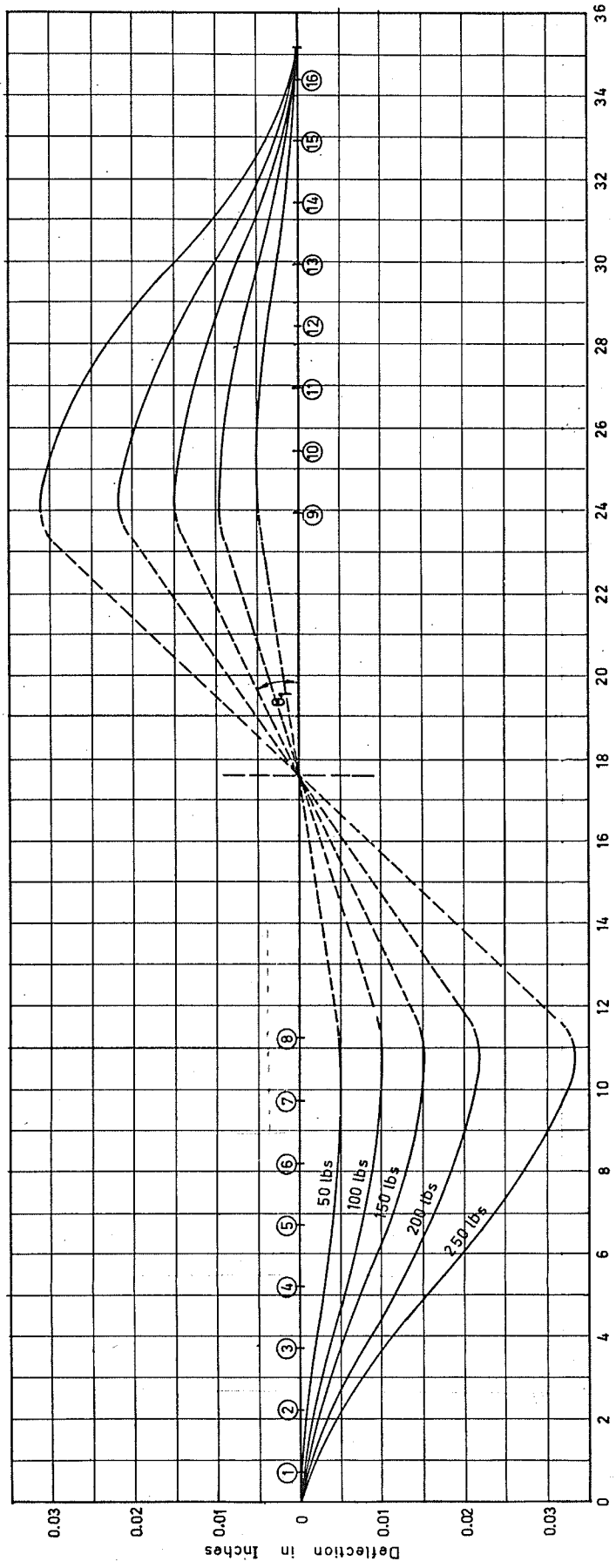

Fig. C-7 Slab Deflections Model C2 Load Type A

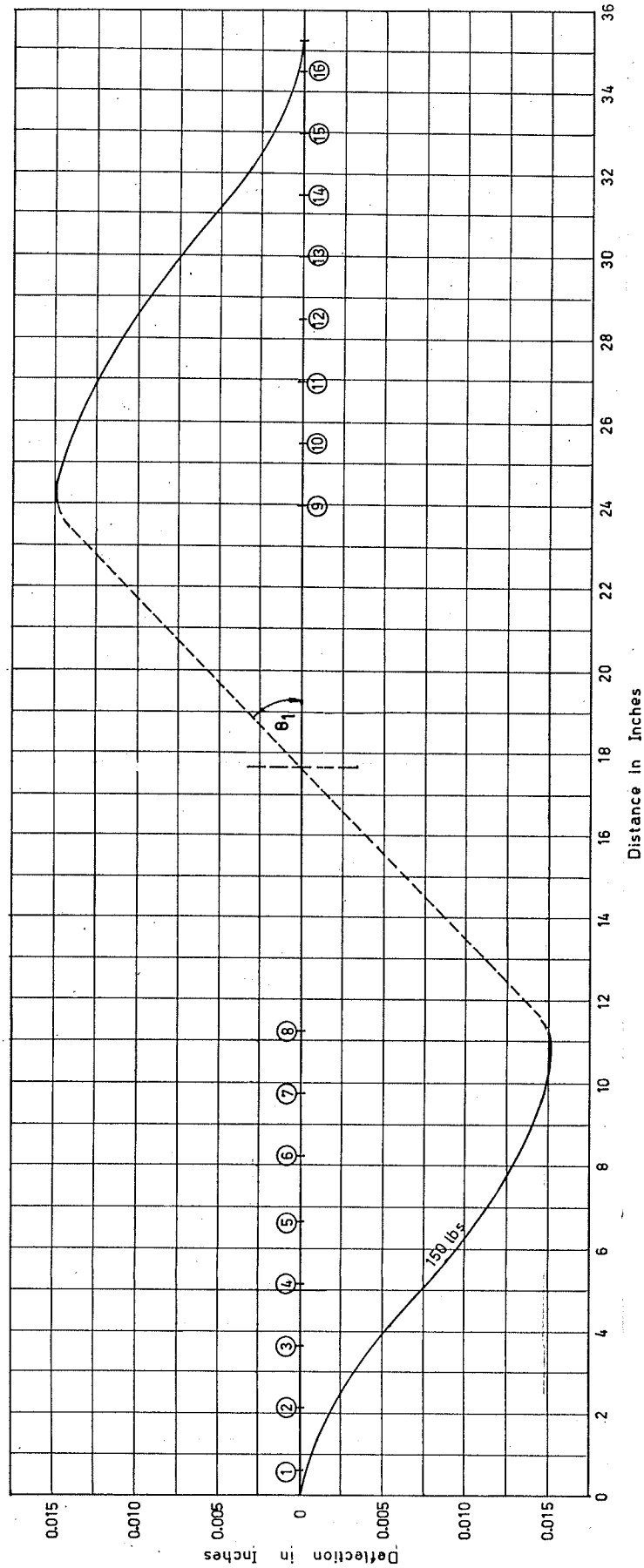

Fig. C-8 Slab Deflections Model C2 Load Type A

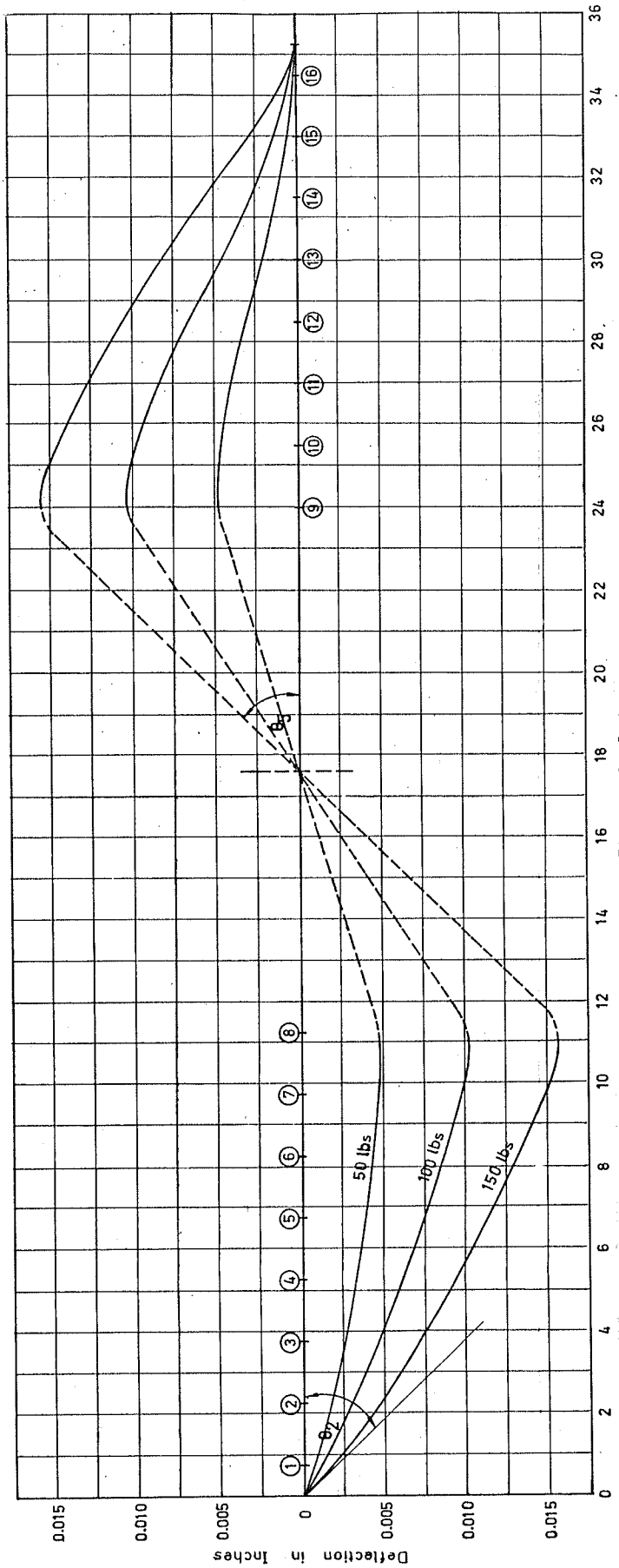

Fig. C-9 Slab Deflections Model C2 Load Type B

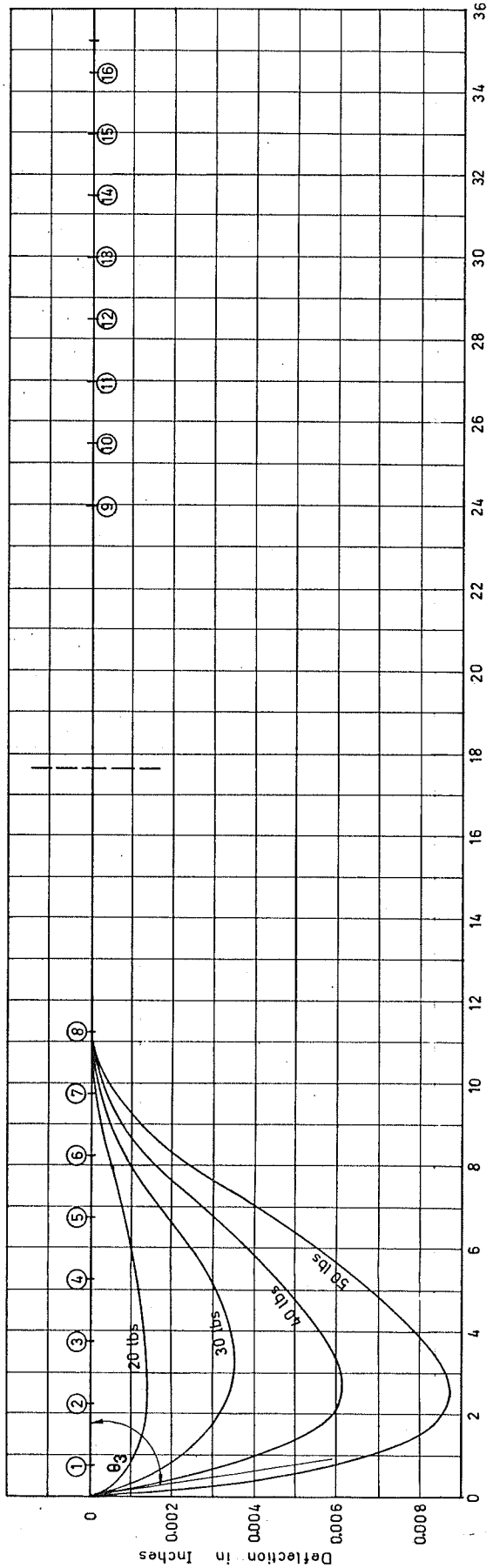

Fig. C-10 Slab Deflections Model C2 Load Type C

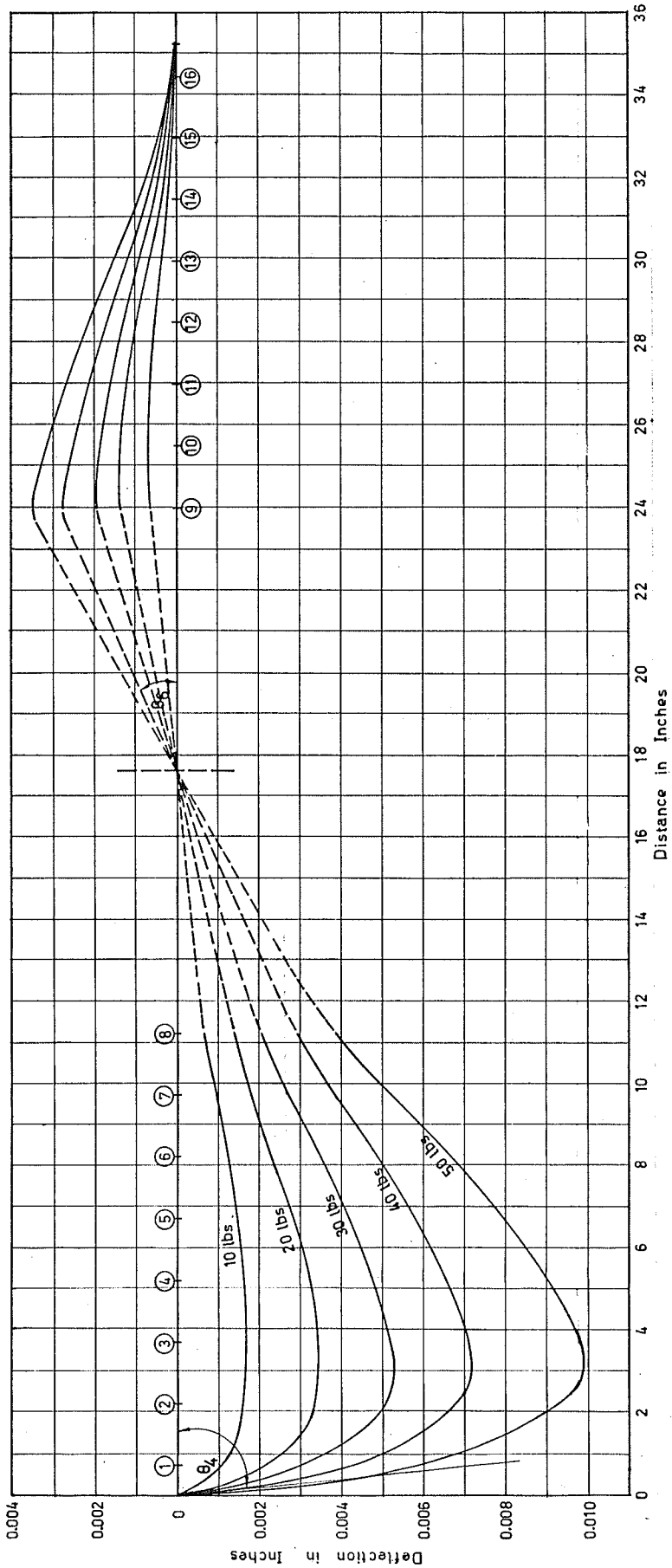

Fig. C-11 Slab Deflections Model C2 Load Type D

Moment applied to centre shear wall (See Fig. C - 6) is:

M_1 = 150 x 7.5 = 1125 lb.-in.

Resulting plate rotations:

Load type A	θ_1 =	0.00238	rad.
Load type B	θ_2 =	0.00259	rad.
and	θ_5 =	0.00256	rad.

Moment applied to exterior column is:

M_2 = 40 x 7.5 = 300 lb.-in.

Resulting plate rotations

Load type C	θ_3 =	0.0066	rad.
Load type D	θ_4 =	0.0096	rad.
and	θ_6 =	0.00045	rad.

(1) Stiffness factor $K_1 = \frac{M_1}{\theta_1} = \frac{1125}{0.00238} = 472{,}000$ lb.-in./rad.

$\frac{4 E I}{L} = 472{,}000$ lb.-in./rad.

Moment of inertia $I_1 = \frac{472{,}000 \times 11.25}{4 \times 2.85 \times 10^6} = 0.465$ $in.^4$

Effective width $b_1 = \frac{0.465 \times 12 \times 8 \times 8 \times 8}{3 \times 3 \times 3} = 105.50$ in.

Calculation of Stiffness and Carry-over Factors and Eff. Widths for Model C2

Table C - 3

(2) Stiffness factor $K_2 = \frac{M_2}{\theta_3} = \frac{300}{0.0066} = 45{,}500$ lb.-in./rad.

$$\frac{4 E I}{L} = 45{,}500$$

Moment ineria $I_2 = \frac{45{,}500 \times 11.25}{4 \times 2.85 \times 10^6} = 0.0449$ in^4.

Effective width $b_2 = \frac{0.0449 \times 12 \times 8 \times 8 \times 8}{3 \times 3 \times 3} = 10.20$ in.

(3) $M_3 = \frac{2 M_2 \theta_2}{\theta_4} = \frac{2 \times 300 \times 0.00259}{0.0096}$ lb.-in.

Carry-Over Factor for Interior Panel $= C_1 = \frac{M_3}{M_1}$

$$= \frac{2 \times 300 \times 0.00259}{0.0096 \times 1125} = 0.144$$

(4) $M_4 = \frac{M_1 \theta_6}{\theta_5} = \frac{1125 \times 0.00045}{0.00256}$ lb.-in.

Carry-Over Factor for Interior Panel $= C_2 = \frac{M_4}{M_2}$

$$= \frac{1125 \times 0.00045}{0.00256 \times 300} = 0.660$$

Calculation of Stiffness and Carry-over Factors and Eff. Widths for Model C2

Table C - 3 (Continued)

Load lbs.	θ_1 rad.	K in.-lb./rad.	$K_{ave.}$ in.-lb./rad.	$b_{ave.}$ in.
50	0.00075	500,000		
100	0.00160	469,000		
150	0.00238	472,000	448,800	101.00
200	0.00340	442,000		
250	0.00520	361,000		

Load Type A

Load lbs.	θ_5 rad.	θ_2 rad.
50	0.0008	0.00090
100	0.00165	0.00160
150	0.00256	0.00259

Load Type B

Plate Rotations

Table C-4

Load lbs.	θ_3 rad.	K in.-lb./rad.	$K_{ave.}$ in.-lb./rad.	$b_{ave.}$ in.
20	0.00276	54,300		
30	0.00450	50,100	47,100	10.60
40	0.00660	45,500		
50	0.00113	38,700		

Load Type C

Load lbs.	θ_6 rad.	θ_4 rad.
10	0.00010	0.00218
20	0.00021	0.0043
30	0.00032	0.0068
40	0.00045	0.0096
50	0.00060	0.0125

Load Type D

Plate Rotations

Table C-4 (Continued)

M_1 (in.-lb.)			θ_2 (rad.)			M_2	θ_4	$c_1 = 2M_2\theta_2/M_1\theta_4$			$c_{1_{ave.}}$
P=50lbs.	P=100lbs.	P=150lbs.	P=50lbs.	P=100lbs.	P=150lbs.	(in.-lb.)	(rad.)	P=50lbs.	P=100lbs.	P=150lbs.	
50x7.5	100x7.5	150x7.5	0.00090	0.00160	0.00259	10x7.5	0.00218	0.1652	0.1468	0.1584	
"	"	"	"	"	"	20x7.5	0.00430	0.1676	0.1488	0.1608	
"	"	"	"	"	"	30x7.5	0.00680	0.1590	0.1410	0.1520	0.1492
"	"	"	"	"	"	40x7.5	0.00960	0.1500	0.1332	0.1440	
"	"	"	"	"	"	50x7.5	0.01250	0.1440	0.1280	0.1382	

Carry-Over Factor of Interior Panel

Table C-5

M_1 (in.-lb.)			θ_5 (rad.)			M_2 (in.-lb.)	θ_6 (rad.)	$c_2 = M_1\theta_6/M_2\theta_5$			$c_{2_{ave.}}$
P=50lbs.	P=100lbs.	P=150lbs.	P=50lbs.	P=100lbs.	P=150lbs.			P=50lbs.	P=100lbs.	P=150lbs.	
50x7.7	100x7.5	150x7.5	0.0008	0.00165	0.00256	10x7.5	0.00011	0.688	0.667	0.645	
"	"	"	"	"	"	20x7.5	0.00021	0.607	0.638	0.615	
"	"	"	"	"	"	30x7.5	0.00032	0.658	0.640	0.615	0.666
"	"	"	"	"	"	40x7.5	0.00045	0.705	0.682	0.660	
"	"	"	"	"	"	50x7.5	0.00060	0.750	0.730	0.705	

Carry-Over Factor of Exterior Panel

Table C-5 (Continued)

APPENDIX D

D - 1 Yield Line Analysis for Model C2. The resisting moment across any line was computed using the formula for ultimate moment.

$$M_u = f'_c\, b\, d^2\, q\, (1 - 0.59q) \qquad \text{..... (D-1)}$$

where $$q = P.\frac{f_y}{f'_c} = \frac{A_s}{bd} \cdot \frac{f_y}{f'_c} \qquad \text{..... (D-2)}$$

and

M_u = Ultimate moment capacity of the section.

A_s = Area of tension reinforcement

f_y = Yield strength of reinforcement

f'_c = Compressive strength of concrete

b = Width of the section

d = Nominal effective depth.

Two failure mechanisms were assumed in the yield line analysis. The first mechanism is shown in Fig. D - 1(a) and the second in Fig. D - 1(b).

The material properties assumed were : f_y = 46,250 psi for the reinforcement and f'_c = 3,080 psi for the concrete. Since the spacing of the reinforcement was not uniform in either direction, the average number of wires in each direction was used in computing slab moment capacities per unit width.

For the negative reinforcement, number of wires per in. was 2.66 in the N - S drection as shown in Fig. D - 2 and 2.10 in the E - W direction.

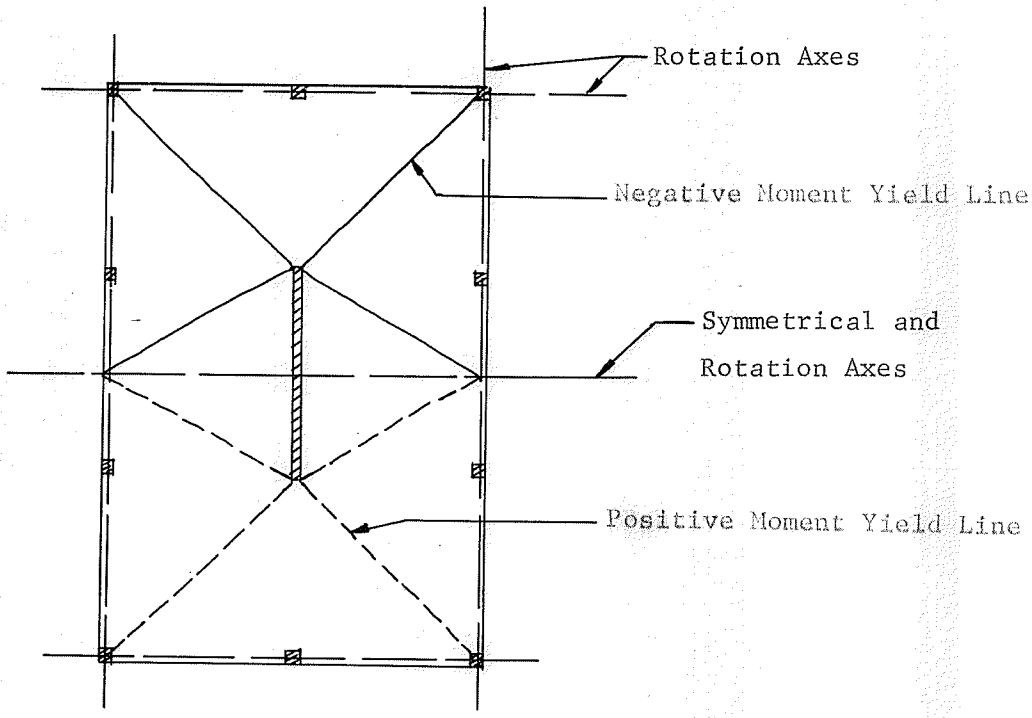

Mechanism 1

(a)

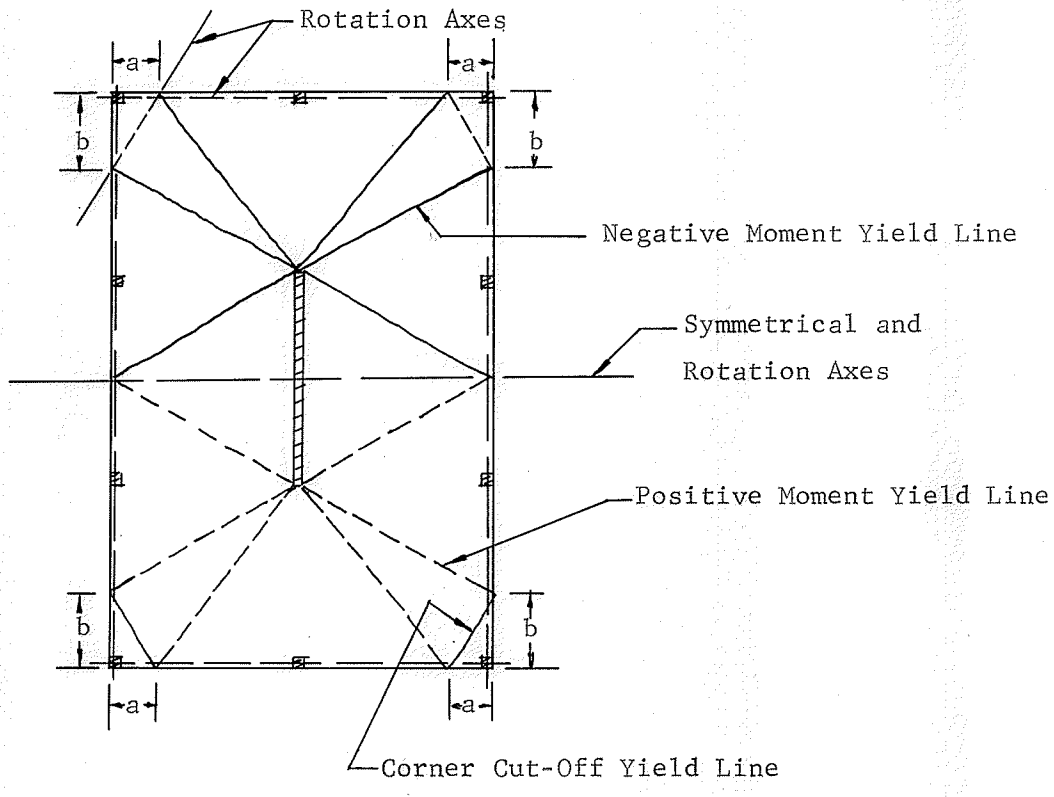

Mechanism 2

(b)

Fig. D-1 Assumed Failure Mechanisms, Model C2

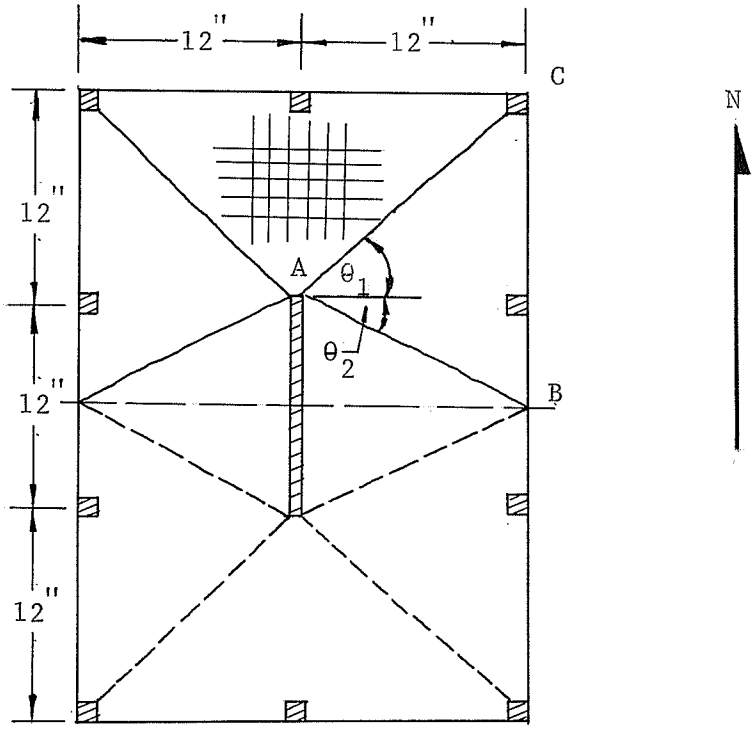

Fig. D-2 Direction of Wires Reinforcement

For 0.038 in. diameter wire, cross-sectional area was 0.001134 sq. in.

The average depth for the slab was 0.288 in.

Thus, for the N-S direction, euqation (D-2) gives:

$$q_1 = \frac{2.66 \times 0.001134}{1 \times 0.288} \times \frac{46250}{3080} = 0.157$$

and from equation (D-1)

$$M_{u1} = 3080 \times 1(0.228)^2 \times 0.157 \ (1 - 0.59 \times 0.157)$$

$= 36.30$ lb.-in./in.

$= m_1$ = unit moment in N-S direction

Similarly for the E-W direction

$q_2 = 0.124$

and $M_{u2} = 29.30$ lb.-in./in.

$= m_2$ = unit moment in E-W direction

The unit moment capacity m_{b1}, in a direction normal to line AC in Fig. D-2 is then:

$$m_{b1} = m_1 \text{Cos}^2\theta_1 + m_2 \text{Sin}^2\theta_1$$

$$= 36.30 \times \frac{1}{2} + 29.30 \times \frac{1}{2}$$

$= 32.80$ lb.-in./in. Since $\theta_1 = 45^o$

Similarly, the unit moment, m_{b2} normal to line AB is:

$$m_{b2} = m_1 \text{Cos}^2\theta_2 + m_2 \text{Sin}^2\theta_2$$

$$= 36.30 \times \frac{4}{5} + 29.30 \times \frac{1}{5}$$

$= 34.90$ lb.-in./in. where $\theta_2 = \text{Tan}^{-1}\frac{6}{12}$

$= 26^o\ 34'$

For the positive reinforcement, number of wires per in. were 2.52 in the N-S direction and 1.77 in the E-W direction.

Thus $q_3 = \frac{2.52 \times 0.001134}{0.288} \times \frac{46250}{3080} = 0.149$

and M_{u3} = 3080 x 0.083 x 0.149(1 - 0.59 x 0.149)

= 34.70 lb.-in./in.

= m_3 = unit moment in N-S direction

Similarly

q_4 = 0.105

and M_{u4} = 25.10 lb.-in./in.

= m_4 = unit moment in E-W direction

The unit moment normal to line AC is then:

m_{b3} = 29.85 lb.-in./in.

And that normal to line AB is:

m_{b4} = 32.76 lb.-in./in.

Analysis for Mechanism 1. Assuming that external moment M applied to the shear wall causes a shear wall rotation of θ radians, the energy dissipation E_D in the slab is:

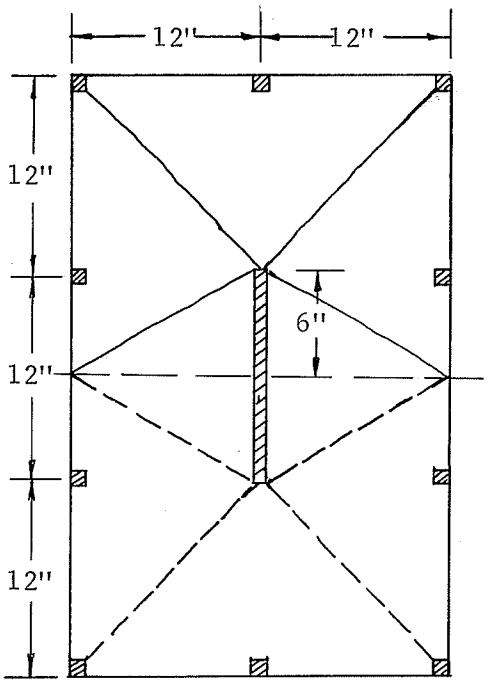

Negative Yield Line

$$E_{D1} = 24 \times 32.80 \times \frac{1}{12} + 12 \times 32.80 + 6 \times 34.90 \times \frac{1}{12} + 24 \times 34.90 \times \frac{1}{6}$$

$$= 305.70 \quad \text{lb.in.rad.}$$

Positive Yield Line

$$E_{D2} = 24 \times 29.85 \times \frac{1}{12} + 2\ 12 \times 29.85 + 6 \times 32.76 \times \frac{1}{12} + 24 \times 32.76 \times \frac{1}{6}$$

$$= 283.20 \quad \text{lb.in.rad.}$$

$\therefore$ Total $E_D = 305.70 + 283.20 = 588.90$ lb.in.rad.

External Workdone

$$M.\theta = P \times 7.5 \times \frac{1}{6} = 1.25P$$

Thus, equating the external and internal work:

$$1.25P = 588.90$$

$$\therefore \quad P = \frac{588.90}{1.25} = \underline{471.0} \text{ lbs.}$$

Analysis for Mechanism 2. Assume parameters a and b to define the points where cracks intersect the free edges of the plate.

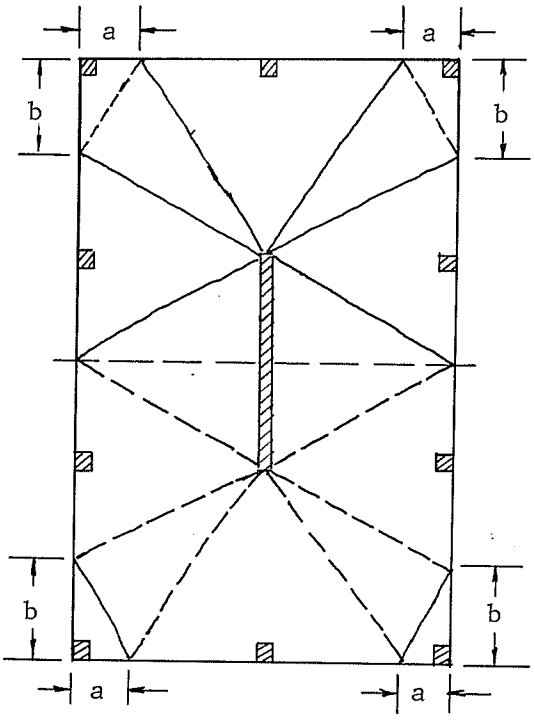

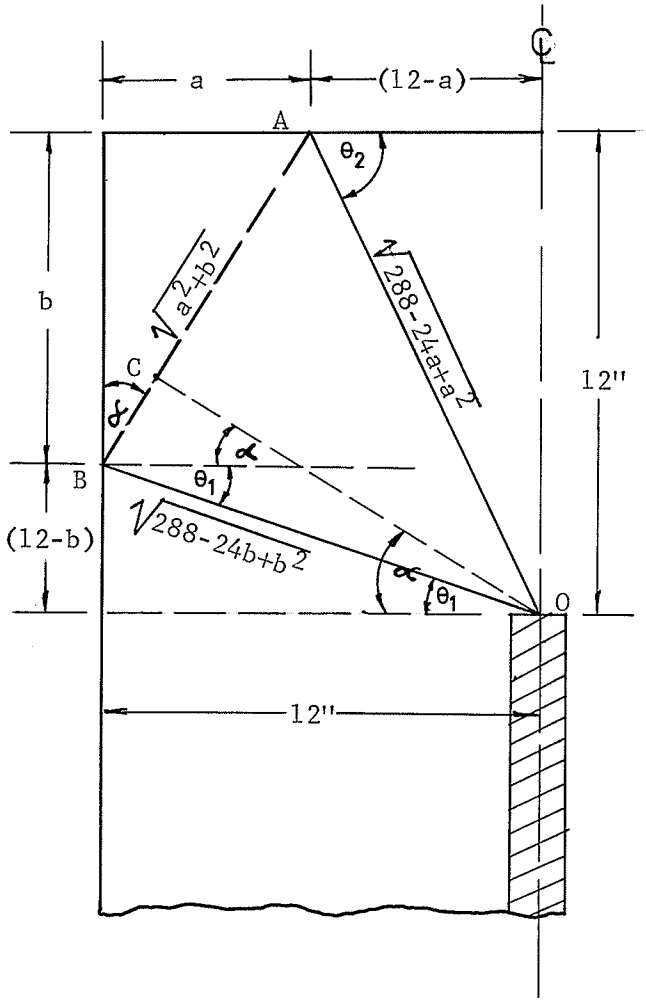

Then, for triangle BCO

$$OC = OB \cos(\alpha - \theta_1)$$

$$" = \sqrt{288 - 24b + b^2}\,(\cos\alpha \cos\theta_1 + \sin\alpha \sin\theta_1)$$

$$" = \sqrt{288 - 24b + b^2}\left[\frac{b}{\sqrt{a^2 + b^2}}\,\frac{12}{\sqrt{288 - 24b + b^2}} + \frac{a}{\sqrt{a^2 + b^2}}\,\frac{12 - b}{\sqrt{288 - 24b + b^2}}\right]$$

$$= \frac{12b}{\sqrt{a^2 + b^2}} + \frac{12a - ab}{\sqrt{a^2 + b^2}}$$

$$= \frac{12(a + b) - ab}{\sqrt{a^2 + b^2}}$$

For negative reinforcement,

The unit moment capacity m_{b1}, in a direction normal to line BO is thus.

$$m_{b1} = m_1 \cos^2\theta_1 + m_2 \cos^2\theta_2$$

where $\sin\theta_1 = \frac{(12 - b)}{\sqrt{288 - 24b + b^2}}$ and $\cos\theta_1 = \frac{12}{\sqrt{288 - 24b + b^2}}$

$$m_{b1} = 36.30\,\frac{144}{288 - 24b + b^2} + \frac{144 - 24b + b^2}{288 - 24b + b^2}\,29.30$$

$$" = \frac{9440 - 703b + 29.3b^2}{288 - 24b + b^2}$$

Similarly, the unit moment, m_{b2} normal to line AO,

when $\text{Sin}\ \theta_2 = \dfrac{12}{\sqrt{288 - 24a + a^2}}$ and $\text{Cos}\ \theta_2 = \dfrac{12 - a}{\sqrt{288 - 24a + a^2}}$

$$m_{b2} = 36.30\ \frac{144 - 24a + a^2}{288 - 24a + a^2} + 29.30\ \frac{144}{288 - 24a + a^2}$$

$$= \frac{9440 - 872a + 36.3a^2}{288 - 24a + a^2}$$

and the unit moment, m_{b3} normal to line AB,

when $\text{Sin}\ \alpha = \dfrac{a}{\sqrt{a^2 + b^2}}$ and $\text{Cos}\ \alpha = \dfrac{b}{\sqrt{a^2 + b^2}}$

$$m_{b3} = 36.30\ \frac{b^2}{a^2 + b^2} + 29.30\ \frac{a^2}{a^2 + b^2} = \frac{29.30a^2 + 36.30b^2}{a^2 + b^2}$$

For positive moment,

The unit moment, m_{b4}, in a direction normal to line BO is:

$$m_{b4} = 34.70\ \frac{144}{288 - 24b + b^2} + 25.10\ \frac{144 - 24b + b^2}{288 - 24b + b^2}$$

$$= \frac{8615 - 602b + 25.10b^2}{288 - 24b + b^2}$$

The unit moment, m_{b5}, normal to line AO is:

$$m_{b5} = 34.70 \frac{144 - 24a + a^2}{288 - 24a + a^2} + 25.10 \frac{144}{288 - 24a + a^2}$$

$$= \frac{8615 - 832a + 34.70a^2}{288 - 24a + a^2}$$

The unit moment, m_{b6}, normal to line AB is:

$$m_{b6} = 34.70 \frac{b^2}{a^2 + b^2} + 25.10 \frac{a^2}{a^2 + b^2}$$

$$= \frac{25.1a^2 + 34.7b^2}{a^2 + b^2}$$

Negative Yield Line,

$$E_{D1} = (24 - 2a)\left[\frac{9440 - 872a + 36.3a^2}{288 - 24a + a^2}\right] \times \frac{1}{12}$$

$$+ 2\sqrt{a^2 + b^2}\left[\frac{9440 - 872a + 36.3a^2}{288 - 24a + a^2} + \frac{9440 - 703b + 29.3b^2}{288 - 24b + b^2}\right.$$

$$\left. + \frac{25.1a^2 + 34.7b^2}{a^2 + b^2}\right] \times \frac{\sqrt{a^2 + b^2}}{12(a + b) - ab}$$

$$+ 2\left[(12 - b)\frac{9440 - 703b + 29.3b^2}{288 - 24b + b^2} + 6 \times 34.90\right] \times \frac{1}{12}$$

$$+ 24 \times 34.9 \times \frac{1}{6} \qquad \text{.....(D-3)}$$

Positive Yield Line,

$$E_{D2} = (24 - 2a)\left[\frac{8615 - 832\,a + 34.7a^2}{288 - 24a + a^2}\right] x \frac{1}{12}$$

$$+ 2\sqrt{a^2 + b^2}\left[\frac{8615 - 832a + 34.7a^2}{288 - 24a + a^2} + \frac{8615 - 602b + 25.10b^2}{288 - 24b + b^2}\right.$$

$$\left. + \frac{29.3a^2 + 36.3b^2}{a^2 + b^2}\right]\frac{\sqrt{a^2 + b^2}}{12(a + b) - ab}$$

$$+ 2\left[(12 - b)\frac{8615 - 602b + 25.10b^2}{288 - 24b + b^2} + 6 \times 32.76\right] x \frac{1}{12}$$

$$+ 24 \times 32.76 \times \frac{1}{6} \qquad \text{.....(D-4)}$$

Adding eq. (D-3) and (D-4), then,

Total energy dissipation = E_D

$$= \frac{(24 - 2a)}{12}\left[\frac{18055 - 1704a + 71a^2}{288 - 24a + a^2}\right] + \frac{2(a^2 + b^2)}{12(a + b) - ab} \quad x$$

$$\left[\frac{18055 - 1704a + 71a^2}{288 - 24a + a^2} + \frac{18055 - 1305b + 54.4b^2}{288 - 24b + b^2} + \frac{54.4a^2 + 71b^2}{a^2 + b^2}\right]$$

$$+ \frac{1}{6}\left[(12 - b)\frac{(18055 - 1305b + 54.4b^2)}{288 - 24b + b^2} + 6 \times 67.66\right]$$

$$+ 4 \times 67.66 \qquad \text{.....(D-5)}$$

Assuming b = 4 in., from eq. (D-5)

$$E_D = \frac{(12 - a)}{6}\left[\frac{18055 - 1704a + 71a^2}{288 - 24a + a^2}\right] + \frac{(a^2 + 16)}{4a + 24}\left[\frac{18055 - 1704a + 71a^2}{288 - 24a + a^2} + 65.8 + \frac{54.4a^2 + 1137}{a^2 + 16}\right] + 425.5 \quad \text{.....(D-6)}$$

Assuming a = 2 in., from eq. (D-6)

E_D = 649.5 lb. in. rad.

$P = \frac{649.5}{1.25} = 520.0$ lbs.

Assuming a = 3 in.,

E_D = 648.45 lb. in. rad.

$P = \frac{648.45}{1.25} = \underline{518.0}$ lbs.

Assuming a = 4 in.,

E_D = 654.86 lb. in. rad.

$P = \frac{654.86}{1.25} = 523.0$ lbs.

use a = 3 in.

Substituting a = 3 in., in eq. (D-5)

$$E_D = 90.45 + \frac{2(9 + b^2)}{36 + 9b}\left[60.3 + \frac{18055 - 1305b + 54.4b^2}{288 - 24b + b^2} + \frac{489.6 + 71b^2}{9 + b^2}\right]$$

$$+ \frac{1}{6}\left[(12 - b)\frac{(18055 - 1305b + 54.4b^2)}{288 - 24b + b^2}\right] + 338.30 \quad \text{.....(D-7)}$$

Assuming b = 1 in., from eq. (D-7)

E_D = 624.95 lb.in.rad.

$P = \frac{624.95}{1.25} = 500.0$ lbs.

Assuming b = 2 in.,

E_D = 624.25 lb.in.rad.

$P = \frac{624.25}{1.25} = \underline{499.0}$ lbs.

Assuming b = 3 in.,

E_D = 633.75 lb.in.rad.

$P = \frac{633.75}{1.25} = 507.0$ lbs.

Thus the smallest load P is 499.0 lbs.

The computed ultimate load for assumed failure mechanism 1 was 471 lbs., and that for assumed failure mechanism 2 was 499 lbs. The experimentally measured ultimate load was 450 lbs. The above computed results based on the concept of the yield line theory, which should be used merely as estimates of the ultimate capacity, are seen to be agree with the experimental value.